Characterization of the Physiological Role of the Deubiquitinase OTUB1 in Mice

---

Dissertation

zur

Erlangung der naturwissenschaftlichen Doktorwürde
(Dr. sc. nat.)

vorgelegt der

Mathematisch-naturwissenschaftlichen Fakultät

der

Universität Zürich

von

Amalia Ruiz Serrano

aus

Spanien

Promotionskommission

Prof. Dr. Roland H. Wenger (Vorsitz)

Dr. Carsten Scholz (Leitung der Dissertation)

Prof. Dr. Thomas A. Lutz

Prof. Dr. Hugo H. Marti

Zürich, 2020

This work has been performed under the supervision of:

Dr. Carsten Scholz
and
Prof. Dr. Roland H. Wenger

at the Institute of Physiology of the University of Zurich, CH-8057 Zurich, Switzerland

within the PhD program in Integrative Molecular Medicine (ImMed)
of the Zurich Center for Integrative Human Physiology (ZIHP)

Table of Contents

Summary

Protein ubiquitination is a key regulatory process in a plethora of physiological and pathological pathways. During ubiquitination, the protein ubiquitin is covalently attached to a substrate protein forming mono- or polyubiquitin chains. Ubiquitination can be reversed via deubiquitinases (DUBs). OTUB1 (ovarian tumor domain-containing ubiquitin aldehyde binding protein 1) is one of the most highly expressed deubiquitinases in cells with a unique enzymatic activity cleaving Lys48 ubiquitin chains and preventing Lys48 and Lys63 ubiquitin chain formation non-enzymatically. OTUB1 regulates various pathways and processes *in vitro*, like proinflammatory and profibrotic signaling, DNA damage response, proliferation and apoptosis.

The cellular oxygen sensor factor inhibiting HIF (FIH) is an asparagine hydroxylase controlling the transactivation activity of the hypoxia inducible factor (HIF), key regulator of the transcriptional response to hypoxia. Our group recently demonstrated that FIH hydroxylates OTUB1 on Asn22, regulating cellular energy metabolism. This thesis aims to investigate the interaction between FIH and OTUB1 in more detail and to assess if OTUB1 is a possible physiological target of FIH.

The molecular interaction between FIH and OTUB1 showed a denaturing-resistant, likely covalently linked protein heterodimer, highly sensitive to hypoxia and depending on FIH enzymatic activity. Several studies have investigated the role of OTUB1 in diseases *in vivo*. However, the physiological function of OTUB1 is unknown. To understand the *in vivo* role of OTUB1 and to assess if it is a likely physiologically relevant FIH target, we characterized mice with constitutive (*Otub1*$^{-/-}$) and conditional whole-body *Otub1* (wb*Otub1*$^{-/-}$) deletion. *Otub1*$^{-/-}$ mice died perinatally due to asphyxiation and showed decreased alveolar space, increased lung cell proliferation and cardiac hypertrophy. wb*Otub1*$^{-/-}$ mice showed pulmonary hyperventilation and cardiac hypertrophy with left ventricular dysfunction. Additionally, adult animals presented with decreased body weight, increased energy expenditure and glucose metabolism. Furthermore, the AKT/mTOR signaling was increased in cells and tissues without *Otub1*. Overall, these results demonstrate that OTUB1 is essential for development, respiration, cardiac function and energy metabolic homeostasis *in vivo*. Interestingly, *Hif1an* (the gene encoding FIH) homozygous knockout (KO) mice display a metabolic phenotype that is virtually identical to the metabolic alterations observed in *Otub1* KO mice.

In summary, we found that FIH forms a stable complex with OTUB1 at a cellular level. Interestingly, the metabolic and respiratory phenotypes of *Otub1* KO mice support that the FIH-dependent regulation of OTUB1 is physiologically relevant. Our studies of *Otub1* KO mice will further help evaluating the potential of OTUB1 as a therapeutic target and possible role in diseases.

List of abbreviations

AKT	RAC-alpha serine/threonine-protein kinase
ALG13	Asparagine-linked glycosylation 13 homolog
CAD	Carbamoyl-phosphate synthetase 2 aspartate transcarbamoylase dihydroorotase
cIAP1	Cellular inhibitor of apoptosis protein-1
CNS	Central nervous system
COPD	Chronic obstructive pulmonary disease
CYLD	Cylindromatosis
DEPTOR	DEP domain containing mTOR interacting protein
DSB	Double strand brand
DUB	Deubiquitinase
EAE	Experimental autoimmune encephalomyelitis
EGFR	Epidermal growth factor receptor
EMT	Epithelial-mesenchymal transition
ER	Estrogen receptor
FIH	Hypoxia-inducible factor 1-alpha inhibitor
FOXO	Forkhead box protein O
FOXM1	Forkhead box protein M1
GLUT4	Solute carrier family 2, facilitated glucose transporter member 4
GSK3β	Glycogen synthase kinase-3 beta
HECT	Homologous to the E6-AP Carboxyl Terminus
HF	Heart failure
HIF	Hypoxia-inducible factor
HIN1L	Hypermethylated in cancer zinc finger/POZ-domain 1 protein
IGF	Insulin-like growth factor
IKKβ	Nuclear factor kappa B inhibitor kinase beta
IL-1R	Interleukin-1 receptor
IRI	Ischemia reperfusion injury
IRS	Insulin receptor substrate
JAK	Janus kinase
JAMM	JAB1/MNP/MOV34 metalloenzymes
JNK	c-Jun N-terminal kinases
KO	Knock-out
MAPK	Mitogen-activated protein kinase
MCPIP	Monocyte chemotactic protein-induced protein

Mdm2	Mouse double minute 2 homolog
MG53	Tripartite motif-containing protein 72
MJD	Machado Joseph Disease
mLST8	Mammalian lethal with Sec13 protein 8
mTOR(C)	Mechanistic target of rapamycin (complex)
MuRF1	Muscle RING-finger protein-1
NASH	Non-alcoholic steatohepatitis
NF-κB	Nuclear factor kappa B
Nur77	Nuclear hormone receptor subfamily 4 group A member
OUT	Ovarian tumor protease
OTUB1	Ovarian tumor domain-containing ubiquitin aldehyde binding protein 1
OTUD(1-6)	Ovarian tumor protease domain-containing protein (1-6)
OTULIN	Ovarian tumor protease deubiquitinase with linear linkage specificity
PDK	Pyruvate dehydrogenase (acetyl-transferring) kinase
PHD	Hypoxia-inducible factor prolyl hydroxylase
PI3K	Phosphoinositide 3-kinase
PIKK	PI3K-related kinase
PPARG	Peroxisome proliferator-activated receptor gamma
PRAS40	Proline rich Akt substrate 40 kDa
PTEN	Phosphatase and tension homolog
Raptor	Regulatory-associated protein of TOR
RhoA	Ras homolog family member A
Rictor	Rapamycin-insensitive companion of mTOR
RIG-I	Retinoic acid-inducible gene I
RING	Really Interesting New Gene
RNF168	Ring Finger Protein 168
RPA	Replication protein A
SENP	Sentrin-specific protease
SGK1	Serum- and glucocorticoid-induced protein kinase 1
S6K	Ribosomal protein S6 kinase
SLC7A11	Cystine/glutamate transporter
SMAD (2/3)	Mothers against decapentaplegic homolog (2/3)
SOCS1	Suppressor of cytokine signaling 1
SREBP	Sterol responsive element binding protein
STAT	Signal transducer and activator of transcription
SUMO	Small ubiquitin-related modifier
TAC	Transverse aortic constriction

TBC1D4	TBC1 domain family member 4
TFEB	Transcription factor EB
TLR	Toll-like receptor
TNFα	Tumor necrosis factor alpha
TRAF	Tumor necrosis factor receptor-associated factor
TSC2	Tuberin
TV	Tidal volume
UBC13	Ubiquitin-conjugating enzyme E2 13
ULK	Serine/threonine-protein kinase
UCH	Ubiquitin C-terminal hydrolase
USP	Ubiquitin-specific protease
VHL	von Hippel-Lindau
YB-1	Y-box-binding protein 1
ZAP	Zinc finger antiviral protein

1. Introduction

1.1. Embryonic development

For over the last 60 years, mice have been used to understand mammalian embryonic development [1]. The mouse is a suitable embryological model due to its early fertility (6 weeks in females and 8 weeks in males), the large number of animals per litter, the possibility to get pregnant again within 4 hours after giving birth, the brief estrous cycle (4 to 6 days) and the short pregnancy period (between 18 and 21 days) [2], allowing for a manageable time frame of analyses. Moreover, mice and humans present a comparable embryonic development, a fertilized egg proliferates and is exposed to cell differentiation forming a primitive streak with anterior-posterior and left-right polarization. From the primitive streak with an epidermal and endodermal layer, the mesoderm is formed by the epidermal to mesodermal transition. The ectoderm, mesoderm and endoderm develop into the different organs and tissues [3]. According to the WHO, 947,000 deaths occurred during preterm birth and 637,000 deaths immediately after birth in humans due to asphyxia and trauma worldwide in 2015 [4]. Due to the previously described advantages and the similarities to the human developmental process, mice constitute a good model to study embryonic development, aiming to understand the causes and to reduce the numbers of pre- and peri-natal deaths in humans.

1.1.1. Mouse lung development

Gas exchange between the environment and organism is required to supply oxygen for the generation of energy by respiration in the mitochondria and to release the carbon dioxide formed by the cells in the body. Respiratory gas exchange occurs in diverse manners in nature ranging from simple diffusion in unicellular organisms to complex avascular air sacs in birds [5]. In mammals, the air enters the lungs from the environment through the mouth and nose and then the gases are exchanged with the body by gas diffusion from lung alveoli into surrounding capillaries. To obtain an efficient gas exchange, humans possess a total lung alveolar surface area of 70m^2 [6] and mice of 80 cm^2 [7]. At the initial phase of the respiratory development, human and mouse embryos present only a laryngo-tracheal tube with reduced surface area and no alveoli. To reach the necessary diffusible interface area at an adult stage, this laryngo-tracheal tube undergoes several complex branching processes [8].

The development of the mouse lung *in utero* includes five different stages (Figure 1) [8]:

(1) Embryonic stage, E9-E12 [8]. From the simple layered blastula, three different layers (endoderm, mesoderm and ectoderm) are formed via gastrulation [9]. The endoderm then

forms a primitive tube surrounded by mesoderm to originate the laryngo-tracheal groove [8]. At E9 in mice or week 4 in humans, the laryngo-tracheal groove constitutes dorso-ventrally the tracheal rudiment and laterally two bronchial buds. In mice, the first observation of a tracheal bifurcation occurs briefly after the laryngo-tracheal groove [10]. From the tracheal diverticulum, symmetric primitive pulmonary buds are formed inside the pleuroperitoneal canals. The reproducible branching is completed at E12 with unilobed left and quadrilobed right lungs in mice. In humans, two left lobes and three right lobes are present at 16 weeks [8]. This branching processing requires high proliferation of epithelial and mesenchymal cells [11]. During this phase, the pulmonary artery travels to the lungs as a branch of the branchial arch arteries [8].

(2) Pseudoglandular stage, E12-E16.5. The bronchial and respiratory tree is formed as an undifferentiated primordial system [8]. During the beginning of this phase neuroendocrine precursor cells are in proximal conducting airways and move towards distal airways [12]. These neuroendocrine cells form clusters and neuroepithelial bodies [12]. Functionally, neuroendocrine cells are key regulators of surrounding cell proliferation and the center of secretory cell differentiation [12]. Together with the neuroendocrine cell differentiation, ciliated, globular and Clara cells begin to differentiate [11].

(3) Canalicular stage, E16.5 to E17.5. The most relevant events are the formation of terminal sacs and vascularization [8]. The morphogenesis of the distal airway and the air-blood barrier occur together with the production of surfactant and epithelial differentiation [10]. Thinning of the alveolar walls is initiated mainly via apoptosis of the interstitial tissue [11]. Furthermore, the pulmonary vascularization level increases in this stage [11].

(4) Saccular stage, E17.5 to P5. Terminal sacs and vascularization increase, and the pneumocytes type I and II are differentiated [8]. The saccular phase is characterized by expansion of the airway spaces [10], transient increase of cell apoptosis during birth with continuous proliferation of epithelial cells and a final surge of apoptosis in order to remove cell excess [11].

(5) Alveolar stage, P5 to P30. Terminal sacs develop into mature alveolar ducts and final alveoli [8]. Mature alveoli are characterized by the thinning of their epithelial-endothelial layer which occurs mainly by apoptosis [11]. The alveolar surface is increased by epithelial cell proliferation [11]. After birth, important morphological and physiological changes occur to reach constant postnatal respiration: body temperature decrease, gaseous distention of the lungs, increase of oxygen partial pressure resulting in decreased carotid oxygen sensitivity, Hering-Breuer reflex activation and functional connectivity between oxygen chemoreceptors and respiratory motoneurons/arousal centers [13, 14].

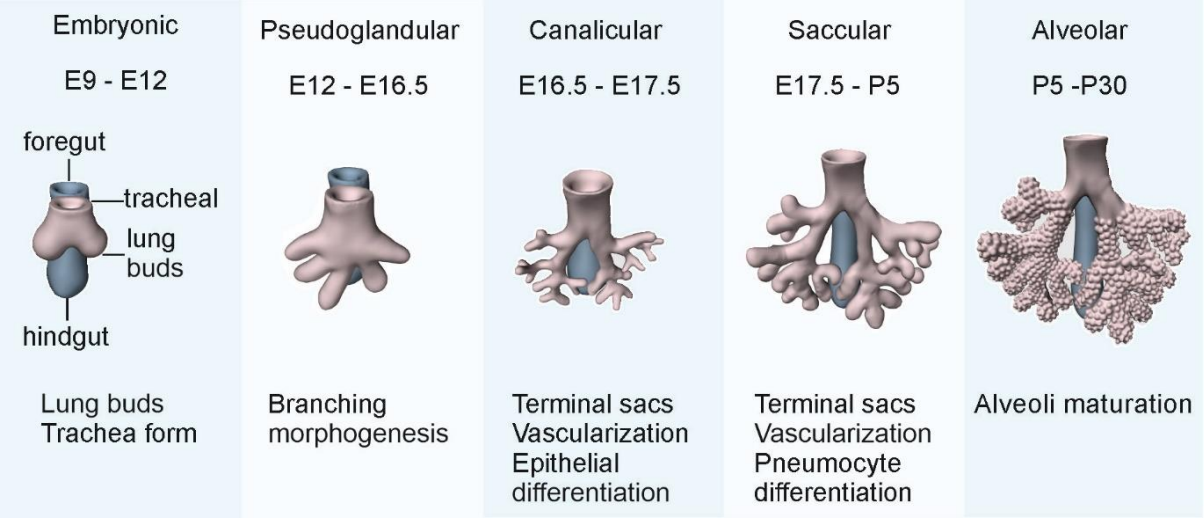

Figure 1: Mouse lung developmental stages. Lung endoderm starts to develop at E9 on the ventral anterior foregut during the embryonic stage. Between E12 and E16.5, branching morphogenesis occurs during the pseudoglandular stage. In the canalicular (E16.5-E17.5) and saccular (E17.5-P5) stages, terminal sacs develop and the lung vascularization level is significantly increased. The last developmental stage of the lung is the alveolar stage between P5 and P30 with alveoli maturation. Figure was adapted from [15].

All changes in the lung during the five distinct development stages are mainly orchestrated by diffusible signals from the mesenchyme, instead of cell intrinsic [12]. During the last two stages of lung development, apoptosis and proliferation are key regulators of the crucial expansion of the alveolar airway space [10, 11, 16-18]. Once the lung development is completed, about 5000 branches in mice and 54000 branches in humans are present. Within the distinct sections of the branches, we can observe a diverse cellular population [10]. The tracheobronchial epithelium contains serous, ciliated, goblet and basal cells. In the proximal bronchi, Clara, ciliated and neuroendocrine cells are present in mice [12]. Finally, bronchioles show ciliated, serous, alveolar type I and II cells [12]. Goblet cells consist of a compact nucleus in the basal area and contains granules with acidic mucin glycoproteins in the apical side of the cytoplasm that can be secreted to the airway lumen to protect the epithelial surface [19]. Serous cells present a similar morphology as the goblet cells but with a higher electron-density in the granules and secrete glandular fluid to hydrate the mucus released by goblet cells and enhance innate immunity [20-22]. Ciliated cells are constituted of up to 300 cilia on the luminal region of each cell and present a high mitochondrial content with the possibility to differentiate morphologically under stress conditions [23, 24]. Basal cells connect through hemodesmosomes to the basement membrane, constitute the attachment source to ciliated and goblet cells and regulates inflammatory response [25, 26]. Clara cells contains granules, can secrete surfactant proteins and proteinases protecting the epithelium and show a high proliferative capacity [27-29]. Neuroendocrine cells are elongated and pyramidal with microvilli displaying a role in the inflammatory response [30]. Alveolar type I cells are placed in the

alveolar surface where the gas exchange occur by this large flat cells [31]. On the other hand, alveolar type II cells are less frequent than type I, show a cuboidal shape with apical microvilli, contain lamellar bodies, secrete surfactant protein and can differentiate into alveolar type I cells [31, 32]. Considering the critical function of the lungs, mutations in genes specifically linked to lung development are typically associated with perinatal lethality [33].

1.1.2. Mouse heart development

In vertebrate embryos, the heart is the first functional organ to be developed (at E8 in mice and at week 3 in humans) [34]. Cardiac congenital malformations constitute 1% of the live births and 8% of the prenatal births in humans [34]. Currently, there are more than 150 gene mutations known in mice that are associated with cardiac development abnormalities which are investigated to increase our understanding of developmental heart formation [35].

Cardiac development can be divided into five different stages in mice (Figure 2):

(1) Cardiac crescent stage, E7.5 [36]. Two different tubes are formed from the cardiogenic mesoderm, the first and second heart fields. The first heart field proliferates and differentiates during this stage whereas the second heart field remains undifferentiated as a myocardial progenitor [36]. Precursor cells in the primitive streak differentiate into cardiomyocytes and travel anterior-laterally to constitute the myocardial primordial with a cranial and caudal peak. In parallel, endothelial cells are differentiated and build two tubes below the myocardial primordial[37].
(2) Linear heart stage, E8 [36, 38]. The heart starts to pump irregularly and the parallel tubes formed by endothelial cells in the previous phase fuse across the ventral midline forming the cardiovascular lumen [37]. During this phase, the myocardium begins to differentiate and is connected to the endocardium via finger-like protrusions [39].
(3) Looping heart stage, E8.5-E10 [36, 38]. The heart starts to pump regularly with the venous pole as a pacemaker. The linear heart turns anti-clockwise forming a premature heart structure with a rostral arterial or aortic sac together with a caudal venous pole (left and right sinus poles)[37, 40]. At a cellular level, the proliferation of cardiomyocytes is increased to a high rate, the highest of all cardiac developmental stages. Specifically, 700 cardiomyocytes are present in 0.0014 mm^3 of heart tissue at E8 and 68000 cardiomyocytes can be found in 0.150 mm^3 of heart tissue at E11. Since the increase in cardiomyocyte numbers and cardiac size occur in parallel, the cardiomyocyte size stays constant at around 2150 μm^3 [39].

(4) Chamber formation stage, E10-12 [36]. A bulboventricular canal connects the left and right ventricle. The right ventricle is connected via an outflow tract to the aortic sac. The four different chambers of the heart are originated from the expansion and bulging of the walls of the looped heart [37]. The cardiac trabeculae in the luminal side of the ventricles are formed from the myocardium [39]. They grow by basal apposition leading towards an outward expansion of the chambers [39].

(5) Maturation/septation stage, overlaps with the previous phase starting after E10 and finishing at birth [36]. In this stage, the heart undergoes sarcomere alignment in their myofibrils, T-tubule formation, a decrease in glycolysis and an increase in mitochondrial number and activity [41]. At the end of the embryonic cardiac development (E17.5), the mouse heart contains approximately 1 million cardiomyocytes with a cellular volume of around 2150 μm^3 [39]. During birth, major changes occur in the heart. When the oxygen and nutrients supplied by the placenta and umbilical cord cease, the circulation to the lungs and of the rest of the newborn begins to be differentiated to allow the adult gas exchange in the alveoli [42]. Those changes in circulation together with the first breath provoke different pressure between the right and left atrium and lead to the closure of the connection between both atria via the foramen ovale [42].

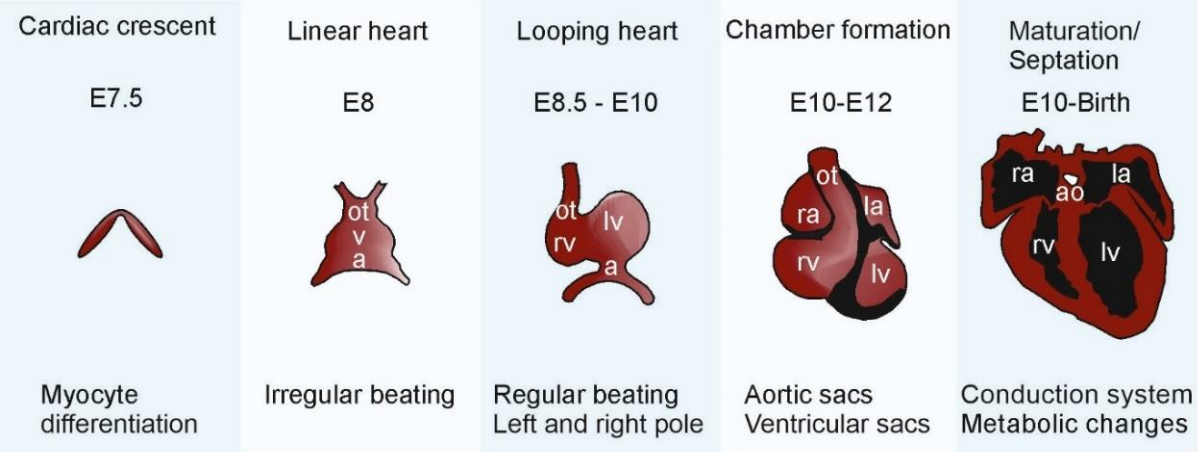

Figure 2: Mouse heart developmental stages. The first stage of cardiac development is the cardiac crescent stage (E7.5) characterized by myocyte differentiation. This is followed by the linear heart stage (E8) with an irregularly beating heart. At stage 3, it follows the looping heart stage (E8.5-E10) with a regularly beating heart and the beginning of the left and right sinus pole differentiation. The different aortic and ventricular sacs are formed during the chamber formation stage (E10-E12). Finally, maturation and septation of the heart occur (E10-birth) together with adaptations of the energy metabolism of cardiomyocytes. Ot: outflow tract; v: ventricle; a: atrium; rv: right ventricle; lv: left ventricle; ra: right atrium; la: left atrium; ao: aorta.

1.2. Adult lung

1.2.1. Mouse pulmonary structure and function

The adult mouse lung is formed by four right lobes and one left lobe [43]. Overall, 18% of the total lung volume is filled by pulmonary parenchymal tissue [44]. Inhaled air travels through the trachea to the main bronchi subsequently to 13-17 bronchioles generations and finally to alveolar ducts with monopodial branching [2]. In the alveoli, diffusion of gases like oxygen and carbon dioxide occur within the bloodstream through a 0.32 μm thick blood-gas barrier [45, 46]. Other functions of the lung include a role in immune defense against inhaled pathogenic particles, conversion of angiotensin I to angiotensin II (a potent vasoconstrictor), and release of diverse substances as surfactant proteins that decrease the alveolar elastic recoil [44, 47-49].

One of the main parameters to assess pulmonary function is the tidal volume (TV), which is the volume of inspired and expired air per breath under resting conditions. In adult mice the average TV is about 0.3 mL. the average respiratory frequency is 168 breaths per minute [50]. This rapid respiratory rate is necessary to dissipate body heat and to maintain the body temperature [51].

The lung includes a wide variety of cells as non-ciliated, dome-shaped, secretory bronchiolar Clara cells and ciliated cells. From the bronchi to the alveoli the cellular general morphology changes from columnar to cuboidal shape [52, 53]. Additionally, the number of Clara cells increases towards the alveoli [54, 55]. These Clara cells are key regulators in anti-inflammatory and immune regulations in the lung epithelium by expressing the P-450 monooxygenase enzymatic system that is involved in metabolism and detoxification of xenobiotics [56]. In the alveolar and acini region of the lung, pneumocytes type I and type II cells can be found. Type I pneumocytes constitute 93-95 % of the alveolar surface of each alveolus, are not able to undergo mitosis and the flat cellular morphology aid gaseous diffusion to the underlying endothelium [57]. Type II pneumocytes represent 3-5 % of the alveolar surface, show a quick repairing capacity, produce surfactant protein to maintain homeostasis of the alveolus and regulates innate immune response [58, 59].

The regulation of the respiration is driven by thoracic neural receptors, peripheral chemoreceptors and central chemoreceptors [60-62]. Thoracic neural receptors are mechanoreceptors located in trachea, airways and pulmonary vessels sending information regarding lung volume, airway stretch and vascular congestion to the respiratory center in the

brain [63, 64]. Peripheral chemoreceptors are divided between carotid bodies that send the information via the glossopharyngeal nerve and aortic bodies that informs via the vagus nerve [60]. Peripheral chemoreceptors are able to sense carbon dioxide and hydrogen ions, but mainly response to low arterial oxygen levels [65]. Central chemoreceptors mostly sense pH modifications in the central nervous system due to changes in arterial carbon dioxide [66]. Carbon dioxide forms hydron ions in the cerebrospinal fluid, producing an acidic pH that is sensed by the chemoreceptors which send the signal to the brain that in turn will stimulate hyperventilation [61].

Whole-body plethysmography is the most commonly used technique to assess the respiratory function in unrestrained and conscious mice in a non-invasive manner [67, 68].

1.2.2. Pulmonary diseases

Lung hypoplasia constitutes the main cause of neonatal lethality and present around 18 % of all perinatal lethality in humans [69-71]. Lung hypoplasia is referred as pulmonary underdevelopment that leads to a decreased pulmonary weight and/or volume due to decreased bronchial branches, alveoli and/or alveolar size. Lung hypoplasia is sub-classified based on the symptoms and causes [72]. For example, primary pulmonary hypoplasia displays with a congenital malformation of the pulmonary parenchyma and a reduced lung volume. The lungs do not respond to treatment with surfactants and neonates do not survive [73, 74]. Current studies try to unravel the mechanisms underlying this disorder [75-78]. Opposite to lung hypoplasia, pulmonary hyperplasia is the enlargement of the lung by the increase on the pulmonary cell number and extremely uncommon in neonates [79, 80].

In general, pulmonary diseases include five of the 30 leading death causes world-wide: chronic obstructive pulmonary disease (COPD) is ranked as third, lower respiratory tract infection is fourth, bronchial and lung cancer is sixth and asthma is ranked as twenty-eighth [81]. COPD is the pulmonary disease with the highest mortality and a wide number of symptoms [82]. COPD displays chronic airway inflammation, decreased numbers of small airways and destruction of parenchymal area, leading to emphysema and shortness of breath. The epithelium airway that functions as a first defense barrier against air pathogens is impaired presenting with squamous metaplasia, goblet cell hyperplasia and loss of epithelial morphology [82]. The epithelium metaplasia or change in the tissue nature may occur by the proliferation of airway epithelial cells. However, the molecular mechanisms underlying the increased cell proliferation and differentiation in COPD remains unknown. COPD

pathogenesis develops in emphysema formation due to the imbalance between proliferation and apoptosis [83], resulting in an excess of mucus and higher infection susceptibility [84]. COPD is irreversible and leads to a decreased parenchymal elasticity due to the degradation of elastin by diverse proteases [85]. Furthermore, COPD affects blood flow and pressure leading to cardiac and renal dysfunction increasing in turn the pulmonary edema [86]. Pulmonary edema is an increase of fluids in the interstitial space and alveoli. At a molecular level, proteoglycans in the extracellular matrix break, leading to decreased intermolecular interactions with the extracellular matrix components facilitating the pulmonary edema [87].

To understand further the function and treatment of pulmonary diseases, different mouse models have been studied. Between the advantages of using the mice are the deeply studied immunologic system, the short reproducible cycle, the wide variety of available mouse reagents, the characterized genome and available transgenic technology applied to this specie [44].

1.3. Adult heart

1.3.1. Mouse cardiac structure and function

The general human and mouse anatomy and function are comparable. The adult heart is a four-chamber organ divided into the right and left heart, each of them formed by one atrium and one ventricle. The main function of the heart is to ensure blood circulation and, thereby, the delivery of nutrients and oxygen in the blood throughout the organism. A cardiac cycle ranges from the contraction of the atria to the relaxation of the ventricles and is divided into two phases: (1) the diastole where the ventricles relax and blood accumulates and (2) the systole corresponding to the contraction and the emptying of the ventricles [88]. The maximal aortic pressure (120 mmHg) is reached during the systole [89] and the lowest arterial pressure (100 mmHg) during the diastole [90] (Figure 3).

The tissue consists of atrial muscle, ventricular muscle, excitatory and conductive muscle fibers (Figure 3). A few anatomical and functional characteristics are different between humans and mice. For example, a mouse adult heart weighs around 150 mg, pumps 20.4 mL blood per minute beating 650 times at rest [91]. A human heart weighs around 275 g and beats on average 65 times per minute and 4 to 6 L per minute under resting conditions [92]. Due to the mouse body position, its heart displays mobility in the pericardial cavity and presents an ellipsoidal shape [93]. Inner, medium and outer epicardium constitute the cardiac layers. The outer surface of the heart is covered by a thin and fragile mesothelium. Underneath the

mesothelium, circumferentially fibrous connective tissue with blood and lymphatic vessels forms the thin pericardium [94, 95]. Below the pericardium, the myocardium incorporates cardiomyocytes surrounded by a rich capillary network [95]. Finally in the inner side of the heart, the endocardium appears with an elevated number of vessels and with cardiomyocyte fibers oblique or parallel to the apical-basal axis [94].

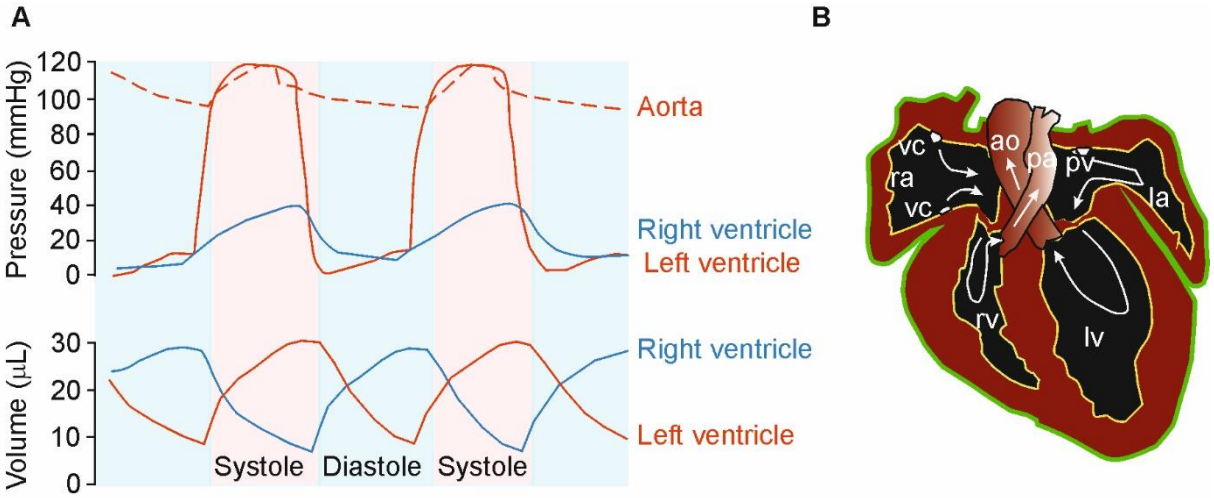

Figure 3: Mouse adult heart function. (A) Cardiac right and left ventricular pressure during systole and diastole, together with the aortic pressure and the corresponding volume of the left and right ventricle. **(B)** Adult mouse heart anatomy showing the different muscle pericardium (green), myocardium (red) and endocardium (yellow) and the blood flow direction with white arrows. rv: right ventricle; lv: left ventricle; ra: right atrium; la: left atrium; ao: aorta; vc: vena cava; pa: pulmonary artery; pv: pulmonary veins.

The heart adjusts its contractile strength and frequency according to the body requirements. Mostly, neural, electrical, hormonal and mechanical signals are sensed affecting cardiac contraction strength and rate [96-98]. The cardiac rhythm is tightly regulated by the electrical activity of the heart. One of the unique characteristics of the heart is the cardiac pacemaker in the superior lateral wall of the right atria, the sinoatrial (SA) node. The SA node is composed of a cluster of specialized cardiomyocytes which have the unique property to spontaneously generate an electrical impulse [99].

The heart responds under different stimuli to pump enough blood to all the body tissues and organs. This cardiac plasticity allows cardiomyocytes to increase their width and length under physiological conditions leading to cardiac hypertrophy [100]. Physiological cardiac hypertrophy is caused by normal animal growth [101], pregnancy [102] and exercise [103, 104], among others. Also, diverse growth hormones such as insulin or thyroid hormone, together with mechanical forcers can lead to cardiac hypertrophy [105]. This cardiac hypertrophy increases cardiac ejection performance and decreases the ventricular wall

pressure [103, 105]. Morphologically, physiological hypertrophy leads to increased ventricular wall thickness together with 10-20% increase in the ventricular volume (eccentric hypertrophy). Under physiological conditions the hypertrophy is reversible and without cardiomyocyte death [105].

There are diverse techniques to measure cardiac morphology and function, such as echocardiography, microCT, PET and MRI. However, due to the costs and accessibility echocardiography is one of the most used techniques [106].

1.3.2. Cardiac diseases

Cardiovascular disease is the leading cause of mortality worldwide in humans, accounting for 31% of all deaths with 17.9 million people in 2016 according to the WHO (https://www.who.int/en/news-room/fact-sheets/detail/cardiovascular-diseases-(cvds)).
Cardiac diseases commonly result in heart failure (HF) constituting the leading reason of morbidity and mortality [107].

HF is typically characterized by systolic or diastolic dysfunction followed by low cardiac output [107].Left-sided HF is usually a precursor of right-sided HF, which is connected to a higher risk of sudden death [108]. Traditionally, left-sided HF can be classified based on reduced (HFrEF; EF < 50 %) or preserved (HFpEF; EF ≥ 50 %) left ventricular ejection fraction. HFrEF presents a ventricle unable to contract normally and is caused by several cardiac disorders as coronary artery disease and cardiomyopathies [109]. These cardiac diseases lead to cardiomyocyte apoptosis and high wall stress, decreasing the contraction capacity of the cardiomyocytes that cause eventually systolic failure. HFrEF presents a higher mortality rate than patients with HFpEF [110]. HFpEF shows diastolic dysfunction, resulting usually from chronic disease as hypertension, aging, obesity or renal dysfunction [109]. HFpEF is observed more frequently in women and older populations [111]. Patients with HFpEF show exercise intolerance, edema, dyspnea, pulmonary edema and pulmonary hypertension, all of the symptoms are related to increased fibrosis, decreased capillary content and cardiac hypertrophy [112].

As previously explained, hypertrophy can occur under physiological conditions. However, several factors including hypertension [113], myocardial infarction [114], gene mutations [115] and valve stenosis [116] can lead to pathological hypertrophy. At a morphological level, pathological hypertrophy is characterized primarily by an increase of the ventricular wall

thickness with larger cardiomyocytes decreasing the ventricular inner chamber volume (concentric hypertrophy). Concentric hypertrophy is found in HF with normal left ventricular ejection fraction [117]. The concentric hypertrophy can lead to an eccentric hypertrophy comparable to physiological hypertrophy, but with a reduced contractile capacity and an increased cardiomyocyte length [105]. Eccentric hypertrophy is found in HF with decreased left ventricular ejection fraction [117]. Pathological hypertrophy is irreversible and associated with cardiomyocyte death, reduced capillary network [118] and fibrosis [119]. Overall, pathologic cardiac hypertrophy has a poor prognosis and generally leads to HFpEF [120], arrythmia [120], pulmonary edema and sudden death due to fibrillation [121].

Murine models represent one of the most relevant models to study cardiac human diseases [122]. For example, mouse models of HF are the most used animal models, mainly due to their genetic similarity with humans and the almost 85 % identical protein-coding regions [123]. Human cardiac diseases has been further understood and their treatment improved by mechanistic studies and candidate gene identification on genetically modified mice [124].

1.4. Energy metabolism in mice

Mice are supplied with energy through a wide variety of metabolic pathways, depending on the available nutrients, energy requirements and others [125-127]. Energy metabolism can be distinguished based on the utilization of molecular oxygen, referred to as aerobic (in the presence of oxygen) or anaerobic (under the absence of oxygen) metabolism [125, 126]. To understand further the metabolism in humans, mice are commonly analyzed. This chapter focuses on mouse glucose metabolism and homeostasis, one of the major metabolic substrates alongside lipids, proteins and molecular oxygen.

1.4.1. Glucose metabolism

Monosaccharides are relevant components of the diet and can be divided between fructose, galactose and glucose [128]. After intestinal tract absorption and transport to the liver, fructose and galactose are mainly transform to glucose [129]. As a result, the glucose transported in the blood represents 95% of the circulating monosaccharides. One mechanism contributing to the circulating glucose content is the elevated amount of glucose phosphatase in liver cells that release glucose in the blood stream hydrolyzing glucose-6-phosphate a product from the metabolism of fructose and galactose, also included in glucose metabolism [130]. Blood glucose concentrations are around 8.8 mM in non-fasted mice [131] and 5.9 mM after 4 hours

of starvation [132]. In humans, blood glucose is around 6.5 mM [133] under non-fasting conditions and around 5 mM after 3 to 8 hours of starvation [133, 134]. Several factors other than nutrient intake affect the blood glucose levels, including the time of day, gender and age [134].

The maintenance of glucose homeostasis is regulated by diverse processes: glycogenesis (formation of glycogen from glucose), glycogenolysis (breakdown of glycogen into glucose), glycolysis (conversion of glucose into pyruvate) and gluconeogenesis (glucose formation from non-carbohydrate substrates) [129]. Glycogen is particularly important for many of these processes. Indeed, this large glucose polymer is mainly stored in liver and skeletal muscle, constituting up to 8% of the liver cell weight [135].

Louis Pasteur first described glucose disruption via glycolysis in 1860 [136]. Glycolysis is the first step of glucose catabolism, breaking glucose into two pyruvic acid molecules [137]. Glycolysis produces energy in form of 2 molecules of ATP and without oxygen [138]. In the presence of oxygen, the catabolic process continues, and the pyruvic acids broken down into acetyl CoA that goes into the citric acid cycle into the mitochondrion. The citric acid cycle releases electrons from the breakdown of acetyl CoA to carbon dioxide [139]. These high-energy electrons are used by the electron transport system that will produce more energy in the form of ATP [137]. Overall, for every molecule of glucose under the presence of oxygen more than 30 ATP molecules can be produced [137, 140].

Glucose is transported via the cellular membrane by different glucose transporters, classified between sodium-glucose linked transporters (SGLTs) and facilitated diffusion glucose transporters (GLUT) [141, 142]. Immediately after entering the cell, glucose is phosphorylated by glucokinase in the liver and hexokinase in most of the other cells to initiate ATP production, facilitate enzyme binding and trap glucose in the cell by changing its charge [141]. Glucose blood concentrations are regulated by the pancreatic hormones glucagon and insulin [143, 144]

1.4.2. Insulin-regulated metabolism

Insulin is a 51 amino acid long anabolic hormone involved in the regulation of glucose [145]. Insulin is synthesized in the beta cells at the islets of Langerhans in the pancreas and cleared in the liver and kidney by the protease insulinase [146]. Its production is regulated by glucose but also affected by the concentration of amino acids, fatty acids, and keto acids in the plasma. As a result, insulin controls energy homeostasis [147].

Insulin is secreted into the blood, having a half-life of about 6 minutes [148]. Insulin interacts with two extracellular alpha subunits of the insulin receptors triggering the phosphorylation of two beta subunits. Intracellularly, tyrosine kinases are activated and phosphorylate several downstream signaling proteins including various insulin receptor substrates (IRS) [149]. The phosphorylation of IRS leads to binding of the lipid kinase PI3K that synthesizes the lipid PIP3 in the plasma membrane, recruiting the kinase PDK that phosphorylates the kinase AKT on Thr308 [150, 151]. AKT is activated by its phosphorylation and phosphorylates in turn several protein substrates at Ser/Thr amino acids [152]. Targets of AKT include the transcription factor family FOXO that regulates glucose production and utilization, the GTPase activator protein TSC2 increases lipid and protein synthesis, the kinase GSK3β induces glycogen synthesis and the Rab GTPase activates the protein TBC1D4 that facilitates glucose uptake [150, 153].

Insulin signaling triggers diverse responses in different organs. In the liver, insulin signaling induce glycogen storage and decrease glucose output [154]. In the skeletal muscle and fat, insulin trigger glucose transport by translocating the glucose transporter GLUT4 to the membrane from intracellular vesicles [129, 149]. In the brain, insulin signaling leads to increased neural activity and downstream decreased hepatic glucose production, food intake and lipoprotein synthesis [150, 155].

One of the most studied diseases due to little or no insulin production or insulin resistance is diabetes where carbohydrate, protein and fat metabolism are abnormal [156]. There are two types of diabetes: type 1 or insulin-dependent diabetes with a lack of insulin secretion and type 2 or non-insulin-dependent diabetes with decreased insulin sensitivity or insulin resistance [157].

1.5. The mTOR pathway

Rapamycin was discovered in a soil sample collected on the island of Rapa Nui in 1964 [158], showing to have immunosuppressive [159], antitumor [160] and antifungal [161] properties. 30 years later, the action mechanism of rapamycin showed the protein mechanistic (initially called mammalian) target of rapamycin (mTOR) [162, 163]. Since then, several studies uncovered the molecular structure, interactions and function of mTOR [164-167].mTOR is a serine/threonine protein kinase belonging to the PI3K-related kinase (PIKK) family [163]. mTOR plays a pleiotropic physiological role, overall controlling the balance between anabolism (production of macromolecules) and catabolism (breakdown of macromolecules) [168]. mTOR exists as the catalytic center in two different protein complexes (mTORC): mTORC1 and mTORC2. mTORC1 is formed by mTOR, Raptor, mLST8 (mammalian lethal with Sec13 protein 8), PRAS40 (proline rich Akt substrate 40 kDa) and DEPTOR (DEP domain containing mTOR interacting protein) [169-171]. Raptor is required for the cellular localization and substrate recruitment of mTORC1 [172]. mLST8 interacts with the catalytic domain of mTOR and is necessary to activate the kinase activity of mTOR [173]. PRAS40 interacts with Raptor and inhibits the kinase activity of mTOR [170, 171, 174-176]. DEPTOR inhibits directly mTOR activity during the inactive forms of mTORC1 [177{Peterson, 2009 #231]}. mTORC2 is formed by mTOR, Rictor, DEPTOR, mLST8 and the regulatory subunits mSin1 and Protor1/2 [178-182]. Rictor is a kinase necessary to phosphorylate the downstream mTORC2 target AKT and is inhibited by DEPTOR [183]. mSin1 is necessary for the assembly of mTORC2 and the phosphorylation of AKT [178]. Protor-1/2 interacts with Rictor and it is only known that Protor-1 functions as an enhancer or adaptor of mTORC2 phosphorylation of the kinase SGK1 (serum- and glucocorticoid-induced protein kinase 1) [180, 184]. Generally, mTORC1 is linked to the regulation of energy metabolism and cell growth, whereas mTORC2 regulates energy metabolism, cell cytoskeleton rearrangement, migration and apoptosis [185]. The main functions of mTOR can be generally grouped as follows (Figure 4):

1. Anabolism: mTOR increases the synthesis of proteins, lipids and nucleotides via mTORC1 [172]. A strong trigger of mTOR is the nutrients that enhances growth and energy storage in mammals [185]. Starvation in turn inhibits mTOR [185]. Overall, there are several ways to stimulate the anabolic property of mTOR, including growth factors such as insulin, the signaling protein Wnt and the inflammatory cytokine TNFα [186-188]. Inhibition of mTOR anabolism can be provoked by low ATP levels, hypoxia and tumor protein p53 regulation of DNA damage [189-191]. Involved in the overall anabolic effect of mTOR are the following processes:

a. mRNA translation: mTORC1 affects protein synthesis by phosphorylation of the p70 S6 kinase 1 (S6K1) [192] and the translation initiation factor 4EBP. mTOR/Raptor phosphorylate S6K1 in its hydrophobic motif (Thr389), allowing the kinase PDK1 to interact with the phosphorylated S6K1 and to phosphorylate the S6K1 activation loop (Thr229). Phosphorylated S6K1 in Thr389 and Thr229 increases protein translation by phosphorylation of the ribosomal protein S6 [192, 193]. mTORC1-dependent phosphorylation of 4EBP impedes the binding of 4EBP with the translation initiation factor eiF4E, allowing eiF4E to position the ribosome to begin mRNA translation [194, 195].

b. Lipid synthesis: mTORC1-dependent phosphorylation of S6K1 also activates the sterol response element binding protein (SREBP) transcription factors that regulate fatty acid and cholesterol formation [196]. Furthermore, mTORC1 is able to phosphorylate the phosphatase lipin1, preventing its nuclear entry and the subsequent downregulation of SREBPs [197, 198].

c. Nucleotide synthesis: following its activation by mTORC1, S6K1 further phosphorylates Ser1859 of carbamoyl-phosphate synthetase 2 aspartate transcarbamoylase dihydroorotase (CAD), increasing the *de novo* pyrimidine synthesis [199, 200]. mTORC1 also promotes the activation of the transcription factor ATF4, which enhances the expression of the dehydrogenase MTHFD2, increasing purine nucleotide production [201].

2. Catabolism: mTOR can inhibit autophagy, lysosome biogenesis and proteasome assembly via mTORC1. Additionally, mTORC1 and mTORC2 induce glycolysis [185]. Generally, food starvation and increased insulin levels in the blood stimulates the catabolic role of mTORC1 and mTORC2 [202]. The role of mTOR in catabolism includes:

a. Autophagy: mTORC1 phosphorylates the kinase ULK1, preventing ULK1 activation via AMPK and subsequent autophagosome formation [203]. mTORC1 also inhibits transcription factors through phosphorylation that are involved in the regulation of proteins involved in the autophagy signaling process, as for example the transcription factor TFEB [204].

b. Lysosome biogenesis: mTORC1 phosphorylates and inhibits the transcription factor TFEB which is also involved in lysosomal biogenesis [191], besides participating in the transcriptional regulation of autophagy-regulating proteins.

c. Proteasome assembly: On the one hand, inactivation of mTORC1 increases the proteasomal-dependent proteolysis via a general activation of the ubiquitin proteasome system [205] or via an increase of proteasomal chaperones inhibiting the kinase Erk5 [206]. On the other hand, hyperactivation of mTORC1 also enhances proteasomal activity by increasing the expression of proteasomal subunits [207]. A

potential reason behind the enhanced proteasomal activity shown via inhibition and activation of mTORC1 could be a different regulation under acute inhibition and prolonged activation of mTORC1 [168]. Acute mTORC1 inhibition promotes proteolysis to obtain free amino acids, whereas prolonged mTORC1 activation leads to a compensatory increase in protein turnover to balance the increasing protein synthesis [168, 205-207].

d. Glycolysis: mTORC1 enhances the expression of the transcription factor HIF1α, which regulates the transcription of several glycolytic genes, such as the phosphofructo kinase (*Pfkp*) leading to the stimulation of glycolysis [196]. mTORC2 phosphorylates AKT which induces the expression of the M2 isoform of pyruvate kinase (PKM2) that catalyzes the last reaction in the glycolytic pathway, promoting glycolysis [208].

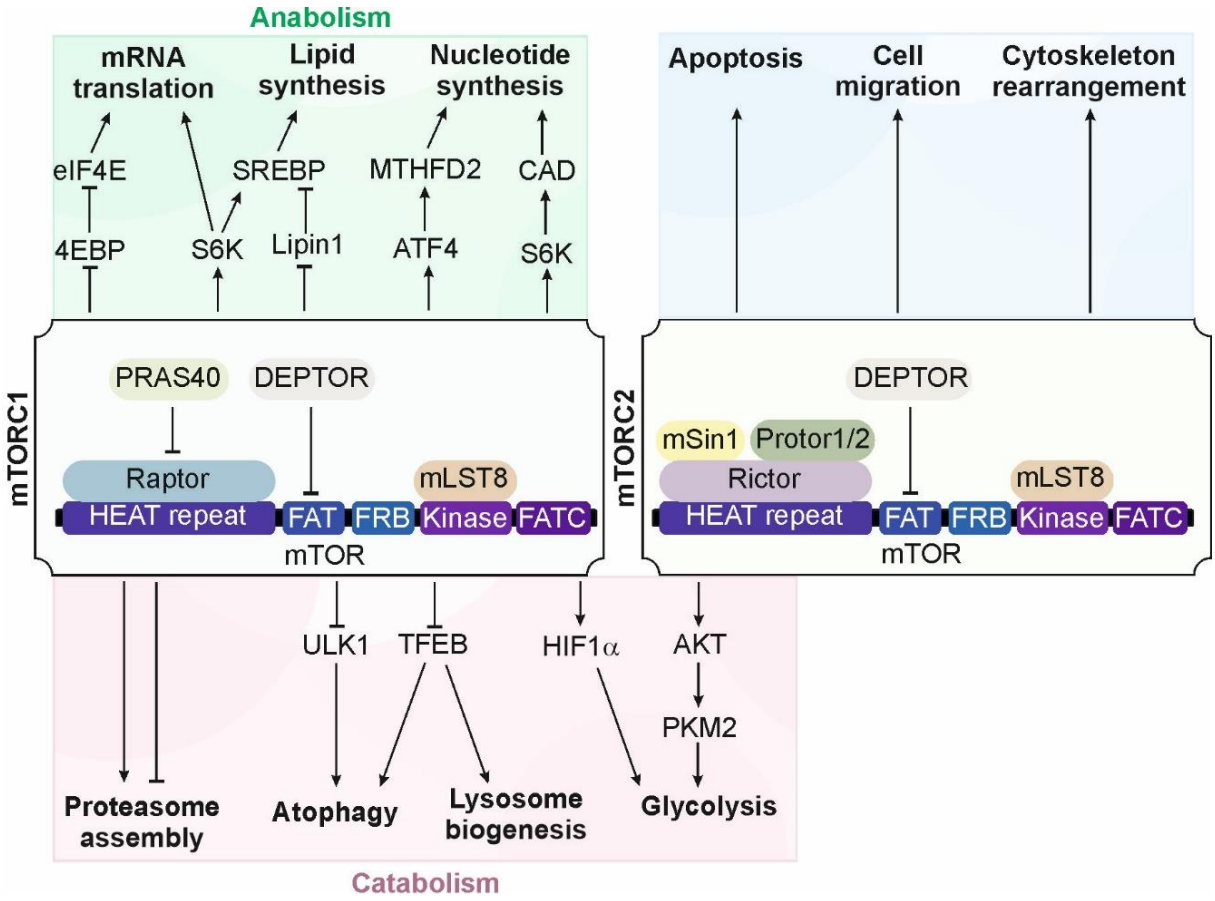

Figure 4: mTORC1 and mTORC2 signaling pathways. mTORC1 (mechanistic target of rapamycin complex 1) and mTORC2 (mechanistic target of rapamycin complex 2) subunits and the mTOR domains are shown in the middle of the figure. The anabolic functions of mTORC1 are highlighted with a green background, catabolic functions of mTORC1 and mTORC2 in a red background and other functions of mTORC2 are indicated with a blue background.

A relevant regulation of mTOR in the metabolism is also through the regulation of insulin signaling [168]. Constitutive deletion of the mTOR inhibitor TSC2 in β–cells led to a biphasic regulation of β–cell mass [209]. In young mice with *TSC2* Knock-out (KO) in β–cells, pancreatic cell mass was increased combined with an enhanced insulin secretion and hypoglycemia [209]. In older mice, β-cell number was decreased combined with hypoinsulinemia and hyperglycemia [209]. In obese rats, mTORC1 is hyperactivated by high fat diet, likely caused by increased amino acid availability and enhanced insulin production and secretion [210]. Hyperactivation of mTORC1 leads to increasing levels of activated S6K1/2, inhibiting the insulin/PI3K/Akt pathway and leading to insulin resistance [211]. Insulin resistance is also reached by direct inhibition of mTORC2, as for example shown with specific *Rictor* KO in liver, muscle or fat [212-215]. Overall, mTOR regulates insulin production as well as insulin regulates the mTOR signaling pathway.

The inhibitor of mTOR, rapamycin, cannot be used to treat diabetes type 2 because it exerts opposite effects on the insulin-mediated regulation of metabolism by mTORC1 and 2 [216, 217]. mTORC1 hyperactivation via genetic or triggered by nutrition leads to insulin resistance, which considered tamoxifen a potential treatment to improve glucose tolerance and treat type 2 diabetes [217, 218]. However, inactivation of mTORC1 by deletion of Raptor in adipocytes in mice shows lipodystrophy with insulin intolerance, hepatomegaly and liver steatosis and loss of mTORC2 activity in adipocytes decreases Akt activity and leads to insulin resistance [212-216]. A more detailed understanding of the specific regulation of mTORC1 and mTORC2 may help identifying possible treatments against type 2 diabetes [168].

Taken together of all the previous mentioned roles of mTOR, energy metabolism is a key target of the mTOR pathway. Other studies relate the mTOR pathway with pathological conditions particularly with cancer. Several proteins upstream of mTOR are mutated in cancer, such as the kinases TSC1/2 [219] or the phosphatase PTEN [220], resulting in increased mTOR signaling and cell survival and proliferation [185]. Furthermore, mTOR inhibits the upstream pathway of the transcription factor NF-κB, which is the major transcriptional regulator of the cellular inflammatory response [221]. Phosphorylated AKT has been shown to activate IKKβ that inhibits the inhibitor NF-κB, IκBα, increasing NF-κB activity [222, 223].

1.5.1. mTOR pathway and cardiac abnormalities

mTOR has been shown to induce striated muscle hypertrophy [224]. mTOR conditional deletion in skeletal muscle mice (Cre-mediated recombination in postmitotic myofibers) led to reduced body weight and muscle atrophy with premature death between 22 and 38 weeks of age [225]. Further studies with *Raptor* (part of mTORC1) and *Rictor* (part of mTORC2) skeletal muscle KO mice showed that mTORC1 plays a role in muscle hypertrophy and mTORC2 shows a similar muscle than wild-type mice [226]. Inhibition of mTORC1 by deletion of *Raptor* increased autophagy, which in turn was the main regulator of the observed muscle hypertrophy [227].

In the cardiac muscle, mTOR has been linked to cardiomyocyte growth and homeostasis during both the embryonic and adult stage [228]. Heart specific *mTOR* KO embryos display decreased cardiomyocyte proliferation, increased apoptosis, a switch from fatty acids as main energy source to glucose oxidation and mitochondrial activity, dilation of the heart and impaired cardiac function [229-231]. Inducible heart specific *Raptor* KO mice display cardiac dilation and dysfunction due to increased cardiomyocyte apoptosis, mitochondrial activity and autophagy leading to mouse death after inducing the KO [230]. Stimulation of mTORC1 *in vivo* can be achieved by high levels of IGF-1, angiotensin-II and β-adrenergic stimulation, ultimately leading to cardiac hypertrophy [232-234]. Furthermore, mTORC1 activity is increased in physiological cardiac hypertrophy due to exercise and in pathological hypertrophy by transverse aortic constriction (TAC) and hypertension [235]. mTORC2 specific cardiac function has only been study under stress condition so far and little is known about its physiological function. Cardiac *Rictor* KO in adult mice shows cardiac dilation, systolic dysfunction and wall thinning after induction of hypertrophy via TAC [236, 237].

1.6. The HIF pathway

Hypoxia occurs, when the available oxygen levels for cells in organism drop below their energy demand [238]. Physiologically, hypoxia occurs for example during development, high altitude exposure or exercise [239, 240]. Hypoxia also occurs in various pathological conditions, such as muscle hypertrophy, HF, cancer, ischemia, stroke or in chronic inflammation [240-248].

To maintain metabolic homeostasis, diverse mechanisms are involved in the production of energy under hypoxia. During normoxia, ATP production occurs mainly through oxidative phosphorylation in the mitochondria. In hypoxia, glycolysis becomes the main source of

cellular energy [249]. Shortly after birth, changes in the energy metabolism of organs occur due to an increase in oxygen availability compared to the situation *in utero* [250]. For example in the heart, mitochondrial biogenesis increases and mitochondrial fusion decreases after birth combined with an increased ATP production [251]. Interestingly, mild hypoxia (10% oxygen) leads to cardiac hypertrophy in cardiomyocytes, inducing a switch to increased glycolysis [252, 253].

Most organisms requires oxygen homeostasis to survive, hence, an oxygen sensing mechanism is required [254]. The best characterized cellular oxygen sensors are the prolyl-4-hydroxylase domain 1-3 (PHD1-3) proteins and the asparagine hydroxylase factor inhibiting HIF (FIH), which use molecular oxygen (O_2) together with 2-oxoglutarate (2-OG) as substrates and iron as well as a reducing agent as co-factors to regulate the HIF transcription factor by hydroxylation [255, 256]. HIF constitutes of heterodimers between one of the oxygen-sensitive HIF-α subunits (HIF-1α, HIF-2α, HIF-3α) and HIF-β [257]. All of those subunits belong to the basic helix-loop-helix PER-ARNT-SIM (bHLH-PAS) family encoded by different genes [258, 259]. Under normal oxygen levels, prolyl hydroxylated HIF-α is recognized by the von Hippel-Lindau (VHL) protein that facilitates the ubiquitination and proteasomal degradation of HIFα [260]. Under hypoxic conditions, HIF-α hydroxylation is decreased, stabilizing the protein and allowing its translocating to the nucleus of the cell where it forms an active transcription complex with HIFβ and the acetyltransferases p300/CBP (CREB-binding protein) as co-activators leading to the enhanced transcription of many genes, including Epo [238]. The ability of cells to sense and adapt to oxygen level is highly relevant leading to the attribution of the 2019 Nobel Prize in Physiology or Medicine [261].

HIFα has been linked to the development and diverse organ malformations. HIF-1α is ubiquitously expressed [262] and plays a vital role *in vivo.* KO of this gene in mice leads to embryonic lethality around E10.5 [263]. *HIF1A* (HIF-1α) KO mouse embryos display vascular regression and malformations in the cephalic region with mesenchymal cell death [263, 264]. Whole-body HIF-2α deletion in mice leads to multi-organ defects including hepatic steatosis, skeletal myopathy and heart hypertrophy together with hypoglycemia, lactic acidosis and deficiency in red blood cells [265-267]. HIF-3α is only present in mammals [268], mainly expressed during late embryonic development and the early postnatal phase [269]. The relevant splice variant of HIF-3α, NEPAS under deletion in mice is associated with a disarrangement of cardiac striated muscle fibers, an enlarged right ventricle and pulmonary hyperplasia [269].

1.6.1. The cellular oxygen sensor FIH

FIH is ubiquitously expressed with highest expression levels in the skeletal muscle and salivary glands [270]. FIH catalyzes the hydroxylation of an asparagine in the C-terminal transactivation domain (CAD) of HIFα, impeding p300/CBP coactivator recruitment [271, 272]. FIH is formed by two sheets of nine β-strands and five β-strands respectively. Eight of those strands constitute the central core dispersed through the structure [273]. FIH functions as homodimer, which is formed by helix-helix interactions located at the C-terminal end of each monomer [273].

Little is known about the regulation of FIH protein levels, *Hif1an* (the gene name of FIH) is not regulated transcriptionally by HIF [274]. At a transcriptional level there are only a few studies showing a transcriptional regulation of FIH. Active kinase PKC ζ in renal carcinoma cells is able to increase the binding between cut-like homeodomain protein (CDP/Cut) and the *HIF1AN* promoter region, inhibiting *HIF1AN* transcription [275]. Also, miR-455 targets *HIF1AN* increasing kinase AMPKα activity and inducing browning of white adipose tissue and mitochondrial production in mice [276]. Ubiquitination of FIH can occur via the E3 ubiquitin ligase Siah-1 in normoxia, targeting FIH for proteasomal degradation [277]. This suggests that Siah-1-dependent regulation of FIH might play a role in the adaptation to hypoxia [277]. FIH is SUMOylated by SUMO2/3 particularly in hypoxia, but also in normoxia, followed by proteasomal degradation [278]. This process can be reversed by the SUMO specific peptidase 3 (SENP3) [278].

Whole-body *Hif1an* KO mice display an energy metabolic phenotype levels [279]. The animals present with a decreased body weight, an increased metabolic rate (increased O_2 consumption and CO_2 production), enhanced glucose and lipid homeostasis and pulmonary hyperventilation levels [279]. Under high fat diet, *Hif1an* KO mice are resistance to body weight gain and liver steatosis levels [279]. These metabolic differences seemed to be regulated at least in part by the brain levels [279]. Neuron-specific FIH deletion also led to a decreased body weight, enhanced metabolic rate, insulin sensitivity and protected against high fat diet-induced body weight gain levels [279]. *Hif1an* KO mouse embryonic fibroblasts (MEFs) showed a suppressed AMPK activation and increased ATP levels [279]. More in-depth analysis demonstrated that FIH regulates a switch between oxidative phosphorylation in the mitochondria and glycolysis in the cytoplasm [270]. *Hif1an* KO cells increased mitochondrial activity in normoxia, glycolytic reserve and oxygen consumption [270]. Genome-wide association studies (GWAS) linked *HIF1AN* to the regulation of body mass index (BMI) and

plasma phospholipid fatty acid concentration [280, 281]. *Hif1an* was also associated with BMI, food conversion and muscle fat content in pigs [282, 283]. The connection between FIH and the metabolic phenotype shown under its deletion, suggest that might be another potential HIF-independent target of FIH leading to the metabolic changes.

FIH has been shown to hydroxylate non-HIF dependent proteins, particularly ankyrin-repeat domain (ARD)-containing proteins[284], including the NF-κB signaling pathway proteins IκBα and p105 [285, 286]. Other FIH substrates such as ASB4 are connected with the ubiquitination and degradation of substrate proteins [285, 287]. Therefore, several proteins outside the HIF pathway have been shown to be FIH substrates, but no known target was linked to the observed metabolic phenotype in *Hif1an* KO mice [285, 288]. Our group recently identify the deubiquitinase OTUB1 as a *bona fide* FIH substrate that is hydroxylated on Asn 22 [289, 290]. Loss of Asn22 hydroxylation increased the interaction of OTUB1 with different metabolic enzymes affecting OTUB1 substrate targeting and the cellular bioenergetic status [290]. Hence, OTUB1 is a target of FIH that might explain the HIF-independent metabolic changes in *Hif1an* KO mice [279, 290].

1.7. Protein ubiquitination

Ubiquitination is a dynamic and widespread cellular post-translational protein modification that was first discovered in 1977 [291-293], gaining the recognition of the 2004 Nobel Prize in Chemistry [294]. Currently, it is known that among the 25,000 genes [295] about 5% are participants of the vast ubiquitin system [296].

Ubiquitination (Figure 5) occurs through an interplay of three different types of enzymes leading to the covalent attachment of the protein ubiquitin (consisting of 76 amino acids) to a substrate requiring the use of ATP in eukaryotes [297]. The contributing enzymes are classified as E1 ubiquitin-activating enzyme, E2 ubiquitin-conjugating enzyme and E3 ubiquitin ligase [297]. E1 activates the C-terminus of ubiquitin attaching it to the sulphur of a cysteine residue in E1 [297]. The ubiquitin is then transferred to an E2. E3 ligases can be differentiated into two different types in humans: HECT (Homologous to the E6-AP Carboxyl Terminus) and RING (Really Interesting New Gene) [298]. HECT E3 enzymes transfer ubiquitin to themselves first and afterwards to the substrate. RING E3 ligases directly transfer ubiquitin from E2 enzymes to the substrate [298].

Ubiquitin is connected to a substrate protein via a covalent amide linkage formed between its the C-terminal Gly76 and an amino group on the side chain of a lysine residue of the substrate [299]. The attachment of the first ubiquitination is referred to as monoubiquitination if no further ubiquitin proteins are attached. Further ubiquitin attachment to the first connected ubiquitin leads to polyubiquitination. The following ubiquitin can bind to 7 different Lys (at positions 7, 11, 27, 29, 33, 48, 63) or the N-terminal Met of ubiquitin [297, 300]. The different protein fate is determined depending on the ubiquitination amino acid residues and the type of ubiquitin chain. Between the different types of polyubiquitin, Lys63- and Lys48-linked ubiquitin chains are the most common ones. Lys63-linked ubiquitin chains plays a role in endocytosis, transport, DNA repair and ribosome function. Whereas Lys48-linked ubiquitin chains regulate proteolysis. Ubiquitin branches (ubiquitin chains attached within a linked ubiquitin chain to the protein substrate) can happen by diverse amino acid linkages increasing the complexity of the system [301-304].

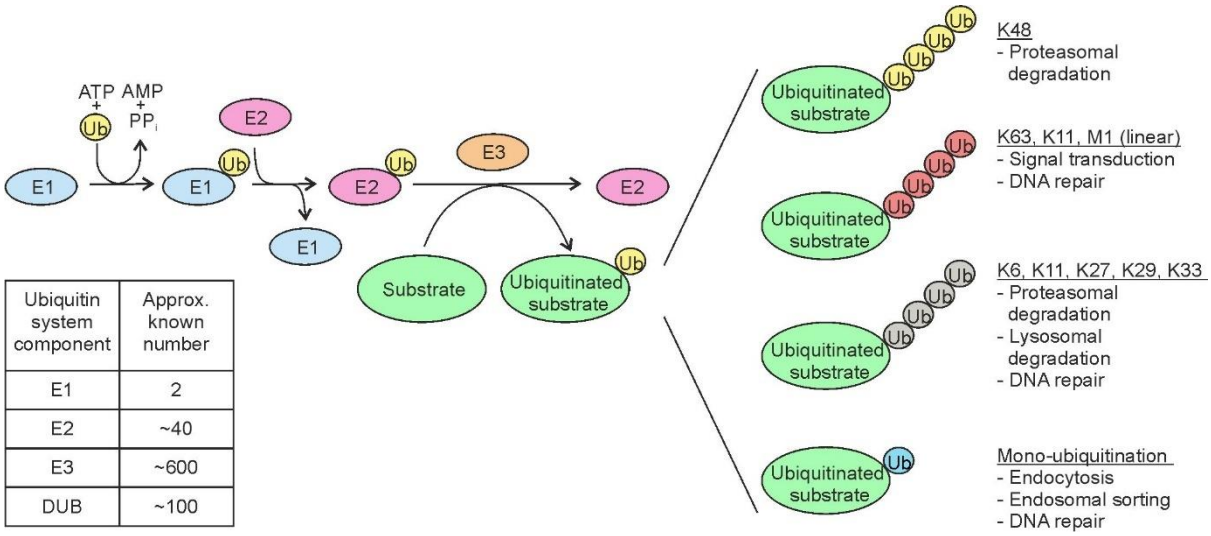

Figure 5: Protein ubiquitination. Two E1 ubiquitin--activating enzymes transfer a protein ubiquitin (Ub) to one out of 40 different E2 ubiquitin-conjugating enzymes. Subsequently, ubiquitin is covalently attached to a protein substrate with the help of an E3 ligase enzyme. If this process occurs once, it leads to monoubiquitination. Several consecutive ubiquitinations can lead to polyubiquitin chains with isopeptide bonds between lysine residues of Ub's. Monoubiquitination and the diverse types of polyubiquitination have different functions. PPi: inorganic diphosphate. Image modified from [297].

Substrate ubiquitination is highly regulated. Phosphorylation is one of the most studied post-translational regulations of ubiquitination [305, 306]. For example, glycogen synthase kinase 3 phosphorylates the transcription factor MYC, facilitating its ubiquitination and proteasomal degradation [307, 308]. Another example is the phosphorylation of the androgen receptor by AKT followed by androgen receptor ubiquitination by the E3 ligase Mdm2 [309]. Phosphorylation can also directly regulate enzymes of the ubiquitin pathway. For example,

the serine/threonine kinase JNK1 phosphorylates the HECT E3 ligase Itch, enhancing its ligase activity [310]. Another case of post-translational modification of the ubiquitination is acetylation, consisting in the addition of an acetyl group to an ubiquitin protein. Acetylation of Lys6 and Lys48 has been shown to block ubiquitin chain formation via those amino acid residues [311].

Ubiquitination plays a significant role in diverse pathologies, such as in muscle-wasting disorders, where there is a loss of skeletal muscle mass caused by cancer, aging and metabolic abnormalities like diabetes [312]. In detail, E3 ligases Atrogin-1 and MuRF1 leads to the degradation of diverse proteins in the myofibrils leading to the disassembly of the muscle filament and breakdown the muscle [313, 314]. Also, the muscle specific E3 ligase MG53 is overexpressed under insulin resistance [315]. MG53 ubiquitinates the insulin receptor and IRS1, leading to its proteasomal degradation [315]. Other significant pathologies associated with abnormal ubiquitination are cardiac diseases. An example of cardiac pathologies is the E3 ligase TRIM63, where mutations are identified in patients with hypertrophy cardiomyopathy [316].

1.7.1. Protein deubiquitination

The ubiquitination process can be reversed by deubiquitinases (DUBs) that cleave ubiquitin from the substrate. There are about 100 DUBs known in humans [317]. DUBs do not only remove ubiquitin chains, but also regulate the available pool of ubiquitin proteins for the ubiquitin pathway [318]. Besides, the modification of the ubiquitin chains can occur via the removal of ubiquitins in a chain modifying the architecture and length [318]. DUBs are classified into six protein families according to their structure and sequence similarity [319]:

(1) Ubiquitin C-terminal hydrolases (UCHs). UCHs are cysteine proteases [297, 301]. The UCH protein family consists of four members: UCHL1 (isozyme L1), UCHL3 (isozyme L3), UCHL5 (isozyme L5) and BAP1 (breast cancer type 1 susceptibility protein associated protein 1) [319]. UCHL1 and UCHL3 include only a catalytic domain. UCHL5 contains also additional 100 amino acids that determine its binding to the proteasome at the subunit Rpn13 of the 19S regulatory particle of the 26S proteasome lid [320-322]. The last and larger component of this family is BAP1 with more than 500 amino acids in a C-terminal prolongation in addition to the catalytic domain [323, 324]. Members of the UCH family hydrolyze ubiquitin chains specifically from the C-terminal end [323, 324]. UCHs play a role in protein stability. *In vivo,* UCHs are important for the maintenance of brain function

[325] and mutations in BAP1 constitute what is called BAP1-related tumor predisposition syndrome which includes lung, ovarian, pancreatic and breast cancer among others [326-328].

(2) Ubiquitin-specific proteases (USPs). USPs are cysteine proteases that encompass the largest DUB family. Most of the USPs contain a catalytic triad consisting of Asp, His and Cys. Asp stabilizes His which deprotonates Cys in the presence of a ubiquitin chain, resulting in a nucleophilic attack on the isopeptide ubiquitin-substrate bond. USPs affect a variety of different processes, including proteasomal degradation, histone modification and cell signaling [329, 330].

(3) Ovarian tumor proteases (OTU). The OTU family comprises four sub-families of cysteine proteases [297, 301]: Otubains (OTUB1 and OTUB2), A20-like OTUs (A20, VCIP135, Cezanne), OTUD (OTUD1-6, ALG13 and HIN1L) and OTULIN (OTULIN, FAM105A) [297, 301]. Within the subfamilies the catalytic domain dimensions differ. The smallest catalytic domain size is reported to be around 150 amino acids in OTUD enzymes. The largest catalytic domain contains around 350 amino acids in A20-like OTUs [331]. OTUs are involved in the regulation of NF-κB signaling, protein degradation, DNA damage repair or angiogenesis [332-334].

(4) Josephins or MJDs. Josephins are cysteine proteases and four different members have so far been identified in humans [297, 301]. The DUB Ataxin-3 is the best characterized member [335]. A characteristic feature of the Josephins is that the catalytic triad shows allosteric impediment when ubiquitin is not present [336]. Josephins are linked to proteasomal degradation or autophagy among others [337]. Josephins are important in neural function, as for example Ataxin-1 modulates transcription important for the dopaminergic pathway [338-340].

(5) JAB1/MNP/MOV34 metalloenzymes (JAMMs). JAMMs are zinc metalloproteases [297, 301], using two zinc molecules in their active sites as well as one water molecule in order to cleave the amide bonds in ubiquitin chains [341-344]. The most studied JAMM deubiquitinase is the proteasome regulatory particle lid subunit RPN11 that is essential for cell viability [345]. JAMMs play a role in DNA repair and proteasomal degradation [346, 347].

(6) Monocyte chemotactic protein-induced protein (MCPIP): MCPIPs were first identified in 2010 through the discovery of MCPIP1 [348]. Bioinformatic analyses indicate that the family is constituted of seven members [319]. This family has only been analyzed in detail regarding MCPIP1 which carries Cys and Asp in the active center of its catalytic domain. MCPIP1 regulates the macrophage inflammatory response by deubiquitinating the TNF receptor associated factors TRAF2, TRAF3 and TRAF6, resulting in negative regulation of JNK and NK-κB activity [348].

The deubiquitination of proteins is additionally regulated in a complex manner by post-translational modifications of DUBs, including phosphorylation, hydroxylation or SUMOylation [349]. These post-translational modifications affect DUB stability, activity, location and/or interactions [350].

1.7.2. Deubiquitinases *in vivo*

DUBs have mainly been studied *in vivo* regarding their role in cancer, but in the last years analyses started to focus on other fields, such as cardiac and metabolic diseases [351]. Hypertrophic and failing mouse hearts show increased UCHL1 level [352]. Cardiac UCHL1 knockdown decreased cardiac hypertrophy induced by pressure overload [352]. Treatment with the UCHL1 inhibitor LDN-57444 ameliorated cardiac hypertrophy [352]. UCHL1 stabilized epidermal growth factor receptor (EGFR), which is a positive regulator of cardiac enlargement by activating diverse downstream pathways including the PI3K/AKT pathway [352]. At the same time, the 19S proteasome-associated DUB inhibitor Auranofin ameliorates cardiac hypertrophy, resulting in the aggregation of IκBα and NF-κB inactivation [353]. *Usp20* KO mice present with an impaired β1 adrenergic receptor-induced cardiac contractility and relaxation, but normal systolic function [354]. It is not well established whether there is a specific involvement of certain ubiquitin chains in the regulation of cardiac homeostasis. However, Lys63-linked ubiquitin chains are a potential target since they are highly linked to cardiac hypertrophy, mainly through their importance for the regulation of the NF-κB pathway [355]. As an example, DUB cylindromatosis (CYLD) cleaves Lys63-linked ubiquitin chains from adaptor protein receptor-interacting protein 1 (RIP1) blocking NF-κB signaling [356].

Several different DUBs were shown to regulate energy metabolism. CYLD suppresses non-alcoholic steatohepatitis (NASH) in monkeys and mice [357]. The E3 ligase TRIM47 degrades CYLD upon interaction correlating with the increased NASH severity. In mice, an increase of hepatic CYLD levels reverses the progression of NASH in mice and of metabolic syndrome in monkeys [357]. In mice, hepatocyte *Cyld* overexpression inhibits insulin resistance, inflammation, fibrosis and lipid accumulation. On a molecular level, CYLD interacts and removes Lys63 of the TAK1 kinase, blocking downstream JNK-p38 cascades [357].

DUBs are also important for the regulation of inflammation. USP13 stabilizes the anti-inflammatory single immunoglobin interleukin-1-related receptor IL-1R/Sigirr leading to suppression of pulmonary inflammation in mice [358]. *Usp13* KO mice are sensitive to lipopolysaccharide or *Pseudomonas aeruginosa* induction of inflammatory lung injury [358].

Otud4 KO mice display enhanced macrophage inflammatory signaling upon Toll-like receptor (TLR) stimulation. Mechanistically, OTUD4 is necessary for the Lys63 deubiquitination of MyD88, an important signaling protein associated to TLR. As a result, OTUD4 inhibits the activation of NF-κB [359]. Interestingly, phosphorylated OTUD4 targets Lys63-linked ubiquitin chains, whereas unmodified OTUD4 hydrolyses Lys48-linked ubiquitin chains [359].

1.8. OTUB1

In 2002, the DUB OTUB1 (ovarian tumor domain-containing ubiquitin aldehyde binding protein 1) was discovered under the name HSPC263 as the first member of the OTU domain family [360]. *Otub1* is located on chromosome 11q13.1 in *Homo sapiens* and on chromosome 19A in *Mus musculus* [361]. OTUB1 gained increasing interest by the research community over the last years due to its unique regulation of ubiquitin chains, its high ubiquitous expression and the modulation of a plethora of cellular processes [362-364]. *In vivo*, homozygous *Otub1* KO mice are perinatally lethal, but no further analysis demonstrate the reason behind the lethality or the detailed phenotype [365, 366]. Furthermore, cell type specific *Otub1* deletion in mice has been further characterized showing anti-inflammatory and pro-inflammatory function [367, 368]. However, the physiological role of OTUB1 remains elusive.

1.8.1. Structure, function and regulation of OTUB1

The active site of OTUB1 is formed by the amino acid triad Asp88, Cys91 and His265 [369]. The active site with the catalytic Cys91 in its center is located at the interface of a β-sheet lobe (β1–β5) and an α-helical lobe (α3-α10) [370]. Isopeptide linkages of K48-linked polyubiquitin chains are hydrolyzed by nucleophilic attack through the Cys91, which is enabled by the proximity of the His265 to Cys91, lowering the Cys91 pKa [371]. OTUB1 contains a conserved OTU domain between residues 85 and 271 [372], that changes the conformation upon binding of free ubiquitin triggering the formation of an ubiquitin binding helix [373]. OTUB1 has a close family homologue, OTUB2. But both proteins differ in their structure and catalytic activity. The OTUB2 catalytic triad is formed by Asn226, Cys91 and His224 displaying a more permissive ubiquitin recognition in its canonical active site than OTUB1 [374, 375]. This is due to the lack of the N-terminal α-helix of OTUB1, which restricts ubiquitin binding in a certain orientation [374, 375]. Besides, OTUB1 presents a unique structure among the cysteine proteases in which the catalytic center is in a non-productive conformation [370]. OTUB2 shows a faster cleavage (Lys48 and Lys63 ubiquitin chains) kinetic compared to OTUB1 due to the hydrogen-

bonding distance between His224 and the Cys91 that facilitates the binding of the substrate [372].

OTUB1 is one of the most highly expressed of all known DUBs [376]. Uniquely, OTUB1 has both catalytic and non-catalytic functions. Beside the catalytic cleavage of Lys48-linked ubiquitin chains, OTUB1 inhibits non-catalytically E2 conjugating enzymes, impeding Lys48-linked and Lys63-linked ubiquitin chain formation [332, 370].

The catalytic activity of OTUB1 targets diverse proteins (Table 1). The canonical function was mainly studied in of the context of cancer progression and metastasis and OTUB1 was shown to stabilize the transcription factors FOXM1 and Snail [377-381]. Inflammation and the cellular response to viral infection are also regulated by OTUB1 by activation of the NF-κB signaling pathway through deubiquitination of cIAP1, UBC13 and/or RIG-I [368, 382, 383]. Also, RhoA is deubiquitinated by OTUB1 rearranging the cytoskeleton and increasing the susceptibility to *Yersinia* infection [384]. In ischemia reperfusion injury, OTUB1 is nephroprotective deubiquitinating Lys48-linked YB-1 and increasing the levels of the anticoagulant nephroprotective aPC [366]. Furthermore, OTUB1 might aggravate neural diseases by deubiquitinating Tau and enhancing the formation of pathological Tau (AT8-positive Tau and oligomeric Tau forms) under an unkown mechanism [385]. Estrogen receptor alpha (ERα) is stabilized at a protein level by OTUB1 through removal of K48-linked ubiquitin chains [386].

Target protein	Regulated Ub chain type	Regulated signalling pathway	Outcome	Ref
FOXM1	Lys48	Avoid proteasomal degr.	Ovarian cancer tumor progression	[377]
	Lys48	Avoid proteasomal degr.	Breast cancer tumor progression	[379]
	Lys48	ECT2-Rho signaling Avoid proteasomal degr.	Renal cell carcinoma progression	[380]
	Lys48	Avoid proteasomal degr.	Hepatic cell carcinoma proliferation	[378]
Snail	Lys48	EMT	Promotion of esophageal squamous cell carcinoma metastasis	[381]
cIAP1	Lys48	Avoid proteasomal degr. NF-κB and MAPK signaling pathways	TNF-dependent cell death Zebrafish vasculature disruption	[382]
UBC13	Lys48	NF-κB signaling	Increased dendritic cells response under infection and inflammation	[368]
RIG-I	Lys48	NF-κB signaling IRF activation	Enhanced response during influenza A virus infection	[383]
RhoA	n.d.	Cytoskeletal rearrangement	Increased susceptibility to *Yersinia* infection	[384]
YB-1	Lys48	n.d.	Nephroprotection following IRI	[366]
Tau	Lys48	n.d.	Formation of pathological Tau forms	[387]
ER-α	n.d.	Estrogen-dependent signaling	Decreased activity of placental alkaline phosphatase*	[386]

Table 1. Target proteins regulated by OTUB1 enzymatic activity. The color code used in the table indicates the regulation of diverse processes or diseases: grey, cancer; blue-gray, immune response; blue, viral and bacterial infection; orange, other diseases; yellow, others. EMT: epithelial-mesenchymal transition. IRI: ischemia reperfusion injury. n.d.: not determined. degr.: degradation.Ub: ubiquitin.* The study only showed the effect of the loss of OTUB1 increasing the activity of placental alkaline phosphatase, no overexpression or recovery experiments were performed.

The non-catalytic activity of OTUB1 has been mainly connected to the regulation of the immune response (Table 2), targeting Nur77, p100, SOCS1 or AKT [367, 388-390]. OTUB1 can bind to several different E2 enzymes, including UBCH5, UBE2E and UBC13 [365]. Furthermore, OTUB1 stabilizes UBE2E1 (UBCH6) by suppressing its autoubiquitination [365]. Interestingly, free ubiquitin and charged ubiquitin E2 enzymes increase the affinity of OTUB1 to E2 [332, 391, 392]. Free ubiquitin binds allosterically to the distal site of OTUB1 and induces the N-terminal ubiquitin-binding helix [332, 391, 392]. The donor ubiquitin of E2 enzymes interacts with the N-terminal ubiquitin-binding helix and provokes the inhibition of E2 enzymes [332, 391, 392]. Besides, OTUB1 prevents the interaction of E2 with E3 enzymes [393, 394]. Interestingly, OTUB1 is monoubiquitinated by UBCH5, increasing the catalytic function of OTUB1 [393, 394]. Moreover, OTUB1 Lys48 cleavage activity is inhibited by the interaction with UBCH5B [391]. Due to the high sequence similarity between E2 enzymes, the inhibition of E2s by OTUB1 may occur via the same mechanism as demonstrated for UBCH5B [332]. Potentially any of the E2 enzymes with which OTUB1 has been shown to interact, as UBE2N, UBE2D, UBE2E [362]. Furthermore, OTUB1 interactome analysis shows an interaction with around 10 E2 enzymes [290]. Overall, a complex interplay between E2 enzymes and OTUB1 occurs, regulating both the activity of E2's and of OTUB1.

Target protein	Regulated E2 enzyme	Regulated Ub chain type	Regulated signaling pathway	Outcome	Ref
RAS	n.d.	n.d.	ERK signaling	Enhanced lung cancer progression	[395]
Nur77	n.d.	Lys48	TNFα signaling	Inhibition of inflammation	[388]
p100	n.d.	Lys48	NF-κB signaling	Prevention of autoimmunity	[389]
SOCS1	n.d.	Lys48	JAK2/STAT1 signaling	Inhibition of CNS autoimmunity	[367]
AKT	n.d.	Lys63	AKT/IL-15R signaling	Homeostasis of CD8+ T and NK cells	[390]
RIG-I	UBCH5	Lys63	NF-κB signaling IRF activation	Enhanced response during IA virus infection	[383]
MDMX	UBCH5	n.d.	p53 signaling	Promotion of mitochondria-mediated apoptosis	[394, 396, 397]
p53	UBCH5	Lys48	p53 signaling	Increased DNA repair	[397]
pSMAD2/3	n.d.	n.d.	TGF-β signaling	Increased cellular migration	[362]
DEPTOR	n.d.	n.d.	mTOR signaling	Decreased cell proliferation, size and autophagy	[398]
RNF168	UBC13	Lys63	ATM signaling	Inhibition of DSB-induced chromatin ubiquitination	[332]
SLC7A11	n.d.	n.d.	Ferroptosis	Increased tumor growth	[399]

Table 2. Target proteins regulated by OTUB1 non-canonical activity. The color code used in the table indicates the regulation of diverse processes or diseases: grey, cancer; blue-gray, immune response; blue, viral and bacterial infection; orange, other diseases; yellow, others. CNS: central nervous system. DSB: double strand brand. IA: influenza A.

Apart from the canonical and non-canonical targets of OTUB1, there are other proteins for which the type of regulation by OTUB1 is unclear (Table 3). Although it was previously reported that OTUB1 cleaves, presumably, Lys48-linked polyubiquitin chains from RhoA reducing the proteasomal degradation of RhoA [384]. Also, OTUB1 stabilizes RhoA via p53 expression increasing prostate cancer invasion [400]. Therefore, additional studies are required to identify OTUB1 regulation of RhoA. Furthermore, OTUB1 suppresses TRIM25 ubiquitination increasing binding of ZAP (Zinc finger antiviral protein) to target mRNA, important process for antiviral activity [401]. Also, the interaction between PTEN (phosphatase and tensin homolog), RPA1 (replication protein A) and OTUB1 enables OTUB1 to deubiquitinate and stabilize RPA1, a protein that protects stalled replication forks and genomic stability [402]. In glomerulonephritis and pulmonary fibrosis, OTUB1 enhanced the pathological response via Decorin or FOXM1, respectively [401, 403].

Target protein	Regulated Ub chain type	Regulated signaling pathway	Outcome	Ref
RhoA	n.d.	Androgen-induced repression of p53 expression	Promotes prostate cancer invasion	[400]
p38MAPK	n.d.	n.d.	Inhibition of dendritic cell immune function Enhanced of phagocytic capacity of dendritic cells	[404]
TRAF6	n.d.	Type I IFNs	Inhibit virus-triggered type I IFN induction	[405]
TRAF3	n.d.	Type I IFNs	Inhibit virus-triggered type I IFN induction	[405, 406]
TRAF3	Lys63	Type I IFNs	Balance antiviral innate immunity	[407]
ZAP	Lys63	n.d.	Increased antiviral activity	[408]
Decorin	n.d.	Proteasomal degr.	Promotes glomerulonephritides	[401]
FOXM1	n.d.	Avoid proteasomal degr. Increased TBFβ by SMAD3/4	Promotes pulmonary fibrosis	[403]
RPA1	n.d.	n.d.	Protects stalled replication forks and genomic stability	[402]

Table 3. Putative targets regulated by unkown OTUB1 activity. The color code used in the table indicates the regulation of diverse processes or diseases: grey, cancer; blue-gray,

immune response; blue, viral and bacterial infection; orange, other diseases; yellow, others. degr.: degradation.

Post-translational modifications of ubiquitin or OTUB1 can affect the deubiquitinating activity of OTUB1. A post-translational modification that regulates OTUB1 is phosphorylation. Phosphorylation at Ser16 by casein kinase 2 increases OTUB1 nuclear localization [409]. As a result, OTUB1 is unable to inhibit chromatin ubiquitination in response to DNA damage in U2OS cells [409]. Also, phosphorylation of Ser65 activates OTUB1 Lys48 catalytic activity [410]. On the other hand, phosphorylation of Ser20 and Ser57 deactivates OTUB1 Lys48 cleavage [410]. Our group previously showed that hydroxylation of OTUB1 Asn22 by FIH altered OTUB1 substrate targeting, particularly for proteins linked to the regulation of cellular energy metabolism [290]. OTUB1 can also be ubiquitinated by the E3 ligase E4B, leading to OTUB1 proteasomal degradation [411].

The mTOR pathway has also been shown to regulate OTUB1 in breast cancer cells and T cells [412-414]. ERK1/2 increases OTUB1 protein levels in breast cancer cells [414]. In lymphocytes, OTUB1 regulates the expression of gene related to anergy (GRAIL). Following the activation of CD4 T cells, Otub1 protein levels are increased, leading to the degradation of GRAIL enhancing cell proliferation [413]. Acute infection of CD4 T cells inhibits the mTOR pathway, which in turn decreases the expression of *Otub1* maintaining GRAIL protein levels [415]. In T cells, upregulation of OTUB1 might be involved in delayed activation and proliferation of CD4+ and CD8+ cells compared to CD3+ T cells [416]. Furthermore, in T cells, inhibition of AKT and mTOR lead to a decreased OTUB1 expression [412, 413]. However, the underlying molecular mechanisms are unknown. OTUB1 protein levels are also affected by other pathways apart from the mTOR. As activated protein C increases OTUB1 expression under ischemia reperfusion injury [366].

1.8.2. Pathological role of OTUB1

The physiological function of OTUB1 *in vivo* remains to be discovered. So far, it has been shown that following homozygous OTUB1 deletion mice die perinatally [365, 366]. During the recent years, the emphasis of OTUB1 studies *in vivo* was directed towards immunology and infection. *In vivo* (Table 4), OTUB1 deletion in T cells increased the activity of CD8+ T and NK cells enhancing anticancer immunity [390]. In B cells, OTUB1 deletion led to hyperplasia, activation of the NF-κB pathway and lupus-like autoimmunity with high IL-6 production [389]. NF-κB pathway activation together with increased MAPK signaling were also observed in mice with specific OTUB1 deletion in dendritic cells [382]. Conditional *Otub1* KO mice are sensitive

to *T.gondii* infection and resistance to lipopolysaccharide sepsis treatment [280, 368]. In zebrafish, knock-down of OTUB1 led to capillary luminal narrowing and capillary detachment from the axial vessel, indicating vascular regression [382].

OTUB1 has also been linked to sclerosis and renal injury [366, 367]. In humans with multiple sclerosis and mouse with experimental autoimmune encephalomyelitis (EAE), OTUB1 levels were increased in astrocytes. Mice with OTUB deletion in astrocytes increased leukocyte accumulation, demyelination in the spinal cord and proinflammatory gene transcription developing more severe EAE [367]. These pathological symptoms are due to the inhibition of the JAK/STAT signaling pathway [367]. Further studies in brain research showed that OTUB1 increases oligomeric Tau forms through its catalytic activity *in vivo*, which are linked to neurodegenerative disorders such as Alzheimer's disease [377]. After intracerebral hemorrhage in rats, OTUB1 is upregulated in the neighboring neurons. This increase in OTUB1 coincided with an increase of apoptotic markers and *in vitro* studies with OTUB1 downregulation of OTUB1 suggested an OTUB1 anti-apoptotic neuronal cell function [417].

In a genome-wide association study, *Otub1* was associated with increased uric acid levels in patients with chronic kidney disease [418]. A Bayesian analysis of available transcriptomic and proteomic studies in renal collecting duct cells indicated that OTUB1 is the DUB with the highest impact on renal transport processes [419]. Under glomerulonephritis, OTUB1 was highly expressed in mesangial cells and decreased the renal disorder antagonizer decorin [401]. *In vivo*, OTUB1 levels were decreased following the inhibition of tubulointerstitial fibrosis in mice by the drug Mycophenolate Mofetil that is commonly used as immunosuppressive for allograft rejection after transplant [420]. *Otub1* heterozygous KO mice showed aggravated ischemia reperfusion injury reducing protein levels of the cold-shock protein YB-1 [366].

OTUB1 mouse model	Specificity	Pathway	Function	Outcome	Ref
Inducible	B-cells	NF-kB signaling	Enhanced p100 levels B-cell hyperplasia Aberrant Ab and IL-6 production	Autoimmunity	[389]
Inducible	Dendritic cells	NF-kB and MAPK signaling	Increased cytokine production	Susceptible to infection Resistance to lipopolysaccharide sepsis	[368]
Inducible	T-cells and whole-body	IL-15 signaling	Increased activation of CD8 T cells and NK cells	CD8+ T cell hyper response to bacterial infection Vitiligo	[390]
Inducible	Astrocyte	JAK2/STAT1 signaling	Increased leukocyte accumulation, enhanced proinflammatory gene transcription Demyelination in the spinal cord	Severe EAE	[367]
Heterozygous	Whole-body	n.d.	n.d.	Aggravated IRI	[366]
Constitutive	Whole-body	n.d.	n.d.	Perinatal lethality	[365, 366]

Table 4. Studies under OTUB1 deletion *in vivo*. The color code used in the table indicates diverse function: blue-gray, immune response; orange, disease; yellow, others. degr.: degradation. Ab: antibody

Another important pathological role of OTUB1 was identified in cancer. OTUB1 interacts with Snail, localizing together in the nucleus and stabilizing Snail in esophageal squamous cell carcinoma [381]. As a result, epithelial mesenchymal transition increases and worsens cancer prognosis *in vitro* and *in vivo* in human glioma cells [381, 421]. In gastric adenocarcinoma, OTUB1 is highly expressed, which was linked to high tumor invasion and cell migration [422]. Upregulation of the non-coding OTUB1 isoform 2 was found in gastric cancer with poor prognosis with decreased survival rate and increased cell proliferation and invasion [423]. In ovarian cancer, OTUB1 interacts with FOXM1 provoking tumor progression, and OTUB1 expression correlates also with poor prognosis [377]. In prostate cancer, OTUB1 induces tumorigenesis *in vivo* and cell invasion via RhoA activation *in vitro* [424]. In hepatocellular carcinoma patients, increased OTUB1 expression was suggested as an independent prognosis parameter. Following the downregulation of OTUB1 in hepatocarcinoma cancer cells, invasion, migration and proliferation was suppressed [425]. In colorectal cancer cells, OTUB1 enhances proliferation, migration and invasion [426-428]. The process can be

inhibited by miR-542-3p treatment targeting OTUB1 [426]. Overall, OTUB1 has been related to bad cancer prognosis in many organs like the lung, ovaries, breast and stomach.

Overall, OTUB1 is a DUB that is ubiquitously expressed in mice and humans. While most of OTUB1 studies were performed *in vitro*, the pathological role of the DUB *in vivo* has gained interest over the last years. Scrutinous characterization of the physiological role of OTUB1 in mice could help to understand further its relevance and its potential use as therapeutic target.

References

1. Brinster, R.L., *A Method for in vitro cultivation of mouse ova from two-cell to blastocyst.* Experimental Cell Research, 1963. **32**: p. 205-208.
2. Pang, S.C., et al., *1 - The Cycling and Pregnant Mouse: Gross Anatomy*, in *The Guide to Investigation of Mouse Pregnancy*, B.A. Croy, et al., Editors. 2014, Academic Press: Boston. p. 3-19.
3. Grapin-Botton, A. and D.A. Melton, *Endoderm development: from patterning to organogenesis.* Trends in Genetics, 2000. **16**: p. 124-130.
4. Organization, W.H. *Congenital anomalies*. 2016.
5. Maina, J.N., *Structure, function and evolution of the gas exchangers: comparative perspectives.* J Anat, 2002. **201**: p. 281-304.
6. Fröhlich, E., et al., *Measurements of Deposition, Lung Surface Area and Lung Fluid for Simulation of Inhaled Compounds.* Frontiers in Pharmacology, 2016. **7**: p. 181.
7. Knust, J., et al., *Stereological estimates of alveolar number and size and capillary length and surface area in mice lungs.* Anat Rec (Hoboken), 2009. **292**: p. 113-22.
8. Warburton, D., et al., *The molecular basis of lung morphogenesis.* Mech Dev, 2000. **92**(1): p. 55-81.
9. Grapin-Botton, A. and D. Constam, *Evolution of the mechanisms and molecular control of endoderm formation.* Mechanisms of Development, 2007. **124**: p. 253-278.
10. Schittny, J.C., *Development of the lung.* Cell and tissue research, 2017. **367**(3): p. 427-444.
11. Del Riccio, V., M. van Tuyl, and M. Post, *Apoptosis in lung development and neonatal lung injury.* Pediatr Res, 2004. **55**: p. 183-9.
12. Rackley, C.R. and B.R. Stripp, *Building and maintaining the epithelium of the lung.* J Clin Invest, 2012. **122**(8): p. 2724-30.
13. Koos, B.J. and A. Rajaee, *Fetal breathing movements and changes at birth.* Adv Exp Med Biol, 2014. **814**: p. 89-101.
14. Wenger, R.H., et al., *Frequently asked questions in hypoxia research.* Hypoxia (Auckl), 2015. **3**: p. 35-43.
15. Beauchemin, K.J., et al., *Temporal dynamics of the developing lung transcriptome in three common inbred strains of laboratory mice reveals multiple stages of postnatal alveolar development.* PeerJ, 2016. **4**: p. e2318.
16. Herriges, M. and E.E. Morrisey, *Lung development: orchestrating the generation and regeneration of a complex organ.* Development, 2014. **141**: p. 502-513.
17. Jesudason, E.C., et al., *Cell proliferation and apoptosis in experimental lung hypoplasia.* Journal of Pediatric Surgery, 2000. **35**: p. 129-133.
18. Saldana, M., et al., *Otubain 1: a non-canonical deubiquitinase with an emerging role in cancer.* Endocr Relat Cancer, 2019. **26**: p. R1-r14.
19. Ganesan, S., A.T. Comstock, and U.S. Sajjan, *Barrier function of airway tract epithelium.* Tissue barriers, 2013. **1**: p. e24997-e24997.
20. Rogers, A.V., et al., *Identification of serous-like cells in the surface epithelium of human bronchioles.* Eur Respir J, 1993. **6**: p. 498-504.
21. Raphael, G.D., et al., *Pathophysiology of rhinitis. Lactoferrin and lysozyme in nasal secretions.* J Clin Invest, 1989. **84**: p. 1528-35.
22. Ballard, S.T. and S.K. Inglis, *Liquid secretion properties of airway submucosal glands.* J Physiol, 2004. **556**: p. 1-10.
23. Serafini, S.M. and E.D. Michaelson, *Length and distribution of cilia in human and canine airways.* Bull Eur Physiopathol Respir, 1977. **13**: p. 551-9.
24. Park, K.S., et al., *Transdifferentiation of ciliated cells during repair of the respiratory epithelium.* Am J Respir Cell Mol Biol, 2006. **34**: p. 151-7.

25. Evans, M.J., et al., *Cellular and molecular characteristics of basal cells in airway epithelium.* Exp Lung Res, 2001. **27**: p. 401-15.
26. Hong, K.U., et al., *Basal cells are a multipotent progenitor capable of renewing the bronchial epithelium.* Am J Pathol, 2004. **164**: p. 577-88.
27. Phelps, D.S. and J. Floros, *Localization of pulmonary surfactant proteins using immunohistochemistry and tissue in situ hybridization.* Exp Lung Res, 1991. **17**: p. 985-95.
28. De Water, R., et al., *Ultrastructural localization of bronchial antileukoprotease in central and peripheral human airways by a gold-labeling technique using monoclonal antibodies.* Am Rev Respir Dis, 1986. **133**: p. 882-90.
29. Widdicombe, J.G. and R.J. Pack, *The Clara cell.* Eur J Respir Dis, 1982. **63**: p. 202-20.
30. Kobayashi, Y. and P.R. Tata, *Pulmonary Neuroendocrine Cells: Sensors and Sentinels of the Lung.* Developmental Cell, 2018. **45**: p. 425-426.
31. Wang, Y., et al., *Pulmonary alveolar type I cell population consists of two distinct subtypes that differ in cell fate.* Proceedings of the National Academy of Sciences, 2018. **115**(10): p. 2407-2412.
32. Mason, R.J., *Biology of alveolar type II cells.* Respirology, 2006. **11 Suppl**: p. S12-5.
33. Turgeon, B. and S. Meloche, *Interpreting neonatal lethal phenotypes in mouse mutants: insights into gene function and human diseases.* Physiol Rev, 2009. **89**: p. 1-26.
34. Bravo-Valenzuela, N.J., A.B. Peixoto, and E. Araujo Júnior, *Prenatal diagnosis of congenital heart disease: A review of current knowledge.* Indian heart journal, 2018. **70**: p. 150-164.
35. Brand, T., *Heart development: molecular insights into cardiac specification and early morphogenesis.* Dev Biol, 2003. **258**: p. 1-19.
36. Paige, S.L., et al., *Molecular regulation of cardiomyocyte differentiation.* Circ Res, 2015. **116**: p. 341-53.
37. Savolainen, S.M., J.F. Foley, and S.A. Elmore, *Histology atlas of the developing mouse heart with emphasis on E11.5 to E18.5.* Toxicol Pathol, 2009. **37**: p. 395-414.
38. Bruneau, B.G., *Transcriptional Regulation of Vertebrate Cardiac Morphogenesis.* Circulation Research, 2002. **90**: p. 509-519.
39. de Boer, B.A., et al., *Growth of the developing mouse heart: an interactive qualitative and quantitative 3D atlas.* Dev Biol, 2012. **368**: p. 203-13.
40. Henderson, D.J., et al., *Cardiovascular defects associated with abnormalities in midline development in the Loop-tail mouse mutant.* Circ Res, 2001. **89**: p. 6-12.
41. Guo, Y. and W.T. Pu, *Cardiomyocyte Maturation.* Circulation Research, 2020. **126**: p. 1086-1106.
42. Cole-Jeffrey, C.T., et al., *Progressive anatomical closure of foramen ovale in normal neonatal mouse hearts.* Anatomical record (Hoboken, N.J. : 2007), 2012. **295**: p. 764-768.
43. Sato, S., et al., *Scale dependence of structure-function relationship in the emphysematous mouse lung.* Frontiers in Physiology, 2015. **6**.
44. Irvin, C.G. and J.H.T. Bates, *Measuring the lung function in the mouse: the challenge of size.* Respiratory Research, 2003. **4**: p. 1.
45. Fallica, J., et al., *Application of carbon monoxide diffusing capacity in the mouse lung.* Journal of applied physiology (Bethesda, Md. : 1985), 2011. **110**: p. 1455-1459.
46. Aeffner, F., B. Bolon, and I.C. Davis, *Mouse Models of Acute Respiratory Distress Syndrome: A Review of Analytical Approaches, Pathologic Features, and Common Measurements.* Toxicol Pathol, 2015. **43**: p. 1074-92.
47. Vanoirbeek, J., et al., *Lung function measurements in mouse models of lung disease: What to expect from FEV_{0.1}?* European Respiratory Journal, 2016. **48**: p. PA4131.
48. Kuba, K., Y. Imai, and J.M. Penninger, *Angiotensin-converting enzyme 2 in lung diseases.* Curr Opin Pharmacol, 2006. **6**: p. 271-6.

49. Veldhuizen, E.J.A. and H.P. Haagsman, *Role of pulmonary surfactant components in surface film formation and dynamics.* Biochimica et Biophysica Acta (BBA) - Biomembranes, 2000. **1467**: p. 255-270.
50. Schulz, H., et al., *Respiratory mechanics in mice: strain and sex specific differences.* Acta Physiologica Scandinavica, 2002. **174**: p. 367-375.
51. Caro, A.C., F.C. Hankenson, and J.O. Marx, *Comparison of thermoregulatory devices used during anesthesia of C57BL/6 mice and correlations between body temperature and physiologic parameters.* Journal of the American Association for Laboratory Animal Science : JAALAS, 2013. **52**: p. 577-583.
52. DeMaio, L., et al., *Characterization of mouse alveolar epithelial cell monolayers.* American Journal of Physiology-Lung Cellular and Molecular Physiology, 2009. **296**: p. L1051-L1058.
53. Schulte, H., C. Mühlfeld, and C. Brandenberger, *Age-Related Structural and Functional Changes in the Mouse Lung.* Frontiers in Physiology, 2019. **10**.
54. Reynolds, S.D. and A.M. Malkinson, *Clara cell: progenitor for the bronchiolar epithelium.* The international journal of biochemistry & cell biology, 2010. **42**: p. 1-4.
55. Rokicki, W., et al., *The role and importance of club cells (Clara cells) in the pathogenesis of some respiratory diseases.* Kardiochirurgia i torakochirurgia polska = Polish journal of cardio-thoracic surgery, 2016. **13**: p. 26-30.
56. Jones, K.G., et al., *Xenobiotic metabolism in Clara cells and alveolar type II cells isolated from lungs of rats treated with beta-naphthoflavone.* J Pharmacol Exp Ther, 1983. **225**: p. 316-9.
57. Lee, D.F., et al., *Isolation and characterisation of alveolar type II pneumocytes from adult bovine lung.* Scientific Reports, 2018. **8**: p. 11927.
58. Uhal, B.D., *Cell cycle kinetics in the alveolar epithelium.* Am J Physiol, 1997. **272**(6 Pt 1): p. L1031-45.
59. Wright, J.L. and A.M. Churg, *Chapter 1 - Macro and Micro Structure of the Lung**, in *Clinical Respiratory Medicine (Fourth Edition)*, S.G. Spiro, G.A. Silvestri, and A. Agustí, Editors. 2012, W.B. Saunders: Philadelphia. p. 1-6.
60. Javaheri, S. and H. Kazemi, *Metabolic alkalosis and hypoventilation in humans.* Am Rev Respir Dis, 1987. **136**: p. 1011-6.
61. Adler, D. and J.P. Janssens, *The Pathophysiology of Respiratory Failure: Control of Breathing, Respiratory Load, and Muscle Capacity.* Respiration, 2019. **97**: p. 93-104.
62. Guyenet, P.G. and D.A. Bayliss, *Neural Control of Breathing and CO2 Homeostasis.* Neuron, 2015. **87**: p. 946-61.
63. Chevalier, M., et al., *Mechanisms Underlying Adaptation of Respiratory Network Activity to Modulatory Stimuli in the Mouse Embryo.* Neural Plast, 2016. **2016**: p. 3905257.
64. Garcia, C.S., et al., *Understanding the mechanisms of lung mechanical stress.* Braz J Med Biol Res, 2006. **39**: p. 697-706.
65. Biscoe, T.J., M.J. Purves, and S.R. Sampson, *The frequency of nerve impulses in single carotid body chemoreceptor afferent fibres recorded in vivo with intact circulation.* The Journal of physiology, 1970. **208**: p. 121-131.
66. Guyenet, P.G., R.L. Stornetta, and D.A. Bayliss, *Central respiratory chemoreception.* The Journal of comparative neurology, 2010. **518**: p. 3883-3906.
67. Au - Mailhot-Larouche, S., et al., *Assessment of Respiratory Function in Conscious Mice by Double-chamber Plethysmography.* JoVE, 2018: p. e57778.
68. Lim, R., et al., *Measuring respiratory function in mice using unrestrained whole-body plethysmography.* Journal of visualized experiments : JoVE, 2014: p. e51755-e51755.
69. Kuwashima, S., et al., *Low-intensity fetal lungs on MRI may suggest the diagnosis of pulmonary hypoplasia.* Pediatr Radiol, 2001. **31**: p. 669-72.
70. Husain, A.N. and R.G. Hessel, *Neonatal pulmonary hypoplasia: an autopsy study of 25 cases.* Pediatr Pathol, 1993. **13**: p. 475-84.

71. Laudy, J.A. and J.W. Wladimiroff, *The fetal lung. 2: Pulmonary hypoplasia.* Ultrasound Obstet Gynecol, 2000. **16**: p. 482-94.
72. Biyyam, D.R., et al., *Congenital Lung Abnormalities: Embryologic Features, Prenatal Diagnosis, and Postnatal Radiologic-Pathologic Correlation.* RadioGraphics, 2010. **30**: p. 1721-1738.
73. Hamel, B.C., *Familial primary pulmonary hypoplasia.* Eur J Pediatr, 1995. **154**: p. 336.
74. Langer, R. and H.J. Kaufmann, *Primary (isolated) bilateral pulmonary hypoplasia: a comparative study of radiologic findings and autopsy results.* Pediatr Radiol, 1986. **16**(3): p. 175-9.
75. Ackerman, K.G., et al., *Fog2 is required for normal diaphragm and lung development in mice and humans.* PLoS Genet, 2005. **1**: p. 58-65.
76. Karolak, J.A., et al., *Complex Compound Inheritance of Lethal Lung Developmental Disorders Due to Disruption of the TBX-FGF Pathway.* Am J Hum Genet, 2019. **104**: p. 213-228.
77. German, K., et al., *Identification of a deletion containing TBX4 in a neonate with acinar dysplasia by rapid exome sequencing.* Am J Med Genet A, 2019. **179**: p. 842-845.
78. Suhrie, K., et al., *Neonatal Lung Disease Associated with TBX4 Mutations.* J Pediatr, 2019. **206**: p. 286-292.e1.
79. Petersen, M., *Chapter 34 - Endometrial Biopsy*, in *Essential Clinical Procedures (Second Edition)*, R.W. Dehn and D.P. Asprey, Editors. 2007, W.B. Saunders: Philadelphia. p. 471-481.
80. Franchi, L.M., et al., *Familial pulmonary nodular lymphoid hyperplasia.* J Pediatr, 1992. **121**: p. 89-92.
81. Wang, H., et al., *Global, regional, and national life expectancy, all-cause mortality, and cause-specific mortality for 249 causes of death, 1980–2015: a systematic analysis for the Global Burden of Disease Study 2015.* The Lancet, 2016. **388**: p. 1459-1544.
82. Hedström, U., et al., *Bronchial extracellular matrix from COPD patients induces altered gene expression in repopulated primary human bronchial epithelial cells.* Scientific Reports, 2018. **8**: p. 3502.
83. Demedts, I.K., et al. *Role of apoptosis in the pathogenesis of COPD and pulmonary emphysema*. Respiratory Research, 2006. **7**, 53 DOI: 10.1186/1465-9921-7-53.
84. Barnes, P.J., S.D. Shapiro, and R.A. Pauwels, *Chronic obstructive pulmonary disease: molecular and cellularmechanisms.* European Respiratory Journal, 2003. **22**: p. 672-688.
85. Stockley, R.A., *Proteases and antiproteases.* Novartis Found Symp, 2001. **234**: p. 189-99; discussion 199-204.
86. de Leeuw, P.W. and A. Dees, *Fluid homeostasis in chronic obstructive lung disease.* European Respiratory Journal, 2003. **22**: p. 33s-40s.
87. Pelosi, P., et al., *The extracellular matrix of the lung and its role in edema formation.* An Acad Bras Cienc, 2007. **79**: p. 285-97.
88. Doevendans, P.A., et al., *Cardiovascular phenotyping in mice.* Cardiovascular Research, 1998. **39**: p. 34-49.
89. Deschepper, C.F., et al., *Characterization of blood pressure and morphological traits in cardiovascular-related organs in 13 different inbred mouse strains.* J Appl Physiol (1985), 2004. **97**: p. 369-76.
90. Mattson, D.L., *Comparison of arterial blood pressure in different strains of mice*.* American Journal of Hypertension, 2001. **14**: p. 405-408.
91. Kreissl, M.C., et al., *Noninvasive measurement of cardiovascular function in mice with high-temporal-resolution small-animal PET.* J Nucl Med, 2006. **47**: p. 974-80.
92. Joyner, M.J. and D.P. Casey, *Regulation of increased blood flow (hyperemia) to muscles during exercise: a hierarchy of competing physiological needs.* Physiological reviews, 2015. **95**: p. 549-601.
93. Wessels, A. and D. Sedmera, *Developmental anatomy of the heart: a tale of mice and man.* Physiological Genomics, 2003. **15**: p. 165-176.

94. Reichardt, M., et al., *Fiber orientation in a whole mouse heart reconstructed by laboratory phase-contrast micro-CT.* Journal of Medical Imaging, 2020. **7**: p. 023501.
95. Dueñas, A., A.E. Aranega, and D. Franco, *More than Just a Simple Cardiac Envelope; Cellular Contributions of the Epicardium.* Frontiers in Cell and Developmental Biology, 2017. **5**(44).
96. Foglia, M.J. and K.D. Poss, *Building and re-building the heart by cardiomyocyte proliferation.* Development (Cambridge, England), 2016. **143**: p. 729-740.
97. Oakley, R.H., et al., *Essential role of stress hormone signaling in cardiomyocytes for the prevention of heart disease.* Proceedings of the National Academy of Sciences of the United States of America, 2013. **110**: p. 17035-17040.
98. Liao, M.-L.C., et al., *Sensing Cardiac Electrical Activity With a Cardiac Myocyte–Targeted Optogenetic Voltage Indicator.* Circulation Research, 2015. **117**: p. 401-412.
99. Hansen, B.J., T.A. Csepe, and V.V. Fedorov, *28 - Mechanisms of Normal and Dysfunctional Sinoatrial Nodal Excitability and Propagation*, in *Cardiac Electrophysiology: From Cell to Bedside (Seventh Edition)*, D.P. Zipes, J. Jalife, and W.G. Stevenson, Editors. 2018, Elsevier. p. 259-271.
100. Shimizu, I. and T. Minamino, *Physiological and pathological cardiac hypertrophy.* Journal of Molecular and Cellular Cardiology, 2016. **97**: p. 245-262.
101. Farrell, E.T., et al., *Increased Postnatal Cardiac Hyperplasia Precedes Cardiomyocyte Hypertrophy in a Model of Hypertrophic Cardiomyopathy.* Frontiers in physiology, 2017. **8**: p. 414-414.
102. Li, J., et al., *New frontiers in heart hypertrophy during pregnancy.* American journal of cardiovascular disease, 2012. **2**: p. 192-207.
103. Maron, B.J., *Structural features of the athlete heart as defined by echocardiography.* Journal of the American College of Cardiology, 1986. **7**: p. 190-203.
104. Pluim, B.M., et al., *The athlete's heart. A meta-analysis of cardiac structure and function.* Circulation, 2000. **101**: p. 336-44.
105. Bernardo, B.C., et al., *Molecular distinction between physiological and pathological cardiac hypertrophy: experimental findings and therapeutic strategies.* Pharmacol Ther, 2010. **128**: p. 191-227.
106. Stypmann, J., et al., *Echocardiographic assessment of global left ventricular function in mice.* Lab Anim, 2009. **43**: p. 127-37.
107. Lips, D.J., et al., *Molecular determinants of myocardial hypertrophy and failure: alternative pathways for beneficial and maladaptive hypertrophy.* European Heart Journal, 2003. **24**: p. 883-896.
108. Chugh, S.S., et al., *Epidemiology of Sudden Cardiac Death: Clinical and Research Implications.* Progress in Cardiovascular Diseases, 2008. **51**: p. 213-228.
109. Borlaug, B.A. and M.M. Redfield, *Diastolic and Systolic Heart Failure Are Distinct Phenotypes Within the Heart Failure Spectrum.* Circulation, 2011. **123**: p. 2006-2014.
110. Palazzuoli, A., et al., *Combined use of lung ultrasound, B-type natriuretic peptide, and echocardiography for outcome prediction in patients with acute HFrEF and HFpEF.* Clinical Research in Cardiology, 2018. **107**: p. 586-596.
111. Hogg, K., K. Swedberg, and J. McMurray, *Heart failure with preserved left ventricular systolic function.* epidemiology, clinical characteristics, and prognosis, 2004. **43**: p. 317-327.
112. Noll, N.A., H. Lal, and W.D. Merryman, *Mouse Models of Heart Failure with Preserved or Reduced Ejection Fraction.* The American Journal of Pathology, 2020. **190**: p. 1596-1608.
113. Kannel, W.B., *Role of blood pressure in cardiovascular morbidity and mortality.* Prog Cardiovasc Dis, 1974. **17**: p. 5-24.
114. Badeer, H.S., *Pathogenesis of cardiac hypertrophy in coronary atherosclerosis and myocardial infarction.* American Heart Journal, 1972. **84**: p. 256-264.

115. Seidman, J.G. and C. Seidman, *The genetic basis for cardiomyopathy: from mutation identification to mechanistic paradigms.* Cell, 2001. **104**: p. 557-67.
116. Kupari, M., H. Turto, and J. Lommi, *Left ventricular hypertrophy in aortic valve stenosis: preventive or promotive of systolic dysfunction and heart failure?* European Heart Journal, 2005. **26**: p. 1790-1796.
117. Little, W.C., *Heart failure with a normal left ventricular ejection fraction: diastolic heart failure.* Transactions of the American Clinical and Climatological Association, 2008. **119**: p. 93-102.
118. Gogiraju, R., M.L. Bochenek, and K. Schäfer, *Angiogenic Endothelial Cell Signaling in Cardiac Hypertrophy and Heart Failure.* Frontiers in Cardiovascular Medicine, 2019. **6**.
119. Goldfine, S.M., et al., *Myocardial collagen in cardiac hypertrophy resulting from chronic aortic regurgitation.* Am J Ther, 1998. **5**: p. 139-46.
120. Heinzel, F.R., et al., *Myocardial hypertrophy and its role in heart failure with preserved ejection fraction.* J Appl Physiol (1985), 2015. **119**: p. 1233-42.
121. van Berlo, J.H., M. Maillet, and J.D. Molkentin, *Signaling effectors underlying pathologic growth and remodeling of the heart.* The Journal of Clinical Investigation, 2013. **123**: p. 37-45.
122. Camacho, P., et al., *Small mammalian animal models of heart disease.* American journal of cardiovascular disease, 2016. **6**: p. 70-80.
123. Uhl, E.W. and N.J. Warner, *Mouse Models as Predictors of Human Responses: Evolutionary Medicine.* Current Pathobiology Reports, 2015. **3**: p. 219-223.
124. Yutzey, K.E. and J. Robbins, Principles of Genetic Murine Models for Cardiac Disease. Circulation, 2007. 115: p. 792-799.
125. Patel, H., M.A. Menouar, and A. Bhardwaj, Physiology, Respiratory Quotient, in StatPearls. 2020, StatPearls Publishing
126. Brinkman, J.E., F. Toro, and S. Sharma, Physiology, Respiratory Drive, in StatPearls. 2020, StatPearls Publishing
127. Lutz, T.A. and S.C. Woods, *Overview of animal models of obesity.* Current protocols in pharmacology, 2012. **Chapter 5**: p. Unit5.61-Unit5.61.
128. Qi, X. and R.F. Tester, *Fructose, galactose and glucose – In health and disease.* Clinical Nutrition ESPEN, 2019. **33**: p. 18-28.
129. Khonsary, S.A., *Guyton and Hall: Textbook of Medical Physiology.* Surgical Neurology International, 2017. **8**: p. 275.
130. van Schaftingen, E. and I. Gerin, *The glucose-6-phosphatase system.* The Biochemical journal, 2002. **362**(Pt 3): p. 513-532.
131. Oosterveer, M.H., et al., *Lxralpha deficiency hampers the hepatic adaptive response to fasting in mice.* J Biol Chem, 2008. **283**: p. 25437-45.
132. Heijboer, A.C., et al., *Sixteen hours of fasting differentially affects hepatic and muscle insulin sensitivity in mice.* J Lipid Res, 2005. **46**: p. 582-8.
133. Fehm-Wolfsdorf, G., et al., *Classically conditioned changes of blood glucose level in humans.* Physiology & Behavior, 1993. **54**: p. 155-160.
134. Moebus, S., et al., *Impact of time since last caloric intake on blood glucose levels.* European journal of epidemiology, 2011. **26**: p. 719-728.
135. Hantzidiamantis, P.J. and S.L. Lappin, *Physiology, Glucose*, in *StatPearls*. 2020, StatPearls Publishing
136. Webster, K.A., *Evolution of the coordinate regulation of glycolytic enzyme genes by hypoxia.* Journal of Experimental Biology, 2003. **206**: p. 2911-2922.
137. Naifeh, J., M. Dimri, and M. Varacallo, *Biochemistry, Aerobic Glycolysis*, in *StatPearls*. 2020, StatPearls Publishing
138. Adeva-Andany, M.M., et al., *Liver glucose metabolism in humans.* Bioscience reports, 2016. **36**: p. e00416.

139. Fernie, A.R., F. Carrari, and L.J. Sweetlove, *Respiratory metabolism: glycolysis, the TCA cycle and mitochondrial electron transport.* Current Opinion in Plant Biology, 2004. **7**: p. 254-261.
140. Bonora, M., et al., *ATP synthesis and storage.* Purinergic signalling, 2012. **8**: p. 343-357.
141. McCall, A.L., *Chapter 22 - Glucose Transport*, in *Stress: Physiology, Biochemistry, and Pathology*, G. Fink, Editor. 2019, Academic Press. p. 293-307.
142. Navale, A.M. and A.N. Paranjape, *Glucose transporters: physiological and pathological roles.* Biophysical reviews, 2016. **8**: p. 5-9.
143. Ruud, J., S.M. Steculorum, and J.C. Brüning, *Neuronal control of peripheral insulin sensitivity and glucose metabolism.* Nature Communications, 2017. **8**: p. 15259.
144. Aronoff, S.L., et al., *Glucose Metabolism and Regulation: Beyond Insulin and Glucagon.* Diabetes Spectrum, 2004. **17**: p. 183-190.
145. Fujita, S., et al., *Effect of insulin on human skeletal muscle protein synthesis is modulated by insulin-induced changes in muscle blood flow and amino acid availability.* American journal of physiology. Endocrinology and metabolism, 2006. **291**: p. E745-E754.
146. Hulse, R.E., L.A. Ralat, and T. Wei-Jen, *Structure, function, and regulation of insulin-degrading enzyme.* Vitamins and hormones, 2009. **80**: p. 635-648.
147. Najjar, S.M. and G. Perdomo, *Hepatic Insulin Clearance: Mechanism and Physiology.* Physiology (Bethesda), 2019. **34**: p. 198-215.
148. Skjaervold, N.K., et al., *Pharmacology of intravenous insulin administration: implications for future closed-loop glycemic control by the intravenous/intravenous route.* Diabetes technology & therapeutics, 2012. **14**: p. 23-29.
149. Whittaker, L., et al., *High-affinity insulin binding: insulin interacts with two receptor ligand binding sites.* Biochemistry, 2008. **47**: p. 12900-12909.
150. Haeusler, R.A., T.E. McGraw, and D. Accili, *Biochemical and cellular properties of insulin receptor signalling.* Nature Reviews Molecular Cell Biology, 2018. **19**: p. 31-44.
151. Ren, L., et al., *The IRS/PI3K/Akt signaling pathway mediates olanzapine-induced hepatic insulin resistance in male rats.* Life Sci, 2019. **217**: p. 229-236.
152. Liao, Y. and M.-C. Hung, *Physiological regulation of Akt activity and stability.* American journal of translational research, 2010. **2**: p. 19-42.
153. Stöckli, J., et al., *Regulation of glucose transporter 4 translocation by the Rab guanosine triphosphatase-activating protein AS160/TBC1D4: role of phosphorylation and membrane association.* Molecular endocrinology (Baltimore, Md.), 2008. **22**(12): p. 2703-2715.
154. Islam, M.S., *Stimulus-Secretion Coupling in Beta-Cells: From Basic to Bedside.* Adv Exp Med Biol, 2020. **1131**: p. 943-963.
155. Lutz, T.A. and E. Osto, *Glucagon-like peptide-1, glucagon-like peptide-2, and lipid metabolism.* Curr Opin Lipidol, 2016. **27**: p. 257-63.
156. Sone, H., *Diabetes Mellitus*, in *Encyclopedia of Cardiovascular Research and Medicine*, R.S. Vasan and D.B. Sawyer, Editors. 2018, Elsevier: Oxford. p. 9-16.
157. O'Donnell, C., *34 - Diabetes*, in *Contact Lens Practice (Third Edition)*, N. Efron, Editor. 2018, Elsevier. p. 314-320.e1.
158. Vézina, C., A. Kudelski, and S.N. Sehgal, *Rapamycin (AY-22,989), a new antifungal antibiotic. I. Taxonomy of the producing streptomycete and isolation of the active principle.* J Antibiot (Tokyo), 1975. **28**: p. 721-6.
159. Martel, R.R., J. Klicius, and S. Galet, *Inhibition of the immune response by rapamycin, a new antifungal antibiotic.* Can J Physiol Pharmacol, 1977. **55**: p. 48-51.
160. Eng, C.P., S.N. Sehgal, and C. Vézina, *Activity of rapamycin (AY-22,989) against transplanted tumors.* J Antibiot (Tokyo), 1984. **37**: p. 1231-7.
161. Sehgal, S.N., H. Baker, and C. Vézina, *Rapamycin (AY-22,989), a new antifungal antibiotic. II. Fermentation, isolation and characterization.* J Antibiot (Tokyo), 1975. **28**: p. 727-32.
162. Brown, E.J., et al., *A mammalian protein targeted by G1-arresting rapamycin-receptor complex.* Nature, 1994. **369**: p. 756-8.

163. Sabatini, D.M., et al., *RAFT1: A mammalian protein that binds to FKBP12 in a rapamycin-dependent fashion and is homologous to yeast TORs.* Cell, 1994. **78**: p. 35-43.
164. Eshleman, J.S., et al., *Inhibition of the mammalian target of rapamycin sensitizes U87 xenografts to fractionated radiation therapy.* Cancer Res, 2002. **62**: p. 7291-7.
165. Lorenz, M.C. and J. Heitman, *TOR mutations confer rapamycin resistance by preventing interaction with FKBP12-rapamycin.* J Biol Chem, 1995. **270**: p. 27531-7.
166. Strömberg, T., et al., *Rapamycin sensitizes multiple myeloma cells to apoptosis induced by dexamethasone.* Blood, 2004. **103**: p. 3138-47.
167. Toth, M.J., et al., *Chronic heart failure reduces Akt phosphorylation in human skeletal muscle: relationship to muscle size and function.* J Appl Physiol (1985), 2011. **110**: p. 892-900.
168. Saxton, R.A. and D.M. Sabatini, *mTOR Signaling in Growth, Metabolism, and Disease.* Cell, 2017. **169**: p. 361-371.
169. Yoon, M.-S. and C.S. Choi, *The role of amino acid-induced mammalian target of rapamycin complex 1(mTORC1) signaling in insulin resistance.* Experimental & Molecular Medicine, 2016. **48**: p. e201-e201.
170. Oshiro, N., et al., *The proline-rich Akt substrate of 40 kDa (PRAS40) is a physiological substrate of mammalian target of rapamycin complex 1.* J Biol Chem, 2007. **282**: p. 20329-39.
171. Wang, L., et al., *PRAS40 regulates mTORC1 kinase activity by functioning as a direct inhibitor of substrate binding.* J Biol Chem, 2007. **282**: p. 20036-44.
172. Kim, J. and K.-L. Guan, *mTOR as a central hub of nutrient signalling and cell growth.* Nature Cell Biology, 2019. **21**: p. 63-71.
173. Kakumoto, K., et al., *mLST8 Promotes mTOR-Mediated Tumor Progression.* PloS one, 2015. **10**(4): p. e0119015-e0119015.
174. Kim, D.H., et al., *GbetaL, a positive regulator of the rapamycin-sensitive pathway required for the nutrient-sensitive interaction between raptor and mTOR.* Mol Cell, 2003. **11**: p. 895-904.
175. Hara, K., et al., *Raptor, a binding partner of target of rapamycin (TOR), mediates TOR action.* Cell, 2002. **110**: p. 177-89.
176. Kim, D.H., et al., *mTOR interacts with raptor to form a nutrient-sensitive complex that signals to the cell growth machinery.* Cell, 2002. **110**: p. 163-75.
177. Zhao, Y., X. Xiong, and Y. Sun, *DEPTOR, an mTOR inhibitor, is a physiological substrate of SCF(βTrCP) E3 ubiquitin ligase and regulates survival and autophagy.* Molecular cell, 2011. **44**: p. 304-316.
178. Frias, M.A., et al., *mSin1 is necessary for Akt/PKB phosphorylation, and its isoforms define three distinct mTORC2s.* Curr Biol, 2006. **16**: p. 1865-70.
179. Jacinto, E., et al., *Mammalian TOR complex 2 controls the actin cytoskeleton and is rapamycin insensitive.* Nature Cell Biology, 2004. **6**: p. 1122-1128.
180. Pearce, L.R., et al., *Identification of Protor as a novel Rictor-binding component of mTOR complex-2.* Biochem J, 2007. **405**: p. 513-22.
181. Dos, D.S., et al., *Rictor, a Novel Binding Partner of mTOR, Defines a Rapamycin-Insensitive and Raptor-Independent Pathway that Regulates the Cytoskeleton.* Current Biology, 2004. **14**: p. 1296-1302.
182. Martinez Calejman, C., et al., *mTORC2-AKT signaling to ATP-citrate lyase drives brown adipogenesis and de novo lipogenesis.* Nature Communications, 2020. **11**: p. 575.
183. Dibble, C.C., J.M. Asara, and B.D. Manning, *Characterization of Rictor phosphorylation sites reveals direct regulation of mTOR complex 2 by S6K1.* Molecular and cellular biology, 2009. **29**: p. 5657-5670.
184. Pearce, L.R., et al., *Protor-1 is required for efficient mTORC2-mediated activation of SGK1 in the kidney.* Biochem J, 2011. **436**: p. 169-79.
185. Liu, G.Y. and D.M. Sabatini, *mTOR at the nexus of nutrition, growth, ageing and disease.* Nature Reviews Molecular Cell Biology, 2020. **21**: p. 183-203.

186. Inoki, K., et al., *TSC2 integrates Wnt and energy signals via a coordinated phosphorylation by AMPK and GSK3 to regulate cell growth.* Cell, 2006. **126**: p. 955-68.
187. Lee, D.F., et al., *IKK beta suppression of TSC1 links inflammation and tumor angiogenesis via the mTOR pathway.* Cell, 2007. **130**: p. 440-55.
188. Menon, S., et al., *Spatial control of the TSC complex integrates insulin and nutrient regulation of mTORC1 at the lysosome.* Cell, 2014. **156**: p. 771-85.
189. Gwinn, D.M., et al., *AMPK phosphorylation of raptor mediates a metabolic checkpoint.* Mol Cell, 2008. **30**: p. 214-26.
190. Brugarolas, J., et al., *Regulation of mTOR function in response to hypoxia by REDD1 and the TSC1/TSC2 tumor suppressor complex.* Genes Dev, 2004. **18**: p. 2893-904.
191. Feng, Z., et al., *The regulation of AMPK beta1, TSC2, and PTEN expression by p53: stress, cell and tissue specificity, and the role of these gene products in modulating the IGF-1-AKT-mTOR pathways.* Cancer Res, 2007. **67**: p. 3043-53.
192. Holz, M.K., et al., *mTOR and S6K1 Mediate Assembly of the Translation Preinitiation Complex through Dynamic Protein Interchange and Ordered Phosphorylation Events.* Cell, 2005. **123**: p. 569-580.
193. Dorrello, N.V., et al., *S6K1- and βTRCP-Mediated Degradation of PDCD4 Promotes Protein Translation and Cell Growth.* Science, 2006. **314**: p. 467-471.
194. Gingras, A.C., et al., *Regulation of 4E-BP1 phosphorylation: a novel two-step mechanism.* Genes Dev, 1999. **13**: p. 1422-37.
195. Brunn, G.J., et al., *Phosphorylation of the Translational Repressor PHAS-I by the Mammalian Target of Rapamycin.* Science, 1997. **277**: p. 99-101.
196. Düvel, K., et al., *Activation of a Metabolic Gene Regulatory Network Downstream of mTOR Complex 1.* Molecular Cell, 2010. **39**: p. 171-183.
197. Porstmann, T., et al., *SREBP Activity Is Regulated by mTORC1 and Contributes to Akt-Dependent Cell Growth.* Cell Metabolism, 2008. **8**: p. 224-236.
198. Peterson, Timothy R., et al., *mTOR Complex 1 Regulates Lipin 1 Localization to Control the SREBP Pathway.* Cell, 2011. **146**: p. 408-420.
199. Ben-Sahra, I., et al., *Stimulation of de Novo Pyrimidine Synthesis by Growth Signaling Through mTOR and S6K1.* Science, 2013. **339**: p. 1323-1328.
200. Robitaille, A.M., et al., *Quantitative Phosphoproteomics Reveal mTORC1 Activates de Novo Pyrimidine Synthesis.* Science, 2013. **339**: p. 1320-1323.
201. Ben-Sahra, I., et al., *mTORC1 induces purine synthesis through control of the mitochondrial tetrahydrofolate cycle.* Science, 2016. **351**: p. 728-733.
202. Yoon, M.-S., *The Role of Mammalian Target of Rapamycin (mTOR) in Insulin Signaling.* Nutrients, 2017. **9**: p. 1176.
203. Jung, C.H., et al., *ULK-Atg13-FIP200 complexes mediate mTOR signaling to the autophagy machinery.* Mol Biol Cell, 2009. **20**: p. 1992-2003.
204. Martina, J.A., et al., *MTORC1 functions as a transcriptional regulator of autophagy by preventing nuclear transport of TFEB.* Autophagy, 2012. **8**: p. 903-14.
205. Zhao, J., et al., *mTOR inhibition activates overall protein degradation by the ubiquitin proteasome system as well as by autophagy.* Proc Natl Acad Sci U S A, 2015. **112**: p. 15790-7.
206. Rousseau, A. and A. Bertolotti, *An evolutionarily conserved pathway controls proteasome homeostasis.* Nature, 2016. **536**: p. 184-9.
207. Zhang, Y., et al., *Coordinated regulation of protein synthesis and degradation by mTORC1.* Nature, 2014. **513**: p. 440-3.
208. Chi, H., *Sin1–mTORC2 signaling drives glycolysis of developing thymocytes.* Journal of Molecular Cell Biology, 2018. **11**: p. 91-92.
209. Shigeyama, Y., et al., *Biphasic response of pancreatic β-cell mass to ablation of tuberous sclerosis complex 2 in mice.* Molecular and Cellular Biology, 2008. **28**: p. 2971-2979.

210. Khamzina, L., et al., *Increased Activation of the Mammalian Target of Rapamycin Pathway in Liver and Skeletal Muscle of Obese Rats: Possible Involvement in Obesity-Linked Insulin Resistance.* Endocrinology, 2005. **146**: p. 1473-1481.
211. Um, S.H., et al., *Absence of S6K1 protects against age- and diet-induced obesity while enhancing insulin sensitivity.* Nature, 2004. **431**: p. 200-205.
212. Hagiwara, A., et al., *Hepatic mTORC2 Activates Glycolysis and Lipogenesis through Akt, Glucokinase, and SREBP1c.* Cell Metabolism, 2012. **15**: p. 725-738.
213. Kumar, A., et al., *Muscle-specific deletion of rictor impairs insulin-stimulated glucose transport and enhances Basal glycogen synthase activity.* Molecular and cellular biology, 2008. **28**: p. 61-70.
214. Kumar, A., et al., *Fat Cell–Specific Ablation of Rictor in Mice Impairs Insulin-Regulated Fat Cell and Whole-Body Glucose and Lipid Metabolism.* Diabetes, 2010. **59**: p. 1397-1406.
215. Yuan, M., et al., *Identification of Akt-independent regulation of hepatic lipogenesis by mammalian target of rapamycin (mTOR) complex 2.* Journal of Biological Chemistry, 2012. **287**: p. 29579-29588.
216. Lamming, D.W., et al., *Rapamycin-Induced Insulin Resistance Is Mediated by mTORC2 Loss and Uncoupled from Longevity.* Science, 2012. **335**: p. 1638-1643.
217. Cunningham, J.T., et al., *mTOR controls mitochondrial oxidative function through a YY1–PGC-1α transcriptional complex.* Nature, 2007. **450**: p. 736-740.
218. Guillén, C. and M. Benito, *mTORC1 Overactivation as a Key Aging Factor in the Progression to Type 2 Diabetes Mellitus.* Frontiers in Endocrinology, 2018. **9**.
219. Mieulet, V. and R.F. Lamb, *Tuberous sclerosis complex: linking cancer to metabolism.* Trends in Molecular Medicine, 2010. **16**: p. 329-335.
220. Chalhoub, N. and S.J. Baker, *PTEN and the PI3-kinase pathway in cancer.* Annual review of pathology, 2009. **4**: p. 127-150.
221. Liu, T., et al., *NF-κB signaling in inflammation.* Signal transduction and targeted therapy, 2017. **2**: p. 17023.
222. Dhingra, R., et al., *Bidirectional regulation of nuclear factor-κB and mammalian target of rapamycin signaling functionally links Bnip3 gene repression and cell survival of ventricular myocytes.* Circ Heart Fail, 2013. **6**: p. 335-43.
223. Zhao, Q.D., et al., *NADPH oxidase 4 induces cardiac fibrosis and hypertrophy through activating Akt/mTOR and NFκB signaling pathways.* Circulation, 2015. **131**: p. 643-55.
224. Jessen, S., et al., *Beta(2) -adrenergic agonist clenbuterol increases energy expenditure and fat oxidation, and induces mTOR phosphorylation in skeletal muscle of young healthy men.* Drug Test Anal, 2020. **12**: p. 610-618.
225. Risson, V., et al., *Muscle inactivation of mTOR causes metabolic and dystrophin defects leading to severe myopathy.* The Journal of cell biology, 2009. **187**: p. 859-874.
226. Bentzinger, C.F., et al., *Skeletal Muscle-Specific Ablation of raptor, but Not of rictor, Causes Metabolic Changes and Results in Muscle Dystrophy.* Cell Metabolism, 2008. **8**: p. 411-424.
227. Castets, P., et al., *Sustained Activation of mTORC1 in Skeletal Muscle Inhibits Constitutive and Starvation-Induced Autophagy and Causes a Severe, Late-Onset Myopathy.* Cell Metabolism, 2013. **17**: p. 731-744.
228. Xin, M., et al., *Regulation of insulin-like growth factor signaling by Yap governs cardiomyocyte proliferation and embryonic heart size.* Sci Signal, 2011. **4**: p. ra70.
229. Zhu, Y., et al., *Mechanistic target of rapamycin (Mtor) is essential for murine embryonic heart development and growth.* PLoS One, 2013. **8**: p. e54221.
230. Shende, P., et al., *Cardiac raptor ablation impairs adaptive hypertrophy, alters metabolic gene expression, and causes heart failure in mice.* Circulation, 2011. **123**: p. 1073-82.

231. Tamai, T., et al., *Rheb (Ras homologue enriched in brain)-dependent mammalian target of rapamycin complex 1 (mTORC1) activation becomes indispensable for cardiac hypertrophic growth after early postnatal period.* J Biol Chem, 2013. **288**: p. 10176-87.
232. Blackwood, E.A., et al., *ATF6 Regulates Cardiac Hypertrophy by Transcriptional Induction of the mTORC1 Activator, Rheb.* Circ Res, 2019. **124**: p. 79-93.
233. Kishore, R., et al., *Interleukin-10 inhibits chronic angiotensin II-induced pathological autophagy.* J Mol Cell Cardiol, 2015. **89**: p. 203-13.
234. Simm, A., et al., *Activation of p70(S6) kinase by beta-adrenoceptor agonists on adult cardiomyocytes.* J Mol Cell Cardiol, 1998. **30**: p. 2059-67.
235. Kemi, O.J., et al., *Activation or inactivation of cardiac Akt/mTOR signaling diverges physiological from pathological hypertrophy.* J Cell Physiol, 2008. **214**: p. 316-21.
236. Kemi, O.J., et al., *Activation or inactivation of cardiac Akt/mTOR signaling diverges physiological from pathological hypertrophy.* Journal of Cellular Physiology, 2008. **214**: p. 316-321.
237. Song, X., et al., *mTOR attenuates the inflammatory response in cardiomyocytes and prevents cardiac dysfunction in pathological hypertrophy.* Am J Physiol Cell Physiol, 2010. **299**: p. C1256-66.
238. Wenger, R.H. and A. Kurtz, *Erythropoietin.* Compr Physiol, 2011. **1**: p. 1759-94.
239. Mohyeldin, A., T. Garzón-Muvdi, and A. Quiñones-Hinojosa, *Oxygen in Stem Cell Biology: A Critical Component of the Stem Cell Niche.* Cell Stem Cell, 2010. **7**: p. 150-161.
240. Giaccia, A.J., M.C. Simon, and R. Johnson, *The biology of hypoxia: the role of oxygen sensing in development, normal function, and disease.* Genes & development, 2004. **18**: p. 2183-2194.
241. Chaillou, T., et al., *Hypoxia transiently affects skeletal muscle hypertrophy in a functional overload model.* American Journal of Physiology-Regulatory, Integrative and Comparative Physiology, 2012. **302**: p. R643-R654.
242. Taylor, C.T. and S.P. Colgan, *Regulation of immunity and inflammation by hypoxia in immunological niches.* Nature Reviews Immunology, 2017. **17**: p. 774-785.
243. Giordano, F.J., *Oxygen, oxidative stress, hypoxia, and heart failure.* J Clin Invest, 2005. **115**(3): p. 500-8.
244. Marti, H.H., *Erythropoietin and the hypoxic brain.* J Exp Biol, 2004. **207**: p. 3233-42.
245. Marti, H.H. and R. Kunze, *Oxygen sensors and neuronal adaptation to ischemia.* Oncotarget, 2017. **8**: p. 1955-1956.
246. Scholz, C.C., et al., *Regulation of IL-1β-induced NF-κB by hydroxylases links key hypoxic and inflammatory signaling pathways.* Proc Natl Acad Sci U S A, 2013. **110**: p. 18490-5.
247. Scholz, C.C. and C.T. Taylor, *Targeting the HIF pathway in inflammation and immunity.* Current Opinion in Pharmacology, 2013. **13**: p. 646-653.
248. Scholz, C.C. and C.T. Taylor, *Hydroxylase-dependent regulation of the NF-κB pathway.* Biol Chem, 2013. **394**: p. 479-93.
249. Solaini, G., et al., *Hypoxia and mitochondrial oxidative metabolism.* Biochimica et Biophysica Acta (BBA) - Bioenergetics, 2010. **1797**: p. 1171-1177.
250. Simon, M.C. and B. Keith, *The role of oxygen availability in embryonic development and stem cell function.* Nat Rev Mol Cell Biol, 2008. **9**: p. 285-96.
251. Neary, M.T., et al., *Hypoxia signaling controls postnatal changes in cardiac mitochondrial morphology and function.* J Mol Cell Cardiol, 2014. **74**: p. 340-52.
252. Bishop, S. and R. Altschuld, *Increased glycolytic metabolism in cardiac hypertrophy and congestive failure.* American Journal of Physiology-Legacy Content, 1970. **218**: p. 153-159.
253. Chu, W., et al., *Mild hypoxia-induced cardiomyocyte hypertrophy via up-regulation of HIF-1α-mediated TRPC signalling.* J Cell Mol Med, 2012. **16**: p. 2022-34.
254. Marti, H.H., *Angiogenesis--a self-adapting principle in hypoxia.* Exs, 2005: p. 163-80.

255. Berra, E., et al., *HIF prolyl-hydroxylase 2 is the key oxygen sensor setting low steady-state levels of HIF-1alpha in normoxia.* The EMBO journal, 2003. **22**: p. 4082-4090.
256. Aragonés, J., et al., *Oxygen Sensors at the Crossroad of Metabolism.* Cell Metabolism, 2009. **9**: p. 11-22.
257. Ziello, J.E., I.S. Jovin, and Y. Huang, *Hypoxia-Inducible Factor (HIF)-1 regulatory pathway and its potential for therapeutic intervention in malignancy and ischemia.* The Yale journal of biology and medicine, 2007. **80**: p. 51-60.
258. Wenger, R.H., *Mammalian oxygen sensing, signalling and gene regulation.* J Exp Biol, 2000. **203**: p. 1253-63.
259. Wenger, R.H., *Cellular adaptation to hypoxia: O2-sensing protein hydroxylases, hypoxia-inducible transcription factors, and O2-regulated gene expression.* Faseb j, 2002. **16**: p. 1151-62.
260. Strowitzki, M.J., E.P. Cummins, and C.T. Taylor, *Protein Hydroxylation by Hypoxia-Inducible Factor (HIF) Hydroxylases: Unique or Ubiquitous?* Cells, 2019. **8**: p. 384.
261. Fandrey, J., et al., *Now a Nobel gas: oxygen.* Pflugers Arch, 2019. **471**: p. 1343-1358.
262. Wiener, C.M., G. Booth, and G.L. Semenza, *In VivoExpression of mRNAs Encoding Hypoxia-Inducible Factor 1.* Biochemical and Biophysical Research Communications, 1996. **225**: p. 485-488.
263. Iyer, N.V., et al., *Cellular and developmental control of O2 homeostasis by hypoxia-inducible factor 1 alpha.* Genes Dev, 1998. **12**: p. 149-62.
264. Kotch, L.E., et al., *Defective Vascularization of HIF-1α-Null Embryos Is Not Associated with VEGF Deficiency but with Mesenchymal Cell Death.* Developmental Biology, 1999. **209**: p. 254-267.
265. Scortegagna, M., et al., *Multiple organ pathology, metabolic abnormalities and impaired homeostasis of reactive oxygen species in Epas1-/- mice.* Nat Genet, 2003. **35**: p. 331-40.
266. Scortegagna, M., et al., *The HIF family member EPAS1/HIF-2α is required for normal hematopoiesis in mice.* Blood, 2003. **102**: p. 1634-1640.
267. Imeri, F., et al., *Generation of renal Epo-producing cell lines by conditional gene tagging reveals rapid HIF-2 driven Epo kinetics, cell autonomous feedback regulation, and a telocyte phenotype.* Kidney International, 2019. **95**: p. 375-387.
268. Taylor, C.T. and J.C. McElwain, *Ancient atmospheres and the evolution of oxygen sensing via the hypoxia-inducible factor in metazoans.* Physiology (Bethesda), 2010. **25**: p. 272-9.
269. Yamashita, T., et al., *Abnormal heart development and lung remodeling in mice lacking the hypoxia-inducible factor-related basic helix-loop-helix PAS protein NEPAS.* Mol Cell Biol, 2008. **28**: p. 1285-97.
270. Sim, J., et al., *The Factor Inhibiting HIF Asparaginyl Hydroxylase Regulates Oxidative Metabolism and Accelerates Metabolic Adaptation to Hypoxia.* Cell Metab, 2018. **27**: p. 898-913.e7.
271. Hewitson, K.S., et al., *Hypoxia-inducible factor (HIF) asparagine hydroxylase is identical to factor inhibiting HIF (FIH) and is related to the cupin structural family.* J Biol Chem, 2002. **277**: p. 26351-5.
272. Lando, D., et al., *FIH-1 is an asparaginyl hydroxylase enzyme that regulates the transcriptional activity of hypoxia-inducible factor.* Genes Dev, 2002. **16**: p. 1466-71.
273. Dann, C.E., R.K. Bruick, and J. Deisenhofer, *Structure of factor-inhibiting hypoxia-inducible factor 1: An asparaginyl hydroxylase involved in the hypoxic response pathway.* Proceedings of the National Academy of Sciences, 2002. **99**: p. 15351-15356.
274. Metzen, E., et al., *Intracellular localisation of human HIF-1 alpha hydroxylases: implications for oxygen sensing.* J Cell Sci, 2003. **116**: p. 1319-26.
275. Li, J., et al., *Protein kinase C-mediated modulation of FIH-1 expression by the homeodomain protein CDP/Cut/Cux.* Mol Cell Biol, 2007. **27**: p. 7345-53.

276. Zhang, H., et al., *MicroRNA-455 regulates brown adipogenesis via a novel HIF1an-AMPK-PGC1α signaling network.* EMBO Rep, 2015. **16**: p. 1378-93.
277. Fukuba, H., et al., *Abundance of aspargynyl-hydroxylase FIH is regulated by Siah-1 under normoxic conditions.* Neurosci Lett, 2008. **433**: p. 209-14.
278. Sallais, J., et al., *Factor inhibiting HIF1-A novel target of SUMOylation in the human placenta.* Oncotarget, 2017. **8**: p. 114002-114018.
279. Zhang, N., et al., *The asparaginyl hydroxylase factor inhibiting HIF-1alpha is an essential regulator of metabolism.* Cell Metab, 2010. **11**: p. 364-78.
280. Locke, A.E., et al., *Genetic studies of body mass index yield new insights for obesity biology.* Nature, 2015. **518**: p. 197-206.
281. Wu, J.H., et al., *Genome-wide association study identifies novel loci associated with concentrations of four plasma phospholipid fatty acids in the de novo lipogenesis pathway: results from the Cohorts for Heart and Aging Research in Genomic Epidemiology (CHARGE) consortium.* Circ Cardiovasc Genet, 2013. **6**: p. 171-83.
282. Zhou, L., et al., *A GWA study reveals genetic loci for body conformation traits in Chinese Laiwu pigs and its implications for human BMI.* Mammalian Genome, 2016. **27**: p. 610-621.
283. Sahana, G., et al., *A genome-wide association scan in pig identifies novel regions associated with feed efficiency trait.* J Anim Sci, 2013. **91**: p. 1041-50.
284. Cockman, M.E., J.D. Webb, and P.J. Ratcliffe, *FIH-Dependent Asparaginyl Hydroxylation of Ankyrin Repeat Domain-Containing Proteins.* Annals of the New York Academy of Sciences, 2009. **1177**: p. 9-18.
285. Cockman, M.E., et al., *Posttranslational hydroxylation of ankyrin repeats in IkappaB proteins by the hypoxia-inducible factor (HIF) asparaginyl hydroxylase, factor inhibiting HIF (FIH).* Proc Natl Acad Sci U S A, 2006. **103**: p. 14767-72.
286. Shin, D.H., et al., *Inhibitor of nuclear factor-kappaB alpha derepresses hypoxia-inducible factor-1 during moderate hypoxia by sequestering factor inhibiting hypoxia-inducible factor from hypoxia-inducible factor 1alpha.* Febs j, 2009. **276**: p. 3470-80.
287. Ferguson, J.E., et al., *ASB4 Is a Hydroxylation Substrate of FIH and Promotes Vascular Differentiation via an Oxygen-Dependent Mechanism.* Molecular and Cellular Biology, 2007. **27**: p. 6407-6419.
288. Cockman, M.E., et al., *Proteomics-based identification of novel factor inhibiting hypoxia-inducible factor (FIH) substrates indicates widespread asparaginyl hydroxylation of ankyrin repeat domain-containing proteins.* Mol Cell Proteomics, 2009. **8**: p. 535-46.
289. Scholz, C.C., et al., *Regulation of IL-1beta-induced NF-kappaB by hydroxylases links key hypoxic and inflammatory signaling pathways.* Proc Natl Acad Sci U S A, 2013. **110**: p. 18490-5.
290. Scholz, C.C., et al., *FIH Regulates Cellular Metabolism through Hydroxylation of the Deubiquitinase OTUB1.* PLoS Biol, 2016. **14**: p. e1002347.
291. Swatek, K.N. and D. Komander, *Ubiquitin modifications.* Cell Research, 2016. **26**(4): p. 399-422.
292. Goldknopf, I.L. and H. Busch, *Isopeptide linkage between nonhistone and histone 2A polypeptides of chromosomal conjugate-protein A24.* Proceedings of the National Academy of Sciences of the United States of America, 1977. **74**: p. 864-868.
293. Hunt, L.T. and M.O. Dayhoff, *Amino-terminal sequence identity of ubiquitin and the nonhistone component of nuclear protein A24.* Biochemical and Biophysical Research Communications, 1977. **74**: p. 650-655.
294. Neefjes, J., T.A. Groothuis, and N.P. Dantuma, *[The 2004 Nobel Prize in Chemistry for the discovery of ubiquitin-mediated protein degradation].* Ned Tijdschr Geneeskd, 2004. **148**: p. 2579-82.
295. Luecken, M.D. and F.J. Theis, *Current best practices in single-cell RNA-seq analysis: a tutorial.* Molecular Systems Biology, 2019. **15**: p. e8746.

296. Ge, Z., et al., *Integrated Genomic Analysis of the Ubiquitin Pathway across Cancer Types.* Cell Rep, 2018. **23**: p. 213-226.e3.
297. Gunter, J., et al., *The functional interplay between the HIF pathway and the ubiquitin system - more than a one-way road.* Exp Cell Res, 2017. **356**: p. 152-159.
298. Metzger, M.B., V.A. Hristova, and A.M. Weissman, *HECT and RING finger families of E3 ubiquitin ligases at a glance.* Journal of Cell Science, 2012. **125**: p. 531-537.
299. Cappadocia, L. and C.D. Lima, *Ubiquitin-like Protein Conjugation: Structures, Chemistry, and Mechanism.* Chem Rev, 2018. **118**: p. 889-918.
300. Suresh, B., et al., *The Importance of Ubiquitination and Deubiquitination in Cellular Reprogramming.* Stem Cells International, 2016. **2016**: p. 6705927.
301. Komander, D., *The emerging complexity of protein ubiquitination.* Biochem Soc Trans, 2009. **37**: p. 937-53.
302. Sadowski, M., et al., *Protein monoubiquitination and polyubiquitination generate structural diversity to control distinct biological processes.* IUBMB Life, 2012. **64**: p. 136-42.
303. Ye, Y. and M. Rape, *Building ubiquitin chains: E2 enzymes at work.* Nat Rev Mol Cell Biol, 2009. **10**: p. 755-64.
304. Kirisako, T., et al., *A ubiquitin ligase complex assembles linear polyubiquitin chains.* Embo j, 2006. **25**: p. 4877-87.
305. Hunter, T., *The Age of Crosstalk: Phosphorylation, Ubiquitination, and Beyond.* Molecular Cell, 2007. **28**: p. 730-738.
306. Nguyen, L.K., W. Kolch, and B.N. Kholodenko, *When ubiquitination meets phosphorylation: a systems biology perspective of EGFR/MAPK signalling.* Cell communication and signaling : CCS, 2013. **11**: p. 52-52.
307. Welcker, M., et al., *The Fbw7 tumor suppressor regulates glycogen synthase kinase 3 phosphorylation-dependent c-Myc protein degradation.* Proceedings of the National Academy of Sciences of the United States of America, 2004. **101**: p. 9085-9090.
308. Yada, M., et al., *Phosphorylation-dependent degradation of c-Myc is mediated by the F-box protein Fbw7.* Embo j, 2004. **23**: p. 2116-25.
309. Lin, H.K., et al., *Phosphorylation-dependent ubiquitylation and degradation of androgen receptor by Akt require Mdm2 E3 ligase.* Embo j, 2002. **21**: p. 4037-48.
310. Gallagher, E., et al., *Activation of the E3 ubiquitin ligase Itch through a phosphorylation-induced conformational change.* Proceedings of the National Academy of Sciences of the United States of America, 2006. **103**: p. 1717-1722.
311. Ohtake, F., et al., *Ubiquitin acetylation inhibits polyubiquitin chain elongation.* EMBO reports, 2015. **16**: p. 192-201.
312. Glass, D.J., *Molecular mechanisms modulating muscle mass.* Trends Mol Med, 2003. **9**: p. 344-50.
313. Cohen, S., et al., *During muscle atrophy, thick, but not thin, filament components are degraded by MuRF1-dependent ubiquitylation.* J Cell Biol, 2009. **185**: p. 1083-95.
314. Sacheck, J.M., et al., *IGF-I stimulates muscle growth by suppressing protein breakdown and expression of atrophy-related ubiquitin ligases, atrogin-1 and MuRF1.* Am J Physiol Endocrinol Metab, 2004. **287**: p. E591-601.
315. Song, R., et al., *Central role of E3 ubiquitin ligase MG53 in insulin resistance and metabolic disorders.* Nature, 2013. **494**: p. 375-9.
316. Chen, S.N., et al., *Human molecular genetic and functional studies identify TRIM63, encoding Muscle RING Finger Protein 1, as a novel gene for human hypertrophic cardiomyopathy.* Circ Res, 2012. **111**: p. 907-19.
317. Günter, J., et al., *The functional interplay between the HIF pathway and the ubiquitin system – more than a one-way road.* Experimental Cell Research, 2017. **356**: p. 152-159.
318. Komander, D., M.J. Clague, and S. Urbé, *Breaking the chains: structure and function of the deubiquitinases.* Nature Reviews Molecular Cell Biology, 2009. **10**: p. 550-563.

319. Fraile, J.M., et al., *Deubiquitinases in cancer: new functions and therapeutic options.* Oncogene, 2012. **31**: p. 2373-2388.
320. Yao, T., et al., *Proteasome recruitment and activation of the Uch37 deubiquitinating enzyme by Adrm1.* Nat Cell Biol, 2006. **8**: p. 994-1002.
321. Jiao, L., et al., *Mechanism of the Rpn13-induced activation of Uch37.* Protein & Cell, 2014. **5**: p. 616-630.
322. Hamazaki, J., et al., *A novel proteasome interacting protein recruits the deubiquitinating enzyme UCH37 to 26S proteasomes.* Embo j, 2006. **25**: p. 4524-36.
323. Jensen, D.E., et al., *BAP1: a novel ubiquitin hydrolase which binds to the BRCA1 RING finger and enhances BRCA1-mediated cell growth suppression.* Oncogene, 1998. **16**: p. 1097-1112.
324. Nishikawa, H., et al., *BRCA1-associated protein 1 interferes with BRCA1/BARD1 RING heterodimer activity.* Cancer Res, 2009. **69**: p. 111-9.
325. Bishop, P., D. Rocca, and J.M. Henley, *Ubiquitin C-terminal hydrolase L1 (UCH-L1): structure, distribution and roles in brain function and dysfunction.* The Biochemical journal, 2016. **473**: p. 2453-2462.
326. D'Arcy, P., X. Wang, and S. Linder, *Deubiquitinase inhibition as a cancer therapeutic strategy.* Pharmacology & Therapeutics, 2015. **147**: p. 32-54.
327. Daou, S., et al., *Monoubiquitination of ASXLs controls the deubiquitinase activity of the tumor suppressor BAP1.* Nature Communications, 2018. **9**: p. 4385.
328. Masoomian, B., J.A. Shields, and C.L. Shields, *Overview of BAP1 cancer predisposition syndrome and the relationship to uveal melanoma.* Journal of Current Ophthalmology, 2018. **30**: p. 102-109.
329. Ye, Y., et al., *Dissection of USP catalytic domains reveals five common insertion points.* Mol Biosyst, 2009. **5**: p. 1797-808.
330. Toko, H., et al., *Csx/Nkx2-5 is required for homeostasis and survival of cardiac myocytes in the adult heart.* J Biol Chem, 2002. **277**: p. 24735-43.
331. Mevissen, T.E., et al., *OTU deubiquitinases reveal mechanisms of linkage specificity and enable ubiquitin chain restriction analysis.* Cell, 2013. **154**: p. 169-84.
332. Nakada, S., et al., *Non-canonical inhibition of DNA damage-dependent ubiquitination by OTUB1.* Nature, 2010. **466**: p. 941-6.
333. Damgaard, R.B., et al., *The Deubiquitinase OTULIN Is an Essential Negative Regulator of Inflammation and Autoimmunity.* Cell, 2016. **166**: p. 1215-1230.e20.
334. Elliott, P.R., et al., *Molecular basis and regulation of OTULIN-LUBAC interaction.* Mol Cell, 2014. **54**: p. 335-48.
335. Liu, H., et al., *The Machado–Joseph Disease Deubiquitinase Ataxin-3 Regulates the Stability and Apoptotic Function of p53.* PLOS Biology, 2016. **14**: p. e2000733.
336. Faggiano, S., et al., *Allosteric regulation of deubiquitylase activity through ubiquitination.* Frontiers in Molecular Biosciences, 2015. **2**.
337. Kwon, Y.T. and A. Ciechanover, *The Ubiquitin Code in the Ubiquitin-Proteasome System and Autophagy.* Trends in Biochemical Sciences, 2017. **42**: p. 873-886.
338. Opal, P., *Ataxin*, in *Encyclopedia of Movement Disorders*, K. Kompoliti and L.V. Metman, Editors. 2010, Academic Press: Oxford. p. 94-95.
339. Sims, J.J. and R.E. Cohen, *Linkage-specific avidity defines the lysine 63-linked polyubiquitin-binding preference of rap80.* Mol Cell, 2009. **33**: p. 775-83.
340. Winborn, B.J., et al., *The deubiquitinating enzyme ataxin-3, a polyglutamine disease protein, edits Lys63 linkages in mixed linkage ubiquitin chains.* The Journal of biological chemistry, 2008. **283**: p. 26436-26443.
341. Cooper, E.M., et al., *K63-specific deubiquitination by two JAMM/MPN+ complexes: BRISC-associated Brcc36 and proteasomal Poh1.* The EMBO journal, 2009. **28**: p. 621-631.

342. Shao, G., et al., *The Rap80-BRCC36 de-ubiquitinating enzyme complex antagonizes RNF8-Ubc13-dependent ubiquitination events at DNA double strand breaks.* Proc Natl Acad Sci U S A, 2009. **106**: p. 3166-71.
343. Wang, B. and S.J. Elledge, *Ubc13/Rnf8 ubiquitin ligases control foci formation of the Rap80/Abraxas/Brca1/Brcc36 complex in response to DNA damage.* Proc Natl Acad Sci U S A, 2007. **104**: p. 20759-63.
344. Cope, G.A., et al., *Role of predicted metalloprotease motif of Jab1/Csn5 in cleavage of Nedd8 from Cul1.* Science, 2002. **298**: p. 608-11.
345. Gallery, M., et al., *The JAMM motif of human deubiquitinase Poh1 is essential for cell viability.* Molecular Cancer Therapeutics, 2007. **6**: p. 262-268.
346. *Structure and Implications of JAMM, a Novel Metalloprotease.* PLOS Biology, 2003. **2**: p. e17.
347. Cao, S., et al., *Structural Insight into Ubiquitin-Like Protein Recognition and Oligomeric States of JAMM/MPN+ Proteases.* Structure, 2017. **25**: p. 823-833.e6.
348. Liang, J., et al., *MCP-induced protein 1 deubiquitinates TRAF proteins and negatively regulates JNK and NF-kappaB signaling.* The Journal of experimental medicine, 2010. **207**: p. 2959-2973.
349. Das, T., et al., *Regulation of Deubiquitinating Enzymes by Post-Translational Modifications.* Int J Mol Sci, 2020. **21**.
350. Das, T., et al., *Regulation of Deubiquitinating Enzymes by Post-Translational Modifications.* International journal of molecular sciences, 2020. **21**: p. 4028.
351. Yang, W.L., X. Zhang, and H.K. Lin, *Emerging role of Lys-63 ubiquitination in protein kinase and phosphatase activation and cancer development.* Oncogene, 2010. **29**: p. 4493-4503.
352. Bi, H.-L., et al., *The deubiquitinase UCHL1 regulates cardiac hypertrophy by stabilizing epidermal growth factor receptor.* Science Advances, 2020. **6**: p. eaax4826.
353. Hu, M., et al., *Deubiquitinase Inhibitor Auranofin Attenuated Cardiac Hypertrophy by Blocking NF-κB Activation.* Cellular Physiology and Biochemistry, 2018. **45**: p. 2421-2430.
354. Yu, S.M., et al., *The deubiquitinase ubiquitin-specific protease 20 is a positive modulator of myocardial β(1)-adrenergic receptor expression and signaling.* J Biol Chem, 2019. **294**: p. 2500-2518.
355. Yan, K., et al., *The role of K63-linked polyubiquitination in cardiac hypertrophy.* Journal of cellular and molecular medicine, 2018. **22**: p. 4558-4567.
356. Wang, X., et al., *TRAF5-mediated Lys-63-linked Polyubiquitination Plays an Essential Role in Positive Regulation of RORγt in Promoting IL-17A Expression.* J Biol Chem, 2015. **290**: p. 29086-94.
357. Ji, Y.X., et al., *The deubiquitinating enzyme cylindromatosis mitigates nonalcoholic steatohepatitis.* Nat Med, 2018. **24**: p. 213-223.
358. Li, L., et al., *The deubiquitinase USP13 stabilizes the anti-inflammatory receptor IL-1R8/Sigirr to suppress lung inflammation.* EBioMedicine, 2019. **45**: p. 553-562.
359. Zhao, Y., et al., *OTUD4 Is a Phospho-Activated K63 Deubiquitinase that Regulates MyD88-Dependent Signaling.* Mol Cell, 2018. **69**: p. 505-516.e5.
360. Borodovsky, A., et al., *Chemistry-Based Functional Proteomics Reveals Novel Members of the Deubiquitinating Enzyme Family.* Chemistry & Biology, 2002. **9**: p. 1149-1159.
361. *Database resources of the National Center for Biotechnology Information.* Nucleic Acids Res, 2018. **46**(D1): p. D8-d13.
362. Herhaus, L., et al., *OTUB1 enhances TGFbeta signalling by inhibiting the ubiquitylation and degradation of active SMAD2/3.* Nat Commun, 2013. **4**: p. 2519.
363. Clague, M.J., C. Heride, and S. Urbe, *The demographics of the ubiquitin system.* Trends Cell Biol, 2015. **25**: p. 417-26.
364. Saldana, M., et al., *Otubain 1: a non-canonical deubiquitinase with an emerging role in cancer.* Endocrine-related cancer, 2019. **26**: p. R1-R14.

365. Pasupala, N., et al., *OTUB1 non-catalytically stabilizes the E2 ubiquitin-conjugating enzyme UBE2E1 by preventing its autoubiquitination.* J Biol Chem, 2018. **293**: p. 18285-18295.
366. Dong, W., et al., *Activated Protein C Ameliorates Renal Ischemia-Reperfusion Injury by Restricting Y-Box Binding Protein-1 Ubiquitination.* J Am Soc Nephrol, 2015. **26**: p. 2789-99.
367. Wang, X., et al., *OTUB1 inhibits CNS autoimmunity by preventing IFN-gamma-induced hyperactivation of astrocytes.* Embo j, 2019. **38**.
368. Mulas, F., et al., *The deubiquitinase OTUB1 augments NF-κB-dependent immune responses in dendritic cells in infection and inflammation by stabilizing UBC13.* Cellular & Molecular Immunology, 2020.
369. Balakirev, M.Y., et al., *Otubains: a new family of cysteine proteases in the ubiquitin pathway.* EMBO reports, 2003. **4**: p. 517-522.
370. Edelmann, M.J., et al., *Structural basis and specificity of human otubain 1-mediated deubiquitination.* Biochem J, 2009. **418**: p. 379-90.
371. Komander, D., M.J. Clague, and S. Urbe, *Breaking the chains: structure and function of the deubiquitinases.* Nat Rev Mol Cell Biol, 2009. **10**: p. 550-63.
372. Edelmann, Mariola J., et al., *Structural basis and specificity of human otubain 1-mediated deubiquitination.* Biochemical Journal, 2009. **418**: p. 379-390.
373. Wiener, R., et al., *The mechanism of OTUB1-mediated inhibition of ubiquitination.* Nature, 2012. **483**: p. 618-22.
374. Altun, M., et al., *The human otubain2-ubiquitin structure provides insights into the cleavage specificity of poly-ubiquitin-linkages.* PLoS One, 2015. **10**: p. e0115344.
375. Sivakumar, D., et al., *Activation and selectivity of OTUB-1 and OTUB-2 deubiquitinylases.* J Biol Chem, 2020. **295**: p. 6972-6982.
376. Schwanhäusser, B., et al., *Global quantification of mammalian gene expression control.* Nature, 2011. **473**: p. 337-342.
377. Wang, Y., et al., *OTUB1-catalyzed deubiquitination of FOXM1 facilitates tumor progression and predicts a poor prognosis in ovarian cancer.* Oncotarget, 2016. **7**: p. 36681-36697.
378. Higurashi, M., et al., *High expression of FOXM1 critical for sustaining cell proliferation in mitochondrial DNA-less liver cancer cells.* Experimental Cell Research, 2020. **389**: p. 111889.
379. Karunarathna, U., et al., *OTUB1 inhibits the ubiquitination and degradation of FOXM1 in breast cancer and epirubicin resistance.* Oncogene, 2016. **35**: p. 1433-44.
380. Zhou, K., et al., *OTUB1-mediated deubiquitination of FOXM1 up-regulates ECT-2 to promote tumor progression in renal cell carcinoma.* Cell & bioscience, 2020. **10**: p. 50-50.
381. Zhou, H., et al., *OTUB1 promotes esophageal squamous cell carcinoma metastasis through modulating Snail stability.* Oncogene, 2018. **37**: p. 3356-3368.
382. Goncharov, T., et al., *OTUB1 modulates c-IAP1 stability to regulate signalling pathways.* Embo j, 2013. **32**: p. 1103-14.
383. Jahan, A.S., et al., *OTUB1 Is a Key Regulator of RIG-I-Dependent Immune Signaling and Is Targeted for Proteasomal Degradation by Influenza A NS1.* Cell Reports, 2020. **30**: p. 1570-1584.e6.
384. Edelmann, M.J., et al., *Post-translational modification of the deubiquitinating enzyme otubain 1 modulates active RhoA levels and susceptibility to Yersinia invasion.* Febs j, 2010. **277**: p. 2515-30.
385. Wang, P., et al., *Tau interactome mapping based identification of Otub1 as Tau deubiquitinase involved in accumulation of pathological Tau forms in vitro and in vivo.* Acta Neuropathol, 2017. **133**: p. 731-749.
386. Stanisić, V., et al., *OTU Domain-containing ubiquitin aldehyde-binding protein 1 (OTUB1) deubiquitinates estrogen receptor (ER) alpha and affects ERalpha transcriptional activity.* J Biol Chem, 2009. **284**: p. 16135-45.

387. Wang, P., et al., *Tau interactome mapping based identification of Otub1 as Tau deubiquitinase involved in accumulation of pathological Tau forms in vitro and in vivo.* Acta Neuropathol, 2017. **133**: p. 731-749.
388. Pei, H.Z., et al., *Ovarian tumor domain-containing ubiquitin aldehyde binding protein 1 inhibits inflammation by regulating Nur77 stability.* Cellular Signalling, 2019. **59**: p. 85-95.
389. Li, Y., et al., *Preventing abnormal NF-kappaB activation and autoimmunity by Otub1-mediated p100 stabilization.* Cell Res, 2019.
390. Zhou, X., et al., *The deubiquitinase Otub1 controls the activation of CD8+ T cells and NK cells by regulating IL-15-mediated priming.* Nature Immunology, 2019. **20**(7): p. 879-889.
391. Juang, Y.C., et al., *OTUB1 co-opts Lys48-linked ubiquitin recognition to suppress E2 enzyme function.* Mol Cell, 2012. **45**: p. 384-97.
392. Sato, Y., et al., *Molecular basis of Lys-63-linked polyubiquitination inhibition by the interaction between human deubiquitinating enzyme OTUB1 and ubiquitin-conjugating enzyme UBC13.* The Journal of biological chemistry, 2012. **287**: p. 25860-25868.
393. Wiener, R., et al., *The mechanism of OTUB1-mediated inhibition of ubiquitination.* Nature, 2012. **483**: p. 618-622.
394. Li, Y., et al., *Monoubiquitination is critical for ovarian tumor domain-containing ubiquitin aldehyde binding protein 1 (Otub1) to suppress UbcH5 enzyme and stabilize p53 protein.* J Biol Chem, 2014. **289**: p. 5097-108.
395. Baietti, M.F., et al., *OTUB1 triggers lung cancer development by inhibiting RAS monoubiquitination.* EMBO molecular medicine, 2016. **8**: p. 288-303.
396. Chen, Y., et al., *Otub1 stabilizes MDMX and promotes its proapoptotic function at the mitochondria.* Oncotarget, 2017. **8**: p. 11053-11062.
397. Sun, X.X., K.B. Challagundla, and M.S. Dai, *Positive regulation of p53 stability and activity by the deubiquitinating enzyme Otubain 1.* Embo j, 2012. **31**: p. 576-92.
398. Zhao, L., et al., *OTUB1 protein suppresses mTOR complex 1 (mTORC1) activity by deubiquitinating the mTORC1 inhibitor DEPTOR.* J Biol Chem, 2018. **293**: p. 4883-4892.
399. Liu, T., et al., *The deubiquitylase OTUB1 mediates ferroptosis via stabilization of SLC7A11.* Cancer Research, 2019: p. canres.3037.2018.
400. Iglesias-Gato, D., et al., *OTUB1 de-ubiquitinating enzyme promotes prostate cancer cell invasion in vitro and tumorigenesis in vivo.* Molecular Cancer, 2015. **14**: p. 8.
401. Zhang, Y., et al., *OTUB1 overexpression in mesangial cells is a novel regulator in the pathogenesis of glomerulonephritis through the decrease of DCN level.* PloS one, 2012. **7**(1): p. e29654.
402. Wang, G., et al., *PTEN regulates RPA1 and protects DNA replication forks.* Cell research, 2015. **25**: p. 1189-1204.
403. Bisserier, M., et al., *AAV1.SERCA2a Gene Therapy Reverses Pulmonary Fibrosis by Blocking the STAT3/FOXM1 Pathway and Promoting the SNON/SKI Axis.* Molecular Therapy, 2020. **28**: p. 394-410.
404. Xuan, N.T., et al., *Regulation of p38MAPK-mediated dendritic cell functions by the deubiquitylase otubain 1.* HLA, 2019. **93**: p. 462-470.
405. Li, S., et al., *Regulation of virus-triggered signaling by OTUB1- and OTUB2-mediated deubiquitination of TRAF3 and TRAF6.* The Journal of biological chemistry, 2010. **285**: p. 4291-4297.
406. Peng, Y., R. Xu, and X. Zheng, *HSCARG negatively regulates the cellular antiviral RIG-I like receptor signaling pathway by inhibiting TRAF3 ubiquitination via recruiting OTUB1.* PLoS Pathog, 2014. **10**: p. e1004041.
407. Xie, M., et al., *Scavenger receptor A impairs interferon response to HBV infection by limiting TRAF3 ubiquitination through recruiting OTUB1.* The FEBS Journal, 2020. **287**: p. 310-324.
408. Zheng, X., et al., *TRIM25 Is Required for the Antiviral Activity of Zinc Finger Antiviral Protein.* J Virol, 2017. **91**.

409. Herhaus, L., et al., *Casein kinase 2 (CK2) phosphorylates the deubiquitylase OTUB1 at Ser16 to trigger its nuclear localization.* Sci Signal, 2015. **8**: p. ra35.
410. Huguenin-Dezot, N., et al., *Synthesis of Isomeric Phosphoubiquitin Chains Reveals that Phosphorylation Controls Deubiquitinase Activity and Specificity.* Cell reports, 2016. **16**: p. 1180-1193.
411. Bhuripanyo, K., et al., *Identifying the substrate proteins of U-box E3s E4B and CHIP by orthogonal ubiquitin transfer.* Sci Adv, 2018. **4**: p. e1701393.
412. Karim, A.F., et al., *Proteomics and Network Analyses Reveal Inhibition of Akt-mTOR Signaling in CD4(+) T Cells by Mycobacterium tuberculosis Mannose-Capped Lipoarabinomannan.* Proteomics, 2017. **17**.
413. Lin, J.T., et al., *Naive CD4 t cell proliferation is controlled by mammalian target of rapamycin regulation of GRAIL expression.* J Immunol, 2009. **182**: p. 5919-28.
414. Hao, M., et al., *Targeting CXCR7 improves the efficacy of breast cancer patients with tamoxifen therapy.* Biochem Pharmacol, 2018. **147**: p. 128-140.
415. Stempin, C.C., et al., *GRAIL and Otubain-1 are Related to T Cell Hyporesponsiveness during Trypanosoma cruzi Infection.* PLoS Negl Trop Dis, 2017. **11**: p. e0005307.
416. Wang, M., D. Windgassen, and E.T. Papoutsakis, *Comparative analysis of transcriptional profiling of CD3+, CD4+ and CD8+ T cells identifies novel immune response players in T-cell activation.* BMC Genomics, 2008. **9**: p. 225.
417. Xie, L., et al., *OTUB1 attenuates neuronal apoptosis after intracerebral hemorrhage.* Mol Cell Biochem, 2016. **422**: p. 171-180.
418. Lee, J., et al., *Genome-wide association analysis identifies multiple loci associated with kidney disease-related traits in Korean populations.* PLoS One, 2018. **13**: p. e0194044.
419. Xue, Z., et al., *Data integration in physiology using Bayes' rule and minimum Bayes' factors: deubiquitylating enzymes in the renal collecting duct.* Physiol Genomics, 2017. **49**: p. 151-159.
420. Petrova, D.T., et al., *Differential kidney proteome profiling in a murine model of renal fibrosis under treatment with mycophenolate mofetil.* Pathobiology, 2011. **78**: p. 162-70.
421. Xu, L., et al., *Silencing of OTUB1 inhibits migration of human glioma cells in vitro.* Neuropathology, 2017. **37**: p. 217-226.
422. Weng, W., et al., *OTUB1 promotes tumor invasion and predicts a poor prognosis in gastric adenocarcinoma.* Am J Transl Res, 2016. **8**: p. 2234-44.
423. Wang, Y.Q., et al., *Upregulation of the Non-Coding RNA OTUB1-isoform 2 Contributes to Gastric Cancer Cell Proliferation and Invasion and Predicts Poor Gastric Cancer Prognosis.* Int J Biol Sci, 2016. **12**: p. 545-57.
424. Iglesias-Gato, D., et al., *OTUB1 de-ubiquitinating enzyme promotes prostate cancer cell invasion in vitro and tumorigenesis in vivo.* Mol Cancer, 2015. **14**: p. 8.
425. Ni, Q., et al., *Expression of OTUB1 in hepatocellular carcinoma and its effects on HCC cell migration and invasion.* Acta Biochim Biophys Sin (Shanghai), 2017. **49**: p. 680-688.
426. Yuan, L., et al., *miR-542-3p inhibits colorectal cancer cell proliferation, migration and invasion by targeting OTUB1.* Am J Cancer Res, 2017. **7**: p. 159-172.
427. Zhou, Y., et al., *OTUB1 promotes metastasis and serves as a marker of poor prognosis in colorectal cancer.* Mol Cancer, 2014. **13**: p. 258.
428. Liu, X., et al., *Colon cancer bears overexpression of OTUB1.* Pathol Res Pract, 2014. **210**: p. 770-3.

2. Aims of the thesis

The deubiquitinase OTUB1 plays an important role in the regulation of several processes *in vitro* and *in vivo* and has been linked to the development and/or progression of diverse pathologies. However, the physiological function of OTUB1 is unknown. Interestingly, we previously discovered that FIH hydroxylates OTUB1 on Asn22, regulating cellular energy metabolism. FIH deletion in mice leads to a metabolic phenotype, but the underlying molecular mechanisms are unclear. Understanding the molecular interaction of FIH and OTUB1 in detail as well as its relevance for physiology would enhance our knowledge about oxygen-dependent and ubiquitin-dependent regulations. In addition, both FIH and OTUB1 are considered as potential therapeutic targets in several different diseases. The characterization of the molecular and physiological interplay of FIH and OTUB1 may help identifying novel therapeutic options.

The goal of this thesis was to analyze the molecular mechanism of the interaction between FIH and OTUB1 further as well as its potential physiologic relevance. To achieve this, the specific aims were:

1) Analysis of the FIH-dependent regulation of OTUB1 in detail.

2) Characterization of the physiological function of OTUB1 in mice.

3. Oxygen-dependent bond formation with FIH regulates the activity of the client protein OTUB1

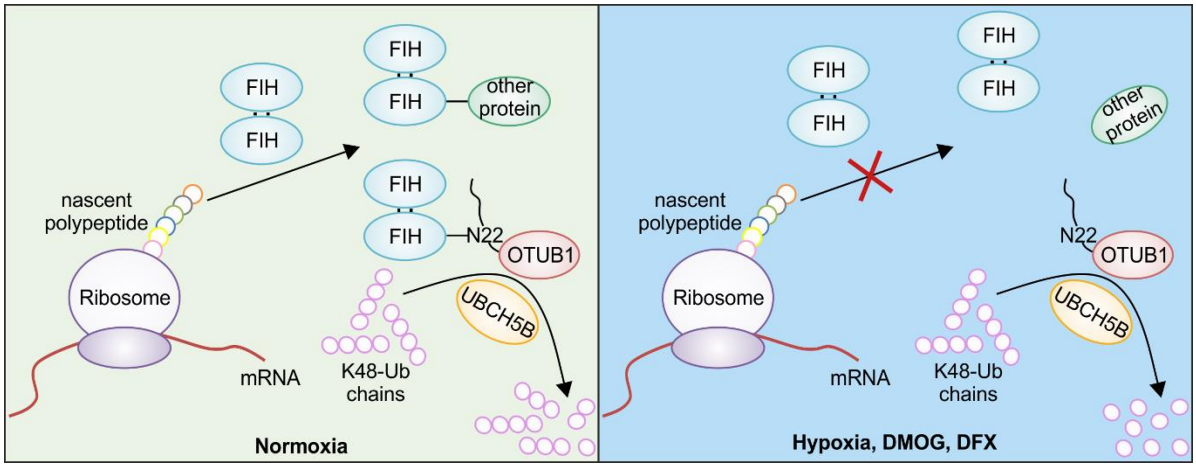

HIGHLIGHTS

- FIH forms a (likely amide) bond with client proteins
- Bond formation is highly hypoxia sensitive and occurs co-translationally
- FIH forms a heterotrimer with the client protein OTUB1 (FIH_2OTUB1_1)
- Complex formation between OTUB1 and FIH regulates OTUB1 deubiquitinase activity
- Bond formation by hydroxylases is an alternative mechanism for hypoxia adaptation

Oxygen-dependent bond formation with FIH regulates the activity of the client protein OTUB1

Christina Pickel[a,1] Julia Günter[a,b], Amalia Ruiz-Serrano[a], Patrick Spielmann[a], Jacqueline-Alba Fabrizio[c], Witold Wolski[d], Daniel J. Peet[c], Roland H. Wenger[a,b,§], Carsten C. Scholz[a,b,§]

[a]Institute of Physiology, University of Zurich, 8057 Zurich, Switzerland

[b]National Centre of Competence in Research 'Kidney.CH', Switzerland

[c]School of Biological Sciences, University of Adelaide, Adelaide, SA, 5005, Australia

[d]Functional Genomics Center Zurich, University of Zurich, 8057 Zurich, Switzerland.

[§]These authors contributed equally.

Short title: FIH regulates OTUB1 deubiquitinase activity.

Correspondence:

Dr. Carsten Scholz
Institute of Physiology
University of Zurich
Winterthurerstr. 190
8057 Zurich
Switzerland
E-mail: carsten.scholz@uzh.ch
Tel: +41 44 635 50 75

Prof. Roland H. Wenger
Institute of Physiology
University of Zurich
Winterthurerstr. 190
8057 Zurich
Switzerland
E-mail: roland.wenger@access.uzh.ch
Tel: +41 44 635 50 65

ABSTRACT

Protein:protein interactions are the basis of molecular communication and are usually of transient non-covalent nature, while covalent interactions other than ubiquitination are rare. For cellular adaptations, the cellular oxygen and peroxide sensor factor inhibiting HIF (FIH) confers oxygen and oxidant stress sensitivity to the hypoxia inducible factor (HIF) by asparagine hydroxylation. We investigated whether FIH contributes to hypoxia adaptation also through other mechanisms and identified a highly hypoxia sensitive, likely covalent, bond formation by FIH with several client proteins, including the deubiquitinase ovarian tumor domain containing ubiquitin aldehyde binding protein 1 (OTUB1). Biochemical analyses were consistent with a co-translational amide bond formation between FIH and OTUB1, occurring within mammalian and bacterial cells but not between separately purified proteins. Bond formation is catalysed by FIH and highly dependent on oxygen availability in the cellular microenvironment. Within cells, a heterotrimeric complex is formed, consisting of two FIH and one covalently linked OTUB1. Complexation of OTUB1 by FIH regulates OTUB1 deubiquitinase activity. Our findings reveal an alternative mechanism for hypoxia adaptation with remarkably high oxygen sensitivity, mediated through covalent protein-protein interactions catalysed by an asparagine modifying dioxygenase.

KEYWORDS: hydroxylase; HIF; hypoxia; oxygen sensor; deubiquitinase; ubiquitin system

INTRODUCTION

Cellular oxygen sensing is of vital importance for cells and tissues in order to adapt to hypoxic conditions when cellular oxygen demand exceeds its supply [1]. The best characterized cellular oxygen sensors are the prolyl-4-hydroxylase domain (PHD) proteins 1-3 and factor inhibiting HIF (FIH) [2]. PHDs hydroxylate two different prolines and FIH hydroxylates one asparagine residue of HIFα subunits [2]. Besides molecular oxygen, these enzymes requires Fe^{2+} and ascorbate or other reducing agents as co-factors and 2-oxoglutarate as co-substrate in order to reduce molecular oxygen and oxidize the substrate protein (hydroxylation) and 2-oxoglutarate (conversion to succinate) [3, 4]. Proline-4-hydroxylation of HIFα leads to its proteasomal degradation whereas asparagine hydroxylation inhibits its interaction with the transcriptional co-activators p300 and CBP, attenuating HIF-dependent gene transactivation [2]. While in higher organisms the only known reaction of 2-oxoglutarate-dependent dioxygenases is hydroxylation [5], in lower organisms they also catalyse ring expansion, rearrangement, desaturation, halogenation and epoxidation [6].

Beside oxygen, FIH also senses peroxide [7]. Interestingly, FIH is more sensitive to H_2O_2 than the PHDs [7]. Peroxide reduces FIH enzymatic activity, leading to decreased HIF-1α asparagine hydroxylation and higher transcriptional activity [7]. This indicates that FIH functionally integrates oxidant stress and hypoxia in cellular signalling.

In vivo, FIH is essential for the regulation of energy metabolism [8, 9]. Amongst others, FIH deletion leads to an increased metabolic rate, increased glucose and lipid homeostasis and increased oxidative metabolism [8, 9]. The FIH-dependent regulation of energy metabolism is at least partly independent of HIF [8]. Therefore, a key question remaining is whether FIH regulates additional substrates outside of the HIF pathway that contribute to the observed phenotype. FIH has previously been shown to target proteins for hydroxylation other than HIFα, including ankyrin repeat domain (ARD)-containing proteins [10-15]. However, whether FIH-dependent hydroxylation of these proteins is functionally relevant for the regulation of energy metabolism is unclear [11, 16]. We recently demonstrated that FIH

interacts with the deubiquitinase (DUB) ovarian tumor domain containing ubiquitin aldehyde binding protein 1 (OTUB1) and hydroxylates it on asparagine 22 (N22), regulating cellular energy metabolism [17, 18].

OTUB1 is a ubiquitously expressed DUB with one of the highest expression levels of all DUBs [19, 20]. OTUB1 cleaves K48-ubiquitin chains through its canonical enzymatic activity, preventing proteasomal degradation of substrate proteins [21, 22]. In addition, OTUB1 inhibits E2 ubiquitin-conjugating enzymes independent of its enzymatic activity, impeding ubiquitin chain formation [23-25]. OTUB1 enzymatic activity is regulated by complexation with E2 enzymes and free ubiquitin [26, 27]. A major characteristic of DUBs is their frequent occurrence in protein complexes, which controls DUB activity [28]. However, whether other proteins in addition to E2 enzymes and free ubiquitin affect OTUB1 activity by protein complexation is unknown.

In this study, we further investigated the molecular interplay between FIH and OTUB1. We show evidence for an unexpected formation of a previously unknown strong, likely covalent, interaction between FIH and OTUB1. We demonstrate that this formation has functional consequences for OTUB1 deubiquitinase activity and is highly oxygen sensitive but relatively slow, indicating a role in chronic hypoxia adaptation. Interestingly, this type of FIH-dependent bond formation is likely not restricted to the substrate OTUB1.

MATERIALS AND METHODS

Cell culture and transient transfection

Human HEK293 (embryonic kidney), MCF7 (breast adenocarcinoma) and Hep3B (hepatocellular carcinoma) cell lines were cultured in DMEM containing 4.5 g/l glucose, sodium pyruvate and L-glutamine (Sigma-Aldrich, St Louis, MO, USA), supplemented with 10% heat-inactivated fetal bovine serum (Gibco by Life Technologies, Carlsbad, Ca, USA) and 100 U/ml penicillin and 100 µg/ml streptomycin (Sigma-Aldrich). Transient transfection of siRNAs and plasmids was performed using lipofectamine 2000 reagent according to the manufacturer's instructions (Invitrogen, Carlsbad, CA, USA) or polyethylenimine (PEI; Polysciences Inc., Warrington, PA) as described previously [29].

Cell treatments

Cycloheximide (CHX; Sigma-Aldrich) was dissolved in ethanol, desferrioxamine (DFX; Sigma-Aldrich), (+)-sodium L-ascorbate (Sigma-Aldrich), 2-oxoglutarate (Sigma-Aldrich), diethyl 2-oxoglutarate (DE-2OG; Sigma-Aldrich) and iron (II) sulfate (Sigma-Aldrich) in H_2O, and dimethyloxalylglycine (DMOG; Frontier Scientific, Logan, UT, USA) and FG-4592 (Roxadustat; Selleckchem, Houston, TX, USA) in dimethylsulfoxide (DMSO, Sigma-Aldrich). Hypoxic incubations were performed using the Invivo$_2$ 400 humidified cell culture workstation (Baker Ruskinn, Bridgend, South Wales, UK) operated at 0.2% O_2 and 5% CO_2 as described previously [29] or in humidified oxygen-regulated cell culture incubators (Binder GmbH, Tuttlingen, Germany) operated at 1% - 8% O_2 and 5% CO_2. If not otherwise indicated, "normoxia" refers to the standard oxygen concentration in the gas phase within a cell culture incubator at 500 m altitude (18.5% O_2) and "hypoxia" to 0.2% O_2 [30].

Plasmids and siRNAs

The plasmid encoding human wildtype FIH-V5 was kindly provided by Dr. Eric Metzen (University of Duisburg-Essen, Essen, Germany). The plasmids encoding FIH H199A-V5 and MBP-FIH have previously been described [31]. The plasmid coding for human wildtype FLAG-OTUB1 (containing two consecutive FLAG tags) [32] was a kind gift of Dr. Mu-Shui Dai (Oregon Health & Science University, Portland, OR, USA). The transfer vector pET3a and the polycistronic expression vector pST39 [33] were kind gifts from Prof. Song Tan (Pennsylvania State University, PA, USA).

Nontargeting siRNA (siNT: 5'-gcuccggagaacuaccagaguauua-3') as well as siRNA targeting human FIH (siFIH: sequence F1, 5'-guugcgcaguuauagcuuctt-3') and the 3'UTR of human OTUB1 (siOTUB1: siRNA-4, 5'-gugguuguaaaugguccuatt-3') were purchased from Microsynth (Balgrach, Switzerland) according to previously reported sequences [10, 34].

Generation of OTUB1 mutants by site-directed mutagenesis

The human FLAG-OTUB1 N22A mutant was previously described [18]. The human FLAG-OTUB1 S16A, S18A, S16A/S18A, C23A, C23S, C91A, C91S point mutants were generated using the Quikchange II XL Site-Directed Mutagenesis kit (Agilent Technologies, Santa Clara, CA, USA) according to the manufacturer's instructions and using the plasmid encoding wildtype FLAG-OTUB1 as template. The mutations of the target sites were confirmed by sequencing.

Immunoblot analysis

Cells were lysed in 150 mM NaCl, 25 mM Tris-HCl (pH 8.0), 1 mM EDTA, 1% NP-40, freshly supplemented with protease inhibitor cocktail (Sigma-Aldrich), 1 mM PMSF and 1 mM Na_3VO_4 and 100 mM iodoacetamide where indicated. Protein concentrations of lysates were determined using the BCA assay (Thermo Fisher Scientific, Waltham, MA, USA). Equal

amounts of proteins were mixed with 5x loading dye (250 mM Tris-HCl pH 6.8, 30% glycerol, 858 mM β-mercaptoethanol, 10% SDS, 0.05% bromophenolblue), separated by SDS-PAGE, electro-transferred to nitrocellulose membranes and detected using anti-FIH antibody (Novus Biologicals, Littleton CO, USA; NBP1-30333), anti-V5 antibody (Invitrogen; R960-025), anti-OTUB1 antibody (Cell Signaling Technology, Danvers, MA, USA; 3783), anti-FLAG antibody (Sigma-Aldrich; F3165), anti-ubiquitin antibody (clone P4D1; Cell Signaling Technology; 3936), anti-HIF-1α antibody (BD Biosciences, San Jose, CA, USA; 610959), anti-HIF-2α antibody (Bethyl Laboratories, Montgomery, TX, USA; A700-003), anti-GFP antibody (Roche Diagnostics, Rotkreuz, Switzerland; 11814460001), anti-β-actin antibody (Sigma-Aldrich; A5441), anti-α-tubulin antibody (Cell Signaling; 2144), anti-SMC1 antibody (Abcam, Cambridge, UK; 9262) and horseradish peroxidase-coupled secondary antibodies (Thermo Fisher Scientific; 31430, 31460). Bound antibodies were detected with SuperSignal enhanced chemiluminescence substrate (Thermo Fisher Scientific) and chemiluminescence was recorded using a CCD camera (LAS 4000 mini, Fujifilm, Tokyo, Japan). ImageQuant TL gel analysis software (GE Healthcare, Version 8.1) was used for quantification as previously described [35]. If not indicated otherwise, values were normalized to the respective loading control and the sum of the intensities of all samples of one signal of each experiment.

Denaturing urea and blue native electrophoresis

For urea electrophoresis, cells were harvested in 30 mM Tris-HCl (pH 8.5), 7 M urea, 2 M thiourea, 0.4% CHAPS, supplemented with protease inhibitor cocktail (Sigma-Aldrich) as described [36]. The protein concentration was determined by Bradford assay and equal protein amounts were separated by 8% urea gel electrophoresis according to the previous description [37, 38]. For blue native electrophoresis, cells were harvested in 20 mM Bis-Tris (pH 7.0), 500 mM ε-aminocaproic acid, 10% glycerol, supplemented with 1 mM PMSF, 10 µg/ml aprotinin, 10 µg/ml leupeptin and 1 mM Na_3VO_4, and lysed by dounce homogenisation. The protein concentration was determined by Bradford assay and equal protein amounts were separated

by 15% blue native gel electrophoresis according to a previous description [39]. Following electrophoresis, proteins were transferred to nitrocellulose membranes and detected using antibodies as described above.

Two-dimensional gel electrophoresis

Cell lysates were prepared for native protein analysis and separated by blue native electrophoresis as described above. Single lanes were cut and separated in the second dimension by SDS-PAGE in 100 mM Tris-HCl (pH 6.8), 12% glycerol, 343 mM β-mercaptoethanol, 4% SDS, 0.02% bromophenolblue [40]. Following transfer to nitrocellulose membranes, proteins were detected using antibodies as described above.

Bacterial expression and purification of His- and MBP-tagged recombinant proteins

The plasmids encoding human pENTR4-OTUB1 WT/N22A were described previously [18] and utilized for generating pDEST17-OTUB1 WT/N22A (coding for His-OTUB1 WT/N22A) using the Gateway system according to the manufacturer's description (Invitrogen). His-OTUB1 WT/N22A was subcloned into the bacterial expression vector pET3a using pDEST17-OTUB1 WT/N22A plasmids as templates. For cloning of MBP-tagged human FIH into pET3a, FIH WT/H199A was subcloned using pFIH WT/H199A-V5 as template, followed by subcloning of an N-terminal MBP tag using human pMBP-FIH as template. *E.coli* BL21(DE3)pLysS (Invitrogen) were transformed with the plasmids and expression of the respective proteins was induced by addition of 0.2 mM isopropyl-ß-D-thiogalactoside (IPTG) for up to 6 h at 30°C. For purification of His-tagged proteins, bacteria were resuspended in 20 mM Tris-HCl (pH 8.0), 500 mM NaCl, 5 mM imidazole, and for purification of MBP-tagged proteins in 20 mM Tris-HCl (pH 8.0), 150 mM NaCl. Lysis buffers were supplemented with 1 mM PMSF and protease inhibitor cocktail (Sigma-Aldrich). Bacteria were lysed using a cell disruptor (TS Series Bench Top, Constant Systems Ltd., Northants, UK) in two cycles at 35 kPsi. Lysates were cleared by ultracentrifugation at 162,000 g, 4°C for 1 h and proteins were affinity purified with $NiSO_4$-

charged sepharose (HiTrap Chelating HP, GE Healthcare, Little Chalfot, UK) or dextrin sepharose (MBPTrap HP, GE Healthcare 28-918-780) columns using the Duo Flow system (Bio-Rad, Hercules, CA, USA). Protein concentrations were determined by Bradford assay. Dot blot, colloidal Coomassie staining [41] and OTUB1 and FIH immunoblotting were used to verify successful protein expression and purification.

Bacterial expression and purification of the stable FIH-OTUB1 complex from a bicistronic expression vector

Cloning of a bicistronic expression vector was performed as described [33]. Briefly, untagged human OTUB1 WT/N22A, FIH WT/H199A, His-OTUB1 WT/N22A and MBP-FIH WT/H199A were cloned into the transfer vector pET3a following PCR amplification. Untagged OTUB1 WT/N22A or His-OTUB1 WT/N22A was subsequently subcloned into cassette 1 of pST39, followed by subcloning of untagged FIH WT/H199A or MBP-FIH WT/H199A into cassette 4. Bacteria lysates were prepared, the protein complex purified by sequential MBP- and Ni^{2+}-affinity purification and analyzed as described above.

Biochemical analyses of the purified stable FIH-OTUB1 complex

Equal amounts of purified FIH-OTUB1 complex or albumin (fraction V, Carl Roth GmbH + Co. KG, Karlsruhe, Germany) were either exposed to 0.1 M NaOH, 10 mM NaOH, 10 mM HCl or 1 M NH_2OH at pH 7 or 10, or left untreated. Following incubation for 1 h at 37°C, samples were neutralized using corresponding amounts of NaOH or HCl and incubated for further 15 min at 37°C and analyzed by SDS-PAGE as described above.

Immunoprecipitation

Immunoprecipitation was performed as previously described [17]. Briefly, for native conditions, cells were lysed with 150 mM NaCl, 20 mM Tris-HCl (pH 7.5), 1 mM $MgCl_2$, 1% Triton X-100, supplemented with protease inhibitor cocktail (Sigma-Aldrich). For denaturing conditions, cells were scraped in PBS and centrifuged for 3 min at 200 g. The cell pellet was resuspended in the same lysis buffer but supplemented with 1% SDS and 0.75 U/µl benzonase (Sigma-Aldrich), boiled for 10 min and the cellular solutes were cleared by centrifugation at 21,000 g and 4°C for 5 min. Cell lysates were incubated with anti-FLAG M2 antibody-coupled beads (Sigma-Aldrich) or anti-V5 agarose affinity gel (Sigma-Aldrich) at 4°C for 1 h. Agarose beads were washed twice with lysis buffer and twice with washing buffer (150 mM NaCl, 20 mM Tris-HCl pH 7.5, 1 mM $MgCl_2$). For analysis by MS, the beads were treated as described below. For analysis by immunoblotting, the beads were resuspended in non-reducing loading buffer (50 mM Tris-HCl pH 6.8, 6% glycerol, 2% SDS, 0.01% bromophenol blue) and boiled for 5 min. 10 mM DTT was added to the supernatant and boiled for further 5 min. For endogenous FIH-specific immunoprecipitation, anti-FIH antibody or anti-β-actin control antibody was bound to protein G-sepharose (GE Healthcare) for 1 h at RT and incubated with non-denatured cell lysates over night at 4°C. Beads were washed and precipitated proteins were analyzed by immunoblotting.

OTUB1 deubiquitinase (DUB) assay

Purified His-OTUB1 WT and MBP-His-heterodimer were quality controlled by SDS-PAGE and colloidal Coomassie staining. Enzymes at the indicated concentration were incubated with 600 nM K48-tetraubiquitin (K48-Ub_4; Boston Biochem, Cambrige, MS, USA) at 37°C in the presence or absence of 25 µM UBCH5B (Enzo Life Science, Inc., Farmingdale, NY, USA). K48-Ub_4 alone was used as negative control. The reaction was stopped by addition of 5x loading dye and samples were incubated for 20 min at RT prior to immunoblot analysis.

Mass spectrometry analysis of the FIH-OTUB1 HD

For analysis of the stable FIH-OTUB1 complex, immunoprecipitated proteins from HEK293 cells were separated by SDS-PAGE. Bands were cut from the Coomassie-stained gel, chopped into small pieces and washed twice with 100 mM NH_4HCO_3, 50% acetonitrile and once with acetonitrile. Digestion with 50 ng trypsin (sequencing grade; Promega, Madison, WI, USA) was performed in buffered conditions (10 mM Tris-HCl pH 8.2, 2 mM $CaCl_2$) for 30 min at 60°C in a microwave oven (Discover System, CEM Corporation, Matthews, NC, USA). The supernatant was collected and lyophilized in a SpeedVac (Thermo Fisher Scientific). For liquid chromatography-tandem MS (LC-MS/MS) analysis, the samples were dissolved in 20 µl 0.1% formic acid and 3 µl were analyzed on a nanoAcquity ultra performance liquid chromatography (UPLC) column (Waters Corporation, Milford, MA, USA) connected to a Q Exactive mass spectrometer (Thermo Fisher Scientific) equipped with a Digital PicoView source (New Objective, Inc., Woburn, MA, USA). Peptides were trapped on a Symmetry C18 trap column (5 µm, 180 µm x 20 mm, Waters Corporation) and separated on a BEH300 C18 column (1.7 µm, 75 µm x 150 m, Waters Corporation) at a flow rate of 250 nl/min using a gradient from 1% solvent B (0.1% formic acid in acetonitrile)/99% solvent A (0.1% formic acid in water) to 40% solvent B/60% solvent A within 30 min. The mass spectrometer was set to data dependent analysis, precursor scan range 350 – 1,500 m/z, resolution 70,000, maximum injection time 100 ms, threshold 3e6. The fragment ion scan range was 200 – 2,000 m/z, resolution 35,000, maximum injection time 120 ms, threshold 1e5. Proteins were identified using the Mascot search engine (Matrix Science; Version 2.5.1.3.). Mascot was set up to

search the human SwissProt database assuming the digestion enzyme trypsin. Mascot was searched with a fragment ion mass tolerance of 0.030 Da and a parent ion tolerance of 10.0 ppm. Oxidation of methionine was specified in Mascot as a variable modification. Scaffold (Proteome Software Inc., Version 4.8.6) was used to validate MS/MS based peptide and protein identifications. Peptide identifications were accepted if they achieved a false discovery rate (FDR) of less than 0.1% by the Scaffold Local FDR algorithm. Protein identifications were accepted if they achieved an FDR of less than 1.0% and contained at least 2 identified peptides. The number of peptides was determined by the number of spectra identifying specific peptide sequences for each protein.

Mass spectrometry analysis of denatured and non-denatured FIH interactomes

For analysis of the stable FIH interactome by label-free quantification (LFQ), human FIH-V5 or tandem EGFP was expressed in HEK293 cells, and cells were lysed in native or denaturing conditions as described above. Following V5-specific IP, the beads were resuspended in 45 µl digestion buffer (10 mM Tris-HCl pH 8.2, 2 mM $CaCl_2$) and the proteins were on-bead digested using 5 µl of 100 ng/µl trypsin in 10 mM HCl (sequencing grade; Promega) in a microwave oven for 30 min at 5 W and 60°C. The supernatants were transferred into new tubes and the beads were additionally digested for 3 h at room temperature. The beads were washed with 100 µl TFA-buffer (0.1% TFA, 10 mM Tris, 2 mM $CaCl_2$) and all supernatants were combined, lyophilized, resolubilized in 25 µl of 3% acetonitrile, 0.1% formic acid spiked with iRT peptides (Biognosys AG, Schlieren, CH), centrifuged at 20,000 g for 10 minutes and analyzed on a Q Exactive mass spectrometer coupled to a Nano Easy 1000 liquid chromatography system (Thermo Fisher Scientific). Solvent composition was 0.1% formic acid for channel A and 0.1% formic acid in acetonitrile for channel B. For each sample, 4 µl of peptides were loaded on a commercial Acclaim PepMap Trap Column (75 µm x 20 mm, Thermo Fisher Scientific) followed by a PepMap RSLC C18 Snail Column (75 µm × 500 mm; Thermo Fisher Scientific). The peptides were eluted at a flow rate of 300 nL/min by a gradient from 5 to 22% B in 79 min, 32% B in 11 min and 95% B in 10 min. Samples were acquired in

a randomized order. The mass spectrometer was operated in data-dependent mode (DDA), acquiring a full-scan MS spectra (300−1,700 m/z) at a resolution of 70,000 at 200 m/z after accumulation to a target value of 3,000,000, followed by higher-energy collision dissociation (HCD) fragmentation on the twelve most intense signals per cycle. HCD spectra were acquired at a resolution of 35,000 using a normalized collision energy of 25 and a maximum injection time of 120 ms. The automatic gain control (AGC) was set to 50,000 ions. Charge state screening was enabled and singly and unassigned charge states were rejected. Only precursors with intensity above 8,300 were selected for MS/MS (2% underfill ratio). Precursor masses previously selected for MS/MS measurement were excluded from further selection for 30 s, and the exclusion window was set at 10 ppm. The samples were acquired using internal lock mass calibration on m/z 371.1010 and 445.1200. The acquired raw mass spectrometry MS data were processed by MaxQuant (Version 1.6.1) [42], followed by protein identification using the integrated Andromeda search engine [43]. Spectra were searched against a UniProt Homo Sapiens (taxonomy 9606) reference proteome (canonical version from 2016-12-09), concatenated to its reversed decoyed fasta database and common protein contaminants. Carbamidomethylation of cysteine was set as fixed, while methionine oxidation and N-terminal protein acetylation were set as variable modifications. MaxQuant Orbitrap default search settings were used. Enzyme specificity was set to trypsin/P. For Label-Free-Quantification, MaxQuant default settings were applied. In the MaxQuant experimental design template, the biological and biochemical replicates were grouped into non-adjacent fractions, to allow match-between-runs within but not between conditions. Each file was treated as a separate experiment to obtain individual quantitative values. Protein fold changes were computed based on intensity values reported in the proteinGroups.txt file. A set of functions implemented in the R package SRMService (http://github.com/protViz/SRMService [44]) was used to filter for proteins with 2 or more peptides, with quantification in at least 4 samples, and to normalize the data with a modified robust z-score transformation and to compute p-values using the t-test with pooled variance. The MS proteomics data were handled using the local laboratory information management system (LIMS) [45]. FIH-specific interactors had an average LFQ

intensity of the four biological replicates of at least 2-fold over control (EGFP) and were statistically significantly different ($p<0.05$). The obtained lists of FIH-specific interactors were analyzed for overlaps using Excel (Microsoft). Functional annotation was performed via the PANTHER database (www.pantherdb.org). For comparison of relative intensities, individual LFQ intensities were normalized to the average intensity of FIH in the samples with ectopic FIH expression.

Primer sequences

The designed Primers for the site-directed mutagenesis of human OTUB1 were as follows (fwd, forward primer; rev, reverse primer):

S16A - fwd: 5'-accttcggagtcggcgcccagcggctcc-3', rev: 5'-ggagccgctgggcgccgactccgaaggt-3'.

S18A - fwd: 5'-gttaacaccttcggcgtcgctgcccagcg-3', rev: 5'-cgctgggcagcgacgccgaaggtgttaac-3'.

S16/18A - fwd: 5'-ttaacaccttcggcgtcggcgcccagcggctcc-3', rev: 5'-ggagccgctgggcgccgacgccgaaggtgttaa-3'.

C23A - fwd: 5'-ttcatcataggccagagcgttaacaccttcggagtcgc-3', rev: 5'-gcgactccgaaggtgttaacgctctggcctatgatgaa-3'.

C23S fwd: 5'-cataggccagagagttaacaccttcggagtcg-3', rev: 5'-cgactccgaaggtgttaactctctggcctatg-3'.

C91A – fwd: 5'-gaaagcccgatagaaagcgttgccgtcaggcctg-3', rev: 5'-caggcctgacggcaacgctttctatcgggctttc-3'.

C91S – fwd: 5'-aaagcccgatagaaagagttgccgtcaggcc-3', rev: 5'-ggcctgacggcaactctttctatcgggcttt-3'.

Primers designed for the cloning of OTUB1 WT and N22A into pET3a - fwd: 5'-actgcatatggcggcggaggaacctcagga-3', rev: 5'-acgtggatccctatttgtagaggatatcgt-3'.

Primers designed for the cloning of FIH WT and H199A into pET3a - fwd: 5'-acgtcatatggcggcgacagcggcgga-3', rev: 5'-acgtggatccctagttgtatcggcccttgatca-3'.

Primers designed for the cloning of His-OTUB1 WT and N22A into pET3a -
fwd 5'-acgtcatatgtcgtactaccatcaccatca-3', rev 5'-acgtagatctctatttgtagaggatatcgt-3'.

Primers designed for the cloning of MBP into pET3a-FIH:
fwd 5'-acgtcatatgaaaatcgaagaaggtaaact-3', rev 5'-actgcatatgggcgccctgaaaatacagg-3'.

Statistical analysis

For the analysis of the significance of difference between two data points, Student's t-test was applied. For comparison of more than two data points, one-way or two-way ANOVA followed by Tukey post-test was applied. P values < 0.05 were considered statistically significant.

Data availability

The MS proteomics data have been deposited to the ProteomeXchange Consortium via the PRIDE [46] partner repository with the dataset identifier PXD011252.

RESULTS

FIH and OTUB1 form a covalently linked protein complex.

Following our previous observations of FIH-dependent hydroxylation of OTUB1 on N22 [17, 18], we here investigated the interplay between FIH and OTUB1 in more detail by immunoprecipitation (IP) of endogenous FIH. Intriguingly, we detected an unexpected signal in immunoblots with antibodies derived against FIH as well as OTUB1 (Fig 1A; marked with "X"). Protein X demonstrated a larger molecular weight than FIH or OTUB1 alone and its signal intensity was decreased following OTUB1 knockdown and abolished by iron chelation with desferrioxamine (DFX) (Fig 1A). Protein X was also detectable using antibodies against ectopically (plasmid-dependently) expressed tagged FIH and OTUB1 (Figs 1B and S1A). Protein X was subsequently investigated using ectopically expressed tagged OTUB1 and FIH to allow detailed analyses with complete control over the experimental conditions. Protein X signal intensity was proportional to OTUB1 protein levels, while mutation of the OTUB1 hydroxylation site (N22A) abrogated it (Fig 1B). Mass spectrometry (MS) identified equimolar amounts of FIH and OTUB1 peptides in protein X (Fig S1B). Taken together, these results are consistent with a heterodimer (HD) consisting of FIH and OTUB1. Furthermore, the FIH-OTUB1 HD was also detected in MCF7 (breast cancer) and Hep3B cells (liver cancer) (Figs S1C and S1D), indicating that HD formation is cell type independent.

HD formation was resistant to denaturing SDS-PAGE, consistent with a possible covalent FIH-OTUB1 conjugation. This was further analyzed following the strategy of the original characterization of the covalent bond between ubiquitin (Ub) and substrate proteins [47]. The complex was resistant to chaotropic urea-PAGE (Fig 1C). The HD was also not disrupted by high concentrations of the reducing agents β-mercaptoethanol (βME) (Figs 1A (lysates), 1D, 1E (lysates) and S1E), iodoacetamide (Fig 1B) and DTT (Figs 1A (IPs) and 1E (IPs)), excluding disulfide bonds as possible connection. For the further assessment of the nature of this conjugation, the HD was purified from bacteria. The purified complex was exposed to high (0.01 and 0.1 M NaOH) and low pH (10 mM HCl) as well as to 1 M

hydroxylamine (pH 7 and 10). NaOH treatment disrupts ester bonds and hydroxylamine disrupts thioester bonds at pH 7 and oxyester bonds at pH 10 [48, 49]. Amide bonds are resistant to these conditions [48, 49]. Low pH disrupts non-covalent bonds and esters. A specific disruption of the bond between FIH and OTUB1 in the HD should yield a decrease of HD levels with simultaneous increase in monomeric FIH and OTUB1. However, no increase in monomeric FIH or OTUB1 levels occurred when the HD decreased (Fig 1D). In addition, when the heterodimer was reduced, the BSA control was decreased to a comparable level as well (Figs 1D and S1F). This indicates that the observed decreases in the HD were due to general effects on protein stability and not due to specific disruption of the FIH-OTUB1 conjugation. Hence, FIH and OTUB1 are covalently attached within the HD and this covalent linkage fulfils all biochemical criteria of an amide bond.

OTUB1 N22A mutation abrogated HD formation (Fig 1B) as well as the non-covalent interaction between FIH and OTUB1 (Figs 1E, S2A and S2B). For a further investigation of the relevance of OTUB1 N22 for HD formation, additional mutations of OTUB1 were introduced within its FIH interaction region (S16, S18, C23) or catalytic domain (C91; leading to a catalytically inactive OTUB1 mutant [21]). Analysis via IP showed that C91 was dispensable, demonstrating that HD formation occurs independent of OTUB1 catalytic activity. The input as well as the FLAG-specific IPs showed that beside N22 also C23 mutation abrogated both the HD and the non-covalent FIH:OTUB1 interaction, while mutations of S16 and/or S18 decreased the HD and the FIH:OTUB1 interaction by roughly 50% (Figs 1E, S2C and S2D). Overall, these results demonstrate that mutations of the OTUB1 hydroxylation site and of its FIH interaction site affect FIH-OTUB1 HD levels and that both are necessary for optimal interaction and HD formation. In addition, they indicate that the OTUB1 amino acid directly involved in the conjugation with FIH is either N22 or C23.

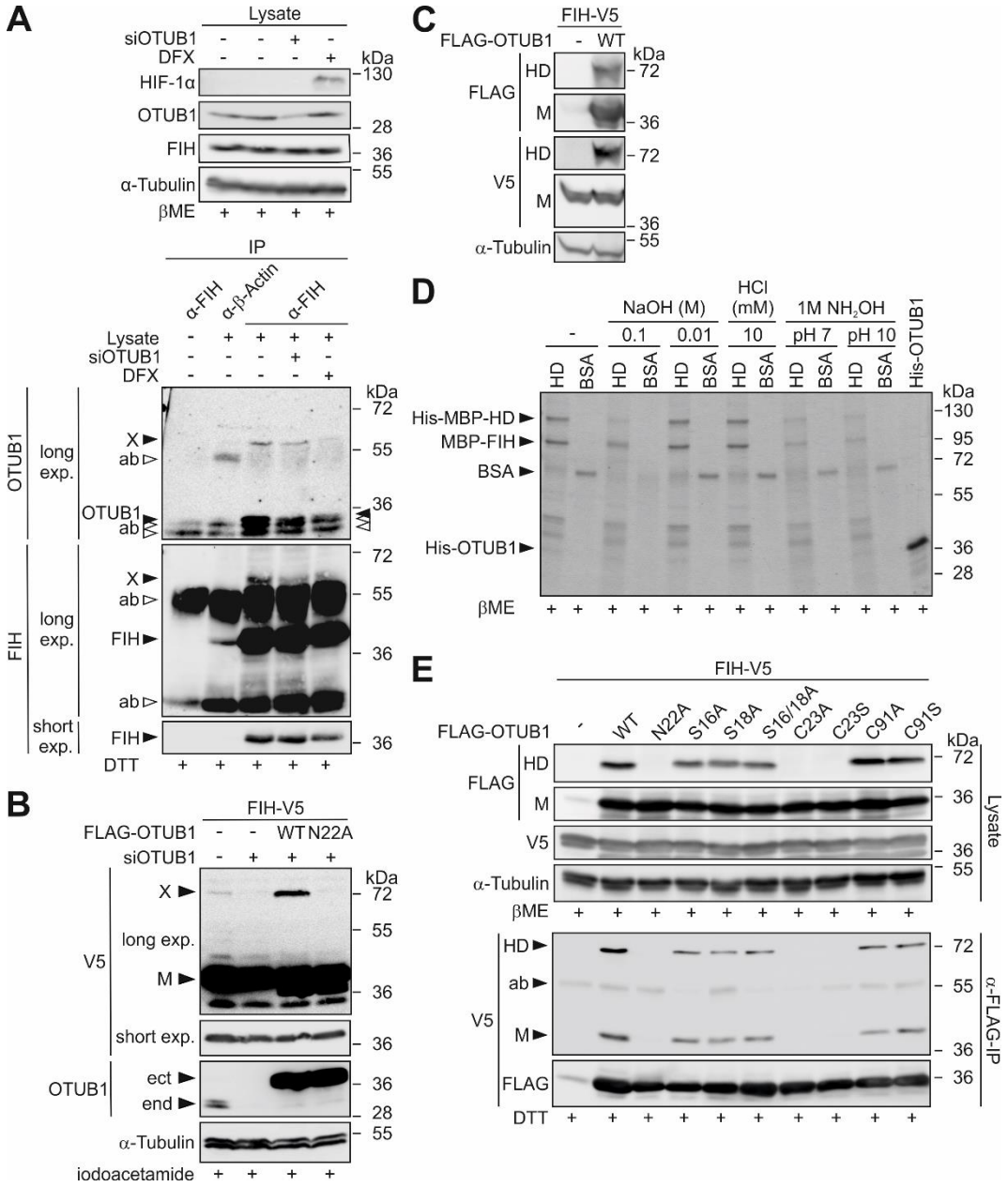

Fig 1: Characterization of the FIH-OTUB1 conjugation. (**A**) Immunoblot analysis of endogenous FIH IP detected the unexpected protein signal ("X"), which was insensitive to 858 mM β-mercaptoethanol (βME) and 10 mM DTT. The same antibody was used for the FIH IP and subsequent FIH immunoblotting and the anti-β-actin antibody was derived from the same species as the anti-FIH antibody, leading to the detection of fragments of the IP antibodies (ab; highlighted by open arrows). Black arrows highlight specific signals of the indicated proteins. (**B**) The intensity of X detected by immunoblotting of cell lysates was proportional to FIH and wildtype OTUB1 (WT) levels, as seen with ectopic FLAG-OTUB1 expression, knockdown and ectopic mutant OTUB1 (N22A) expression. Protein signal X was insensitive to 100 mM iodoacetamide, the only agent present that disrupts disulfide bonds. (**C**) Investigation of the resistance of the FIH-OTUB1 HD interaction to a chaotropic agent by urea-PAGE followed by immunoblotting. (**D**) Investigation of the effect of treatments disrupting thioesters and oxyesters using purified HD. The samples were analysed by Coomassie-stained SDS-PAGE, which included boiling in the presence of 858 mM βME during sample preparation. (**E**) Residues of the FIH interaction site of OTUB1 were mutated and their relevance for HD formation investigated by ectopic expression of the mutated proteins and

anti-FLAG-IP. All samples were boiled in the presence of 858 mM βME or 10 mM DTT as indicated followed by immunoblot. exp, exposure; HD, heterodimer; M, monomer; ect, ectopic (plasmid-dependent) expression; end, endogenous protein. The data represent (A) two, (C, D, E (IPs)) three, (B) four or (E (lysates)) six independent experiments.

FIH-dependent FIH-OTUB1 heterodimer formation is a hypoxia-regulated mechanism.

While OTUB1 enzymatic activity was dispensable for HD formation, the OTUB1 hydroxylation site as well as the FIH interaction site were necessary. Therefore, we hypothesized that FIH catalyzes the formation of the putative covalent bond. In agreement with this hypothesis, hypoxia (0.2% O_2), a 2-oxoglutarate (2-OG) competitor (dimethyloxalylglycine, DMOG) and the iron chelator DFX prevented HD formation (Fig 2A). The PHD-specific inhibitor FG-4592 (roxadustat) [50] did not affect HD levels (Fig 2A). Accordingly, knockdown of endogenous FIH with parallel expression of a catalytically inactive FIH mutant (H199A) [31] completely abolished formation of the HD (Fig 2B). Overall, these results demonstrated that FIH enzymatic activity is required for covalent bond formation. A possibly limiting availability of FIH co-factors in cell culture affecting the FIH catalytic cycle could be excluded (Fig S2E).

In order to investigate the sensitivity of HD formation to oxygen availability, 8 different oxygen levels were used in the range of 18.5% to 0.2% O_2. HIF-1α and HIF-2α stabilization were determined as biological readout for the obtained level of hypoxia and for the comparison with the PHD sensitivity. We observed an unusually high hypoxia sensitivity with an EC_{50} of 4.1% O_2, which was even higher than the hypoxia sensitivity of the PHD-dependent HIF-1α and HIF-2α stabilization with EC_{50} values of 2.15% and 3.5% O_2, respectively (Figs 2C and 2D). Of note, this is in stark contrast to the known hypoxia sensitivity for FIH-dependent HIF-1α hydroxylation, which is below 1% O_2 [51, 52].

Taken together, our results demonstrate that FIH catalyses HD formation with OTUB1, which is remarkably sensitive to changes in oxygen availability within the physiologically relevant range, suggesting a function in oxygen-dependent signalling.

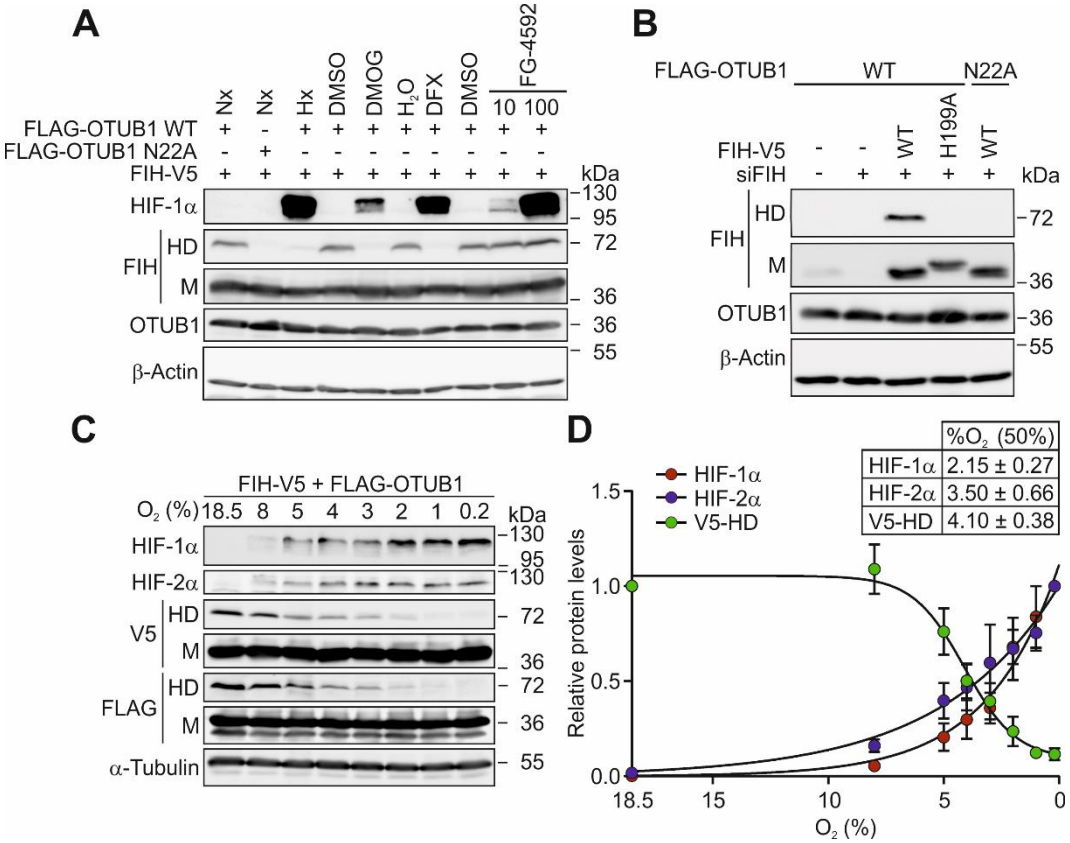

Fig 2: Hypoxia sensitivity of the FIH-dependent FIH-OTUB1 heterodimer formation. (**A**) Heterodimer (HD) formation was sensitive to hypoxia (Hx, 0.2% O_2), DMOG and DFX, but not to the PHD-specific inhibitor FG-4592. (**B**) Immunoblotting of cell lysates with the indicated ectopic expressions. The H199A FIH mutant is catalytically inactive and was incapable of forming the HD. (**C**) Hypoxia sensitivity of HD formation in comparison with HIF-1α and HIF-2α stabilization following 24 h of incubation at the indicated O_2 levels. (**D**) Quantification of the experiment described in (C) and calculation of the oxygen sensitivity of HD formation and HIF-1α and HIF-2α stabilization based on this quantification. Nx, normoxia; M, monomer. Data are shown as mean ± SEM from four independent experiments or are representative for (A, B) three or (C) four independent experiments.

The FIH-OTUB1 heterodimer forms co-translationally and is extraordinarily stable.

As next step, the stability of the HD was analyzed *in cellulo*. First, transiently transfected cells were allowed to form the HD for 24 h with subsequent inhibition of further HD formation by exposing these cells to 0.2% O_2. The HD showed a pronounced stability with first significant decreases in HD levels after 24 h only (Figs 3A and S3A).

For the investigation of the HD formation time, HEK293 cells were transfected with FIH and OTUB1 expressing plasmids for 5 h and subsequently incubated for 16 h in 0.2% O_2 in order to inhibit FIH activity to express both FIH and OTUB1 without HD formation (Fig S3B). Media was replaced with normoxic media for instantaneous re-oxygenation and the time of

HD formation was analysed (Fig S3B). HD formation was unexpectedly slow with a half-maximal level after 2.5 h, reaching a level comparable with normoxia after 8.7 h (Figs 3B and S3C; values calculated from Fig S3C). Re-oxygenation following hypoxia leads to active FIH within approximately 1 min [52], which can therefore not explain the slow HD formation. Hence, we assumed that a mechanism independent of FIH enzymatic activity was involved and investigated if HD formation occurred co-translationally using cycloheximide (CHX; Fig S3B). Simultaneous addition of CHX with the start of the re-oxygenation had no effect on the formation of the HD (Fig. 3C; Re-ox ctrl vs. Re-ox CHX). However, the simultaneous start of two different treatments such as CHX and re-oxygenation can make it difficult to interpret the result due to different kinetics involved. Therefore, we also included samples in which we pre-treated the cells for 1 h with CHX prior to the start of re-oxygenation to allow for an efficient inhibition of translation at the time of re-oxygenation. In these samples, HD formation was markedly reduced after 6 h of re-oxygenation (Fig 3C; Re-ox ctrl vs. Re-ox CHX pre), indicating that translation might be important for HD formation. Interestingly, purified FIH and OTUB1 did not form the HD under cell-free conditions (data not shown). However, a bicistronic expression vector [33] for FIH and OTUB1 (Fig S3D), expressing both proteins in the same bacterium, resulted in HD formation which was dependent on the presence of the OTUB1 N22 hydroxylation site and on active FIH (H199A abrogated HD formation) (Fig 3D). Co-inoculation of bacterial cultures that expressed either FIH or OTUB1 did not lead to detectable HD formation (Fig S3E). Taken together, these results strongly suggest that HD formation occurs co-translationally.

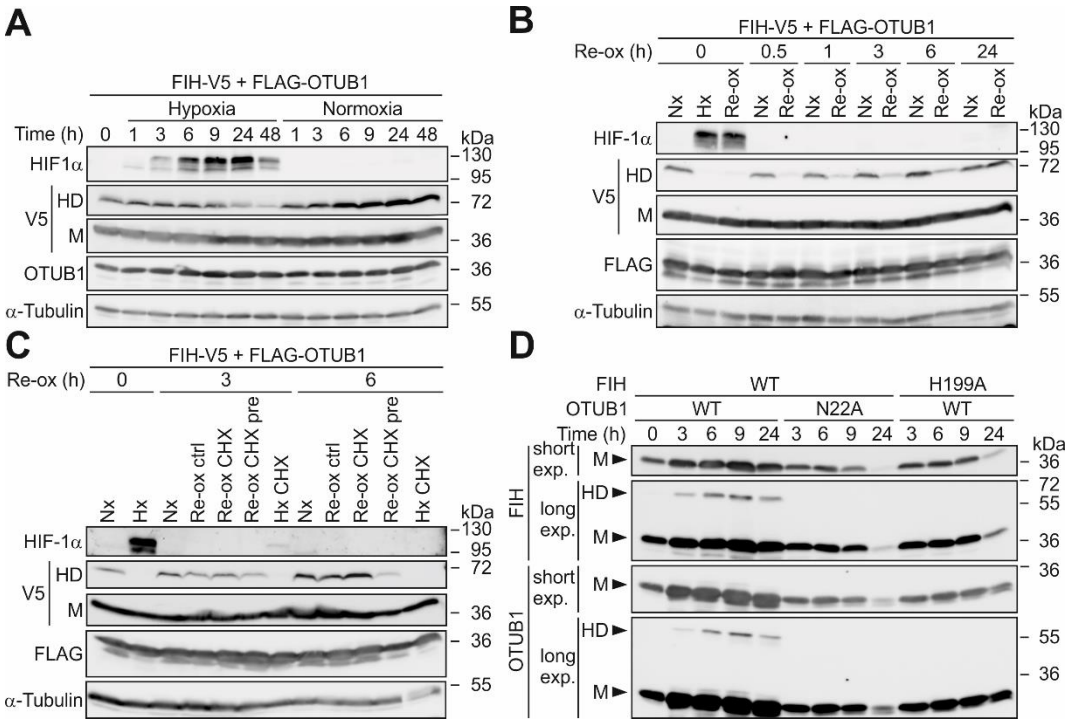

Fig 3: Co-translational formation of the extraordinarily stable FIH-OTUB1 HD. (**A**) Following ectopic expression of the indicated proteins, the FIH-OTUB1 heterodimer (HD) was allowed to form for 24 h prior to the analysis of the HD stability in hypoxia when FIH is inhibited and no additional HD can be formed. (**B**) HD formation kinetics and (**C**) HD formation during translation inhibition by cycloheximide (CHX) according to the experimental setups described in Fig S3B. Re-Ox CHX, addition of CHX at the same time as re-oxygenation was started; Re-Ox CHX pre, pre-incubation of cells with CHX for 1 h prior to the start of re-oxygenation. (**D**) Bicistronic expression of the indicated His-OTUB1-MBP-FIH in *E.coli* followed by immunoblot analysis. Time points indicate the time after induction of protein production by addition of isopropyl-ß-D-thiogalactoside (IPTG). Nx, normoxia; M, monomer. Data are representative for three independent experiments throughout.

The FIH-OTUB1 HD is part of a native FIH:FIH-OTUB1 heterotrimer.

The active form of FIH is a non-covalent FIH:FIH homodimer [53]. Therefore, we sought to investigate, if both FIH proteins of the homodimer form a covalent bond with OTUB1 and if HD formation interferes with the interaction of the FIH proteins within the FIH homodimer. Following native gel electrophoresis, ectopic FIH-V5 expression alone showed two bands in the immunoblot, which corresponded to monomeric FIH and homodimeric FIH, as homodimeric FIH was not detectable anymore after denaturation of the same sample (Fig 4A). With ectopic FIH-V5 and FLAG-OTUB1 co-expression, a complex was detectable that was composed of FIH and OTUB1 (detected with both antibodies) and moved slower in the electric field than the FIH homodimer (Fig 4A). Next, the composition of this complex was analyzed in

a second denaturing dimension following native gel electrophoresis. Alongside the HD, a further signal was observed in the anti-V5 immunoblot at the same molecular weight as the V5 signal obtained from FIH-V5 expression alone (Fig 4B). This revealed that the native complex contained an additional, non-covalently bound FIH protein. Non-covalently interacting (monomeric) OTUB1 was not detected within the complex (Fig. 4B). In summary, only covalently linked OTUB1 was present in the complex combined with a covalently linked FIH and a second, non-covalently interacting FIH. Hence, *in cellulo* a FIH:FIH-OTUB1 heterotrimer (HT) is formed.

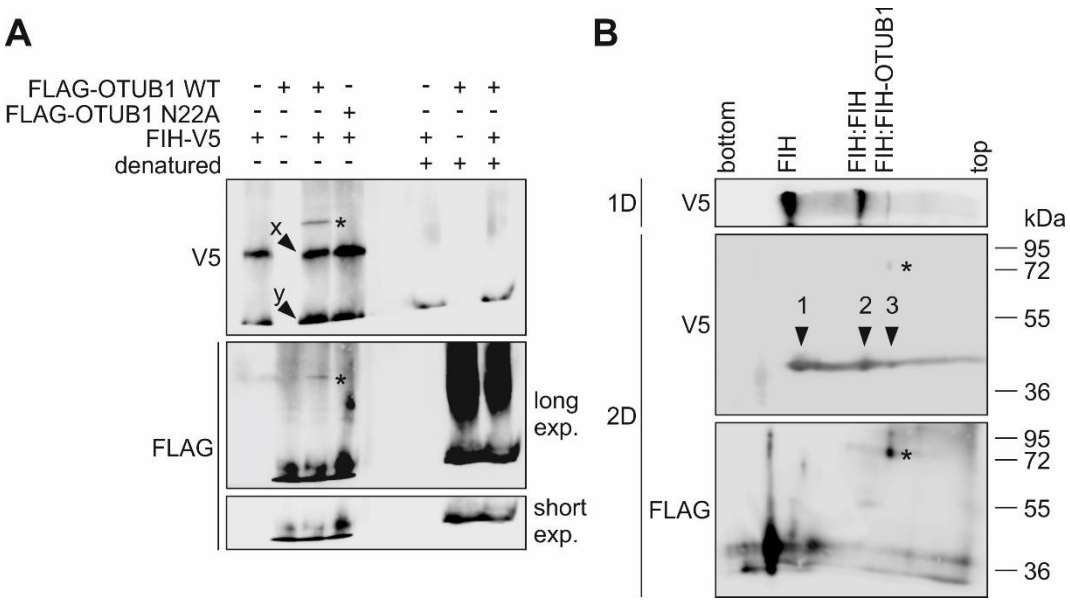

Fig 4: FIH:FIH-OTUB1 heterotrimer formation. Analysis of the composition of the covalently linked FIH-OTUB1 complex by (**A**) blue native-PAGE (first dimension, 1D) following ectopic expression in HEK293 cells and by (**B**) SDS-PAGE as second dimension (2D). *, FIH-OTUB1 heterodimer; x, FIH homodimer; y, FIH monomer; arrows 1-3, monomeric FIH originating from FIH monomers (1), FIH:FIH homodimers (2) or the FIH:FIH-OTUB1 heterotrimer (3). Data are representative for three independent experiments throughout.

Covalent complex formation with FIH regulates OTUB1 enzymatic activity.

To assess possible functional consequences of HT formation for OTUB1 enzymatic activity (hydrolysis of K48-linked Ub chains), monomeric free OTUB1 and the native HT were purified from bacterial lysates (Figs S4A and S4B). To account for a small contamination of the HT by monomeric OTUB1, indicating that non-covalently bound OTUB1 was co-purified, molar

concentrations of the control (monomeric OTUB1) were matched with the contamination. Within the HT sample, there was a significant increase in cleavage of K48-Ub chains in comparison to monomeric OTUB1 following 5 min of incubation, as shown by significant decreases in Ub_4 chains paralleled by significant increases in Ub_3 chains (Figs 5A and 5B). This demonstrated a higher deubiquitinase activity within the HT sample over monomeric OTUB1, which could only be derived from the HT itself. Hence, OTUB1 enzymatic activity was maintained in the HT. Interestingly, at later time points this activity was decreased in comparison to monomeric OTUB1 (Figs 5A and 5B).

Interaction of the OTUB1 N-terminus with uncharged E2s (such as UBCH5B) increases OTUB1 activity towards K48-ubiquitin chains by stabilizing the structure of an OTUB1 Ub-binding site [26]. Because the OTUB1 N-terminus also contains the FIH interaction site, we investigated if the stimulating effect of UBCH5B on OTUB1 enzymatic activity was affected by HT formation. The activity of purified monomeric OTUB1 was strongly increased in the presence of UBCH5B, as demonstrated by a faster turnover of K48-linked Ub_4 into smaller Ub chains when UBCH5B was present (Figs 5C, 5D and S4C). In contrast, HT-dependent cleavage of Ub_4 chains was reduced in the presence of UBCH5B in comparison to HT alone, as shown by higher residual levels of Ub_4 chains in samples containing both the HT and UBCH5B compared to samples containing the HT alone (Figs 5C, 5D and S4C). This demonstrated that UBCH5B had the opposite effect on OTUB1 activity when OTUB1 was bound by FIH (forming the HT) than on monomeric OTUB1.

These results show that OTUB1 maintains its enzymatic activity within the heterotrimeric complex with FIH, but the important regulation of its activity by the E2 enzyme UBCH5B is inverted, demonstrating a functional effect of FIH:FIH-OTUB1 HT formation.

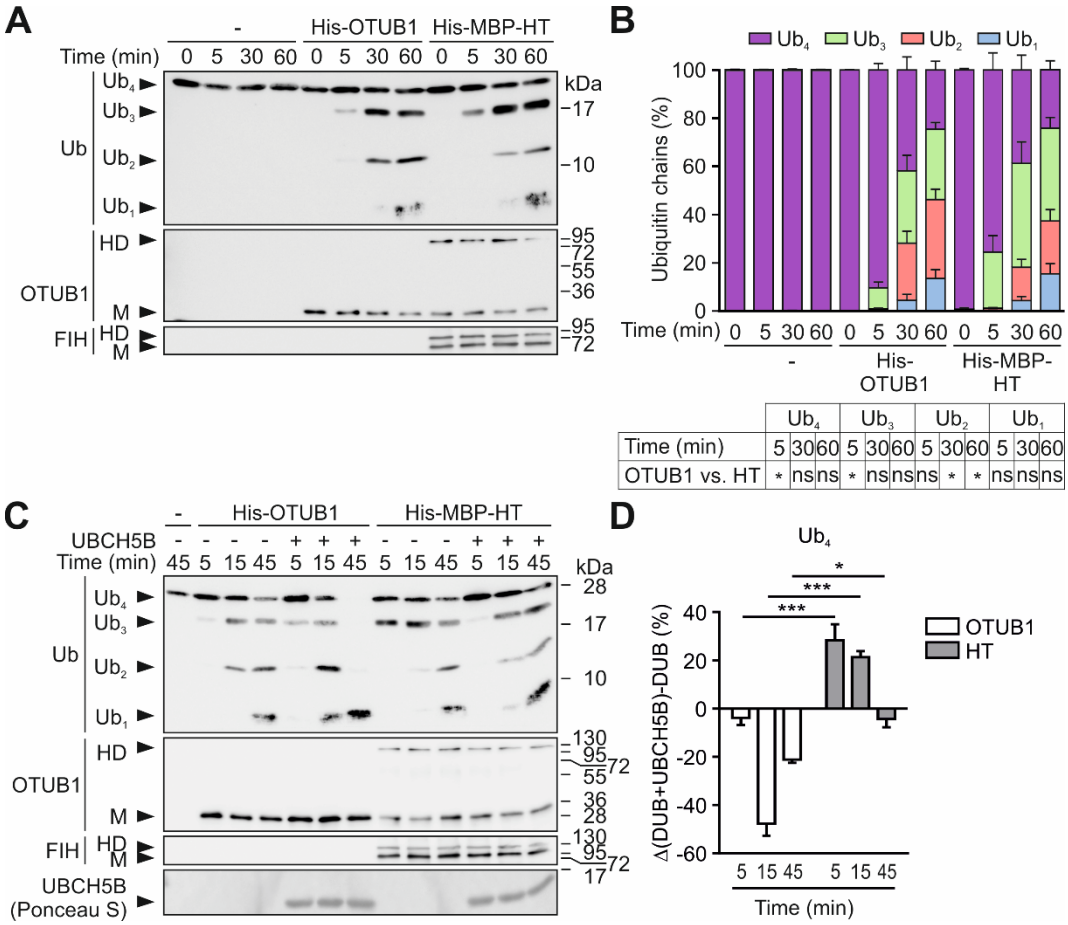

Fig 5: UBCH5B-dependent regulation of OTUB1 DUB activity in the FIH:FIH-OTUB1 heterotrimer. (**A-D**) Comparison of the OTUB1 enzymatic activity in purified monomeric OTUB1 and in the FIH:FIH-OTUB1 heterotrimer (HT) in (**A**, **B**) the absence or (**C**, **D**) presence of the E2 protein UBCH5B using (**A**, **C**) a DUB assay and (**B**, **D**) quantification. (**D**) The relative levels of Ub_4 chains were quantified in each sample of the experiment described in (C). Quantified Ub_4 chain amounts in the samples containing His-Otub1 alone were subtracted from the quantified Ub_4 chain amounts in samples with His-OTUB1 + UBCH5B (clear bars). The same analysis was carried out for the His-MBP-HT: quantified amounts of Ub_4 chains in samples with His-MBP-HT alone were subtracted from the quantified amounts in the samples containing His-MBP-HT + UBCH5B (grey bars). DUB, indicates the deubiquitinases OTUB1 or HT, respectively. HD, heterodimer; M, monomer, Ub_n, K48-linked ubiquitin chains with n number of Ub proteins; ns, not significant. Data are shown as mean + SEM from three independent experiments or are representative for three independent experiments. *, $p<0.05$; **, $p<0.01$; ***, $p<0.001$ by two-way ANOVA followed by Tukey post-test.

FIH forms denaturation resistant complexes with a specific subset of its interactome.

During our analyses, we observed further higher molecular weight bands in addition to the HD that were also detected with an antibody against FIH (Fig S5A). Intriguingly, these bands disappeared when FIH activity was inhibited (Fig S5A). This indicated that FIH-dependent covalent bond formation was not restricted to OTUB1. For the investigation of such potential further covalent complexes formed by FIH, we utilized an assay previously described for the discrimination of covalent and non-covalent ubiquitin interactions [54]. In this assay, the FIH-OTUB1 HD was pulled down under denaturing conditions without non-covalently interacting FIH (Fig 6A). When FIH-V5 was expressed alone, the same approach showed several high molecular weight complexes, of which some were maintained under denaturing conditions ("+SDS") (Fig 6B). This further indicated that a subset of the FIH interactome forms covalent complexes with FIH similar to OTUB1. MS identified 71 proteins that interacted with FIH following native lysis ("- SDS"), while 375 proteins were observed following IP from denatured cell lysates (Fig 6C). The higher number of co-precipitants in the IP from denatured cell lysates was surprising, but denaturing lysis will lead to the extraction of more proteins, which could explain the difference in the number of detected proteins. Thirteen FIH interactors were present under denaturing as well as native conditions, including OTUB1 (Figs 6C, 6D and S5B). The interactomes covered a broad spectrum of different biological processes (Fig S5C). Among the 12 novel candidates for covalent complex formation, the previously described FIH interactors IκBβ and CDK1 were present [13, 17]. These results demonstrate that FIH forms stable complexes with a subset of its interactome.

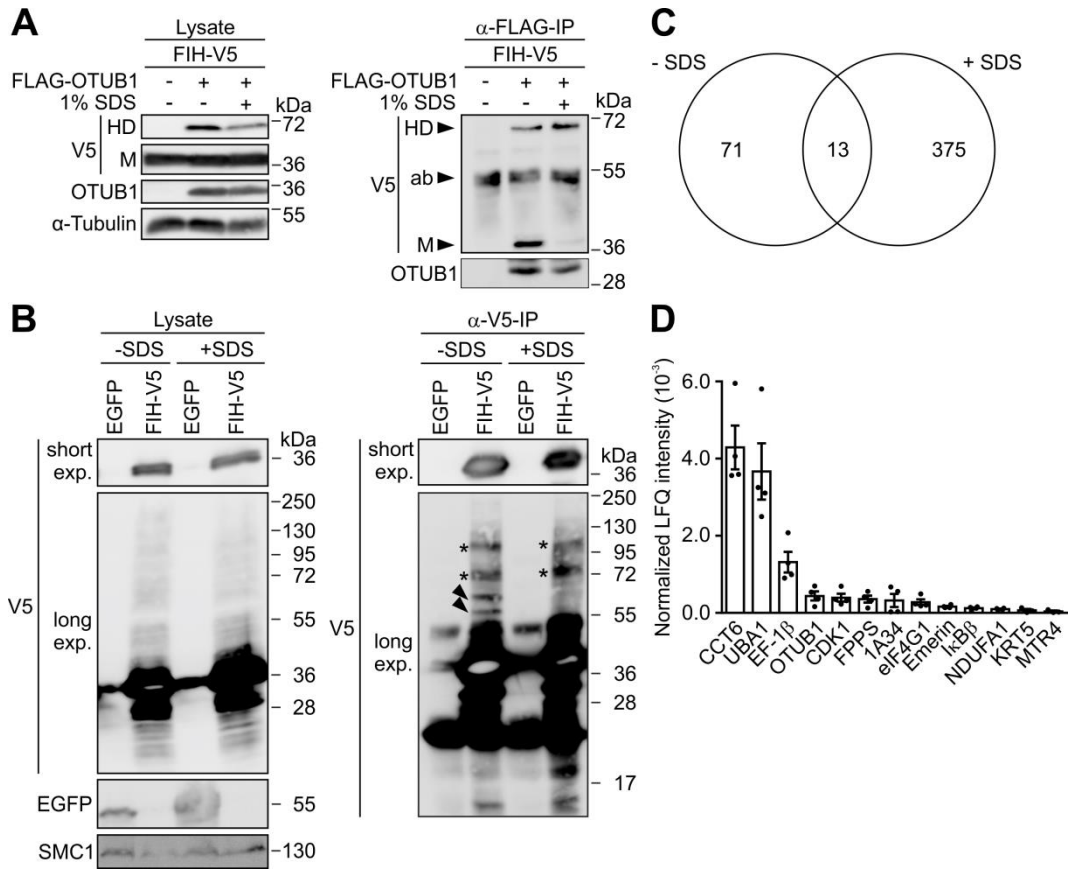

Fig 6: Denaturing condition-resistant FIH interactome composition. (**A**) Following ectopic expression of the indicated proteins, HEK293 cells were lysed under native or denaturing (boiling in 1% SDS) conditions followed by anti-FLAG IP and immunoblot analysis. HD, heterodimer; M, monomer; ab, antibody. (**B**) Following ectopic expression of either FIH-V5 or tandem EGFP, HEK293 cells were lysed as described in (A) followed by anti-V5 IP and immunoblot analysis. exp, exposure. (**C**) Following the same sample preparation as in (B), the samples were analysed by MS. Venn diagram displaying the overlap between FIH interactors under native (-SDS) and denaturing (+SDS) conditions. (**D**) Rank order of the 13 proteins interacting with FIH under both conditions shown in (C), according to the relative label free quantification (LFQ) intensity following IP in the presence of SDS and normalized to FIH pull-down. Data are shown as mean ± SEM. HD, heterodimer; M, monomer; ab, antibody; exp, exposure. Data are shown as mean ± SEM from (C, D) four biological replicates or are representative for (A) three or (B) one independent experiment. (B-D) Samples were processed in parallel and only differ in the analysis (immunoblot or MS).

DISCUSSION

The formation of protein complexes is the basis for cellular processes and functions [55]. Hence, the understanding of protein complex formation is fundamental for our understanding of health and disease. Cellular oxygen sensing is vital for cells in order to be able to monitor oxygen availability in their local microenvironment and to adjust to changes accordingly [3]. In this study, we provide insights into a previously unknown cross-talk between FIH and OTUB1 through amide bond formation catalysed by FIH, with unprecedented oxygen sensitivity and with functional relevance for OTUB1, regulating its K48-Ub chain cleavage activity. The covalent FIH-OTUB1 HD formation may represent an alternative molecular mechanism for the cellular adaptation to oxygen changes over longer time periods, linking oxygen sensing and deubiquitinase activity. Furthermore, we provided results indicating that FIH-dependent covalent bond formation is not exclusive for OTUB1.

The covalent bond of the FIH-OTUB1 HD fulfils all biochemical criteria of an amide bond [47-49, 56, 57]. FIH enzymatic activity was necessary for HD formation and hence FIH appears to have amide synthase activity. This activity required the same co-factors and co-substrates as FIH-dependent hydroxylation. But in contrast to amide bond formation in the ubiquitin system, FIH is not known to utilize ATP. Furthermore, the catalyzing protein (FIH) attaches itself instead of a third moiety, such as an ubiquitin or a hydroxyl group. Hence, the proposed FIH amide synthase activity on OTUB1 would be based on an unprecedented molecular mechanism.

FIH can oxidize hydrophilic, hydrophobic, acidic, basic, polar and neutral amino acid side chains and FIH may catalyze the formation of β–oxo-histidine and dehydrohistidine [58-60]. This demonstrates that FIH catalytic activity is highly promiscuous and that FIH may be capable of catalyzing more than asparagine hydroxylation. In our experiments, point mutations of OTUB1 indicated that N22 and C23 are necessary for HD formation. Cysteines such as C23 can form disulfide bonds or thioesters, but both types of covalent bonds were excluded by our analyses. N22 can be hydroxylated by FIH [18], demonstrating that N22 is accessible for FIH catalytic activity. Therefore, N22 is likely the OTUB1 amino acid that is involved in the

covalent bond formation. However, peptides corresponding to the suspected regions of FIH-OTUB1 HD formation could not be detected by MS, which is likely due to the unknown molecular weight of these unique peptides, and excludes a direct examination of the nature of the FIH-OTUB1 bond.

Interestingly, asparagine can non-enzymatically form succinimide intermediates, which lead to amide bond formations with lysine residues during aging [61]. Furthermore, in specific bacterial proteins asparagine can auto-catalytically form succinimide intermediates that lead to amide bond formation with lysyl residues, provided that an additional glutamate or aspartate is present within a hydrophobic pocket [62]. FIH contains an aspartate (D201; iron coordination) and a lysyl residue (K214; 2-OG coordination) within its active center [63, 64]. Unfortunately, the involvement of K214 in covalent bond formation cannot be assessed since the enzymatic activity of FIH is likely lost following K214 mutation.

FIH-dependent asparagine hydroxylation of HIF still occurs at lower oxygen levels than PHD dependent prolyl hydroxylation [52, 65]. Here, we report an even higher oxygen sensitivity for FIH-mediated HD formation than for PHD-mediated HIFα destabilization. The half-maximal oxygen concentration (gas phase) for HD formation was determined as 4.1% O_2, which is in stark contrast to the previously determined sensitivity for FIH-dependent HIFα hydroxylation, being below 1% O_2 [51, 52]. Interestingly, the oxygen sensitivity of FIH-dependent hydroxylation depends on the used substrate and its length [66, 67]. Therefore, it is likely that the here observed unprecedentedly high oxygen sensitivity of FIH is encoded within the interacting peptide of the specific substrate.

Functionally, OTUB1 maintained enzymatic activity within the FIH:FIH-OTUB1 HT, while the regulation of its activity by UBCH5B was affected. OTUB1 enzymatic activity is regulated by E2 enzymes dependent on the presence of free mono-Ub and whether the E2 is charged with a covalently attached Ub. Mono-Ub in combination with Ub-charged E2 enzymes inhibits OTUB1 enzymatic activity due to interaction of the Ub of the charged E2 enzyme with an Ub binding site at the OTUB1 N-terminus and the interaction of the free mono-Ub with a second Ub binding site, preventing OTUB1 from binding its substrate (K48-linked Ub chains)

[23, 26, 27]. Uncharged E2 enzymes in turn stimulate OTUB1 activity by stabilizing the structure of the N-terminal Ub-binding site that is disordered in the apoenzyme [21, 26, 27]. When we assessed if OTUB1 DUB activity was preserved within the HT (in the absence of UBCH5B), we observed an initial increase of OTUB1 activity at 5 min, which decreased in comparison to non-complexed OTUB1 at later time points, coinciding with an increased release of mono-Ub. An E2 was not present, but FIH might mimic the effect of a charged E2 enzyme within the HT, as it also binds to the OTUB1 N-terminus. The stimulation of OTUB1 activity by uncharged UBCH5B was inverted when OTUB1 was complexed by FIH. This effect was again comparable to the regulation of OTUB1 activity by a charged E2 enzyme, although this time in the absence of free Ub. Overall, it seems likely that the functional regulation of OTUB1 by covalently bound FIH:FIH is due to its localization and its resemblance to an interacting charged E2 enzyme.

We observed that the formation of the FIH-OTUB1 heterodimer is slow (within the range of several hours) combined with slow degradation kinetics (up to 24 h). This is in stark contrast to the fast HIF-1α stabilization and degradation kinetics (seconds to minutes) [68]. The fast HIF-1α kinetic is crucial for its role as the main transcription factor for the cellular adaptation especially to acute changes in oxygen levels. The observed slow formation and degradation kinetics of the FIH-OTUB1 HD will make it insensitive to brief fluctuations of oxygen levels (minutes to possibly a few hours). Hence, the FIH-OTUB1 complex is likely not involved in acute but rather in chronic cellular adaptations to hypoxia, providing a further set point for cellular oxygen availability besides HIFα.

Interestingly, the monomeric prolyl-3-hydroxylase 2-OG and Fe(II)-dependent oxygenase domain-containing protein 1 (OGFOD1) has been shown to form an OGFOD1 activity-dependent SDS-PAGE resistant complex with its substrate ribosomal protein S23 (RPS23) [69, 70]. However, the oxygen sensitivity of the complex formation, a possible functional consequence or the nature of the interaction remained unclear. Of note, a point mutation in RPS23 that impairs its hydroxylation and stable complex formation with OGFOD1

has recently been linked to ribosomopathy in humans [71], indicating that covalent HD formation of hydroxylases with their substrates may be involved in human diseases.

ACKNOWLEDGEMENTS: We thank the Functional Genomics Center Zurich, Dr. Peter Hunziker and Dr. Paolo Nanni for performing mass spectrometry analyses; Daniel Prata for excellent technical support; Dr. Mu-Shui Dai (Oregon Health and Science University, Portland, Oregon, US) and Prof. Eric Metzen (University of Duisburg-Essen, Essen, Germany) for the kind gifts of plasmids.

The work was supported by the Swiss National Science Foundation (31003A_165679) (R.H.W.); a *Forschungskredit* of the University of Zurich (FK-15-046) (C.C.S.); and a Junior Grant of the NCCR Kidney.CH (C.C.S.).

DECLARATIONS OF INTEREST: none

REFERENCES

1. Semenza GL. Regulation of oxygen homeostasis by hypoxia-inducible factor 1. Physiology (Bethesda). 2009;24:97-106.

2. Kaelin WG, Jr., Ratcliffe PJ. Oxygen sensing by metazoans: the central role of the HIF hydroxylase pathway. Mol Cell. 2008;30(4):393-402.

3. Schofield CJ, Ratcliffe PJ. Oxygen sensing by HIF hydroxylases. Nat Rev Mol Cell Biol. 2004;5(5):343-354.

4. Scholz CC, Taylor CT. Hydroxylase-dependent regulation of the NF-κB pathway. Biol Chem. 2013;394(4):479-493.

5. Ploumakis A, Coleman ML. OH, the Places You'll Go! Hydroxylation, Gene Expression, and Cancer. Mol Cell. 2015;58(5):729-741.

6. Islam MS, Leissing TM, Chowdhury R, Hopkinson RJ, Schofield CJ. 2-Oxoglutarate-Dependent Oxygenases. Annu Rev Biochem. 2018;87:585-620.

7. Masson N, Singleton RS, Sekirnik R, Trudgian DC, Ambrose LJ, Miranda MX, Tian YM, Kessler BM, Schofield CJ, Ratcliffe PJ. The FIH hydroxylase is a cellular peroxide sensor that modulates HIF transcriptional activity. EMBO Rep. 2012;13(3):251-257.

8. Zhang N, Fu Z, Linke S, Chicher J, Gorman JJ, Visk D, Haddad GG, Poellinger L, Peet DJ, Powell F, Johnson RS. The asparaginyl hydroxylase factor inhibiting HIF-1alpha is an essential regulator of metabolism. Cell Metab. 2010;11(5):364-378.

9. Sim J, Cowburn AS, Palazon A, Madhu B, Tyrakis PA, Macias D, Bargiela DM, Pietsch S, Gralla M, Evans CE, Kittipassorn T, Chey YCJ, Branco CM, Rundqvist H, Peet DJ, Johnson RS. The Factor Inhibiting HIF Asparaginyl Hydroxylase Regulates Oxidative Metabolism and Accelerates Metabolic Adaptation to Hypoxia. Cell Metab. 2018;27(4):898-913.e897.

10. Cockman ME, Lancaster DE, Stolze IP, Hewitson KS, McDonough MA, Coleman ML, Coles CH, Yu X, Hay RT, Ley SC, Pugh CW, Oldham NJ, Masson N, Schofield CJ, Ratcliffe PJ. Posttranslational hydroxylation of ankyrin repeats in IkappaB proteins by the hypoxia-inducible factor (HIF) asparaginyl hydroxylase, factor inhibiting HIF (FIH). PNAS. 2006;103(40):14767-14772.

11. Cockman ME, Webb JD, Ratcliffe PJ. FIH-dependent asparaginyl hydroxylation of ankyrin repeat domain-containing proteins. Ann N Y Acad Sci. 2009;1177:9-18.

12. Karttunen S, Duffield M, Scrimgeour NR, Squires L, Lim WL, Dallas ML, Scragg JL, Chicher J, Dave KA, Whitelaw ML, Peers C, Gorman JJ, Gleadle JM, Rychkov GY, Peet DJ. Oxygen-dependent hydroxylation by FIH regulates the TRPV3 ion channel. J Cell Sci. 2015;128(2):225-231.

13. Rodriguez J, Pilkington R, Garcia Munoz A, Nguyen LK, Rauch N, Kennedy S, Monsefi N, Herrero A, Taylor CT, von Kriegsheim A. Substrate-Trapped Interactors of PHD3 and FIH Cluster in Distinct Signaling Pathways. Cell Rep. 2016;14(11):2745-2760.

14. Nagarajan Y, Rychkov GY, Peet DJ. Modulation of TRP Channel Activity by Hydroxylation and Its Therapeutic Potential. Pharmaceuticals (Basel, Switzerland). 2017;10(2).

15. Janke K, Brockmeier U, Kuhlmann K, Eisenacher M, Nolde J, Meyer HE, Mairbaurl H, Metzen E. Factor inhibiting HIF-1 (FIH-1) modulates protein interactions of apoptosis-stimulating p53 binding protein 2 (ASPP2). J Cell Sci. 2013;126(Pt 12):2629-2640.

16. Devries IL, Hampton-Smith RJ, Mulvihill MM, Alverdi V, Peet DJ, Komives EA. Consequences of IkappaB alpha hydroxylation by the factor inhibiting HIF (FIH). FEBS letters. 2010;584(23):4725-4730.

17. Scholz CC, Cavadas MA, Tambuwala MM, Hams E, Rodriguez J, von Kriegsheim A, Cotter P, Bruning U, Fallon PG, Cheong A, Cummins EP, Taylor CT. Regulation of IL-1β-

induced NF-κB by hydroxylases links key hypoxic and inflammatory signaling pathways. PNAS. 2013;110(46):18490-18495.

18. Scholz CC, Rodriguez J, Pickel C, Burr S, Fabrizio JA, Nolan KA, Spielmann P, Cavadas MA, Crifo B, Halligan DN, Nathan JA, Peet DJ, Wenger RH, Von Kriegsheim A, Cummins EP, Taylor CT. FIH regulates cellular metabolism through hydroxylation of the deubiquitinase OTUB1. PLoS Biol. 2016;14(1):e1002347.

19. Herhaus L, Al-Salihi M, Macartney T, Weidlich S, Sapkota GP. OTUB1 enhances TGFbeta signalling by inhibiting the ubiquitylation and degradation of active SMAD2/3. Nature communications. 2013;4:2519.

20. Clague MJ, Heride C, Urbe S. The demographics of the ubiquitin system. Trends Cell Biol. 2015;25(7):417-426.

21. Edelmann MJ, Iphofer A, Akutsu M, Altun M, di Gleria K, Kramer HB, Fiebiger E, Dhe-Paganon S, Kessler BM. Structural basis and specificity of human otubain 1-mediated deubiquitination. Biochem J. 2009;418(2):379-390.

22. Wang T, Yin L, Cooper EM, Lai MY, Dickey S, Pickart CM, Fushman D, Wilkinson KD, Cohen RE, Wolberger C. Evidence for bidentate substrate binding as the basis for the K48 linkage specificity of otubain 1. J Mol Biol. 2009;386(4):1011-1023.

23. Wiener R, Zhang X, Wang T, Wolberger C. The mechanism of OTUB1-mediated inhibition of ubiquitination. Nature. 2012;483(7391):618-622.

24. Nakada S, Tai I, Panier S, Al-Hakim A, Iemura S, Juang YC, O'Donnell L, Kumakubo A, Munro M, Sicheri F, Gingras AC, Natsume T, Suda T, Durocher D. Non-canonical inhibition of DNA damage-dependent ubiquitination by OTUB1. Nature. 2010;466(7309):941-946.

25. Juang YC, Landry MC, Sanches M, Vittal V, Leung CC, Ceccarelli DF, Mateo AR, Pruneda JN, Mao DY, Szilard RK, Orlicky S, Munro M, Brzovic PS, Klevit RE, Sicheri F, Durocher D. OTUB1 co-opts Lys48-linked ubiquitin recognition to suppress E2 enzyme function. Mol Cell. 2012;45(3):384-397.

26. Wiener R, DiBello AT, Lombardi PM, Guzzo CM, Zhang X, Matunis MJ, Wolberger C. E2 ubiquitin-conjugating enzymes regulate the deubiquitinating activity of OTUB1. Nat Struct Mol Biol. 2013;20(9):1033-1039.

27. Wolberger C. Mechanisms for regulating deubiquitinating enzymes. Protein Sci. 2014;23(4):344-353.

28. Mevissen TET, Komander D. Mechanisms of Deubiquitinase Specificity and Regulation. Annu Rev Biochem. 2017;86:159-192.

29. Stiehl DP, Wirthner R, Köditz J, Spielmann P, Camenisch G, Wenger RH. Increased prolyl 4-hydroxylase domain proteins compensate for decreased oxygen levels. Evidence for an autoregulatory oxygen-sensing system. J Biol Chem. 2006;281(33):23482-23491.

30. Wenger RH, Kurtcuoglu V, Scholz CC, Marti HH, Hoogewijs D. Frequently asked questions in hypoxia research. Hypoxia. 2015;3:35-43.

31. Lando D, Peet DJ, Gorman JJ, Whelan DA, Whitelaw ML, Bruick RK. FIH-1 is an asparaginyl hydroxylase enzyme that regulates the transcriptional activity of hypoxia-inducible factor. Genes Dev. 2002;16(12):1466-1471.

32. Sun XX, Challagundla KB, Dai MS. Positive regulation of p53 stability and activity by the deubiquitinating enzyme Otubain 1. EMBO J. 2012;31(3):576-592.

33. Tan S. A modular polycistronic expression system for overexpressing protein complexes in Escherichia coli. Protein Expr Purif. 2001;21(1):224-234.

34. Pickel C, Taylor CT, Scholz CC. Genetic Knockdown and Pharmacologic Inhibition of Hypoxia-Inducible Factor (HIF) Hydroxylases. Methods Mol Biol. 2018;1742:1-14.

35. Gutsche K, Randi EB, Blank V, Fink D, Wenger RH, Leo C, Scholz CC. Intermittent hypoxia confers pro-metastatic gene expression selectively through NF-kappaB in inflammatory breast cancer cells. Free Radic Biol Med. 2016;101:129-142.

36. Peach M, Marsh N, Macphee DJ. Protein solubilization: attend to the choice of lysis buffer. Methods Mol Biol. 2012;869:37-47.

37. Anderson BL, Berry RW, Telser A. A sodium dodecyl sulfate--polyacrylamide gel electrophoresis system that separates peptides and proteins in the molecular weight range of 2500 to 90,000. Anal Biochem. 1983;132(2):365-375.

38. Bradford MM. A rapid and sensitive method for the quantitation of microgram quantities of protein utilizing the principle of protein-dye binding. Anal Biochem. 1976;72:248-254.

39. Swamy M, Siegers GM, Minguet S, Wollscheid B, Schamel WW. Blue native polyacrylamide gel electrophoresis (BN-PAGE) for the identification and analysis of multiprotein complexes. Sci STKE. 2006;2006(345):pl4.

40. Camacho-Carvajal MM, Wollscheid B, Aebersold R, Steimle V, Schamel WW. Two-dimensional Blue native/SDS gel electrophoresis of multi-protein complexes from whole cellular lysates: a proteomics approach. Mol Cell Proteomics. 2004;3(2):176-182.

41. Neuhoff V, Arold N, Taube D, Ehrhardt W. Improved staining of proteins in polyacrylamide gels including isoelectric focusing gels with clear background at nanogram sensitivity using Coomassie Brilliant Blue G-250 and R-250. Electrophoresis. 1988;9(6):255-262.

42. Cox J, Mann M. MaxQuant enables high peptide identification rates, individualized p.p.b.-range mass accuracies and proteome-wide protein quantification. Nat Biotechnol. 2008;26(12):1367-1372.

43. Cox J, Neuhauser N, Michalski A, Scheltema RA, Olsen JV, Mann M. Andromeda: a peptide search engine integrated into the MaxQuant environment. J Proteome Res. 2011;10(4):1794-1805.

44. Wolski W, Grossmann J, Panse C. SRMService - R-Package to Report Quantitative Mass Spectrometry Data. 2018. Available from: http://github.com/protViz/SRMService.

45. Turker C, Akal F, Joho D, Panse C, Barkow-Oesterreicher S, Rehrauer H, Schlapbach R, editors. B-Fabric: The Swiss Army Knife for Life Sciences. EDBT 2010; 2010 March 22–26, 2010; Lausanne, Switzerland.

46. Vizcaino JA, Csordas A, del-Toro N, Dianes JA, Griss J, Lavidas I, Mayer G, Perez-Riverol Y, Reisinger F, Ternent T, Xu QW, Wang R, Hermjakob H. 2016 update of the PRIDE database and its related tools. Nucleic Acids Res. 2016;44(D1):D447-456.

47. Ciechanover A, Heller H, Elias S, Haas AL, Hershko A. ATP-dependent conjugation of reticulocyte proteins with the polypeptide required for protein degradation. PNAS. 1980;77(3):1365-1368.

48. Hershko A, Ciechanover A, Heller H, Haas AL, Rose IA. Proposed role of ATP in protein breakdown: conjugation of protein with multiple chains of the polypeptide of ATP-dependent proteolysis. PNAS. 1980;77(4):1783-1786.

49. Kostiuk MA, Keller BO, Berthiaume LG. Non-radioactive detection of palmitoylated mitochondrial proteins using an azido-palmitate analogue. Methods Enzymol. 2009;457:149-165.

50. Yeh TL, Leissing TM, Abboud MI, Thinnes CC, Atasoylu O, Holt-Martyn JP, Zhang D, Tumber A, Lippl K, Lohans CT, Leung IKH, Morcrette H, Clifton IJ, Claridge TDW, Kawamura A, Flashman E, Lu X, Ratcliffe PJ, Chowdhury R, Pugh CW, Schofield CJ. Molecular and cellular mechanisms of HIF prolyl hydroxylase inhibitors in clinical trials. Chem Sci. 2017;8(11):7651-7668.

51. Singleton RS, Trudgian DC, Fischer R, Kessler BM, Ratcliffe PJ, Cockman ME. Quantitative mass spectrometry reveals dynamics of factor-inhibiting hypoxia-inducible factor-catalyzed hydroxylation. J Biol Chem. 2011;286(39):33784-33794.

52. Tian YM, Yeoh KK, Lee MK, Eriksson T, Kessler BM, Kramer HB, Edelmann MJ, Willam C, Pugh CW, Schofield CJ, Ratcliffe PJ. Differential sensitivity of hypoxia inducible factor

hydroxylation sites to hypoxia and hydroxylase inhibitors. J Biol Chem. 2011;286(15):13041-13051.

53. Lancaster DE, McNeill LA, McDonough MA, Aplin RT, Hewitson KS, Pugh CW, Ratcliffe PJ, Schofield CJ. Disruption of dimerization and substrate phosphorylation inhibit factor inhibiting hypoxia-inducible factor (FIH) activity. Biochem J. 2004;383(Pt. 3):429-437.

54. Emmerich CH, Cohen P. Optimising methods for the preservation, capture and identification of ubiquitin chains and ubiquitylated proteins by immunoblotting. Biochem Biophys Res Commun. 2015;466(1):1-14.

55. Wells JN, Bergendahl LT, Marsh JA. Co-translational assembly of protein complexes. Biochem Soc Trans. 2015;43(6):1221-1226.

56. Pao KC, Wood NT, Knebel A, Rafie K, Stanley M, Mabbitt PD, Sundaramoorthy R, Hofmann K, van Aalten DMF, Virdee S. Activity-based E3 ligase profiling uncovers an E3 ligase with esterification activity. Nature. 2018;556(7701):381-385.

57. Termathe M, Leidel SA. The Uba4 domain interplay is mediated via a thioester that is critical for tRNA thiolation through Urm1 thiocarboxylation. Nucleic Acids Res. 2018;46(10):5171-5181.

58. Yang M, Hardy AP, Chowdhury R, Loik ND, Scotti JS, McCullagh JS, Claridge TD, McDonough MA, Ge W, Schofield CJ. Substrate selectivity analyses of factor inhibiting hypoxia-inducible factor. Angewandte Chemie (International ed in English). 2013;52(6):1700-1704.

59. Yang M, Ge W, Chowdhury R, Claridge TD, Kramer HB, Schmierer B, McDonough MA, Gong L, Kessler BM, Ratcliffe PJ, Coleman ML, Schofield CJ. Asparagine and aspartate hydroxylation of the cytoskeletal ankyrin family is catalyzed by factor-inhibiting hypoxia-inducible factor. J Biol Chem. 2011;286(9):7648-7660.

60. Yang M, Chowdhury R, Ge W, Hamed RB, McDonough MA, Claridge TD, Kessler BM, Cockman ME, Ratcliffe PJ, Schofield CJ. Factor-inhibiting hypoxia-inducible factor (FIH) catalyses the post-translational hydroxylation of histidinyl residues within ankyrin repeat domains. Febs J. 2011;278(7):1086-1097.

61. Friedrich MG, Wang Z, Schey KL, Truscott RJW. Spontaneous cross-linking of proteins at aspartate and asparagine residues is mediated via a succinimide intermediate. Biochem J. 2018;475(20):3189-3200.

62. Sridharan U, Ponnuraj K. Isopeptide bond in collagen- and fibrinogen-binding MSCRAMMs. Biophys Rev. 2016;8(1):75-83.

63. Dann CE, 3rd, Bruick RK, Deisenhofer J. Structure of factor-inhibiting hypoxia-inducible factor 1: An asparaginyl hydroxylase involved in the hypoxic response pathway. PNAS. 2002;99(24):15351-15356.

64. Elkins JM, Hewitson KS, McNeill LA, Seibel JF, Schlemminger I, Pugh CW, Ratcliffe PJ, Schofield CJ. Structure of factor-inhibiting hypoxia-inducible factor (HIF) reveals mechanism of oxidative modification of HIF-1 alpha. J Biol Chem. 2003;278(3):1802-1806.

65. Stolze IP, Tian YM, Appelhoff RJ, Turley H, Wykoff CC, Gleadle JM, Ratcliffe PJ. Genetic analysis of the role of the asparaginyl hydroxylase factor inhibiting hypoxia-inducible factor (FIH) in regulating hypoxia-inducible factor (HIF) transcriptional target genes [corrected]. J Biol Chem. 2004;279(41):42719-42725.

66. Wilkins SE, Hyvarinen J, Chicher J, Gorman JJ, Peet DJ, Bilton RL, Koivunen P. Differences in hydroxylation and binding of Notch and HIF-1alpha demonstrate substrate selectivity for factor inhibiting HIF-1 (FIH-1). Int J Biochem Cell Biol. 2009;41(7):1563-1571.

67. Ehrismann D, Flashman E, Genn DN, Mathioudakis N, Hewitson KS, Ratcliffe PJ, Schofield CJ. Studies on the activity of the hypoxia-inducible-factor hydroxylases using an oxygen consumption assay. Biochem J. 2007;401(1):227-234.

68. Jewell UR, Kvietikova I, Scheid A, Bauer C, Wenger RH, Gassmann M. Induction of HIF-1alpha in response to hypoxia is instantaneous. FASEB J. 2001;15(7):1312-1314.

69. Singleton RS, Liu-Yi P, Formenti F, Ge W, Sekirnik R, Fischer R, Adam J, Pollard PJ, Wolf A, Thalhammer A, Loenarz C, Flashman E, Yamamoto A, Coleman ML, Kessler BM, Wappner P, Schofield CJ, Ratcliffe PJ, Cockman ME. OGFOD1 catalyzes prolyl hydroxylation of RPS23 and is involved in translation control and stress granule formation. PNAS. 2014;111(11):4031-4036.

70. Horita S, Scotti JS, Thinnes C, Mottaghi-Taromsari YS, Thalhammer A, Ge W, Aik W, Loenarz C, Schofield CJ, McDonough MA. Structure of the ribosomal oxygenase OGFOD1 provides insights into the regio- and stereoselectivity of prolyl hydroxylases. Structure. 2015;23(4):639-652.

71. Paolini NA, Attwood M, Sondalle SB, Vieira CM, van Adrichem AM, di Summa FM, O'Donohue MF, Gleizes PE, Rachuri S, Briggs JW, Fischer R, Ratcliffe PJ, Wlodarski MW, Houtkooper RH, von Lindern M, Kuijpers TW, Dinman JD, Baserga SJ, Cockman ME, MacInnes AW. A Ribosomopathy Reveals Decoding Defective Ribosomes Driving Human Dysmorphism. Am J Hum Genet. 2017;100(3):506-522.

Supplementary Data

FIH regulates OTUB1 deubiquitinase activity through oxygen-dependent covalent complex formation

Christina Pickel, Julia Günter, Amalia Ruiz-Serrano, Patrick Spielmann, Jacqueline-Alba Fabrizio, Witold Wolski, Daniel J. Peet, Roland H. Wenger, and Carsten C. Scholz

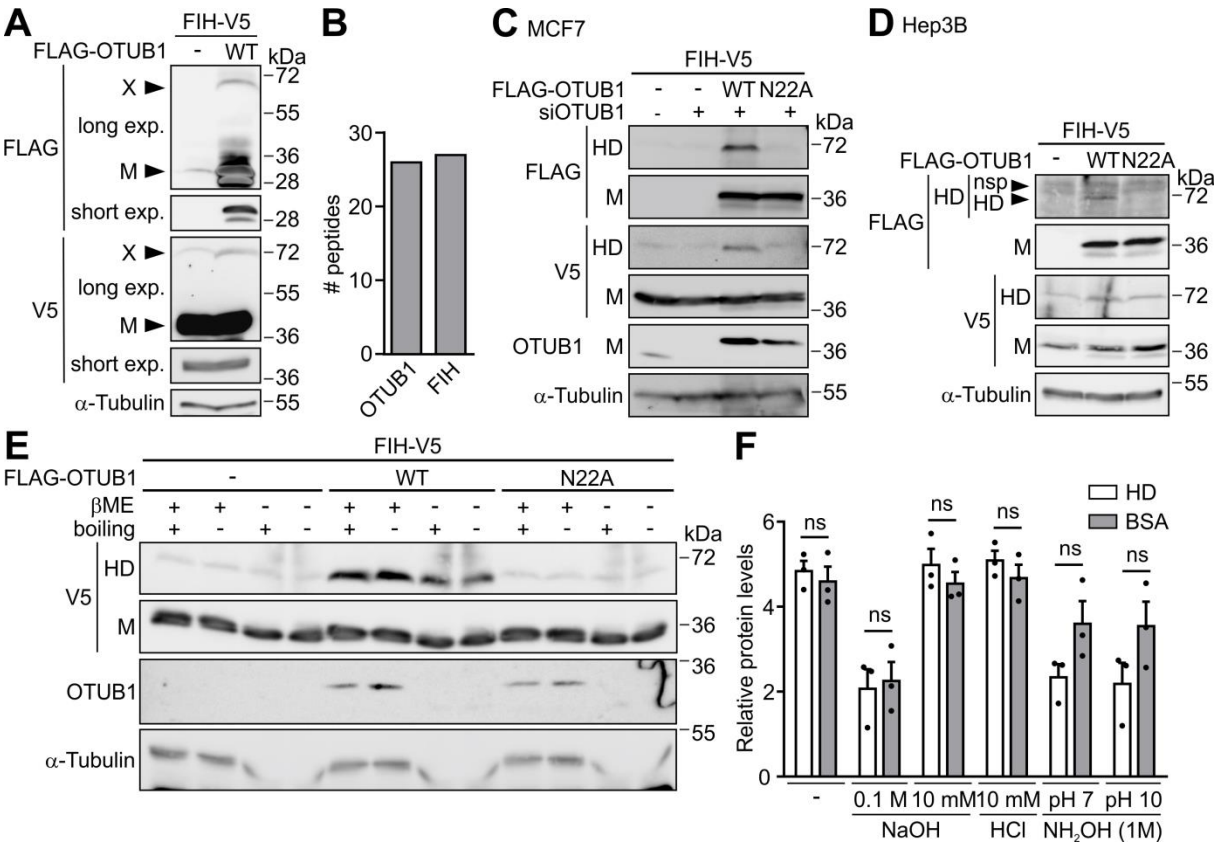

Fig S1. Cell-type independent covalent FIH-OTUB1 HD formation. (**A**) Ectopic expression of FLAG-OTUB1 in combination with FIH-V5 led to the detection of protein signal "X" at 72 kDa with both anti-FLAG and anti-V5 antibodies. (**B**) MS analysis of protein X excised from a SDS-PAGE gel following IP from HEK293 cell lysates demonstrated that protein X contained both OTUB1 and FIH. (**C**, **D**) Detection of the heterodimer (HD) by immunoblotting in MCF7 breast adenocarcinoma (C) and Hep3B liver carcinoma cell lysates (D) with the indicated plasmid-dependent expressions and knockdowns. (**E**) Immunoblot analysis of HEK293 lysates with the indicated ectopic expression in the presence or absence of 858 mM β-mercaptoethanol (βME) and boiling. (**F**) Quantification of the experiment described in Fig 1D. M, monomer; ab, antibody; nsp, non-specific. Data are shown as mean + SEM from (F) three independent experiments or are representative for (B) one or (A, C-F) three independent experiments. Statistical analysis by two-way ANOVA followed by Tukey post-test (ns, not significant).

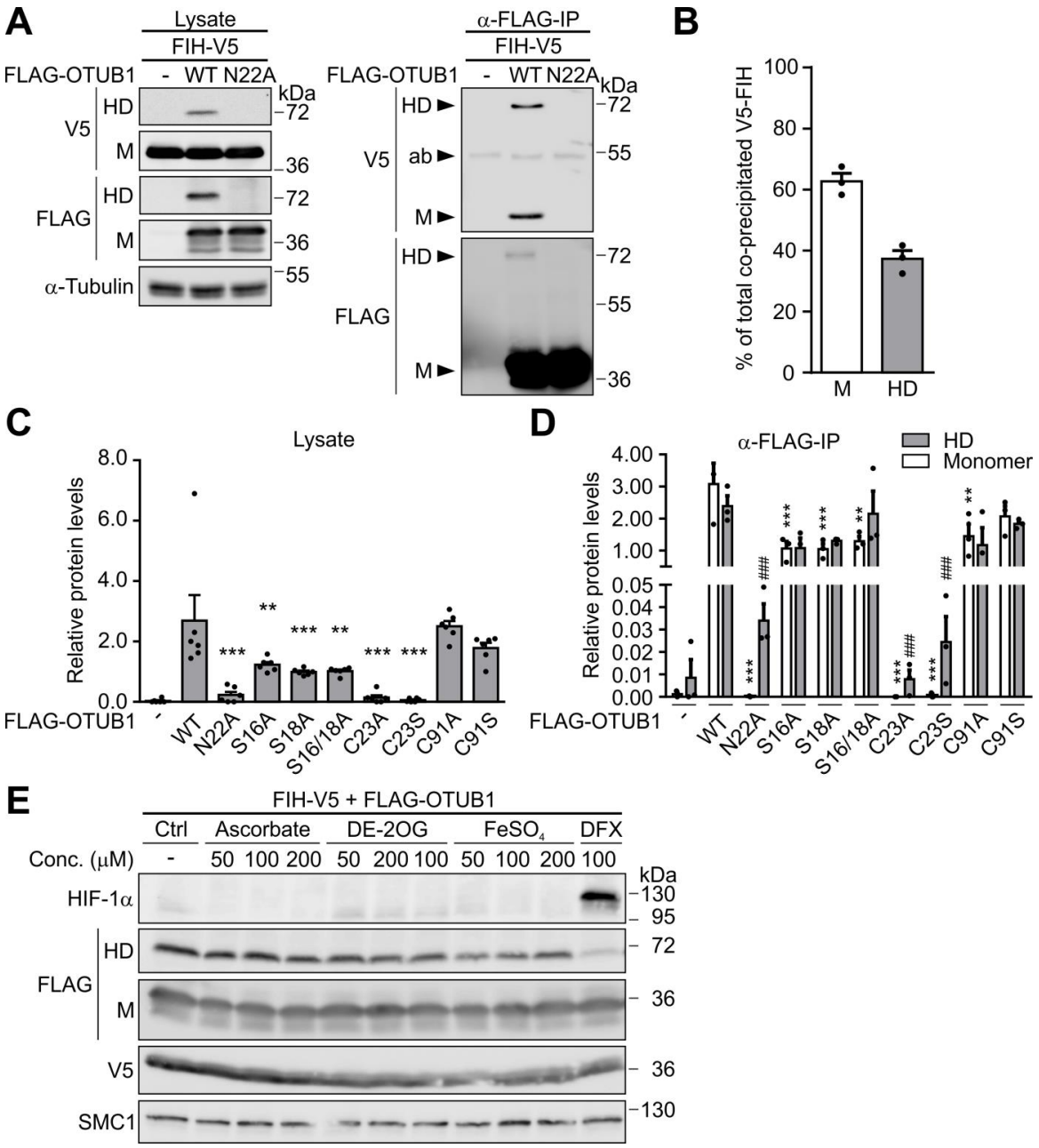

Fig S2. Formation of the FIH-OTUB1 HD depends on the OTUB1 hydroxylation site and FIH activity. (**A**) Immunoblotting following anti-FLAG IP of HEK293 lysates containing the indicated ectopic expressions. (**B**) Quantification of monomeric FIH (M) and of the FIH-OTUB1 HD of the experiments shown in (A). (**C**, **D**) Quantification of the experiments shown in Fig 1E. (**E**) Immunoblot analysis of HEK293 cells following the addition of FIH co-factors/substrates or the iron chelator DFX. HD, heterodimer; M, monomer; ab, antibody. Data are shown as mean + SEM from (B, D) three or (C) six independent experiments or are representative of (A, E) three independent experiments. **, p<0.01; ***/###, p<0.001 by one-way ANOVA followed by Tukey post-test. *, statistically significant compared with HD WT; #, statistically significant compared with M WT.

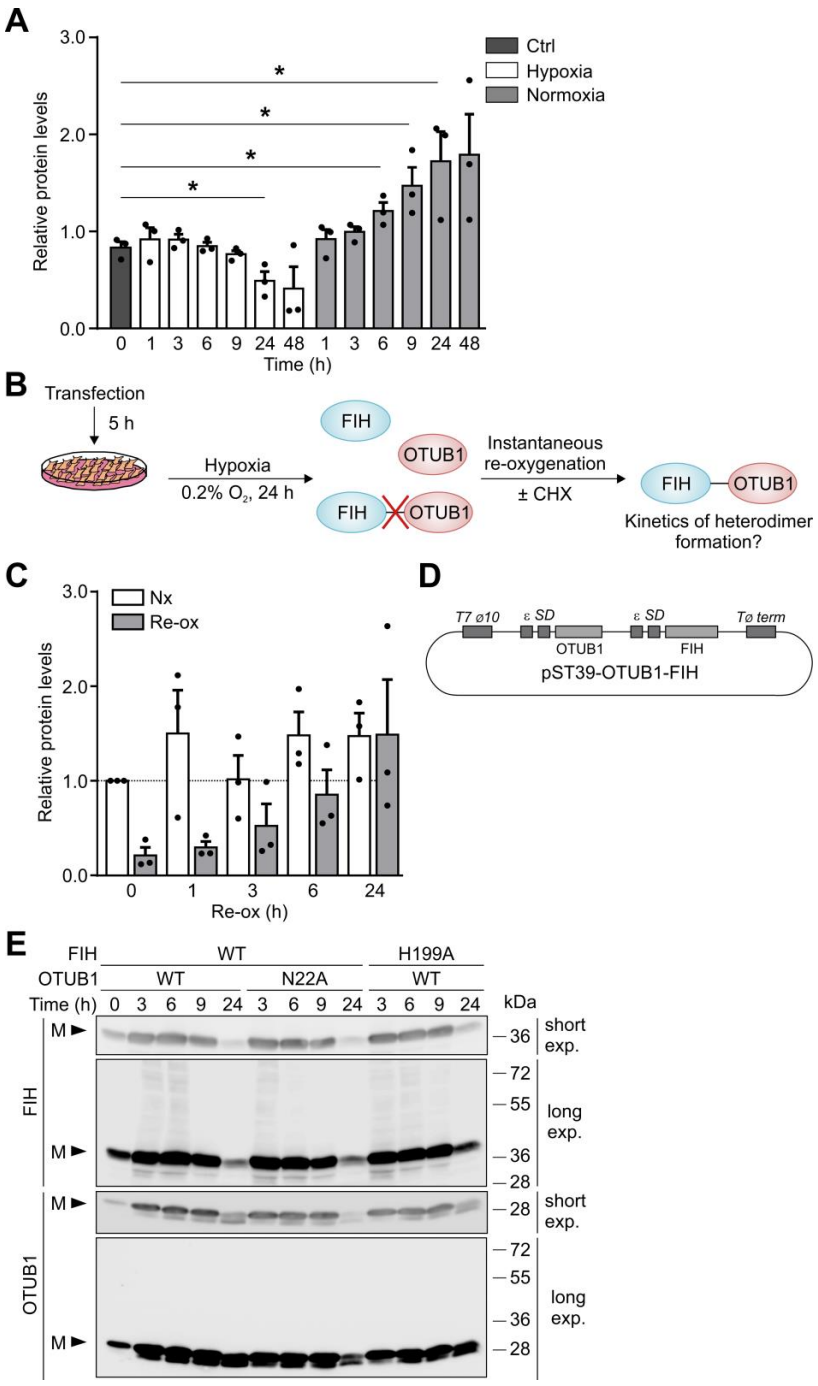

Fig S3. FIH-OTUB1 HD stability and formation kinetics. (**A**) Quantification of the experiment depicted in Fig 3A. (**B**) Illustration of the experimental procedures performed in Fig 3B and 3C. HEK293 cells were transiently co-transfected with FIH-V5 and FLAG-OTUB1 WT, incubated in hypoxia (0.2% O_2) for 24 h and instantaneously re-oxygenated in the presence or absence of 400 µM cycloheximide (CHX). (**C**) Quantification of the experiment depicted in Fig 3B. (**D**) Plasmid map of the bacterial bicistronic expression vector pST39-His-OTUB1-MBP-FIH. T7 Ø10, T7 promotor; T7 term, T7 terminator; ε, translational enhancer; SD, Shine-Dalgarno sequence. (**E**) Immunoblot analysis of co-inoculated bacterial cultures expressing either OTUB1 or FIH. Bacteria were transformed with either OTUB1 or FIH expression plasmids, cultivated separately and then mixed in a 1:1 ratio followed by induction of the indicated protein expression. HD, heterodimer; M, monomer; exp., exposure. Data are shown as mean + SEM from three independent experiments or are representative for (E) two independent experiments.

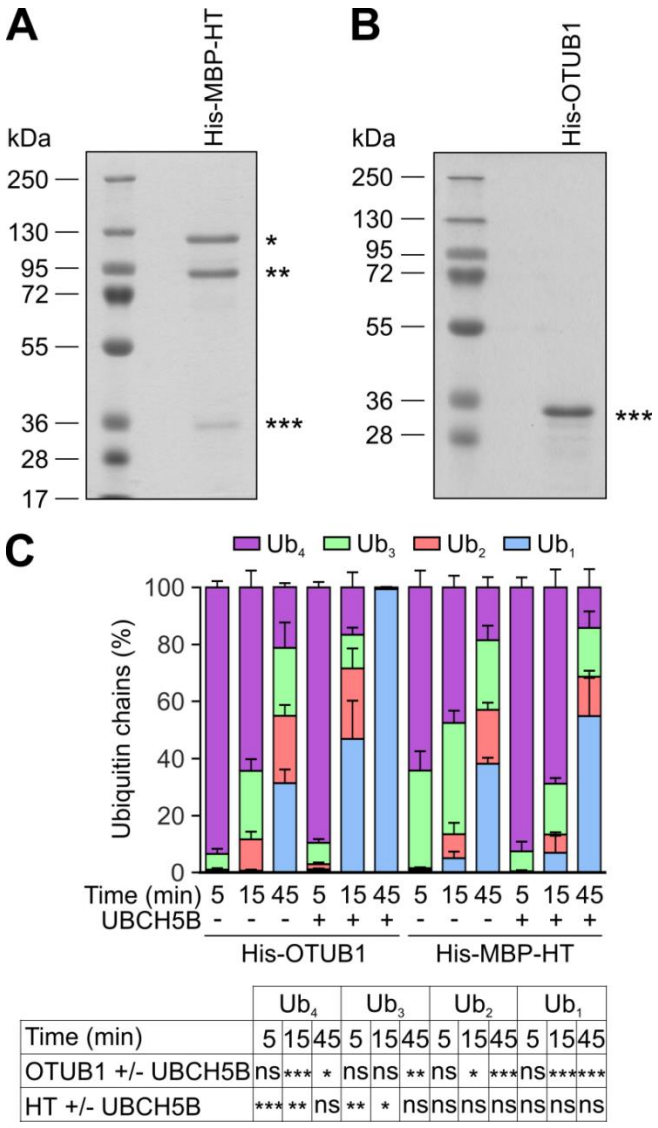

	Ub_4			Ub_3			Ub_2			Ub_1		
Time (min)	5	15	45	5	15	45	5	15	45	5	15	45
OTUB1 +/- UBCH5B	ns	***	*	ns	ns	**	ns	*	***	ns	***	***
HT +/- UBCH5B	***	**	ns	**	*	ns	ns	ns	ns	ns	ns	ns

Fig S4. Quality control of purified FIH:FIH-OTUB1 HT and His-tagged OTUB1 for *in vitro* activity assays. (**A**) His-OTUB1-MBP-FIH:FIH-MBP heterotrimer (His-MBP-HT) was purified from *E. coli* by sequential MBP- and Ni^{2+}-affinity purification and analyzed by SDS-PAGE and colloidal Coomassie staining. (**B**) His-OTUB1 was purified from *E. coli* by Ni^{2+}-affinity purification and analyzed by SDS-PAGE and colloidal Coomassie staining. *, FIH-OTUB1 heterodimer (predicted MW: 117.82 kDa); **, monomeric MBP-FIH originating from the native protein complex (predicted MW: 83.78 kDa); ***, monomeric His-OTUB1 (predicted MW: 34.04 kDa). (**C**) Quantification of each single Ub chain of the experiment depicted in Fig. 5C. Data are shown as mean + SEM from three independent experiments. *, $p<0.05$; **, $p<0.01$; ***, $p<0.001$ by two-way ANOVA followed by Tukey post-test.

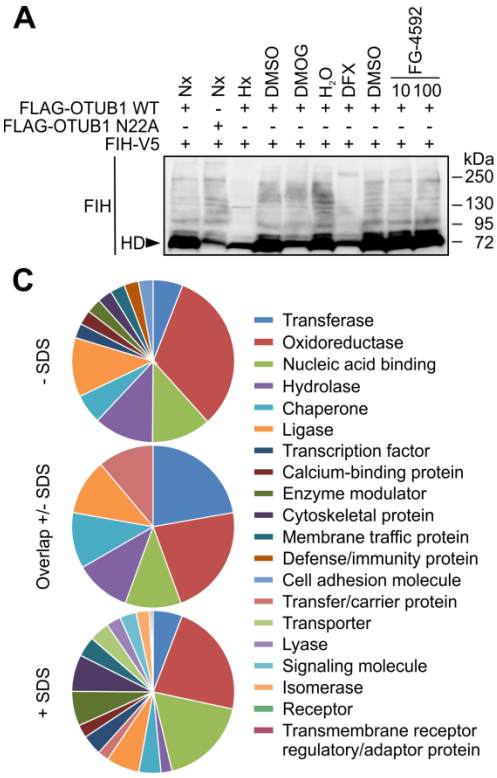

B

Abbreviation	Full protein name	UniProt Access. No.
CCT6A	T-complex protein 1 subunit zeta	P40227
UBA1	Ubiquitin-like modifier-activating enzyme 1	P22314
EF-1β	Elongation factor 1-beta	P24534
OTUB1	Ubiquitin thioesterase OTUB1	Q96FW1
CDK1	Cyclin-dependent kinase 1	P06493
FPPS	Farnesyl pyrophosphate synthase	P14324
1A34	HLA class I histocompatibility antigen, A-34 alpha chain	P30453
eIF4G1	Eukaryotic translation initiation factor 4 gamma 1	Q04637
Emerin	Emerin	P50402
IκBβ	NF-kappa-B inhibitor beta	Q15653
NDUFA9	NADH dehydrogenase [ubiquinone] 1 alpha subcomplex subunit 9, mitochondrial	Q16795
KRT5	Keratin, type I, cytoskeletal 5	P13647
MRT4	Exosome RNA helicase MRT4	P42285

Fig S5. FIH interactome under native and denaturing conditions. (**A**) Longer exposure of the FIH immunoblot shown in Fig 2A. (**B**) Protein abbreviations, full names and uniprot.org identifiers of proteins detected as FIH interactors under both lysis conditions. (**C**) Proteins shown in Fig 6C were analyzed and categorized for protein class using the Panther classification system (www.pantherdb.org). HD, heterodimer. Data were analyzed from (B, C) four biological replicates or are representative for (A) three independent experiments.

4. The deubiquitinase OTUB1 is essential for development, respiration, energy metabolism and cardiac function

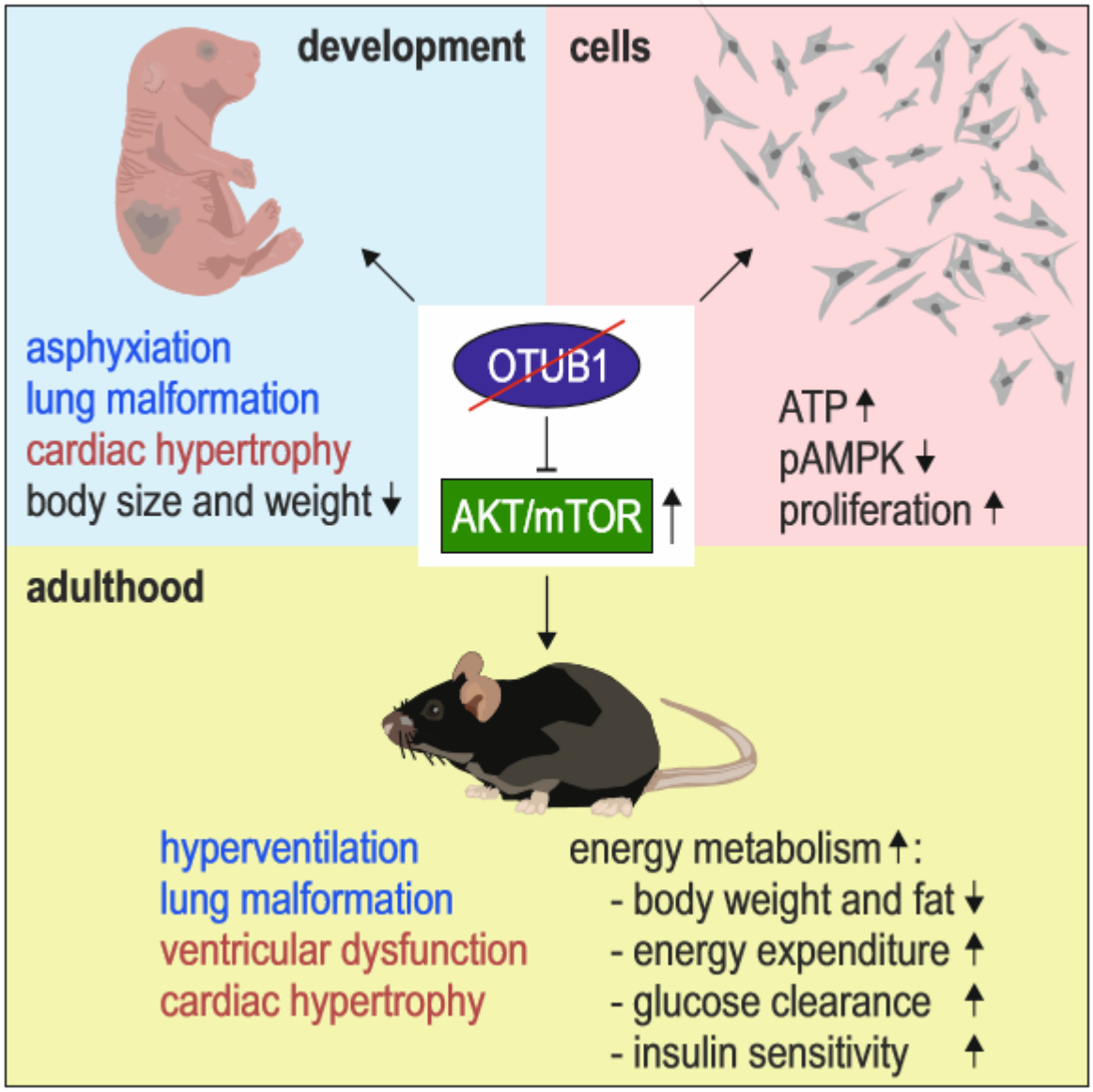

The deubiquitinase OTUB1 is essential for development, energy metabolism, respiration, and cardiac function

Amalia Ruiz-Serrano[1], Josep Monné Rodríguez[2], Christina N. Boyle[3], Julia Günter[1,4], Sarah Costantino[5], Pascal Flüchter[1], Svende Pfundstein[1], Andreas M. Bapst[1], Giovanni Pellegrini[2], Carsten A. Wagner[1,4], Thomas A. Lutz[3], Francesco Paneni[5], Roland H. Wenger[1,4,*], and Carsten C. Scholz[1,4,*]

[1]Institute of Physiology, University of Zurich, Zurich, Switzerland.
[2]Laboratory for Animal Model Pathology (LAMP), Institute of Veterinary Pathology, University of Zurich, Zurich, Switzerland.
[3]Institute of Veterinary Physiology, University of Zurich, Zurich, Switzerland.
[4]National Centre of Competence in Research 'Kidney.CH', Switzerland.
[5]Center for Molecular Cardiology, Schlieren Campus, University of Zurich, Schlieren, Switzerland; University Heart Center, Cardiology, University Hospital Zurich, Switzerland; Department of Research and Education, University Hospital Zurich, Switzerland.

Running title: Physiological functions of OTUB1 in mice.

Keywords: ubiquitin, deubiquitinating enzyme, respiratory distress syndrome, cardiac dysfunction, diabetes, insulin resistance, metabolic syndrome, FIH, HIF1AN, hypoxia.

***Correspondence to:**

Dr. Carsten Scholz
Institute of Physiology
University of Zurich
Winterthurerstr. 190
8057 Zurich
Switzerland
E-mail: carsten.scholz@uzh.ch
Tel: +41 44 635 50 75

Prof. Roland H. Wenger
Institute of Physiology
University of Zurich
Winterthurerstr. 190
8057 Zurich
Switzerland
E-mail: roland.wenger@access.uzh.ch
Tel: +41 44 635 50 65

ABSTRACT

Deubiquitinases (DUBs) are key regulators of the ubiquitin system, which is an integral part of most cellular signalling pathways. The DUB OTUB1 is ubiquitously expressed with one of the highest cellular protein levels of all DUBs. However, the physiological function of OTUB1 is unknown. Here we show that constitutive *Otub1* deletion in mice leads to perinatal lethality caused by asphyxiation. Adult mice with conditional whole-body *Otub1* deletion (wb*Otub1*$^{-/-}$) hyperventilated and were unable to adapt their respiratory pattern to hypoxia. wb*Otub1*$^{-/-}$ mice developed cardiac hypertrophy and left ventricular dysfunction. Moreover, wb*Otub1*$^{-/-}$ led to an increase in energy metabolism, including reduced body weight gain, accelerated energy expenditure and enhanced insulin sensitivity. *Otub1* deletion elevated basal and stimulated AKT/mTOR signalling in cells and tissues, which likely caused the observed phenotypes. These results demonstrate that OTUB1 has an essential role in energy metabolism as well as for embryonic development, respiratory and cardiac function.

INTRODUCTION

The ubiquitin system plays an essential role in virtually all cellular signalling pathways and, hence, in cell and tissue homeostasis[72]. The ubiquitin system regulates cellular proteins by conjugation of ubiquitin proteins (Ub) via Ub-conjugating enzymes (E1s, E2s, E3s)[72]. Poly-Ub chains can differ in the amino acid residue(s) used to inter-connect Ub proteins within the chains (either via the Ub N-terminal methionine or through seven different lysine residues), leading to distinct three-dimensional chain structures and different downstream effects[73]. K48-linked Ub chains are the most abundant Ub modification in cells, targeting modified proteins for proteasomal degradation[20]. K63-Ub chains are the second most abundant Ub-chain type[20], serving as inducible scaffolds in multiple signalling pathways[74].

Deubiquitinases (DUBs) are negative regulators of the Ub system, removing or trimming Ub chains and regulating the available pool of free Ub[72, 73]. DUBs recently gained interest as therapeutic targets for various diseases[72]. However, the function and regulation of many DUBs is insufficiently understood. The DUB ovarian tumor (OTU) domain-containing ubiquitin aldehyde binding protein 1 (OTUB1) shows one of the highest cellular protein levels of all known approximately 100 DUBs[20, 72]. OTUB1 exhibits a unique combination of canonical and non-canonical functions. Canonically, OTUB1 specifically cleaves K48-ubiquitin chains, preventing proteasomal degradation of substrate proteins[22, 75]. In addition, OTUB1 inhibits E2 enzymes independent of its enzymatic activity, impeding K48- and K63-linked ubiquitin chain formation[19, 24, 25, 76]. OTUB1 has been implicated in the regulation of various pathways and processes *in vitro*, ranging from pro-inflammatory signalling[77-79], to pro-fibrotic signalling[19], the DNA damage response[24], proliferation[80, 81] and apoptosis[77].

We previously showed that the cellular oxygen sensor factor inhibiting HIF (FIH) interacts with OTUB1[82-85] and hydroxylates it on asparagine 22[85], regulating cellular energy metabolism[85]. Furthermore, FIH and OTUB1 form a denaturation-resistant protein-protein complex, regulating OTUB1 enzymatic activity[83].

Constitutive whole-body deletion of *Otub1* in mice is lethal during development[86, 87], but the induced developmental defects, the underlying cause(s) of the lethality and the involved molecular mechanism(s) are unknown. Some central nervous system (CNS) and immune cell-specific functions of OTUB1 were recently analysed in mice. In a mouse model of CNS autoimmunity, deletion of *Otub1* in astrocytes increased neuroinflammation[87]. *Otub1* ablation in dendritic cells decreased the immune response to parasite infection and LPS stimulation[88]. Conditional deletion of *Otub1* in B cells led to a hyperactive B cell state[89]. CD8+ T cells with *Otub1* knockout (KO) revealed an increased sensitivity to IL-15[90]. Natural killer cells without *Otub1* were hypersensitive to cytokine-dependent stimulation[90]. OTUB1 recently gained interest as possible novel therapeutic target in cancer, because it was linked to the regulation of many cancer-associated pathways, such as p53, RhoA, AKT, mTOR, MAPK and FOXM1[90, 91]. Furthermore, increased OTUB1 levels were associated with increased tumor invasiveness and metastasis in different cancer types[91].

Overall, various links exist between OTUB1, cancer, inflammation and immunity, leading to an increasing interest in OTUB1 as pharmacologic target. However, the physiological function of OTUB1 is still unclear. Therefore, we aimed to characterize the physiological role of OTUB1 in mice to increase our understanding of its function *in vivo* and its value as pharmacologic target.

RESULTS

Homozygous *Otub1* deletion induces lethal developmental defects

OTUB1 is ubiquitously expressed in humans and mice (Supplementary Fig. 1a-c). To elucidate OTUB1 function *in vivo*, we therefore characterized mice with constitutive whole-body heterozygous and homozygous *Otub1* deletion (Fig. 1a). Homozygous *Otub1* KO was lethal, while *Otub1* haploinsufficient mice were viable (Fig. 1b,c). Absence of OTUB1 did not affect the sex ratio (Fig. 1b,c). Most *Otub1*$^{-/-}$ mice died perinatally, but there were still less *Otub1*$^{-/-}$ mice observed at E18.5 (births occurred on average at E19.5) than expected when assuming a Mendelian distribution (Fig. 1b,c). On a few occasions, remnants of absorptions were observed at E18.5, two of which could be identified as *Otub1*$^{-/-}$, suggesting that a small number of *Otub1*$^{-/-}$ mice died during earlier developmental processes. While *Otub1*$^{+/-}$ embryos were comparable in size and weight to *Wt* mice, *Otub1*$^{-/-}$ embryos were significantly lighter and smaller than *Otub1*$^{+/-}$ mice (Fig. 1d,e). The ventricular wall diameter and the heart weight of *Otub1*$^{-/-}$ animals were increased (Fig. 1f,g). Other organs showed no gross histological abnormalities (Supplementary Fig. 1d) or weight differences (Supplementary Fig. 1e).

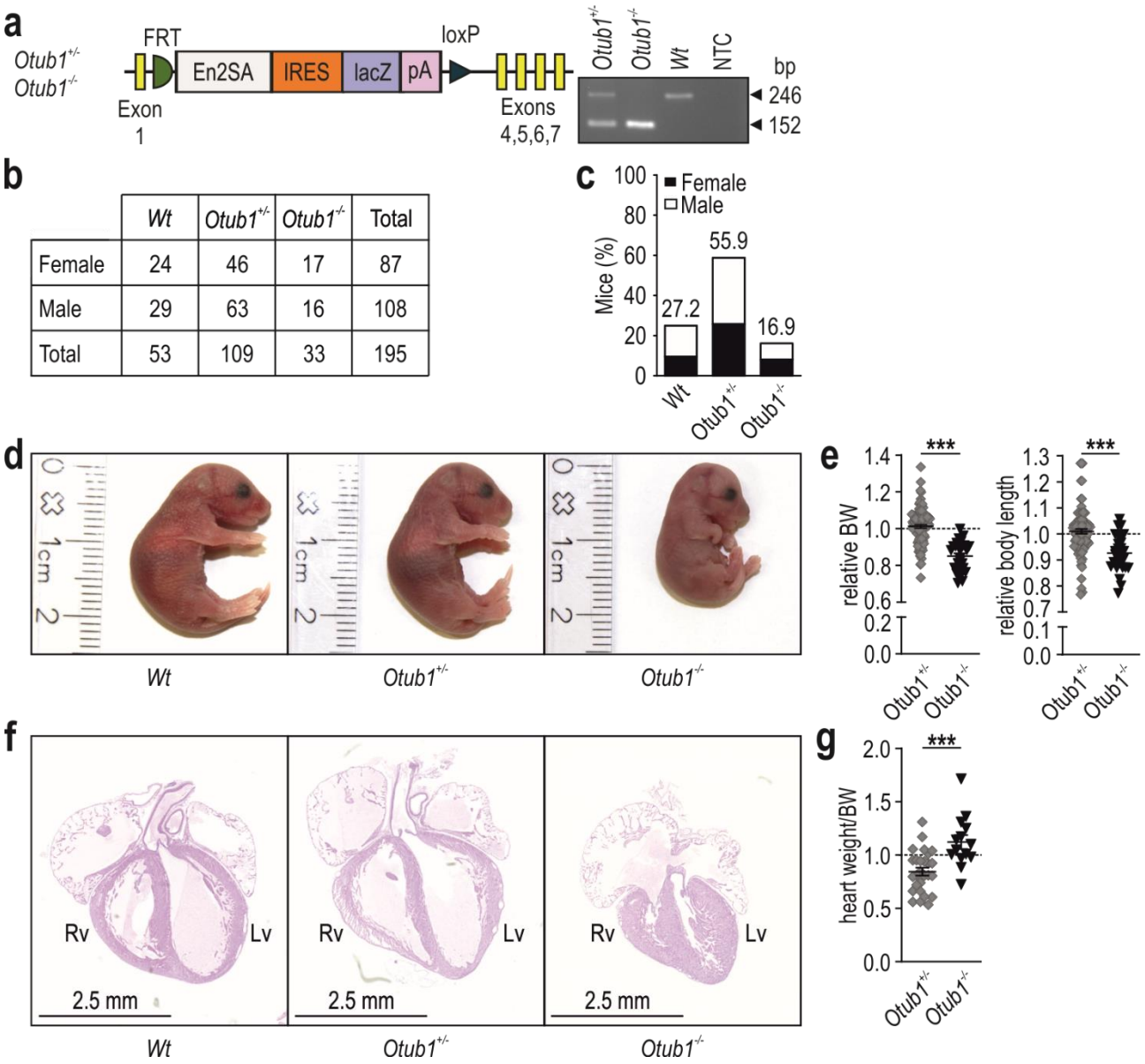

	Wt	Otub1+/-	Otub1-/-	Total
Female	24	46	17	87
Male	29	63	16	108
Total	53	109	33	195

Fig. 1: Gross developmental defects in *Otub1*$^{-/-}$ mice. a, Genotype of mice with heterozygous or homozygous *Otub1* deletion (*Otub1*$^{+/-}$ or *Otub1*$^{-/-}$). Image shows PCR results determining the genotype. En2SA, engrailed 2 gene splice acceptor; IRES, internal ribosome entry site; lacZ, β-galactosidase gene; pA, polyadenylation; FRT, flippase recognition target; loxP, locus of X (cross)-over in P1; *Wt*, wildtype; NTC, non-template control. **b,** Total numbers of observed mice and gender distribution within each genotype following *Otub1*$^{+/-}$ mating (E18.5 and P0). **c,** Relative distribution of genotypes and genders following *Otub1*$^{+/-}$ mating. The numbers in the graph indicate the total percentage of each genotype. **d,** Representative images of *wildtype* (*Wt*), *Otub1*$^{+/-}$ and *Otub1*$^{-/-}$ mice (P0). **e,** Body weight (BW) and body length relative to *Wt* littermates (E18.5; *Otub1*$^{+/-}$, n = 94; *Otub1*$^{-/-}$, n = 27) **f,** H&E staining of frontal heart sections (P0). Rv/Lv, right/left ventricle. **g,** *Otub1*$^{+/-}$ (n=27) and *Otub1*$^{-/-}$ (n = 14) heart weight corrected for BW and normalised to the corresponding *Wt* (n=15) littermates (E18.5). The dashed line indicates *Wt* littermates. Data are presented as mean ± SEM. ***, p<0.001 by two-tailed Student's t-test. Exact P values: **e,** relative BW: <0.0001; relative body length: <0.0001; **g,** 0.0003.

Constitutive *Otub1* deletion prevents respiration

Although the lung of *Otub1*$^{-/-}$ mice showed no difference in weight and gross morphology, we observed gasping in *Otub1*$^{-/-}$ new-born pups (P0) and E18.5 embryos (excised by caesarean section). In contrast to *Wt* and *Otub1*$^{+/-}$ lungs, *Otub1*$^{-/-}$ lungs sank during a floating test, demonstrating that *Otub1*$^{-/-}$ animals were unable to inflate their lungs (Fig. 2a). Histological analyses of the lungs showed that the saccular air space was significantly decreased in *Otub1*$^{-/-}$ mice (Fig. 2b). While glycogen is necessary for the production of surfactant phospholipids[92], we found no difference in glycogen stained by periodic acid-Schiff (PAS) (Fig. 2c). Also surfactant protein C (SPC) showed comparable levels by immunohistochemistry (IHC) between the genotypes (Fig. 2d) and transmission electron microscopy depicted a normal visual appearance of lamellar bodies in *Otub1*$^{-/-}$ embryos (Supplementary Fig. 1f). These results indicated a normal surfactant production in *Otub1*$^{-/-}$ embryos. IHC detection of CD31, a marker of vascular endothelial cells[93], showed a significant decrease for *Otub1*$^{-/-}$ lungs compared to *Wt* but not to *Otub1*$^{+/-}$ lungs (Fig. 2e). *Otub1*$^{+/-}$ embryos showed a (non-significant) decrease in CD31 lung staining compared to *Wt* without developing a lung phenotype (Fig. 2e) and the difference between *Otub1*$^{+/-}$ and *Otub1*$^{-/-}$ embryos was rather small and also not significant (Fig. 2e). Therefore, it appeared implausible that the pulmonary vessel density was a major contributor to the *Otub1*$^{-/-}$ lung phenotype.

OTUB1 has previously been shown to regulate apoptosis via e.g. increased cleaved caspase 3 (clCasp3) levels[77]. In E18.5 *Otub1*$^{-/-}$ lungs, clCasp3 levels were comparable to *Wt* lungs but significantly increased compared to *Otub1*$^{+/-}$ (Fig. 2f). The groups displayed a large variability in clCasp3 levels, but, importantly, the clCasp3 levels were overall very low (Fig. 2f). Hence, apoptosis was unlikely to contribute to the *Otub1*$^{-/-}$ lung phenotype.

OTUB1 has also been reported to regulate proliferation[80, 81]. Analysis of proliferation by Ki67 IHC demonstrated that *Otub1* deletion significantly enhanced proliferation in the developing lung compared to both *Otub1*$^{+/-}$ and *Wt* mice (Fig. 2g). In HEK293 cells, OTUB1 knockdown increased proliferation, and rescue by OTUB1 ectopic expression

decreased the proliferation back to levels comparable to control cells (Supplementary Fig. 1g). In summary, we suggest that *Otub1* ablation decreased the saccular air space through increased cell proliferation, which led to the inability of *Otub1*$^{-/-}$ mice to inflate their lungs and caused the perinatal lethality.

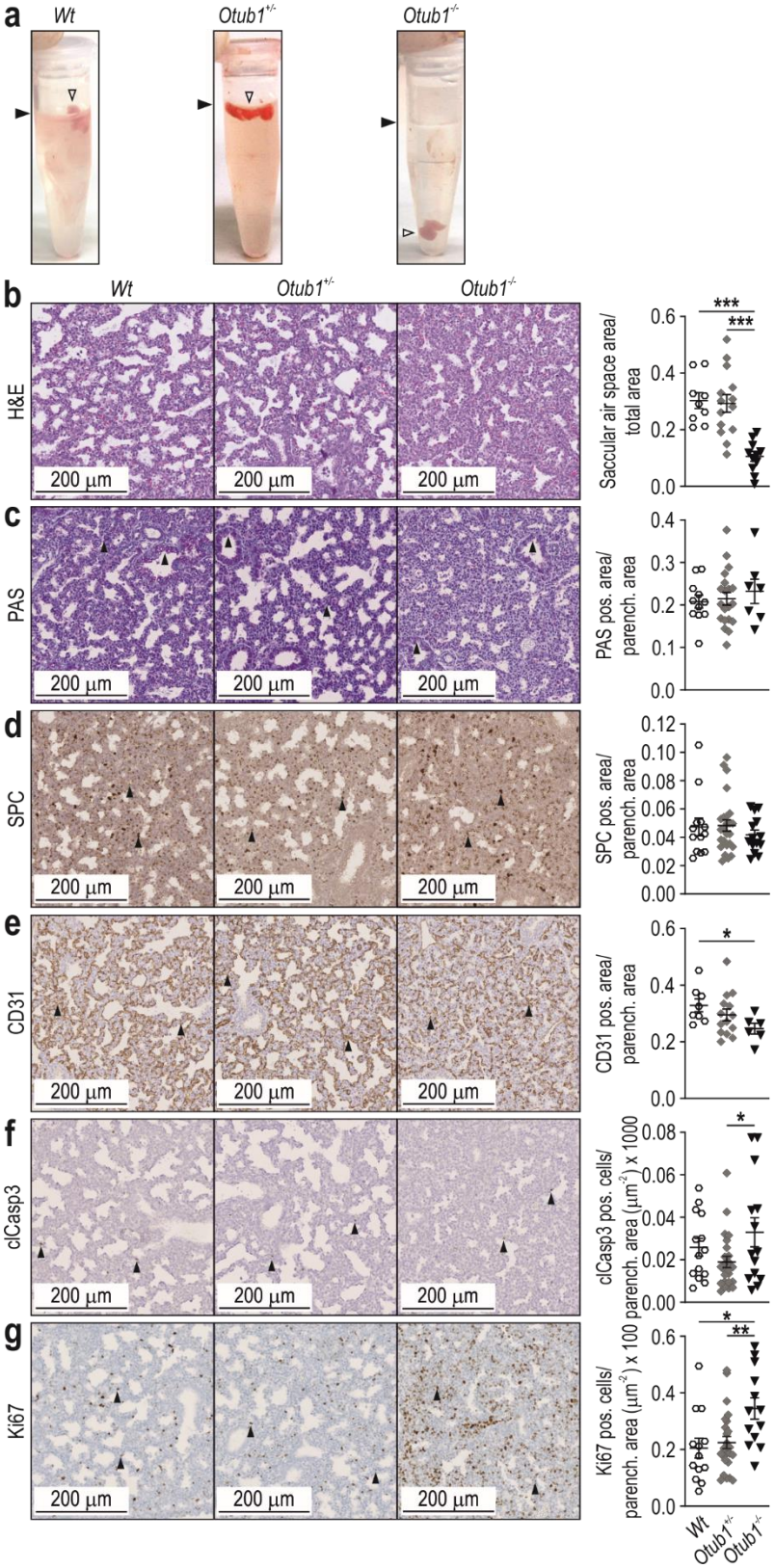

Fig. 2: Lung tissue and respiratory alterations in *Otub1*$^{-/-}$ mice. a, Floating test for P0 *Wt*, *Otub1*$^{+/-}$ and *Otub1*$^{-/-}$ lungs. Filled arrowheads indicate the surface, empty arrowheads indicate the lung. **b-g,** Histological analyses and quantification of E18.5 transversal lung sections by H&E (**b**), PAS (**c**), anti-surfactant C (SPC) antibody (**d**), anti-cluster of differentiation 31 (CD31) antibody (**e**), anti-cleaved caspase 3 (clCasp3) antibody (**f**) and anti-Ki67 antibody (**g**). Quantifications of the stainings in E18.5 *Wt* (n = 9-14), *Otub1*$^{+/-}$ (n = 14-25) and *Otub1*$^{-/-}$ (n = 11-14) lung tissues were normalised to parenchymal (parench.) tissue area. pos., positive. Data are presented as mean ± SEM. *, p<0.05, **, p<0.01, ***, p<0.001 by two-tailed Student's t-test. Exact P values: **b,** *Wt* versus *Otub1*$^{-/-}$: <0.0001; *Otub1*$^{+/-}$ versus *Otub1*$^{-/-}$: <0.0001; **e,** 0.0213; **f,** *Otub1*$^{+/-}$ versus *Otub1*$^{-/-}$: 0.0313; **g,** *Wt* versus *Otub1*$^{-/-}$: 0.0116; *Otub1*$^{+/-}$ versus *Otub1*$^{-/-}$: 0.0047.

Conditional whole-body *Otub1* deletion causes hyperventilation in adult mice

To analyse the physiological relevance of OTUB1 in adult mice, we established a mouse strain with tamoxifen (Tx)-inducible whole-body *Otub1* ablation (Fig. 3a). The deletion of *Otub1* was highly efficient with some intra- and inter-organ variations (Fig. 3b and Supplementary Fig. 2a).

Because *Otub1* deletion affected lung development, we analysed whether a deletion during adulthood impacted upon respiration and lung tissue. Under normal oxygen conditions (normoxia; 21% O_2), the respiratory frequency was not significantly altered in *Otub1* KO mice, but the tidal volume was increased relative to Tx-treated control mice and the minute volume was significantly higher in comparison to both controls (Fig. 3c), demonstrating that mice lacking *Otub1* were hyperventilating. Following normoxia, the respiration of the same mice was determined in hypoxia (10% O_2). Acute hypoxia increased tidal and minute volume in all groups (Fig. 3c, 10% O_2, early), but *Otub1* KO mice maintained an increased tidal and minute volume relative to both controls (Fig. 3c, 10% O_2, early) whereas after 25-30 min in hypoxia (Fig. 3c, 10% O_2, late), the control mice adapted and showed comparable respiration to normoxia (Fig. 3c). *Otub1* KO mice did not adjust and maintained increased respiratory frequency, tidal volume and minute volume (Fig. 3c). These findings demonstrated that OTUB1 is integral for the regulation of respiration and the adaptation of respiration to hypoxia. The respiration of mice with constitutive *Otub1* haploinsufficiency was not altered (Supplementary Fig. 2b), indicating that a partial loss of *Otub1* can be compensated for.

Interestingly, the weight of lungs lacking *Otub1* was significantly increased compared to controls (Fig. 3d). Lungs of *Otub1*$^{+/-}$ mice showed no weight difference (Supplementary Fig. 2c). An increased number of proliferating and total cells was detected in adult *Otub1* KO lungs (Fig. 3e), which was comparable to our findings in *Otub1*$^{-/-}$ E18.5 lungs (Fig. 2g). Hence, *Otub1* deletion induced proliferation in lung tissue independent of development. In summary, OTUB1 is essential for lung tissue homeostasis, regulation of respiration and the adaptation of respiration to hypoxia.

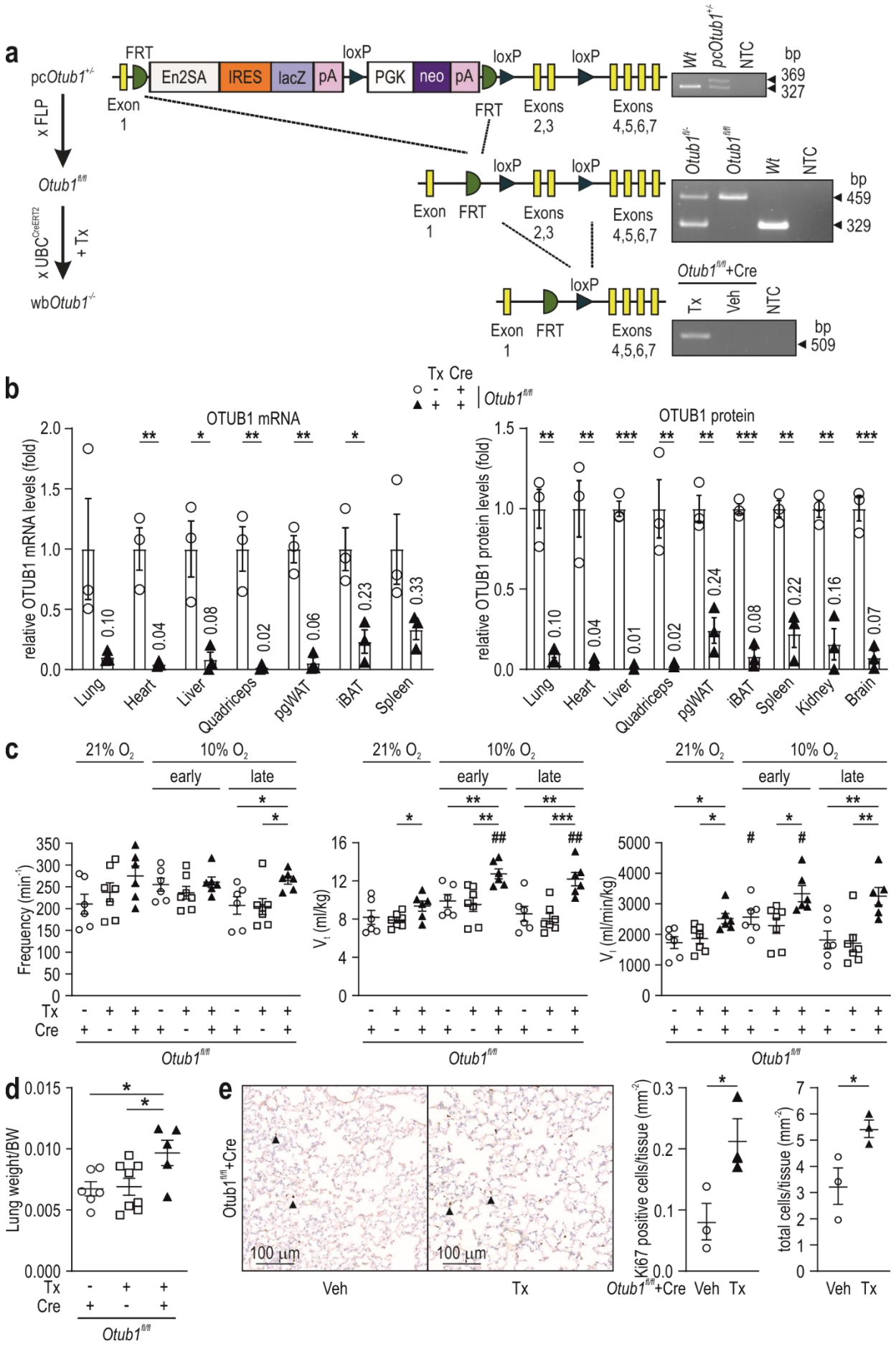
a
pcOtub1+/-
x FLP
Otub1fl/fl
x UBCCreERT2
+ Tx
wbOtub1-/-
FRT
En2SA
IRES
lacZ
pA
loxP
PGK
neo
pA
Exon 1
Exons 2,3
Exons 4,5,6,7
Wt
pcOtub1+/-
NTC
bp
369
327
Otub1fl/-
Otub1fl/fl
459
329
Otub1fl/fl+Cre
Tx
Veh
509
b
Tx
Cre
Otub1fl/fl
OTUB1 mRNA
relative OTUB1 mRNA levels (fold)
OTUB1 protein
relative OTUB1 protein levels (fold)
Lung
Heart
Liver
Quadriceps
pgWAT
iBAT
Spleen
Kidney
Brain
c
21% O2
10% O2
early
late
Frequency (min-1)
Vt (ml/kg)
V̇t (ml/min/kg)
d
Lung weight/BW
e
Otub1fl/fl+Cre
100 µm
Veh
Tx
Ki67 positive cells/tissue (mm-2)
total cells/tissue (mm-2)

Fig. 3 (see figure legend on p. 13).
Fig. 3: Lung tissue and respiratory alterations in adult mice with induced whole-body *Otub1* deletion. a, *Otub1*$^{fl/fl}$ mice were generated by crossing mice with the potential of conditional *Otub1* deletion (pc*Otub1*$^{+/-}$) with mice transgenic for *Flippase (Flp)*. To obtain conditional whole-body *Otub1* KO (wb*Otub1*$^{-/-}$) mice, *Otub1*$^{fl/fl}$ mice were crossed with mice carrying one transgene of a Cre^{ERT2} expressed under the control of the ubiquitin C (UBC) promoter (UBC-Cre^{ERT2}), followed by gavage of 200 μg tamoxifen (Tx)/g BW during 5 consecutive days. Images show PCR results determining the genotypes. PGK, phosphoglycerol kinase promoter; neo, neomycin resistance gene; *Otub1*$^{fl/fl}$+Cre, *Otub1*$^{fl/fl}$ mice carrying one UBC-Cre^{ERT2} transgene; NTC, non-template control; Veh, vehicle; bp, base pairs. **b,** Quantification of OTUB1 mRNA (RT-qPCR) and protein (immunoblotting) in the indicated tissues (5 months after *Otub1* deletion; 6.5 months old mice; n = 3). Numbers show the residual fraction of OTUB1. OTUB1 mRNA values were normalised to murine S12 mRNA levels. pgWAT, perigonadal white adipose tissue; iBAT, interscapular brown adipose tissue. **c,** Consecutive analysis of the respiration of unrestrained mice (2 month after *Otub1* deletion; 4 months old mice; *Otub1*$^{fl/fl}$ + Cre + Veh, n = 6; *Otub1*$^{fl/fl}$ - Cre + Tx, n = 7; *Otub1*$^{fl/fl}$ + Cre + Tx, n = 6) determined by barometric pressure plethysmography in normoxia (21% O_2) and hypoxia (10% O_2). V_t, tidal volume; V_I, minute volume; early, first 5 min in hypoxia; late, 25-30 min in hypoxia. **d,** Lung weight normalised to BW of the mice analysed in (C) (3.5 months after *Otub1* deletion; 5.5 months old mice; *Otub1*$^{fl/fl}$ + Cre + Veh, n = 6; *Otub1*$^{fl/fl}$ - Cre + Tx, n = 8; *Otub1*$^{fl/fl}$ + Cre + Tx, n = 5). **e,** Immunohistology and quantification of Ki67 and total cell number in lung tissue (3.5 months after *Otub1* deletion; 5.5 months old mice; n = 3). All data are presented as mean ± SEM. #/*, p<0.05; ##/**, p<0.01; ***, p<0.001 by two-tailed Student's t-test. #/##, compared to the corresponding measurements of the same mice in normoxia. Exact P values: **b,** mRNA - heart: 0.0057; liver: 0.0188; quadriceps: 0.0061; pgWAT: 0.0014; iBAT: 0.0189; protein - lung: 0.0019; heart: 0.0057; liver: <0.0001; quadriceps: 0.0059; pgWAT: 0.0028; iBAT: <0.0001; spleen: 0.0014; kidney: 0.0016; brain: 0.0004; **c,** frequency +Cre -Tx versus +Cre +Tx: 0.0254; frequency -Cre +Tx versus +Cre +Tx: 0.0169; V_t 21% O_2 -Cre +Tx versus +Cre +Tx: 0.0273; V_t 10% O_2 early +Cre -Tx versus +Cre +Tx: 0.0074; V_t 10% O_2 early -Cre +Tx versus +Cre +Tx: 0.0046; V_t 21% O_2 +Cre +Tx versus V_t 10% O_2 early +Cre +Tx: 0.0011; V_t 10% O_2 late +Cre -Tx versus +Cre +Tx: 0.0062; V_t 10% O_2 late -Cre +Tx versus +Cre +Tx: 0.0006; V_t 21% O_2 +Cre +Tx versus V_t 10% O_2 late +Cre +Tx: 0.0097; V_I 21% O_2 +Cre -Tx versus +Cre +Tx: 0.0122; V_I 21% O_2 -Cre +Tx versus +Cre +Tx: 0.0164; V_I 10% O_2 early -Cre +Tx versus +Cre +Tx: 0.0147; V_I 21% O_2 +Cre -Tx versus V_I 10% O_2 early +Cre -Tx: 0.0213; V_I 21% O_2 +Cre +Tx versus V_I 10% O_2 early +Cre +Tx: 0.0263; V_I 10% O_2 late +Cre -Tx versus +Cre +Tx: 0.0055; V_I 10% O_2 late -Cre +Tx versus +Cre +Tx: 0.0029; **d,** +Cre -Tx versus +Cre +Tx: 0.0298; -Cre +Tx versus +Cre +Tx: 0.0412; **e,** Ki67 Veh versus Tx: 0.0469; total cells Veh versus Tx: 0.0474.

Mice lacking *Otub1* develop cardiac hypertrophy and ventricular dysfunction

Heart size and function were assessed in adult mice with induced *Otub1* deletion using echocardiography (Fig. 4a), because of the previously observed cardiac phenotype in *Otub1*$^{-/-}$ embryos (Fig. 1). Over time, *Otub1* ablation increased the left ventricular mass (LVM) (Fig. 4b). The isovolumic relaxation time (IVRT) was prolonged at one and four months following *Otub1* deletion (Fig. 4c), indicating a diastolic dysfunction. The isovolumic contraction time (IVCT), an important part of the systole, was significantly increased four months after *Otub1* KO (Fig. 4d). The myocardial performance index (MPI)[94] was significantly raised at both

time points after *Otub1* KO (Fig. 4e) and the E and A myocardial velocities ratio (E/A) was increased four months after *Otub1* deletion (Fig. 4f), both further supporting a diastolic dysfunction. The ejection fraction and fractional shortening were significantly decreased four months after *Otub1* KO (Fig. 4g and Supplementary Fig. 3a). But the extent of these regulation was relatively small and the ejection fraction remained on average above 50% (Fig. 4g), which is considered to be a preserved ejection fraction[95]. Other parameters showed no significant difference (Supplementary Fig. 3b-f), whereas tissue Doppler imaging (TDI) confirmed the observations for IVRT, IVCT and MPI (Supplementary Fig. 3g-i). Six months after *Otub1* KO, the heart weight relative to tibia length showed a tendency to be increased (Fig. 4h). In an additional group of mice, the heart weight relative to tibia length was significantly increased in mice with *Otub1* deletion (5.5 months after KO) compared to vehicle control (Supplementary Fig. 3j), overall supporting the observed increase in LVM. A cardiac failure did not develop following *Otub1* KO in this group of mice at the analysed time point, because the wet versus dry lung weight - a read-out for lung congestion - was not changed (Fig. 4i). Constitutive haploinsufficiency of *Otub1* did not affect cardiac tissue or function (Supplementary Fig. 3k-aa), indicating that a partial loss of OTUB1 can be compensated for.

We next analysed heart rate, systolic (SBP) and diastolic blood pressure (DBP) using a tail-cuff system. The heart rate of mice with *Otub1* deletion was significantly decreased 1.5 and 3.5 months after *Otub1* KO (Fig. 4j). The DBP was unaltered 1.5 months after *Otub1* KO and decreased 3.5 months after *Otub1* KO compared to the Tx but not to the vehicle control (Fig. 4k). Of note, the Tx control group increased the DBP over time, whereas mice with *Otub1* KO maintained the DBP (Fig. 4k). This indicates that the difference between the Tx and the *Otub1* KO group was not caused by *Otub1* KO. A significant decrease of the SBP was observed 1.5 months after *Otub1* KO compared to the Tx but not to the vehicle control (Fig. 4l). 3.5 months after *Otub1* KO there was no difference between the groups (Fig. 4l). An increased SBP or DBP could have contributed to the alterations in *Otub1* KO hearts. But there were no indications for an increase in either SBP or DBP following *Otub1* KO. Therefore, the

observed changes in ventricular wall size and cardiac function were likely due to intrinsic heart tissue alterations rather than an adaptive response to external stimuli.

Ki67 levels were analysed in cardiac tissue to determine if proliferation contributed to the increased ventricular wall size. Only very little Ki67 positive cells were detected and there was no difference between the groups (Supplementary Fig. 3ab). FITC-WGA staining showed a cardiomyocyte hypertrophy in both ventricles (Fig. 4m), which likely led to the increased ventricular mass.

In summary, our results demonstrated that conditional *Otub1* KO leads to cardiac hypertrophy, left ventricular dysfunction and a decreased heart rate without affecting SBP and DBP. Hence, OTUB1 is an important regulator of cardiac homeostasis and function.

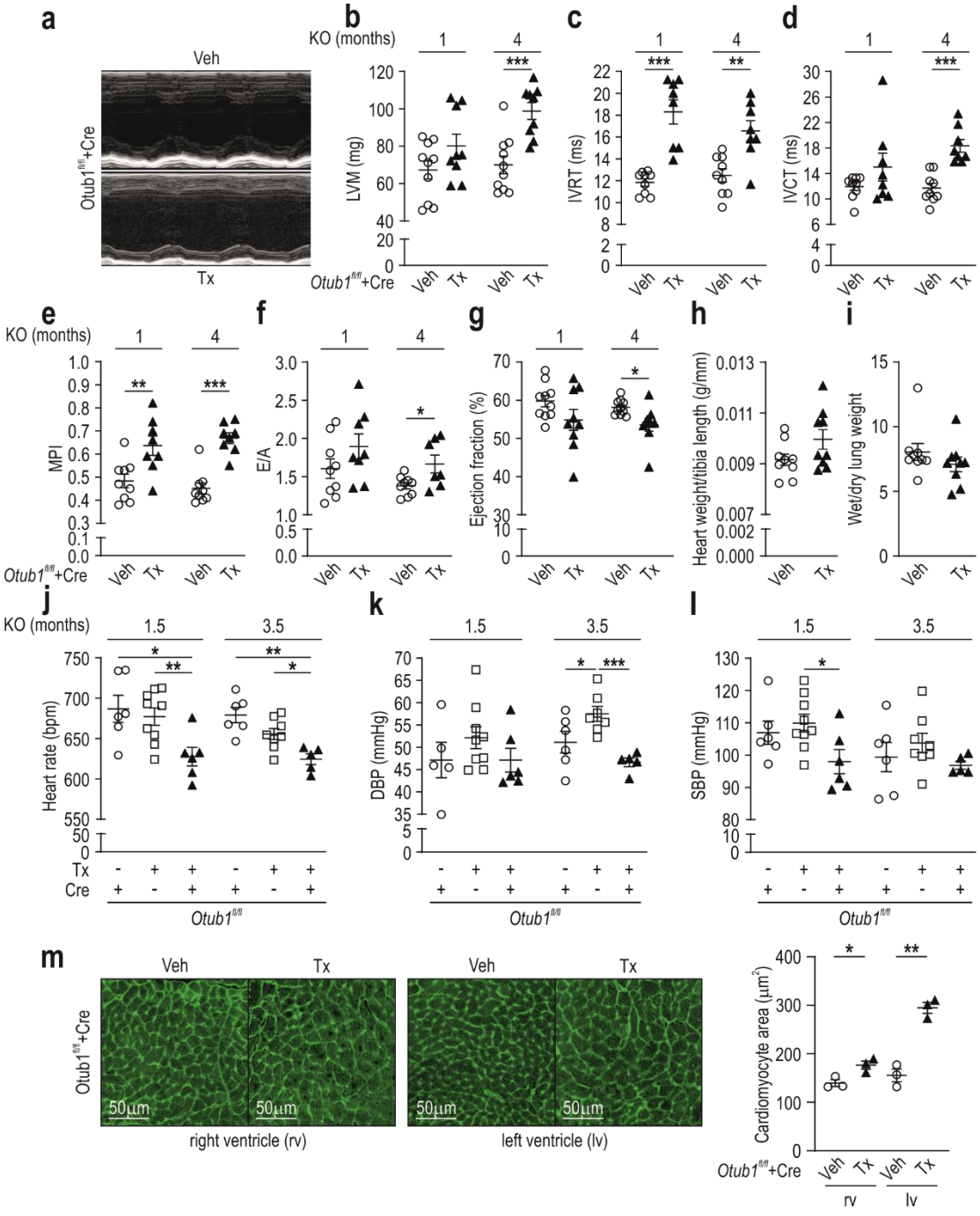

Fig. 4: Cardiac function in adult mice with induced *Otub1* KO. a, Representative M-mode scans of the left ventricle in short-axis view. **b-g,** Echocardiography of the left ventricular mass (LVM) (**b**), isovolumic relaxation time (IVRT) (**c**), isovolumic contraction time (IVCT) (**d**), myocardial performance index (MPI) (**e**), E and A myocardial velocities ratio (E/A) (**f**) and ejection fraction (**g**) at the indicated time points after *Otub1* KO (3.5 and 6.5 months of age, Veh, n = 9-10; Tx, n = 7-9). **h,** Heart weight normalised to tibia length (n = 9) and **l,** wet to dry lung weight ratio (6 months after *Otub1* deletion; 8.5 months old mice; Veh, n = 8; Tx, n = 9). **j-l,** Tail-cuff-dependent assessment of heart rate (**j**), diastolic blood pressure (DBP) (**k**) and systolic blood pressure (SBP) (**l**) at the indicated time points after *Otub1* KO (3.5 and 5.5 months of age; $Otub1^{fl/fl}$ + Cre + Veh, n = 5-6; $Otub1^{fl/fl}$ - Cre + Tx, n = 7-9; $Otub1^{fl/fl}$ + Cre + Tx, n = 5-6). **m,** FITC-WGA staining of heart tissue and quantification of transversal cardiomyocyte area (6 months after *Otub1* KO; 8.5 months old mice; n = 3). Data are presented as mean ± SEM. *, p<0.05; **, p<0.01; ***, p<0.001 by two-tailed Student's t-test**.**

Exact P values: **b,** 4 months KO: 0.0004; **c,** 1 month KO: <0.0001; 4 months KO: 0.0019; **d,** 4 months KO: <0.0001; **e,** 1 month KO: 0.0082; 4 months KO: <0.0001; **f,** 4 months KO: 0.0249; **g,** 4 months KO: 0.0158; **j,** 1.5 months KO: +Cre -Tx versus +Cre +Tx: 0.0157; -Cre +Tx versus +Cre +Tx: 0.0089; 3.5 months KO: +Cre -Tx versus +Cre +Tx: 0.0015; -Cre +Tx versus +Cre +Tx: 0.0108; **k,** 3.5 months KO: +Cre -Tx versus -Cre +Tx: 0.0482; -Cre +Tx versus +Cre +Tx: 0.0005; **l,** 1.5 months KO: -Cre +Tx versus +Cre +Tx: 0.0212; **m,** rv: 0.0246; lv: 0.0015.

Otub1 deletion increases AKT/mTOR signalling

MEFs were produced from *Wt* and *Otub1*$^{-/-}$ mice (Supplementary Fig. 4a) to analyse possible molecular mechanisms underlying the observed phenotypes. Total Ub chains, K48-linked and K63-linked Ub chains showed no difference in MEFs or heart tissue (Supplementary Fig. 4b,c). Therefore, *Otub1* deletion had likely a more specific effect than altering general ubiquitin chain levels.

OTUB1 was previously linked to the regulation of the phosphorylation of the serine/threonine kinase AKT following IL-15 stimulation of CD8+ T cells and NK cells[90] as well as to mammalian target of rapamycin (mTOR) activity in HeLa, HEK293T and H1299 cells[96]. AKT/mTOR signalling plays a pivotal role in lung development[92, 97, 98], respiration[92, 99] and cardiac homeostasis[100, 101]. Therefore, we analysed whether OTUB1 affected the AKT/mTOR pathway in MEFs. *Otub1* KO increased both AKT Thr308 and Ser473 phosphorylation under basal conditions (Fig. 5a). Following FCS and amino acid depletion, both AKT phosphorylations were also increased compared to *Wt* cells (Fig. 5a). After the re-addition of FCS (to stimulate AKT/mTOR signalling), both AKT phosphorylations were increased as well (Fig. 5a). This demonstrated that *Otub1* deletion leads to increased AKT phosphorylation under both basal and stimulated conditions. To investigate mTOR activity, the phosphorylation status of the ribosomal protein S6 kinase (S6K) Thr389 was analysed, a direct target of mTOR complex 1 (mTORC1)[102]. Under baseline conditions, the phosphorylation of S6K Thr389 was comparable, but following stimulation, the phosphorylation of S6K was decreased in *Otub1*$^{-/-}$ MEFs relative to *Wt* (Fig. 5a), suggesting a decreased mTOR activity. OTUB1 has been reported to directly regulate DEPTOR protein stability[96], a negative regulator of mTORC1 and mTORC2[103]. Interestingly, in *Otub1*$^{-/-}$ MEFs DEPTOR levels were increased (Fig. 5b), which was inconsistent with a direct

regulation of the DEPTOR protein half-life by OTUB1, but consistent with the observed decrease in mTOR activity. Overall, these results demonstrated that *Otub1* deletion affects the AKT/mTOR pathway in MEFs.

Next, we analysed if *Otub1* KO also led to a differential AKT/mTOR signalling *in vivo*. In E18.5 *Otub1*$^{-/-}$ lungs, AKT phosphorylation was not altered, but S6K phosphorylation and S6K total levels were increased compared to *Wt* mice (Fig. 5c). Interestingly, *Otub1* haploinsufficiency also led to an increase in phosphorylated S6K, but only in some of the tested animals (Fig. 5c), indicating a gene dosage-dependent effect. DEPTOR levels were decreased (Fig. 5c), which could explain the increase in phosphorylation of S6K and would be in line with a direct regulation of DEPTOR protein half-life by OTUB1. In summary, these results demonstrated that mTOR-dependent signalling was increased in OTUB1 deficient E18.5 lungs.

In adult lungs with *Otub1* KO, no difference in AKT phosphorylation was observed, but an increase in phosphorylated and total S6K levels (Fig. 5d) comparable to the results in E18.5 lungs. DEPTOR levels showed a tendency to be increased (Fig. 5d). Because DEPTOR levels were differentially regulated between E18.5 and adult lungs with *Otub1* KO, whereas phosphorylated and total S6K levels were affected in the same manner, DEPTOR may not play a major role in the observed effects in the lung. In adult *Otub1* KO hearts, AKT phosphorylation was not altered, but S6K phosphorylation was increased and total S6K levels were decreased (Supplementary Fig. 4d). The observed alterations were not in complete agreement between the heart and the lung, indicating a tissue specific effect of *Otub1*. Overall, these findings demonstrate that *Otub1* deletion leads to an increased activity of AKT/mTOR signalling in cells and tissues.

The AKT/mTOR pathway is a major determinant of cellular metabolism [102, 104]. To analyse if the OTUB1-dependent effect on AKT/mTOR was functionally relevant, the metabolic energy status was compared between *Wt* and *Otub1* KO MEFs. We observed a decrease in AMPK phosphorylation in *Otub1*$^{-/-}$ MEFs (Fig. 5e). Furthermore, ATP levels were

increased in the absence of *Otub1* (Fig. 5f). These results were in agreement with an increased AKT activation in cells [105], indicating a functionally relevant regulation by OTUB1.

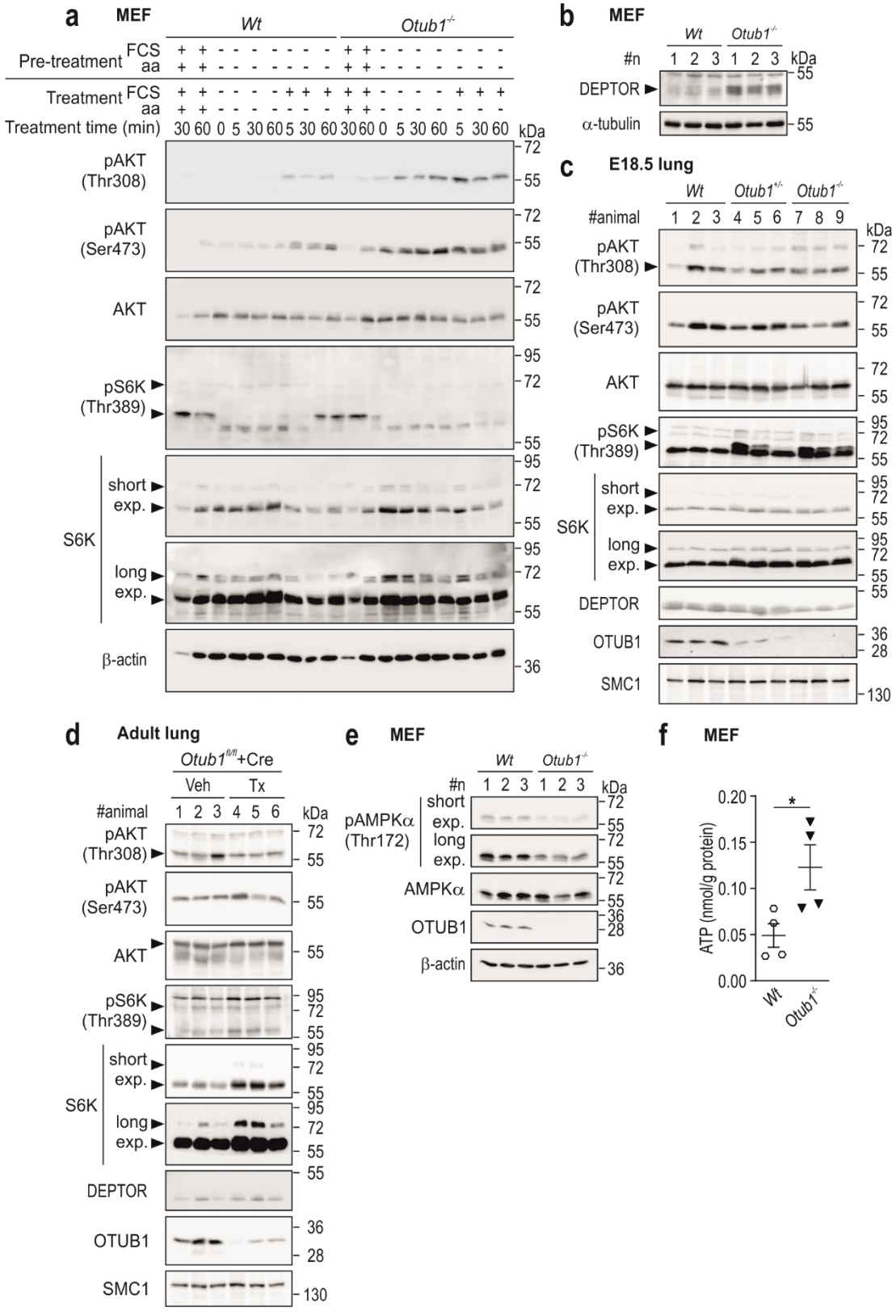

Fig. 5: AKT/mTOR signalling in MEFs and mouse tissues with *Otub1* deletion. a, Immunoblotting of the indicated (phospho)proteins (pAKT, pS6K) in *Wt* and *Otub1* homozygous KO (*Otub1*$^{-/-}$) mouse embryonic fibroblasts (MEFs; n = 3) following the indicated (pre-)treatments (pre-treatment: 4 hours). **b,** DEPTOR protein levels in *Wt* and *Otub1*$^{-/-}$ MEFs (n = 3). **c,** Immunoblotting of the indicated (phospho)proteins in E18.5 mouse lung tissue lysates (n = 3). **d,** Immunoblotting of the indicated (phospho)proteins in lung tissue lysates

following 4 hours of starvation during the light cycle (5 months after *Otub1* KO; 6.5 months old mice; n = 3). **e,** Immunoblotting of (phospho)AMPKα in MEFs (n = 3). **f,** Intracellular ATP levels normalised to protein levels in MEFs (n = 4). Representative images are shown and all data are presented as mean ± SEM. *, p<0.05 by two-tailed Student's t-test**.** Exact P values: **f,** 0.0363.

Loss of *Otub1* leads to a hypermetabolic state *in vivo*

We hypothesised that a relevant regulation of cellular energy metabolism by OTUB1 would lead to a corresponding phenotype *in vivo*. Following five days of Tx treatment to ablate *Otub1* in adult mice, BW progression was monitored for 122 days. Mice with *Otub1* gained around 20 g in 127 days, while mice without *Otub1* only gained around 11.5 g (Fig. 6a). The same mice showed a decreased fat/lean mass ratio 3 and 4.5 months after *Otub1* KO (Fig. 6b). Both subcutaneous white adipose tissue (sWAT) and perigonadal (pgWAT) WAT were significantly decreased in mice lacking *Otub1* (Fig. 6c). Interscapular brown adipose tissue (iBAT) was comparable between the groups (Fig. 6c). The liver weight was increased in mice with *Otub1* KO (Fig. 6c) without gross histological difference (Supplementary Fig. 5a). The quadriceps weight showed a tendency to be increased (Supplementary Fig. 5b). The brain weight was significantly increased, but the difference was rather small, while the weight of the spleen and kidneys was not altered (Supplementary Fig. 5b). Overall, these results showed weight changes in several organs that are important for energy metabolism *in vivo*. A reduced organ weight was only observed for WAT, suggesting that the reduced BW was due to a decreased WAT.

Interestingly, despite a decreased BW gain, food and water intake showed a tendency to be increased in mice lacking *Otub1* (Fig. 6d). In agreement with a higher intake, also the faeces weight and the urine volume were increased (Fig. 6d). The body temperature showed a tendency to be higher in mice lacking *Otub1* (Fig. 6e). O_2 consumption, CO_2 production and energy expenditure were increased during the light cycle in *Otub1* KO mice (Fig. 6f). The respiratory exchange ratio (RER) was not altered (Fig. 6f), indicating that the utilized nutrients for energy production were the same between the groups. In the dark cycle, comparable results were observed to the light cycle (Supplementary Fig. 5c). Overall, these results

demonstrated a hypermetabolic state in mice with *Otub1* deletion, which was in agreement with an increased ATP production in MEFs (Fig. 5f).

Mice with *Otub1* KO showed a lower maximal exercise capacity than control mice (Supplementary Fig. 5d), but a similar lactate concentration despite a shorter running period (Supplementary Fig. 5e), demonstrating a comparable physical exhaustion. These results indicate that lactate was either produced at a higher rate or consumed at a lower rate following *Otub1* ablation.

Hypermetabolism can be caused by hyperthyroidism[106]. Plasma levels of thyroid-stimulating hormone (TSH) are commonly used as primary read-out for thyroid dysfunction[106]. However, plasma TSH levels were not altered between the groups (Supplementary Fig. 5f), rendering a thyroid dysfunction unlikely as reason for the observed metabolic phenotype.

In summary, *Otub1* deletion in adult mice leads to a hypermetabolic state with reduced weight gain, decreased fat mass, increased nutrient and water intake combined with increased waste production as well as an increased energy expenditure and reduced exercise capacity. This metabolic phenotype was not caused by thyroid dysfunction.

To further improve our understanding of the physiological role of OTUB1, haploinsufficient *Otub1*$^{+/-}$ mice were also analysed for a metabolic phenotype. Interestingly, the analysed group of *Otub1*$^{+/-}$ mice showed in most aspects the opposite regulation compared to mice with conditional *Otub1* ablation. *Otub1*$^{+/-}$ mice had an increased BW and fat over lean mass ratio (Supplementary Fig. 6a-b). In the analysed group, excised sWAT, pgWAT and iBAT showed a tendency to be increased, whereas the liver weight was significantly decreased (Supplementary Fig. 6c). Food and water intake as well as faeces weight and urine volume showed a tendency to be decreased (Supplementary Fig. 6d). Indirect calorimetry demonstrated decreased O_2 consumption, CO_2 production and energy expenditure (Supplementary Fig. 6e,f). The RER was not significantly altered (Supplementary Fig. 6e,f). There was no histological difference observed in liver tissue (Supplementary Fig. 6g). In

summary, *Otub1* haploinsufficiency in mice appears to lead to a hypometabolic state, but with a low penetrance.

Maximal exercise capacity was decreased in the same *Otub1*$^{+/-}$ mice, with comparable lactate levels relative to control (Supplementary Fig. 6h), demonstrating a comparable physical exhaustion. This observation was similar to the results obtained in mice with induced *Otub1* deletion despite an otherwise opposite regulation of energy metabolism. This indicates that the running time was not directly determined by the metabolic phenotype in these mice.

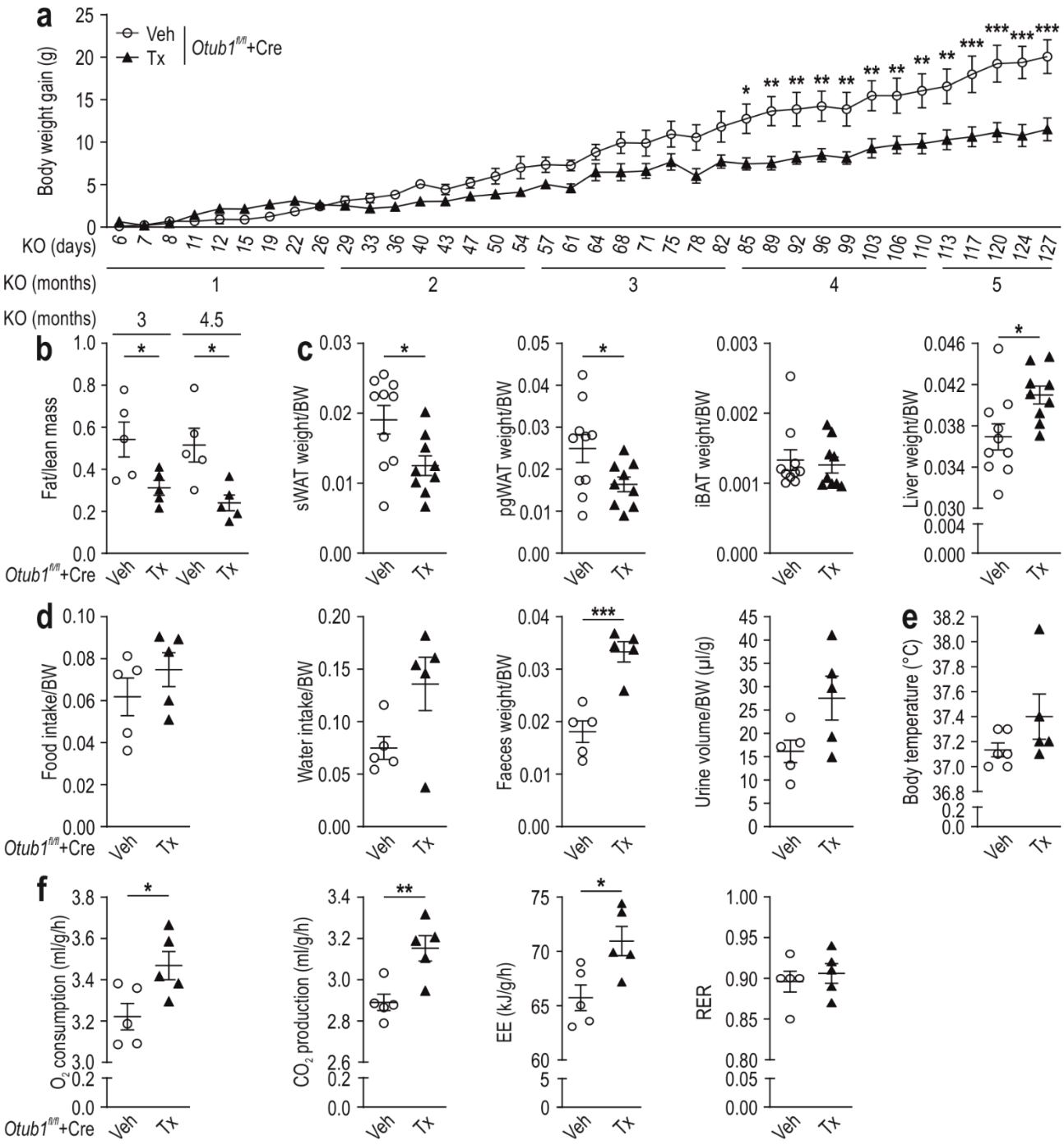

Fig. 6: Energy metabolism in adult mice with induced *Otub1* KO*.* a, Body weight gain after *Otub1* KO during days 1-5 (n=5). **b,** Fat mass to lean mass ratio analysed by Echo-MRI in the mice shown in (**a**) at the indicated time after *Otub1* KO (4.5 and 6 months of age; n = 5). **c,** Weight of indicated organs relative to BW (6 months after *Otub1* KO; 8.5 months old mice; Veh, n = 10; Tx, n = 9). sWAT, subcutaneous WAT; pgWAT, perigonadal WAT; iBAT, interscapular brown AT. **d,** Food and water intake, faeces weight and urine volume over 72 hours, collected in metabolic cages (4.5 months after *Otub1* KO; 6 months old mice, n = 5). **e,** Rectal body temperature (2.5 months after *Otub1* deletion; 5 months old mice; Veh, n = 6; Tx, n = 5). **f,** O_2 consumption, CO_2 production, energy expenditure (EE) and respiratory exchange ratio (RER) of 3 consecutive days during the light cycle (5 months after *Otub1* deletion; 6.5 months old mice; n = 5). All data are presented as mean ± SEM. *, p<0.05; **, p<0.01; ***, p<0.001 by two-way ANOVA with Bonferroni post-test (**a**) or two-tailed Student's t-test (**b-f**). Exact P values: **a,** 85 days: 0.0230; 89 days: 0.0032; 92 days: 0.0084; 96 days: 0.0076; 99 days: 0.0084; 103 days: 0.0026; 106 days: 0.0076; 110 days: 0.0023; 113 days: 0.0020; 117 days: 0.0001; 120 days: <0.0001; 124 days: <0.0001; 127 days: <0.0001; **b,** 3 months after KO: 0.0342; 4.5 months after KO: 0.0146; **c,** sWAT: 0.0189; pgWAT: 0.0434; liver: 0.0191; **d,** 0.0007; **f,** O_2 consumption: 0.0291; CO_2 production: 0.0071; EE: 0.0317.

Otub1 deletion increases insulin-dependent signalling

Next, we aimed to assess the underlying cause for the observed metabolic phenotype in adult mice with induced *Otub1* KO. The AKT/mTOR pathway is activated by insulin and plays a key role in insulin-regulated metabolism[107]. In an intraperitoneal glucose tolerance test (IPGTT), *Otub1* KO mice showed a faster glucose clearance than control mice (Fig. 7a). An intraperitoneal insulin tolerance test (IPITT) confirmed increased insulin sensitivity in mice with *Otub1* deletion (Fig. 7b). Basal insulin levels (after 4 h of fasting) were decreased in *Otub1* KO mice (Fig. 7c). These results demonstrated increased insulin sensitivity in mice lacking *Otub1*. Haploinsufficient *Otub1*$^{+/-}$ mice (the same group that was analysed for the metabolic phenotype) showed a tendency towards decreased insulin sensitivity (Supplementary Fig. 7a-c).

Analysing AKT/mTOR signalling in the liver, no difference was observed in the phosphorylation of AKT or S6K under basal conditions (analysed 4 h after fasting; Fig. 7d). There was also no difference in AKT phosphorylation in heart and lung under basal conditions, and S6K phosphorylation was increased in both tissues (Fig. 5d and Supplementary Fig. 4d). But the same mice had decreased basal insulin levels (Fig. 7c). Therefore, a maintained or increased AKT/mTOR signalling in the presence of decreased basal insulin levels indicated an enhanced sensitivity of AKT/mTOR signalling to insulin-dependent stimulation when *Otub1*

was deleted. Consequently, we next analysed the response of AKT/mTOR signalling to insulin stimulation *in vivo*. 15 minutes after insulin injection, the phosphorylation of AKT on Ser473 was increased in livers with *Otub1* KO (Fig. 7e). The effect on AKT Thr308 was less clear (Fig. 7e). The phosphorylation of S6K was not altered, but total levels of S6K showed a tendency to be decreased in both basal as well as stimulated conditions (Fig. 7d,e), indicating that additional regulation may have occurred. In the hearts of the same animals, phosphorylation of AKT Ser473 was also at least in some animals increased in response to insulin stimulation, which could also be observed for the phosphorylation of S6K (Supplementary Fig. 7d).

The phosphorylation of ERK1/2, another insulin target[108], was not altered in the liver under basal conditions (Fig. 7d). In response to insulin stimulation, ERK1/2 phosphorylation was increased in livers with *Otub1* KO (Fig. 7e), indicating that the OTUB1-dependent regulation of insulin signalling was either not confined to AKT/mTOR or occurred upstream of the bifurcation point of both signalling cascades. The phosphorylation of ERK1/2 showed a tendency to be decreased in hearts with *Otub1* KO following insulin stimulation, again supporting a tissue-specific effect of *Otub1* KO on cellular signalling pathways (Supplementary Fig. 7d). In summary, *Otub1* deletion led to increased insulin sensitivity under basal and stimulated conditions, which likely contributed to the hypermetabolic state.

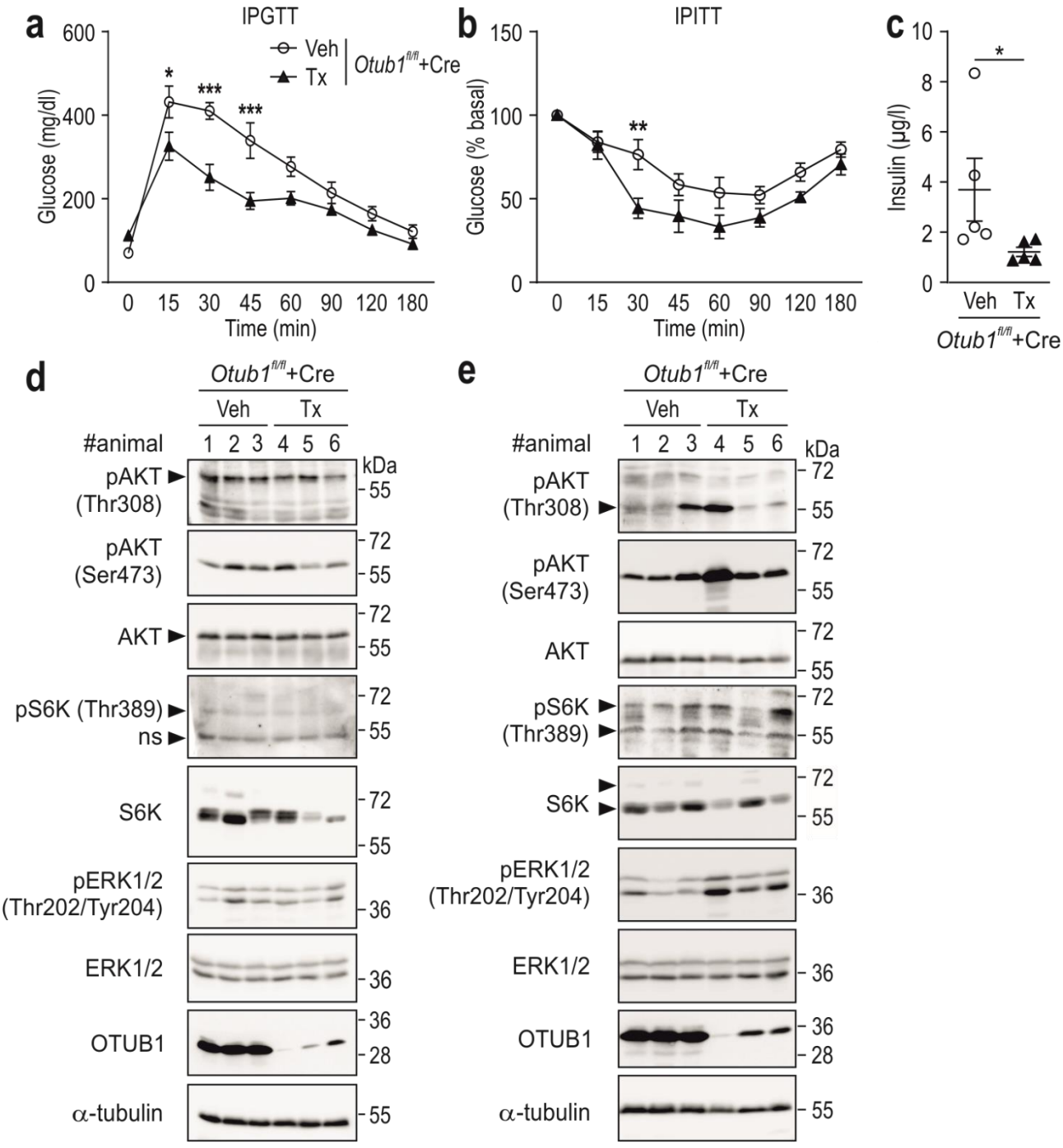

Figure 7. Insulin sensitivity of adult mice with induced *Otub1* KO. a, Intraperitoneal glucose tolerance test (IPGTT; 2 mg glucose/g BW; Veh, n = 4; Tx, n = 5) and **b,** IP insulin tolerance test (IPITT; 0.75 mU insulin/g BW; 4 months after *Otub1* KO; 5.5 months old mice; n=5). **c,** Plasma insulin levels in the mice shown in a and b (5 months after *Otub1* KO; 6.5 months old mice; n = 5) following 4 hours of starvation during the light cycle. **d,** Immunoblotting of liver lysates from the mice in (**c**) (n = 3). **e,** Immunoblotting of liver lysates from mice (10 days after *Otub1* KO; 2 months old mice; n = 3) starved overnight (16 h) followed by IP insulin application (0.75 mU insulin/g BW) 15 min prior to tissue harvest. *, p<0.05; **, p<0.01; ***, p<0.001 by two-way ANOVA with Bonferroni post-test (**a, b**) or two-tailed Mann-Whitney t-test (**c**). Exact P values: **a,** 15 min: 0.0131; 30 min: <0.0001; 45 min: 0.0003; **b,** 30 min: 0.0056; **c,** 0.0159.

DISCUSSION

We provide *in vivo* evidence that the DUB OTUB1 is essential for embryonic development, respiration, lung and heart tissue homeostasis, cardiac function and energy metabolism. Previous investigations of OTUB1 in mice focussed on the relevance of OTUB1 for specific immune cells and/or a cell type-specific role of OTUB1 during inflammation[87-90]. Our analyses of mice with whole-body *Otub1* deletion indicate that the general physiological function of OTUB1 differs from its specific role in immune cells and during inflammation.

We propose that the failure of *Otub1*$^{-/-}$ mice to inflate their lungs is caused by the observed increased proliferation and decreased saccular air space, which may augment the lung tissue resistance against mechanical stretch. In adult mice, OTUB1 is important for the control of the oxygen-dependent regulation of respiration. Therefore, OTUB1 may play a key role in oxygen sensing by the carotid body, the main sensor of arterial oxygenation regulating lung function[109]. Future investigations should assess if *Otub1* deletion specifically in the carotid body contributes to the perinatal lethality.

Cells derived from mice lacking *Otub1* showed increased ATP levels and a decreased AMPK phosphorylation, which corresponds with our previous observation that OTUB1 overexpression elevates AMPK phosphorylation[85]. *Otub1*$^{-/-}$ embryos were lighter and smaller than their littermates, which may at least in part be caused by an altered energy metabolism. In adult mice, our results show that OTUB1 defines a set-point for whole-body glucose metabolism, with *Otub1* deletion leading to increased glucose utilization and a hypermetabolic state.

Lack of *Otub1* generally enhanced AKT/mTOR signalling in MEF cells and in all investigated organs, although the detailed underlying mechanisms somewhat differed. The variability may be explained by the presence of different stimuli of the AKT/mTOR signalling pathway which is not exclusively regulated by insulin[102, 104]. AKT/mTOR signalling affects cellular ATP levels and AMPK phosphorylation[105], controls body weight and size during development[101], and plays a key role in lung development[97, 98]. Increased AKT/mTOR signalling causes death by respiratory failure following caesarean section at E18.5[92]. In adult

mice, increased AKT/mTOR signalling leads to decreased body weight and fat mass, increased oxygen consumption, improved glucose clearance and insulin sensitivity as well as decreased serum insulin levels[110, 111]. In the heart, enhanced AKT/mTOR signalling leads to cardiac hypertrophy[100, 101]. Inhibition of AKT and ERK1/2 signalling decreased the response of the carotid body to hypoxia[99]. Of note, OTUB1 directly regulates the phosphorylation of AKT in CD8+ T and NK cells following IL-15 stimulation and *Otub1* deletion led to increased phosphorylation of AKT and S6K in these cell types[90]. OTUB1 furthermore regulates DEPTOR, a negative regulator of mTORC1 and 2[96]. Therefore, we conclude that OTUB1 is a negative regulator of AKT/mTOR signalling and that an increased AKT/mTOR signalling underlies at least in part the observed phenotypes in mice with *Otub1* deletion.

While *Otub1* haploinsufficiency neither affected embryonic development nor respiratory or cardiac function, at least some animals showed changes in energy metabolism, indicating that tissues important for the regulation of energy metabolism have a higher sensitivity to a partial loss of *Otub1* than the lung or the heart. The observed decrease in energy metabolism in *Otub1* hypomorphs is in contrast to the hypermetabolic state in mice with a (nearly) complete loss of *Otub1* and demonstrates an unexpected gene dosage-response curve of OTUB1. A similar gene dosage-response curve has previously been described for a negative regulator of PI3K/AKT/mTOR signalling, the phosphatase and tensin homolog located on chromosome 10 (PTEN). The partial loss of PTEN leads to spontaneous tumor development in mice, but a complete PTEN deletion can obstruct tumor growth[112]. Because the metabolic phenotype showed a low penetration in *Otub1*$^{+/-}$ mice, OTUB1-dependent regulation of energy metabolism may not only depend on OTUB1 protein levels but likely also on additional mechanisms. Previously, it was shown for another regulator of AKT/mTOR signalling, the IQ motif containing GTPase activating protein 1 (IQGAP1), that its effect on AKT/mTOR is governed by the input of different stimuli. IQGAP1 can increase or decrease AKT/mTOR activity and downstream insulin synthesis as well as secretion, depending on the available amount of nutrients in concert with EGF-dependent signalling[113]. For OTUB1, it was shown that its interaction with DEPTOR is partially

dependent on amino acid availability[96]. We showed that O_2 availability can regulate OTUB1 interactions and enzymatic activity[83, 85]. The OTUB1-dependent effect on AKT/mTOR signalling may hence integrate different stimuli depending on the OTUB1 protein levels.

We previously reported that the oxygen sensor FIH regulates cellular energy metabolism through hydroxylation of OTUB1[85]. Mice lacking the gene encoding FIH (*Hif1an*) present with a decreased body weight gain, a decreased fat mass, increased insulin sensitivity, increased food and water intake as well as increased O_2 consumption, CO_2 production and energy expenditure, while maintaining the RER[114]. Furthermore, *Hif1an* deletion led to hyperventilation[114]. While not lethal, these phenotypes of *Hif1an* KO mice are otherwise identical with our observations in *Otub1* KO mice, supporting our hypothesis that FIH is an important regulator of OTUB1[83, 85].

In summary, OTUB1 has multiple physiological roles, ranging from its essential function during embryonic development to the control of respiratory and cardiac function as well as general energy metabolism. These results highlight the physiological relevance of this DUB and indicate that pharmacologic targeting of OTUB1 – as for example suggested for cancer treatment[91] - may not be without severe side effects. Furthermore, our findings may help identifying previously unknown causes of developmental, respiratory and heart diseases as well as metabolic disorders.

METHODS

Mice

Mice with heterozygous *Otub1* deletion (*Otub1*$^{+/-}$, strain C57BL/6N-Otub1$^{tm1b(EUCOMM)Hmgu/H}$) were purchased from the EUCOMM consortium (http://www.mousephenotype.org; via the EMMA repository, https://www.infrafrontier.eu/) [115] and bred to generate *Otub1*$^{-/-}$ mice (Fig. 1a). Mouse Contract Services were provided by the Mary Lyon Centre at MRC Harwell (http://www.har.mrc.ac.uk; UK). Wildtype mice (*Wt*; C57BL/6N, Charles River, MA, USA) were used for maintenance breeding with *Otub1*$^{+/-}$ mice. Mice with induced whole-body *Otub1* (wb*Otub1*$^{-/-}$) deletion were generated by crossing heterozygous mice with potential of conditional *Otub1* deletion (pc*Otub1*$^{+/-}$; strain *Otub1*$^{tm1a(EUCOMM)Hmgu/IcsORI}$; purchased from the EUCOMM consortium via the EMMA repository and provided by the Institut Clinique de la Souris, ICS, Illkirch, France) with *Flp* deleter mice (129S4/svJaeSor-Gt(Rosa)26Sor$^{tm1(FLP1)Dym}$), leading to the removal of the inserted *lacZ* gene and neomycin cassette and resulting in mice with floxed *Otub1* exons 2 and 3 (*Otub1*$^{fl/fl}$; Fig. 3a). *Otub1*$^{fl/fl}$ mice were crossed with mice carrying one copy of a Cre^{ERT2} transgene under the control of the ubiquitin C promoter (UBC-Cre^{ERT2}; strain B6.Cg-Ndor1$^{Tg(UBC-cre/ERT2)1Ejb/2J}$; purchased from The Jackson Laboratory; https://www.jax.org/strain/008085). For the induction of *Otub1* deletion, *Otub1*$^{fl/fl}$ x UBC-Cre^{ERT2} (*Otub1*$^{fl/fl}$+Cre) mice were treated with 200 μg of tamoxifen/g BW (Sigma-Aldrich, St. Louis, MO, USA). Mice were maintained at a constant ambient temperature (21±1°C) with 12 hours light/dark cycles, standard chow diet (Provimi Kliba, Gossau, Switzerland) and water available *ad libitum* under optimal hygienic conditions (OHC), unless indicated otherwise. Both genders were used for the investigations of developmental phenotypes, in adult mice female mice were analysed. All animal experiments were approved by the veterinary office of the canton Zurich, Switzerland.

Cell culture

MDA-MB468 (breast cancer), HepG2 and Hep3B (hepatocarcinoma), Caco-2 (colon carcinoma) as well as HEK293 (immortalized kidney) cells were cultured in DMEM (Sigma-

Aldrich) containing 4.5 mM sodium pyruvate, glucose and L-glutamine (Sigma-Aldrich), supplemented with 10% heat-inactivated fetal calf serum (FCS; Gibco by Life Technologies, Carlsbad, Ca, USA), 100 μg/ml streptomycin (S) and 100 U/ml penicillin (P; Sigma-Aldrich). SUM149PT (breast cancer) cells were cultured in 50% DMEM and 50% RPMI (Sigma-Aldrich) supplemented with 10%FCS and 100 μg/ml S and 100 U/ml P. AB8/13 cells (kidney) were cultured in RPMI supplemented with 10% FCS, 50 IU/ml P, 50 µg/ml S, supplemented with 5 µg/ml insulin, 5 µg/ml transferrin and 5 ng/ml sodium selenite (Roche, Mannheim, Germany). AB8/13 cells were propagated at 33°C and differentiated for 10-14 days at 37°C. Kelly (neuroblastoma) cells were cultured in RPMI, 10% FCS, 100 μg/ml S and 100 U/ml P. If not otherwise indicated, cells were maintained under standard conditions (humidified atmosphere at 37ºC with 18.5% O_2 and 5% CO_2). *Wt* and *Otub1* KO mouse embryonic fibroblasts (MEFs) were obtained at day 12.5 of gestation. MEFs were cultured in DMEM containing 10% FCS, 1% GlutaMAX (Gibco), 200 μM 2-mercaptoethanol (Gibco), 100 μg/ml S and 100 U/ml P and maintained at 5% O_2. For transient transfection of cells, Lipofectamine 2000 reagent (Invitrogen) or polyethylenimine (PEI; Polysciences, Warrington) was used as described previously[116]. For FCS and/or amino acid deprivation, MEFs were kept in RPMI 1640 medium containing glucose but no FCS or amino acids for 4 hours. To reintroduce FCS, the media was exchanged with RPMI 1640 containing 10% FCS and the cells were harvested at the indicated time points.

Protein extraction and determination of protein concentration

Protein extraction was performed with lysis buffer containing 150 mM NaCl, 1 mM EDTA, 25 mM Tris-HCl pH 8.0, 1% NP-40, 1 mM Na_3VO_4, 1 mM PMSF and 1 mM NaF. For cell lysis, protease inhibitor cocktail (Sigma-Aldrich) was added to the lysis buffer. For tissue lysis, 1 μg/ml aprotinin, 1 μg/ml leupeptin and 1 μg/ml pepstatin A were included in the lysis buffer, and tissue samples were homogenised using a polytron homogenizer (VWR International, Amsterdam, Netherlands). For the analysis of insulin-dependent signaling *in vivo*, mice were

intraperitoneally injected with 0.75 U/kg insulin, following an overnight fasting period. Organs were harvested 15 minutes after injection and proteins were extracted. For the analysis of polyubiquitin chains, the deubiquitinase inhibitor[117] N-ethylmaleimide (50 mM; Sigma-Aldrich) was added to the lysis buffer. Protein concentrations were determined by the BCA assay (Thermo Fisher Scientific, Waltham, MS, USA).

RNA analyses

RNA was extracted from tissues using the guanidine thiocyanate-acid phenol-chloroform method as previously described[118]. The RNA was converted to cDNA by reverse transcription of 2 μg of total RNA using AffinityScript transcriptase (Agilent, Santa Clara, CA, USA). The cDNA was analysed using the SYBR Green qPCR reagent kit (Kapa Biosystems, London, UK) in a MX3000P light cycler (Agilent). Transcript levels were normalised to mouse ribosomal protein S12 mRNA levels. OTUB1 RNA-sequencing data from human organs were extracted from a previous analysis[119].

ATP assay

Intracellular ATP levels were measured with the CellTiter-Glo 2.0 Assay according to the manufacturer's description (Promega, Madison, WI, USA). Cells were lysed with Passive Lysis Buffer (Promega) and diluted 1:100 in cell culture media. Samples were mixed with equal amounts of CellTiter-Glo 2.0 reagent for 2 minutes on an orbital shaker followed by additional 10 minutes of incubation at room temperature. Luminescence was determined in a microplate luminometer (Berthold Technologies, Bad Wildbach, Germany) and normalized to protein concentration determined by the Bradford method[120].

Cell proliferation analysis

Stably transfected HEK293 cells (shControl, shRNA targeting OTUB1 or shRNA targeting OTUB1 + Flag-OTUB1)[34, 85] were seeded and counted every 24 hours with the Vi-Cell XR cell counter (Beckham, Indianapolis, IN, USA).

Plasmids and siRNAs

The plasmid encoding human FLAG-OTUB1 was generously provided by Dr. Mu-Shui Dai (Oregon Health & Science University, Portland, OR, USA)[121]. Nontargeting siRNA (siNT, 5'-GCUCCGGAGAACUACCAGAGUAUUATT-3') and siRNA targeting the 3'UTR of hOTUB1 (siOTUB1, 5'-GUGGUUGUAAAUGGUCCUATT-3') were previously described[83, 121] and were purchased from Microsynth (Balgach, Switzerland).

Immunoblot analysis

Equal protein amounts were separated by SDS-PAGE, transferred to nitrocellulose or polyvinylidene difluoride membranes and detected using anti-FIH (Novus Biologicals, Littleton, CO, USA; npb1-3033), anti-OTUB1 (Cell Signaling, Danvers, MA, USA; 3783), anti-DEPTOR (Novus Biologicals; nbp1-49674), anti-p70 S6 kinase (Cell Signaling; CST9202), anti-phospho-p70 S6 kinase (Cell Signaling; 9234), anti-Akt (pan; Cell Signalling; 2920), anti-phospho-Akt (Ser473; Cell Signaling; 4060), anti-phospho-Akt (Thr308; Cell Signalling; 2965), anti-p44/42 MAPK (Erk1/2; Cell Signaling, 4695), anti-phospho-p44/42 MAPK (Erk1/2; Thr202/Tyr204; Cell Signaling; 4376), anti-AMPK (Cell Signaling; 2603), anti-phospho-AMPK (Thr172; Cell Signaling; 2535), anti-poly-ubiquitin (clone P4D1; Cell Signaling; 3936), anti-Lys48-linked poly-ubiquitin chains (Millipore, Darmstadt, Germany; 05-1307), anti-Lys-63-linked poly-ubiquitin chains (Millipore; 05-1308), anti-β-actin (Sigma-Aldrich; A5441), anti-α-tubulin (Cell Signaling; 2144), anti-SMC1 antibodies (Abcam, Cambridge, UK; 9262) and horseradish peroxidase (HRP)-coupled secondary antibodies (Thermo Fisher Scientific; 31430, 31460). Chemiluminescence detection was performed with Supersignal West Dura (Thermo Fisher Scientific) and recorded with a CCD camera (LAS-4000; GE Healthcare,

Chalfont, St. Giles, UK) as previously described[116]. Quantification was perfomed with ImageQuant TL gel analysis software (GE Healthcare, Version 8.1).

Lung inflation test

The trachea of P0 mice was tied shut, the lung was excised and its floatability was tested in PBS. Inflated lungs float, non-inflated lungs sink.

Tissue staining

Organs were fixed in 4% formaldehyde for 24 hours (Sigma-Aldrich). The sections were deparaffinised with xylene and rehydrated with decreasing concentrations of ethanol in water. Tissue sections (3-5 μm thick) were stained with haematoxylin and eosin (H&E), periodic acid-schiff (PAS), fluorescein isothiocyanate-coupled wheat germ agglutinin (FITC-WGA; Sigma-Aldrich) or subjected to immunohistochemistry (IHC) for cleaved caspase 3 (Asp175; Cell Signaling; 9664), SP-C (Santa Cruz Biotechnology, Dallas, TX, USA; sc-13979), Ki67 (Ventana Medical Systems, Tucson, AZ, USA; 790-4286) or CD31 (Santa Cruz Biotechnology; sc-1506R). Discovery XT research instrument (Ventana Medical Systems) was used for the detection of cleaved caspase 3 and Ki67. An autostainer (Dako) was employed for SP-C and CD31. All antibody blocking steps were performed with H_2O_2 (Dako) and REAL Antibody Diluent (Dako). Conditioning 1 pre-treatment (Cell conditioning 1 (CC1), Ventana Medical Systems) was used for the antigen retrieval for subsequent analysis with the Discovery XT systems and antigen retrieval with EDTA buffer (pH 9) was used for the Dako autostainer. For IHC signal detection, HRP-coupled secondary antibodies were used (Ventana Medical Systems; 760-4311; Jackson ImmunoResearch; 711-065-152) together with DAB substrate buffer (Dako, Glostrup, Denmark; K3468). Quantification was performed with ImageJ 1.53a (NIH, MD, USA)[122, 123]. Lipidosis and extramedullary hematopoiesis (EMH) analyses were performed by a certified mouse pathologist in a blinded manner using PAS-stained livers (0, no abnormality; 1, minimal abnormality; 2, mild abnormality; 3, moderate abnormality; 4, severe abnormality; 5, very severe abnormality).

Transmission electron microscopy (TEM)

Tissue samples of the cranial right lung lobe were fixed for 24 hours in 2.5% glutaraldehyde in 0.2 M sodium phosphate buffer (pH 7.3) for TEM examination in the TEM Unit (Institute of Veterinary Pathology, Laboratory for Animal Model Pathology, University of Zurich). Briefly, specimens were washed in sodium phosphate buffer and fixed in 1% osmium tetroxide in phosphate buffer/distilled water for 60 min. Tissues were dehydrated in ascending concentrations of ethanol, followed by propylene oxide. Specimens were subsequently infiltrated with 50% resin (Epoxy embedding medium, Sigma Aldrich, Germany) and incubated overnight. The tissues were then incubated in polyethylene embedding capsules filled with 100% resin for 3 days. Semi-thin sections (1 μm) were prepared using an ultramicrotome (Reichert-Jung Ultracut, Munich, Germany) with a diamond knife (Diatome, Biel, Switzerland), stained with toluidine blue and areas of interest for the preparation of ultrathin sections were chosen under the light microscope. Ultrathin sections (90 nm) were prepared with a diamond knife, mounted on copper grids, stained with uranyl acetate and Reynold's lead citrate and examined with a transmission electron microscope (Philips CM10, FEI, Thermo Fisher Scientific) operating with a Gatan Orius Sc1000 digital camera (Digital Micrograph, Gatan, Pleasanton, CA, USA).

Blood pressure measurement

Heart rate, systolic and diastolic blood pressure were measured with a tail-cuff system (Visitech Systems, Apex, NC, USA) in restrained mice. Mice were acclimatised during 5 days prior to the beginning of the experiment. For each mouse, 20 consecutive measurements were analysed. The experiment was performed between 2 and 4 hours after the beginning of the light cycle at 37°C.

Maximal acute exercise capacity

Mice were run on a Simplex II metabolic rodent treadmill (Columbus Instruments, Columbus, OH, USA). Following 1 hour of acclimatization on the previous day, each mouse was placed in a closed individual treadmill lane during 15 minutes without exercise. The exercise was started at 6 m/min at 0° inclination and the intensity was increased every minute by 1 m/minute and every two minutes by 5° inclination, until reaching 20° inclination. The mice were stimulated to run until exhaustion by a mild electric shock (1 mA, pulse 200 ms, 1 Hz) experienced on a shock grid at the bottom of the running belt. Complete exhaustion of a mouse was reached when the mouse spent more than 3 consecutive seconds on the shock grid or jumped more than 3 times on the shock grid without reengaging the treadmill. Prior to and immediately after the experiment, blood samples were taken and analysed for lactate levels using the StatStrip Xpress Lactate Meter (Nova Biomedical, Waltham, MA, USA).

Intraperitoneal glucose tolerance test (IPGTT)

After fasting for 16 hours over night, 2 mg of glucose/g BW (20% w/v; Braun, Hessen, Germany) were intraperitoneally injected into the mice. Blood samples from the tip of the tail were analysed after the indicated time points using a StatStrip Xpress Glucose Meter (Nova Biomedical).

Intraperitoneal insulin tolerance test (IPITT)

Following fasting for 16 hours over night, mice were intraperitoneally injected with 0.75 IU/kg BW (Lilly Humalog, Indianapolis, IN, USA). Blood glucose levels were measured in blood from the tip of the tail at the indicated time points after injection using the StatStrip Xpress Glucose Meter.

ELISAs

Basal insulin levels were determined in plasma taken from mice starved for 4 hours during the light cycle using an anti-insulin enzyme-linked immunosorbent assay (ELISA) following the manufacturer’s description (Mercodia, Uppsala, Sweden). Thyroid-stimulating hormone (TSH)

plasma values were analysed with an anti-TSH ELISA following the manufacturer's description (Cloud-clone Corporation, Katy, TX, USA). Absorbance was determined with a microplate reader (Infinite 200 Pro, Tecan, Maennedorf, Switzerland).

Body composition analysis

An EchoMRI whole body composition analyser was used to analyse lean and fat mass non-invasively according to the manufacturer's instructions (Echo Medical systems, Houston, TX, USA).

Whole-body plethysmography

Basal respiration as well as the adaptation of respiration to hypoxia were assessed in unrestrained conscious mice using a whole-body plethysmograph and BioSystem XA software (Buxco Research Systems, Wilmington, NC, USA). Each mouse was placed in a 1 dm^3 chamber and allowed to adapt for 1 hour. Respiratory parameters were analysed over a 5 minute interval at 21% O_2 and during the first 5 min after reaching 10% O_2 (referred to as "early"). In addition, the respiration was assessed after 25-30 min at 10% O_2 (referred to as "late"). To exclude measurements of non-basal respiration, data was not taken into account if at least 3 consecutive respiratory frequencies showed a variability of above 70 breaths/min and/or a total frequency of 400 breaths/min or above.

Indirect calorimetry

Animals were single housed in acrylic glass airtight metabolic cages attached to an open calorimetry system (TSE Systems, Bad Homburg, Germany). Food and water were provided *ad libitum.* O_2 consumption and CO_2 production were measured during 3 days and the average was calculated. Energy expenditure (EE) was calculated according to the Weir equation and normalised to the corresponding lean mass + 0.2 times the fat mass, as determined by body composition analysis by EchoMRI[124, 125].

Echocardiography

Mouse echocardiography including tissue Doppler imaging (TDI) was performed under isofluorane anesthesia with a high resolution Micro-Ultrasound System (Vevo 3100, Visualsonics, Toronto, ON, Canada) as previously described[94]. The myocardial performance index (MPI) was calculated as: MPI = (isovolumetric contraction time [IVCT] + isovolumetric relaxation time [IVRT])/aortic ejection time (AET)[94].

Food/water intake, urine/faeces production

Mice were single housed in metabolic cages with grid surfaces (Technoplast, Schwerzenbach, Switzerland) and food, water, urine, faeces and BW were monitored every 24 hours for 72 hours. Urine was collected under light mineral oil (Sigma-Aldrich) to avoid evaporation.

Genotyping primers

Otub1$^{+/-}$ and *Otub1*$^{-/-}$:

Otub1-5arm-WTF: 5'-TAGATGCTACACAGTGCTTTTAGA-3'

Otub1-Ctrl-WTR: 5'-TTAGAGATCAGCTCTGGAAATATAG-3'

5mut-R1: 5'-GAACTTCGGAATAGGAACTTCG-3'

pc*Otub1* KO$^{+/-}$:

Kr_3209: 5'-CCAACAGCTTCCCCACAACGG-3'

Ef_5272: 5'-TCCACCCCTTCATCCTGCTTTCT-3'

Otub1$^{fl/fl}$:

Ef_5272: 5'-TCCACCCCTTCATCCTGCTTTCT-3'

Er_5277: 5'-CAGACCAGAGCAGGATTAAGAAGCCTA-3'

UBC-Cre^{ERT2}:

UBCre 25285: 5'-GACGTCACCCGTTCTGTTG-3'

UBCre-oIMR7338: 5'-CTAGGCCACAGAATTGAAAGATCT-3'

UBCre-oIMR7339: 5'-GTAGGTGGAAATTCTAGCATC-3'

UBCre-oIMR9074: 5'-AGGCAAATTTTGGTGTACGG-3'

wb*Otub1* KO:

Ef_5273: 5'-GAAGGACAAAGGGCGTGTCTCAGT-3'

L3r_ 5274: 5'-TCTACCCATCCCAACACCAGCAAG-3'

loxP:

Primer 1307 forw: 5'-GGCAGAAGCACGCTTATCG-3'

Primer 1307 rev: 5'-GACAAGCGTTAGTAGGCACAT-3'

Sex determination[126]:

Smcx-1: 5'-CCGCTGCCAAATTCTTTGG-3'

Smc4-1: 5'-TGAAGCTTTTGGCTTTGAG-3'

Statistical analysis

For the statistical analysis between two different data points, two-tailed Student's t-test or Mann-Whitney test were applied as indicated. Comparison of more than two data points included One-Way ANOVA followed by Tukey post-test analysis or Two-Way ANOVA followed by Bonferroni post-test as indicated.

Data availability

All main data of this study are included in the main part of the manuscript or supplementary information. All underlying raw data will be available on https://datadryad.org/ upon acceptance of this article and the accession code will be inserted in this paragraph prior to publication.

ACKNOWLEDGEMENTS

We thank the Zurich Integrative Rodent Physiology (ZIRP) facility for the expert contributions; D. M. Katschinski for advice and support; B. Becher for the *Flp* deleter strain. The work was supported by the Swiss National Science Foundation (31003A_165679) (R.H.W.), by a Junior Grant of the NCCR “Kidney.CH” (C.C.S.) and by the Hartmann Müller-Stiftung (C.C.S.). F.P. is the recipient of a H.H. Sheikh Khalifa bin Hamad Al Thani Foundation Assistant Professorship at the Faculty of Medicine, University of Zurich.

AUTHOR CONTRIBUTIONS

A.R.S., J.M.P., C.N.B., J.G., S.C., P.F., S.P., A.M.B., G.P., C.A.W., T.A.L., F.P., R.H.W., C.C.S. performed experiments and/or analysed/interpreted the data. J.M.P., G.P., C.A.W., T.A.L., F.P., R.H.W., C.C.S. provided essential resources. C.C.S. wrote the paper and conceptualized and supervised the study. All authors critically reviewed the results and the manuscript.

COMPETING INTERESTS

The authors declare no competing interests.

REFERENCES

1 Clague, M. J., Urbe, S. & Komander, D. Breaking the chains: deubiquitylating enzyme specificity begets function. *Nat Rev Mol Cell Biol* **20**, 338-352 (2019).
2 Günter, J., Ruiz-Serrano, A., Pickel, C., Wenger, R. H. & Scholz, C. C. The functional interplay between the HIF pathway and the ubiquitin system - more than a one-way road. *Exp Cell Res* **356**, 152-159 (2017).
3 Clague, M. J., Heride, C. & Urbe, S. The demographics of the ubiquitin system. *Trends Cell Biol* **25**, 417-426 (2015).
4 Vandenabeele, P. & Bertrand, M. J. The role of the IAP E3 ubiquitin ligases in regulating pattern-recognition receptor signalling. *Nat Rev Immunol* **12**, 833-844 (2012).
5 Edelmann, M. J. *et al.* Structural basis and specificity of human otubain 1-mediated deubiquitination. *Biochem J* **418**, 379-390 (2009).
6 Wang, T. *et al.* Evidence for bidentate substrate binding as the basis for the K48 linkage specificity of otubain 1. *J Mol Biol* **386**, 1011-1023 (2009).
7 Wolberger, C. Mechanisms for regulating deubiquitinating enzymes. *Protein science : a publication of the Protein Society* **23**, 344-353 (2014).
8 Nakada, S. *et al.* Non-canonical inhibition of DNA damage-dependent ubiquitination by OTUB1. *Nature* **466**, 941-946 (2010).
9 Juang, Y. C. *et al.* OTUB1 co-opts Lys48-linked ubiquitin recognition to suppress E2 enzyme function. *Mol Cell* **45**, 384-397 (2012).
10 Herhaus, L., Al-Salihi, M., Macartney, T., Weidlich, S. & Sapkota, G. P. OTUB1 enhances TGFbeta signalling by inhibiting the ubiquitylation and degradation of active SMAD2/3. *Nat Commun* **4**, 2519 (2013).
11 Goncharov, T. *et al.* OTUB1 modulates c-IAP1 stability to regulate signalling pathways. *EMBO J* **32**, 1103-1114 (2013).
12 Li, S. *et al.* Regulation of virus-triggered signaling by OTUB1- and OTUB2-mediated deubiquitination of TRAF3 and TRAF6. *J Biol Chem* **285**, 4291-4297 (2010).
13 Peng, Y., Xu, R. & Zheng, X. HSCARG negatively regulates the cellular antiviral RIG-I like receptor signaling pathway by inhibiting TRAF3 ubiquitination via recruiting OTUB1. *PLoS Pathog* **10**, e1004041 (2014).
14 Lin, J. T. *et al.* Naive CD4 t cell proliferation is controlled by mammalian target of rapamycin regulation of GRAIL expression. *J Immunol* **182**, 5919-5928 (2009).
15 Zhou, K. *et al.* OTUB1-mediated deubiquitination of FOXM1 up-regulates ECT-2 to promote tumor progression in renal cell carcinoma. *Cell Biosci* **10**, 50 (2020).
16 Sulser, P. *et al.* HIF hydroxylase inhibitors decrease cellular oxygen consumption depending on their selectivity. *FASEB J.* **34**, 2344-2358 (2020).
17 Pickel, C. *et al.* Oxygen-dependent bond formation with FIH regulates the activity of the client protein OTUB1. *Redox Biol* **26**, 101265 (2019).
18 Scholz, C. C. *et al.* Regulation of IL-1beta-induced NF-kappaB by hydroxylases links key hypoxic and inflammatory signaling pathways. *PNAS* **110**, 18490-18495 (2013).
19 Scholz, C. C. *et al.* FIH Regulates Cellular Metabolism through Hydroxylation of the Deubiquitinase OTUB1. *PLoS Biol* **14**, e1002347 (2016).
20 Pasupala, N. *et al.* OTUB1 non-catalytically stabilizes the E2 ubiquitin-conjugating enzyme UBE2E1 by preventing its autoubiquitination. *J Biol Chem* **293**, 18285-18295 (2018).
21 Wang, X. *et al.* OTUB1 inhibits CNS autoimmunity by preventing IFN-gamma-induced hyperactivation of astrocytes. *EMBO J* **38** (2019).
22 Mulas, F. *et al.* The deubiquitinase OTUB1 augments NF-kappaB-dependent immune responses in dendritic cells in infection and inflammation by stabilizing UBC13. *Cell Mol Immunol* (2020).
23 Li, Y. *et al.* Preventing abnormal NF-kappaB activation and autoimmunity by Otub1-mediated p100 stabilization. *Cell Res* **29**, 474-485 (2019).

24 Zhou, X. *et al.* The deubiquitinase Otub1 controls the activation of CD8(+) T cells and NK cells by regulating IL-15-mediated priming. *Nat Immunol* **20**, 879-889 (2019).

25 Saldana, M., VanderVorst, K., Berg, A. L., Lee, H. & Carraway, K. L. Otubain 1: a non-canonical deubiquitinase with an emerging role in cancer. *Endocrine-related cancer* **26**, R1-R14 (2019).

26 Ikeda, H. *et al.* Increased Akt-mTOR signaling in lung epithelium is associated with respiratory distress syndrome in mice. *Mol Cell Biol* **31**, 1054-1065 (2011).

27 Lertkiatmongkol, P., Liao, D., Mei, H., Hu, Y. & Newman, P. J. Endothelial functions of platelet/endothelial cell adhesion molecule-1 (CD31). *Curr Opin Hematol* **23**, 253-259 (2016).

28 Costantino, S. *et al.* Obesity-induced activation of JunD promotes myocardial lipid accumulation and metabolic cardiomyopathy. *Eur Heart J* **40**, 997-1008 (2019).

29 Riehle, C. & Bauersachs, J. Small animal models of heart failure. *Cardiovasc Res* **115**, 1838-1849 (2019).

30 Zhao, L. *et al.* OTUB1 protein suppresses mTOR complex 1 (mTORC1) activity by deubiquitinating the mTORC1 inhibitor DEPTOR. *J Biol Chem* **293**, 4883-4892 (2018).

31 Land, S. C., Scott, C. L. & Walker, D. mTOR signalling, embryogenesis and the control of lung development. *Semin Cell Dev Biol* **36**, 68-78 (2014).

32 Wang, J. *et al.* PI3K-AKT pathway mediates growth and survival signals during development of fetal mouse lung. *Tissue Cell* **37**, 25-35 (2005).

33 Iturri, P., Joseph, V., Rodrigo, G., Bairam, A. & Soliz, J. Inhibition of Protein Kinases AKT and ERK1/2 Reduce the Carotid Body Chemoreceptor Response to Hypoxia in Adult Rats. *Adv Exp Med Biol* **860**, 269-277 (2015).

34 Xu, L. & Brink, M. mTOR, cardiomyocytes and inflammation in cardiac hypertrophy. *Biochim Biophys Acta* **1863**, 1894-1903 (2016).

35 Dummler, B. & Hemmings, B. A. Physiological roles of PKB/Akt isoforms in development and disease. *Biochem Soc Trans* **35**, 231-235 (2007).

36 Saxton, R. A. & Sabatini, D. M. mTOR Signaling in Growth, Metabolism, and Disease. *Cell* **168**, 960-976 (2017).

37 Caron, A., Briscoe, D. M., Richard, D. & Laplante, M. DEPTOR at the Nexus of Cancer, Metabolism, and Immunity. *Physiol Rev* **98**, 1765-1803 (2018).

38 Manning, B. D. & Toker, A. AKT/PKB Signaling: Navigating the Network. *Cell* **169**, 381-405 (2017).

39 Hahn-Windgassen, A. *et al.* Akt activates the mammalian target of rapamycin by regulating cellular ATP level and AMPK activity. *J Biol Chem* **280**, 32081-32089 (2005).

40 De Leo, S., Lee, S. Y. & Braverman, L. E. Hyperthyroidism. *Lancet* **388**, 906-918 (2016).

41 Haeusler, R. A., McGraw, T. E. & Accili, D. Biochemical and cellular properties of insulin receptor signalling. *Nat Rev Mol Cell Biol* **19**, 31-44 (2018).

42 Taniguchi, C. M., Emanuelli, B. & Kahn, C. R. Critical nodes in signalling pathways: insights into insulin action. *Nat Rev Mol Cell Biol* **7**, 85-96 (2006).

43 Lopez-Barneo, J., Macias, D., Platero-Luengo, A., Ortega-Saenz, P. & Pardal, R. Carotid body oxygen sensing and adaptation to hypoxia. *Pflugers Arch* **468**, 59-70 (2016).

44 Akasaki, Y. *et al.* Glycolytic fast-twitch muscle fiber restoration counters adverse age-related changes in body composition and metabolism. *Aging cell* **13**, 80-91 (2014).

45 Chakraborty, A. *et al.* Inositol pyrophosphates inhibit Akt signaling, thereby regulating insulin sensitivity and weight gain. *Cell* **143**, 897-910 (2010).

46 Carracedo, A., Alimonti, A. & Pandolfi, P. P. PTEN level in tumor suppression: how much is too little? *Cancer Res* **71**, 629-633 (2011).

47 Osman, M. A., Sarkar, F. H. & Rodriguez-Boulan, E. A molecular rheostat at the interface of cancer and diabetes. *Biochim Biophys Acta* **1836**, 166-176 (2013).

48 Zhang, N. *et al.* The asparaginyl hydroxylase factor inhibiting HIF-1alpha is an essential regulator of metabolism. *Cell Metab* **11**, 364-378 (2010).
49 Dickinson, M. E. *et al.* High-throughput discovery of novel developmental phenotypes. *Nature* **537**, 508-514 (2016).
50 Gutsche, K. *et al.* Intermittent hypoxia confers pro-metastatic gene expression selectively through NF-kappaB in inflammatory breast cancer cells. *Free Radic Biol Med* **101**, 129-142 (2016).
51 Emmerich, C. H. & Cohen, P. Optimising methods for the preservation, capture and identification of ubiquitin chains and ubiquitylated proteins by immunoblotting. *Biochem Biophys Res Commun* **466**, 1-14 (2015).
52 Imeri, F. *et al.* Generation of renal Epo-producing cell lines by conditional gene tagging reveals rapid HIF-2 driven Epo kinetics, cell autonomous feedback regulation, and a telocyte phenotype. *Kidney Int* **95**, 375-387 (2019).
53 Uhlen, M. *et al.* Proteomics. Tissue-based map of the human proteome. *Science* **347**, 1260419 (2015).
54 Bradford, M. M. A rapid and sensitive method for the quantitation of microgram quantities of protein utilizing the principle of protein-dye binding. *Anal Biochem* **72**, 248-254 (1976).
55 Pickel, C., Taylor, C. T. & Scholz, C. C. Genetic Knockdown and Pharmacologic Inhibition of Hypoxia-Inducible Factor (HIF) Hydroxylases. *Methods Mol Biol* **1742**, 1-14 (2018).
56 Sun, X. X., Challagundla, K. B. & Dai, M. S. Positive regulation of p53 stability and activity by the deubiquitinating enzyme Otubain 1. *EMBO J* **31**, 576-592 (2012).
57 Schindelin, J. *et al.* Fiji: an open-source platform for biological-image analysis. *Nat Methods* **9**, 676-682 (2012).
58 Schneider, C. A., Rasband, W. S. & Eliceiri, K. W. NIH Image to ImageJ: 25 years of image analysis. *Nat Methods* **9**, 671-675 (2012).
59 Weir, J. B. New methods for calculating metabolic rate with special reference to protein metabolism. *J Physiol* **109**, 1-9 (1949).
60 Wielinga, P. Y., Alder, B. & Lutz, T. A. The acute effect of amylin and salmon calcitonin on energy expenditure. *Physiol Behav* **91**, 212-217 (2007).
61 Clapcote, S. J. & Roder, J. C. Simplex PCR assay for sex determination in mice. *Biotechniques* **38**, 702, 704, 706 (2005).

SUPPLEMENTARY INFORMATION

The deubiquitinase OTUB1 is essential for development, energy metabolism, respiration, and cardiac function

Amalia Ruiz-Serrano[1], Josep Monné Rodríguez[2], Christina N. Boyle[3], Julia Günter[1,4], Sarah Costantino[5], Pascal Flüchter[1], Svende Pfundstein[1], Andreas M. Bapst[1], Giovanni Pellegrini[2], Carsten A. Wagner[1,4], Thomas A. Lutz[3], Francesco Paneni[5], Roland H. Wenger[1,4,*], and Carsten C. Scholz[1,4,*]

[1]Institute of Physiology, University of Zurich, Zurich, Switzerland.
[2]Laboratory for Animal Model Pathology (LAMP), Institute of Veterinary Pathology, University of Zurich, Zurich, Switzerland.
[3]Institute of Veterinary Physiology, University of Zurich, Zurich, Switzerland.
[4]National Centre of Competence in Research 'Kidney.CH', Switzerland.
[5]Center for Molecular Cardiology, Schlieren Campus, University of Zurich, Schlieren, Switzerland; University Heart Center, Cardiology, University Hospital Zurich, Switzerland; Department of Research and Education, University Hospital Zurich, Switzerland.
*, emails: roland.wenger@access.uzh.ch, carsten.scholz@uzh.ch

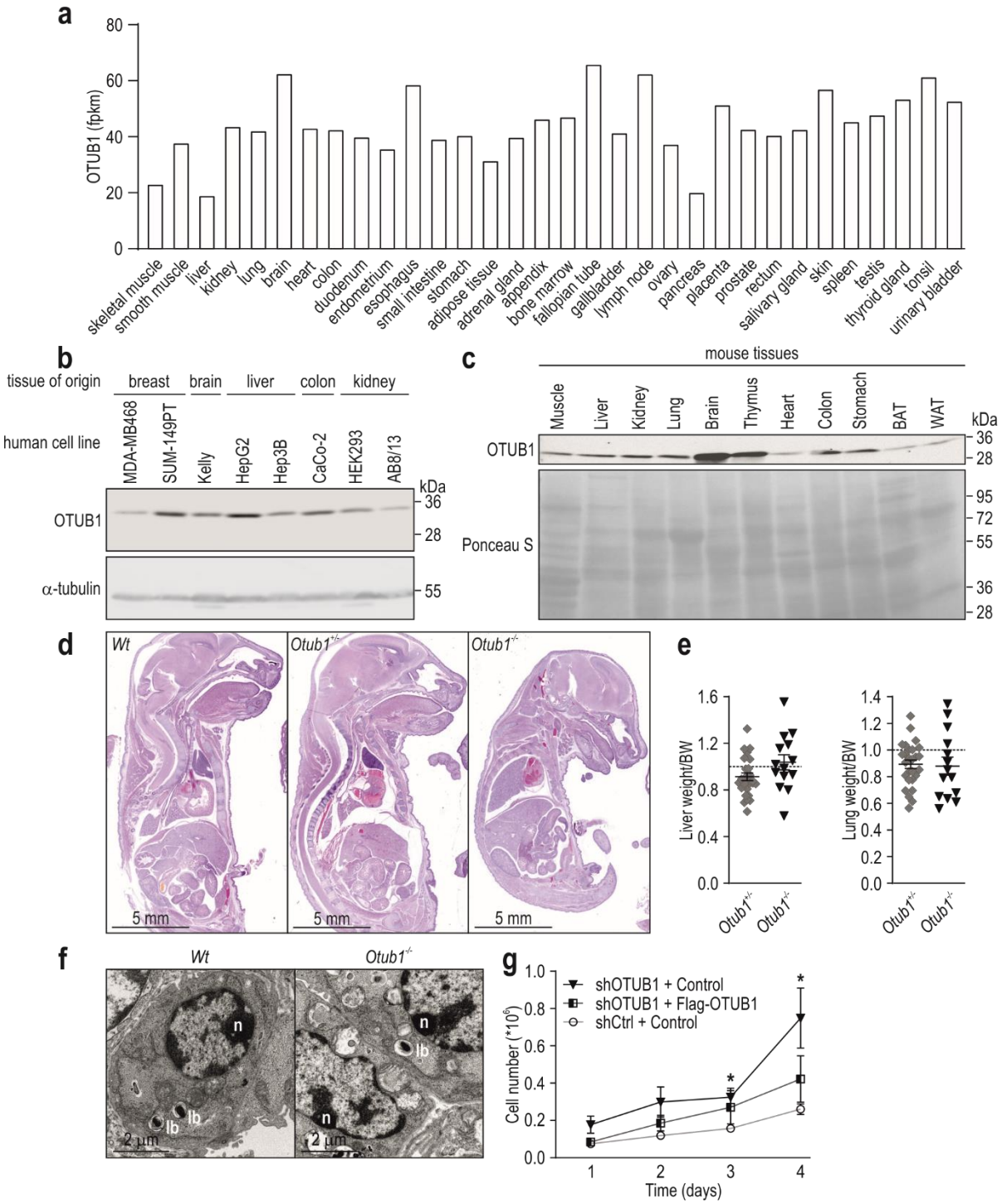

Supplementary Figure 1. OTUB1 tissue expression levels and developmental effects of *Otub1* deletion. a, Human OTUB1 RNA-sequencing analysis of the indicated organs [119]. **b,** Immunoblot analysis of OTUB1 protein levels in the indicated human cancer cell lines. α-Tubulin served as loading and blotting control. **c,** Immunoblotting of OTUB1 in murine *Wt* tissues. Ponceau S staining of the membrane served as loading and blotting control. BAT, brown adipose tissue; WAT, white adipose tissue. **d,** H&E staining of sagittal sections of *Wt*, *Otub1*$^{+/-}$ and *Otub1*$^{-/-}$ mice (E18.5). **e,** *Otub1*$^{+/-}$ (n=27) and *Otub1*$^{-/-}$ (n=14) liver and lung weight corrected for BW and normalised to the corresponding *Wt* littermates (E18.5). The dashed line indicates *Wt* littermates. **f,** Transmission electron microscopy of lung tissue from *Wt* and *Otub1*$^{-/-}$ mice (E18.5). lb, lamellar body; m, mitochondrium; n, nucleus. **g,** Cell proliferation analysis of HEK293 cells stably co-transfected with shRNA targeting OTUB1 (shOTUB1)

together with an empty vector (control), or shOTUB1 together with an expression construct for FLAG-OTUB1, or an shRNA without target (shCtrl) together with the empty control vector (n=3). Representative pictures of three independent experiments are displayed. All data are shown as mean ± SEM. *, $p < 0.05$ by Student's t-test. Exact P values: **g,** 3 days shCtrl + Control versus shOTUB1 + Control: 0.0267; 4 days shCtrl + Control versus shOTUB1 + Control: 0.0402.

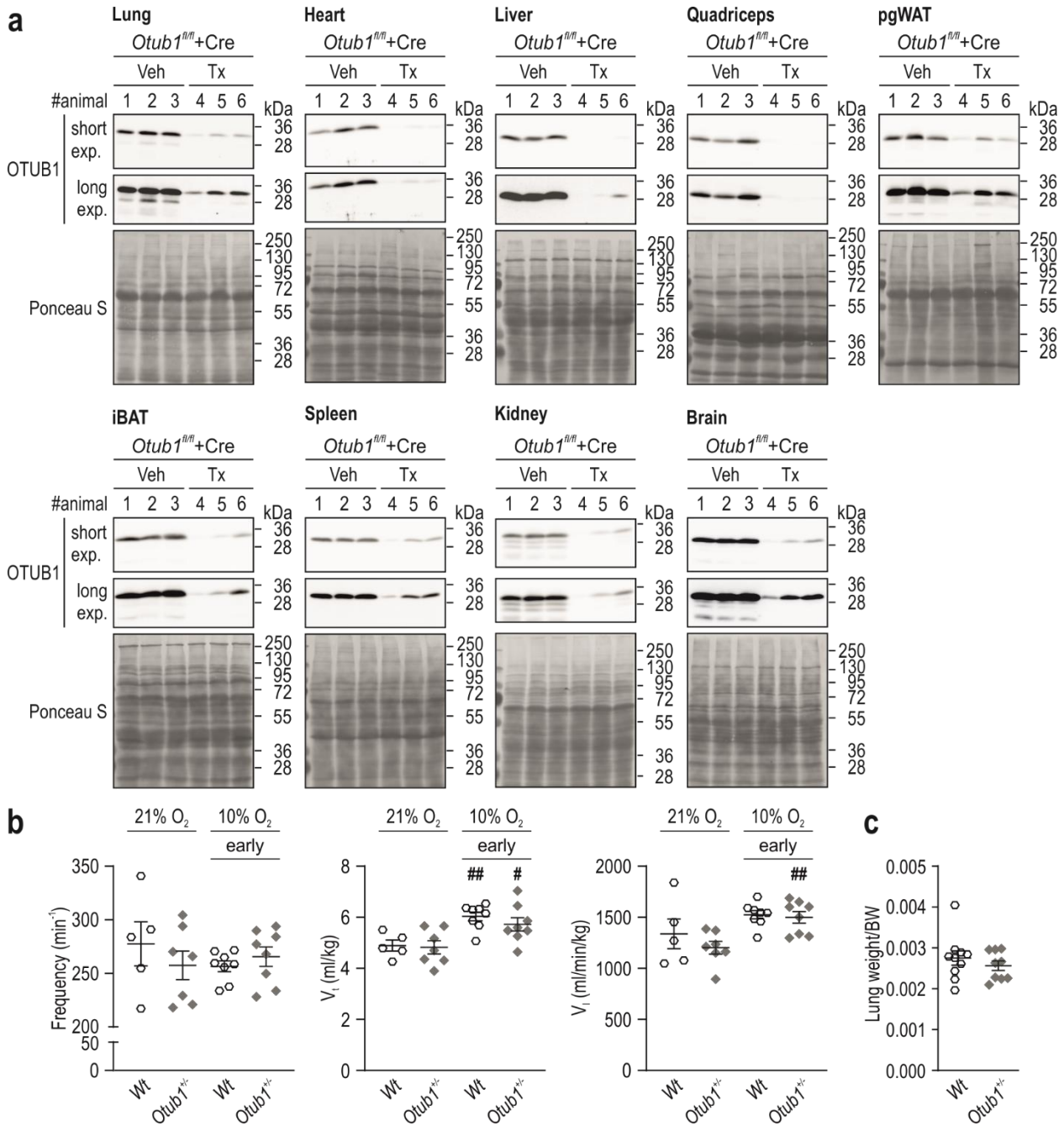

Supplementary Figure 2. Efficiency of induced *Otub1* KO and lung function analysis in *Otub1*$^{+/-}$ mice. a, OTUB1 protein levels were analysed by immunoblotting 5 months after the induction of *Otub1* deletion. pgWAT, perigonadal white adipose tissue; iBAT, interscapular brown adipose tissue. **b,** Consecutive analysis of the lung function of unrestrained *Wt* (n = 5-8) *Otub1*$^{+/-}$ mice (6 months old mice; n = 7-8) determined by barometric pressure plethysmography in normoxia (21% O_2) and hypoxia (10% O_2). V_t, tidal volume; V_l, minute volume; early, first 5 min in hypoxia. **c,** Lung weight normalised to BW of *Wt* (n=10) and *Otub1*$^{+/-}$ (n=9) mice (10 months old). Representative pictures of three independent experiments are displayed. All data are shown as mean ± SEM. #, $p < 0.05$; ##, $p < 0.01$ by Student's t-test compared to the corresponding analysis of the same mice in normoxia. Exact P values: **b,** V_t 10% O_2 early *Wt* versus V_t 21% O_2 *Wt*: 0.0015; V_t 10% O_2 early *Otub1*$^{+/-}$ versus V_t 21% O_2 *Otub1*$^{+/-}$: 0.0295; V_l 10% O_2 early *Otub1*$^{+/-}$ versus V_l 21% O_2 *Otub1*$^{+/-}$: 0.0037.

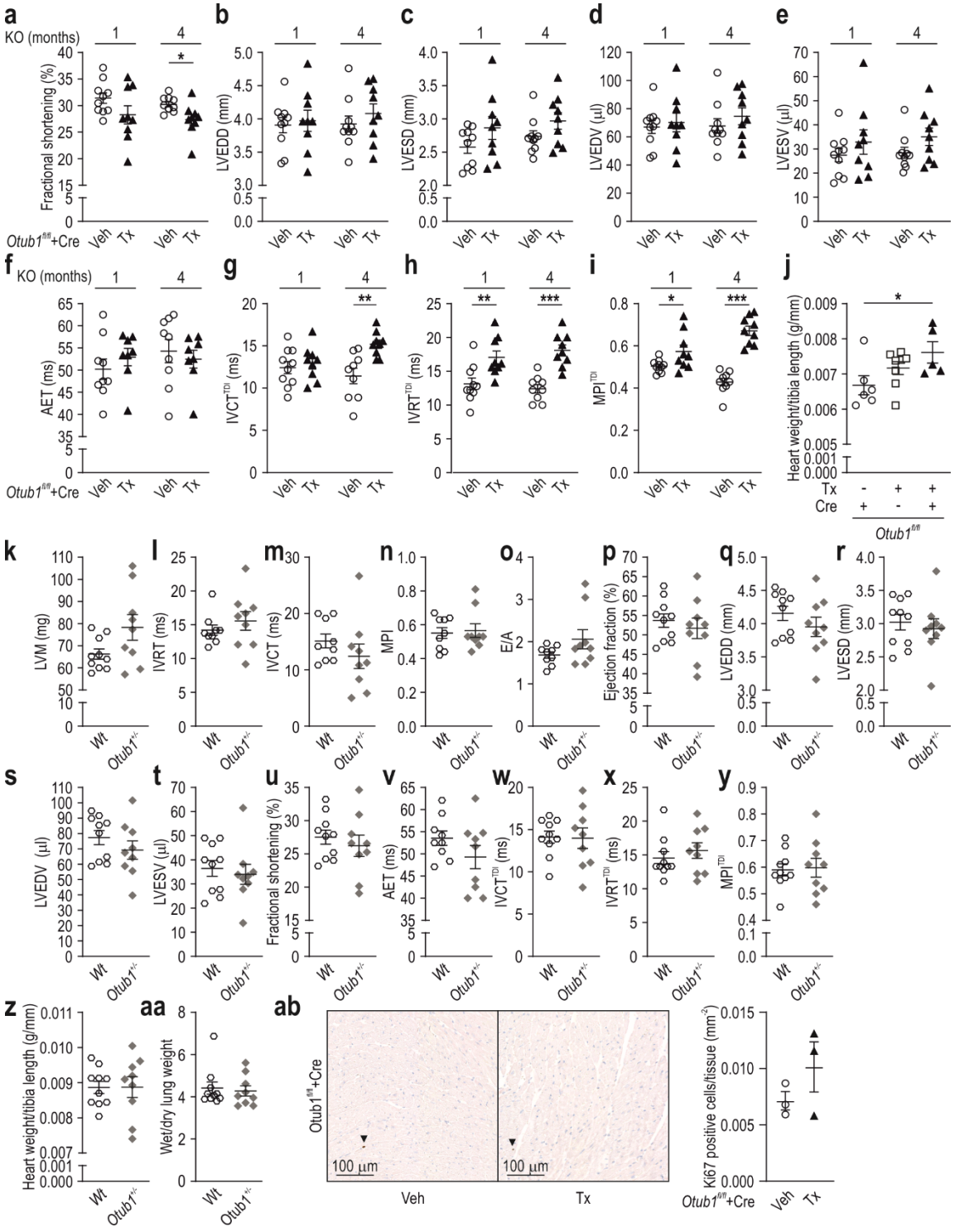

Supplementary Figure 3. Cardiac function in mice with *Otub1* KO. a-i, Echocardiography of the fractional shortening (**a**), left ventricular end diastolic diameter (LVEDD) (**b**), left ventricular end systolic diameter (LVESD) (**c**), left ventricular end diastolic volume (LVEDV) (**d**), left ventricular end systolic volume (LVESV) (**e**), aortic ejection time (AET) (**f**), isovolumic contraction time determined by tissue Doppler imaging ($IVCT^{TDI}$) (**g**), isovolumic relaxation time determined by tissue Doppler imaging ($IVRT^{TDI}$) (**h**) and the myocardial performance index determined by tissue Doppler imaging (MPI^{TDI}) (**i**) at the indicated time points after *Otub1* KO (3.5 and 6.5 months of age; Veh, n = 9-10; Tx, n = 8-9). **j,** Heart weight normalised to tibia length (3.5 months after *Otub1* KO; *Otub1*$^{fl/fl}$ + Cre + Veh, n = 6; *Otub1*$^{fl/fl}$ - Cre + Tx, n = 8; *Otub1*$^{fl/fl}$ + Cre + Tx, n = 5). **k-y,** Echocardiography of the left ventricular mass (LVM) (**k**), IVRT

(**l**), isovolumic contraction time (IVCT) (**m**), myocardial performance index (MPI) (**n**), E and A myocardial velocities ratio (E/A) (**o**), ejection fraction (**p**), LVEDD (**q**), LVESD (**r**), LVEDV (**s**), LVESV (**t**), fractional shortening (**u**), AET (**v**), $IVCT^{TDI}$ (**w**), $IVRT^{TDI}$ (**x**) and MPI^{TDI} (**y**) in the indicated mice (10 months old; *Wt*, n = 9-10; $Otub1^{+/-}$, n = 9). **z,** Heart weight normalised to tibia length and **aa,** wet over dry lung ratio in *Wt* (n=10) and $Otub1^{+/-}$ (n=9) mice (10 months old). **ab,** Immunohistochemistry of transversal heart sections with anti-Ki67 antibody and subsequent quantification (3.5 months after *Otub1* deletion, 5.5 months of age; n=3). All data are shown as mean ± SEM. *, $p < 0.05$ by Student's t-test. Exact P values: **a,** 4 months KO: 0.0164; **g,** 4 months KO: 0.0023; **h,** 1 month KO: 0.0073; 4 months KO: <0.0001; **i,** 1 month KO: 0.0345; 4 months KO: <0.0001; **j,** +Cre -Tx versus +Cre +Tx: 0.0486.

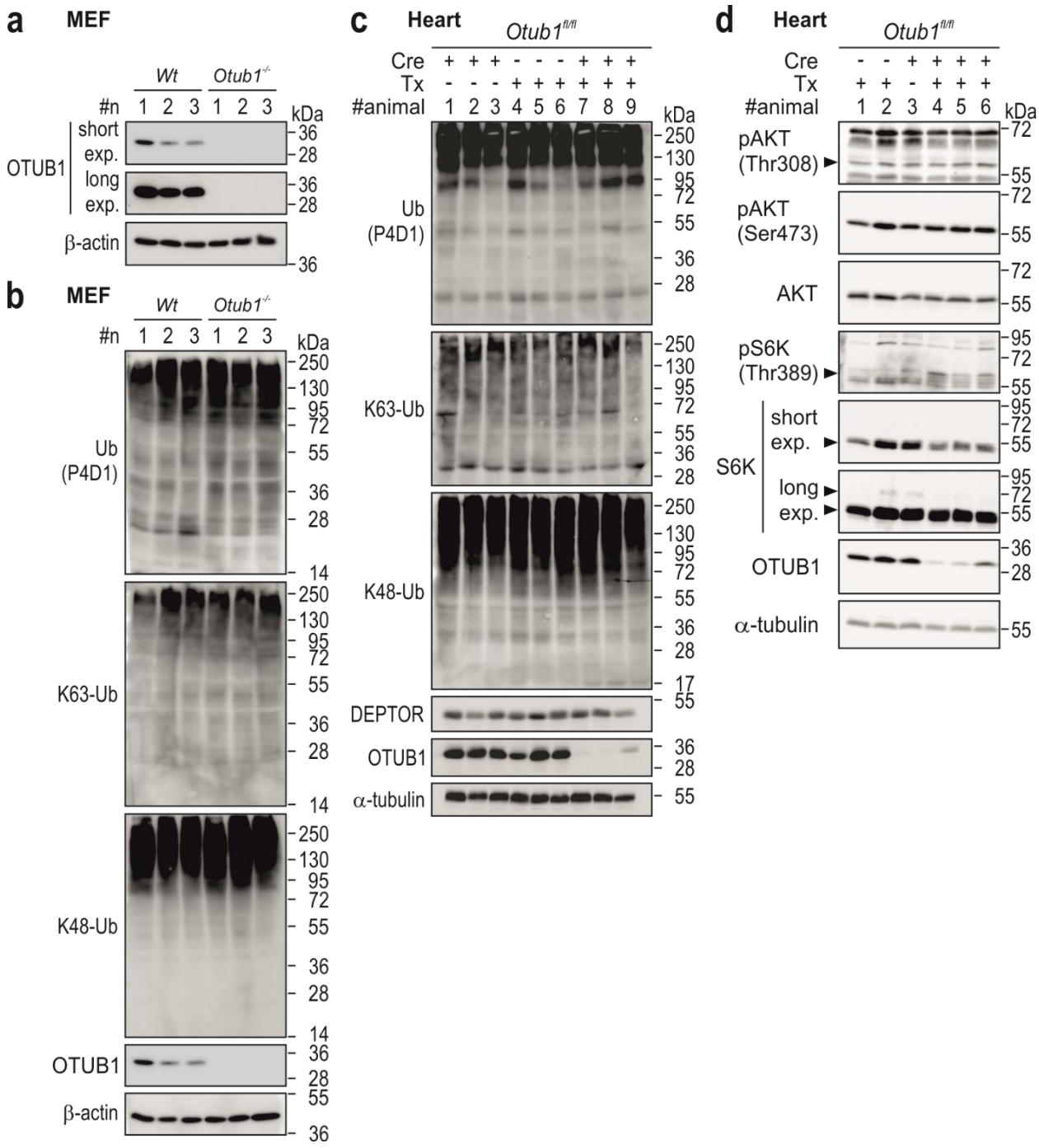

Supplementary Figure 4. Protein levels in mouse embryonic fibroblasts and hearts with homozygous *Otub1* deletion. a,b, Immunoblotting of the indicated proteins in *Wt* and *Otub1*$^{-/-}$ MEFs (n = 3). K63-Ub, K63-linked ubiquitin chains; K48-Ub, K48-linked Ub chains. **c,d,** Immunoblotting of the indicated proteins in heart tissue from mice with the indicated genotype and treatment 3.5 (**c**) or 6 (**d**) months after *Otub1* deletion (n = 3).

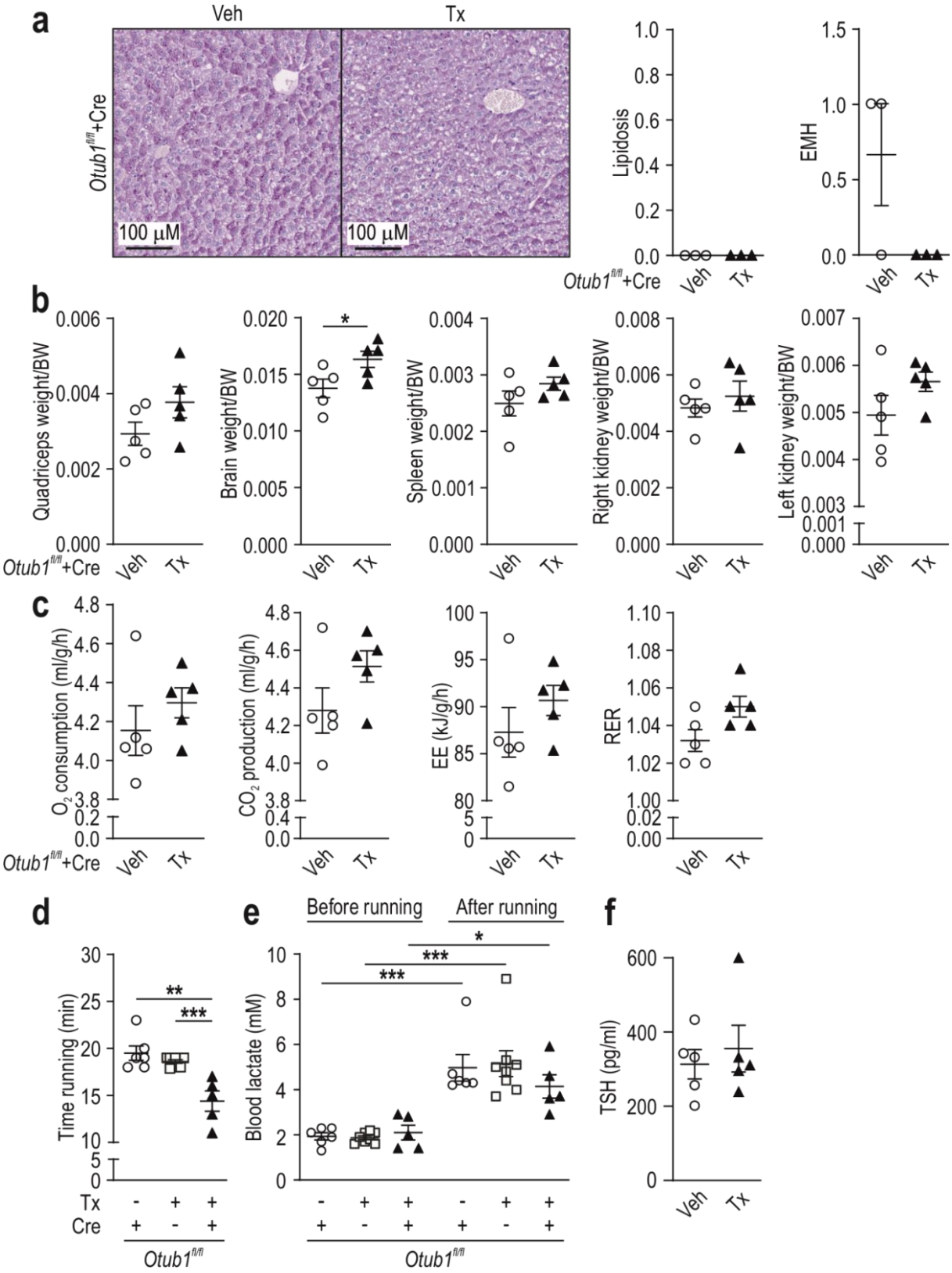

Supplementary Figure 5. Energy metabolism in mice with induced *Otub1* ablation. a, Representative PAS staining of transversal liver slices with scored lipidosis levels and extramedullary hematopoiesis (EMH) assessed 5 months after *Otub1* deletion (5 months after *Otub1* deletion; 6.5 months old mice, n=3). **b,** Weight of the indicated tissues normalised to BW (5 months after *Otub1* deletion; 6.5 months old mice, n=5). **c,** Averaged O_2 consumption, CO_2 production, energy expenditure (EE) and respiratory exchange ratio (RER) of 3

consecutive days during the night cycle (5 months after *Otub1* deletion; 6.5 months old mice; n=5). **d,** Total running time during a maximal exercise capacity analysis (3 months after *Otub1* deletion; 4.5 months old mice; *Otub1*$^{fl/fl}$ + Cre + Veh, n = 6; *Otub1*$^{fl/fl}$ - Cre + Tx, n = 8; *Otub1*$^{fl/fl}$ + Cre + Tx, n = 5). **e,** Blood lactate analyses prior to and following the maximal exercise shown in (**d**). **f,** Thyroid-stimulating hormone (TSH) plasma levels (5 months after *Otub1* deletion; 6.5 months old mice; n=5). *, $p < 0.05$; **, $p<0.01$; ***, $p<0.001$ by Student's t-test. Exact P values: **b,** brain weight: 0.0460; **d,** +Cre -Tx versus +Cre +Tx: 0.0033; -Cre +Tx versus +Cre +Tx: 0.0005; **e,** +Cre -Tx: 0.0006; -Cre +Tx: <0.0001; +Cre +Tx: 0.0102.

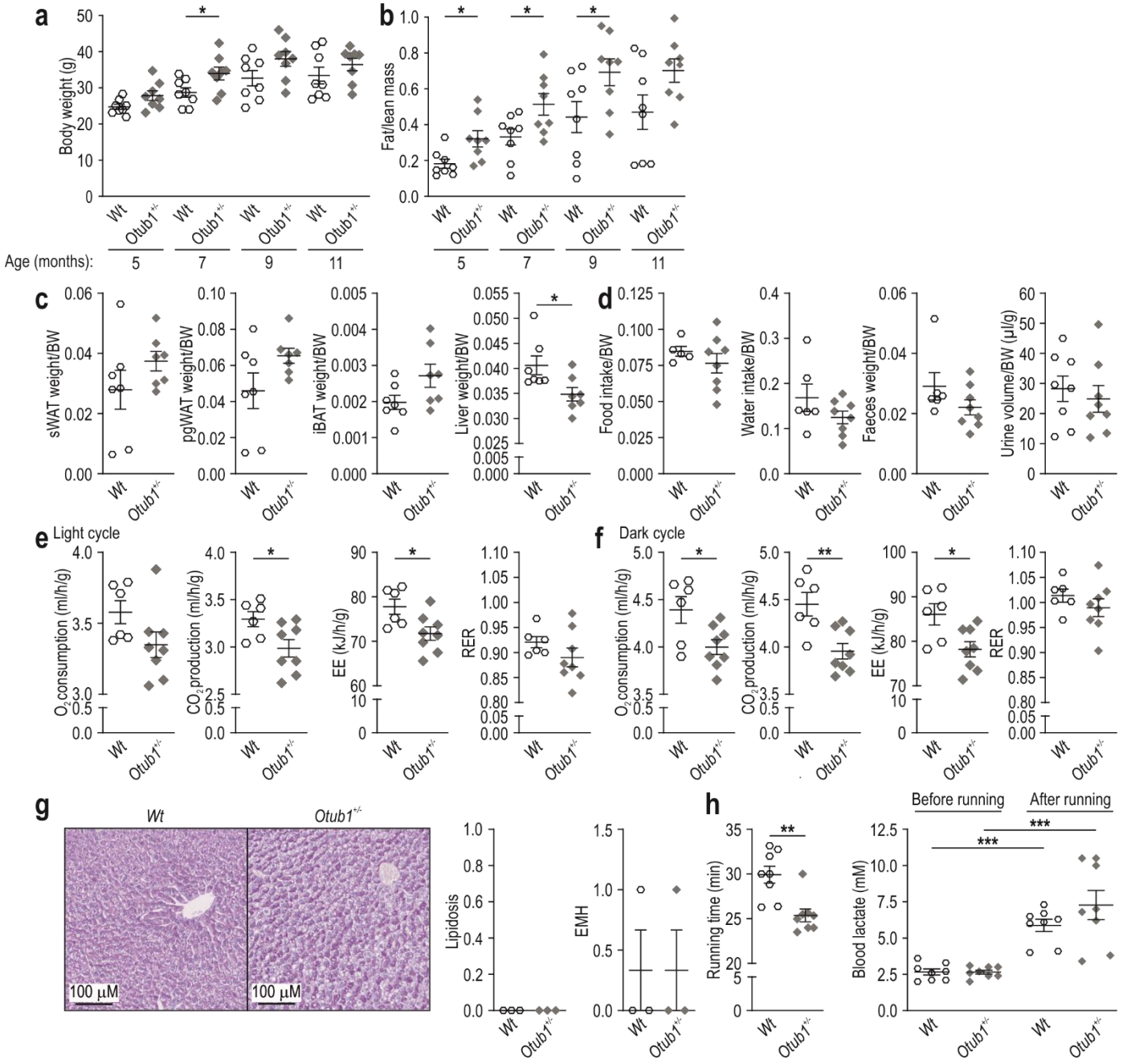

Supplementary Figure 6. Energy metabolism in adult *Otub1*$^{+/-}$ mice. a, Age-dependent weight development of *Otub1*$^{+/-}$ mice (n=8) **b,** Fat mass to lean mass ratio analysed by Echo-MRI in the same mice as shown in (**a**). **c,** Organ weight relative to BW in the same mice as shown in (**a, b**) (12 months of age; n = 7). **d,** Averaged food and water intake, faeces weight and urine volume over 72 hours, collected in metabolic cages (9.5 months of age; *Wt*, n = 5-8; *Otub1*$^{+/-}$, n = 8). **e,** O_2 consumption, CO_2 production, energy expenditure (EE) and respiratory exchange ratio (RER) of three consecutive days during the dark and **f,** light cycle (11.5 month old mice; *Wt*, n = 6; *Otub1*$^{+/-}$, n = 8). **g,** Representative PAS staining of transversal liver slices with scored lipidosis levels and extramedullary hematopoiesis (EMH) assessed in 4 month old mice (n=3). **h,** Total running time and blood lactate measurements before and after maximal exercise capacity analyses (7 month old mice; n = 8). All analyses were performed with the same group of mice. *, $p < 0.05$; **, $p<0.01$; ***, $p<0.001$ by Student's t-test. Exact P values: **a,** 0.032; **b,** 5 months: 0.0181; 7 months: 0.0295; 9 months: 0.0465; **c,** liver weight: 0.0283; **e,** CO_2 production: 0.0322; EE: 0.0216; **f,** O_2 consumption: 0.0237; CO_2 production: 0.0046; EE: 0.0172; **h,** running time: 0.0018; blood lactate: *Wt*: <0.0001; *Otub1*$^{+/-}$: 0.0005.

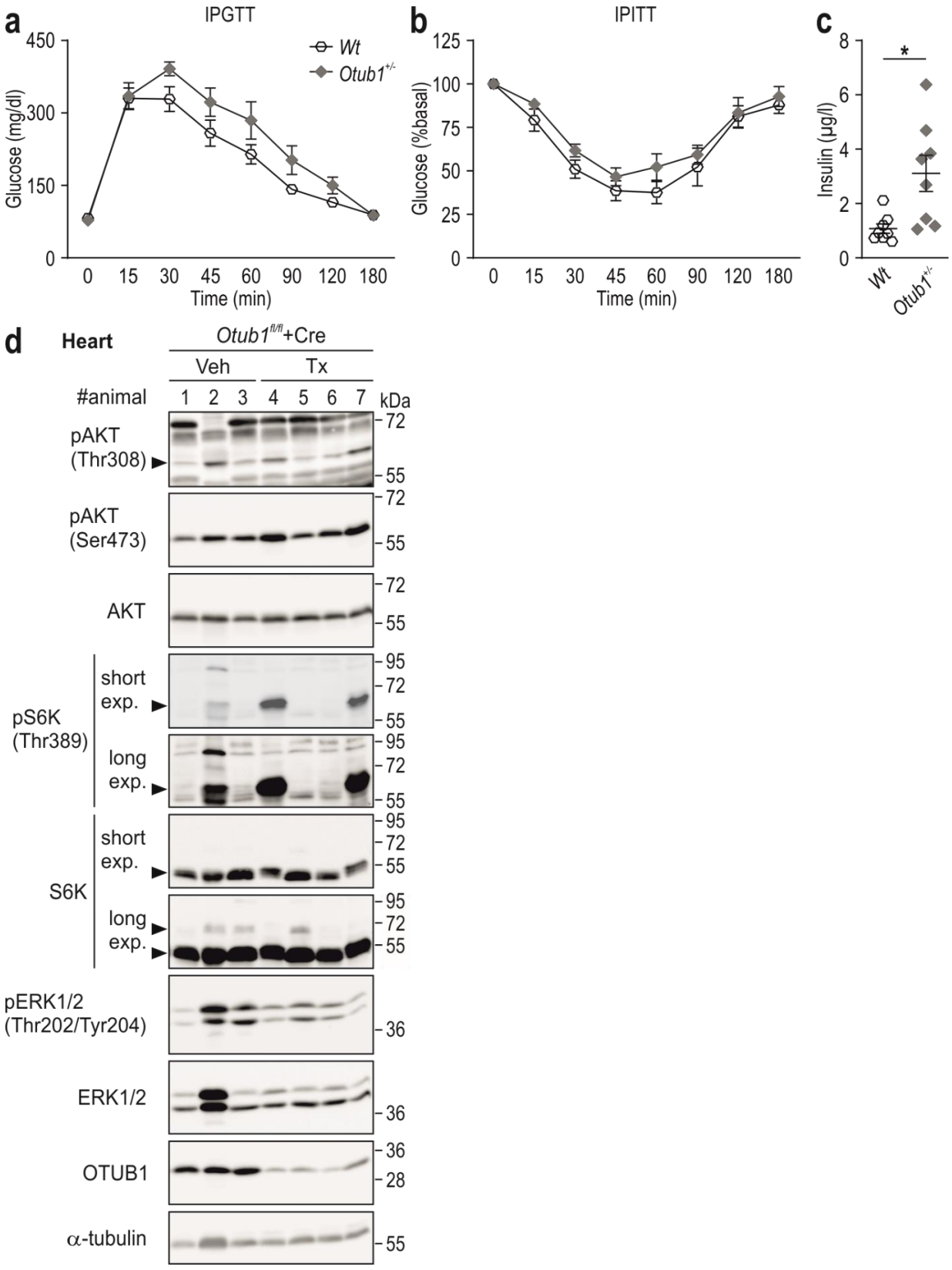

Supplementary Figure 7. Insulin sensitivity in mice with *Otub1* KO. a, Intraperitoneal glucose tolerance test (IPGTT; 2 mg glucose/g BW) and **b,** intraperitoneal insulin tolerance test (IPITT; 0.75 mU insulin/g BW) in 7 month-old mice (n = 7-8). **c,** Plasma insulin levels determined in 7 month-old mice (n = 8). **d,** Immunoblotting of heart lysates from mice (10 days after *Otub1* KO; 2 months old) starved overnight (16 h) followed by insulin IP application (0.75 mU insulin/g BW) 15 min prior to tissue harvest (Veh, n = 3; Tx, n = 4). *, $p < 0.05$ by two-way ANOVA with Bonferroni post-test (**a,b**) or Student's t-test (**c**). Exact P values: **c,** 0.0105.

5. Conclusions and future perspectives

Protein ubiquitination plays a crucial role in a plethora of physiological processes, such as cell apoptosis, cell metabolism and inflammation [127]. DUBs negatively regulate ubiquitination and are currently investigated as possible novel therapeutic targets. This possible role of the DUBs is especially due to their role as regulators in cancer, chronic inflammation or autoimmune disorders [128]. However, further understanding of the function and regulation of DUBs is necessary to understand their mechanism of action. One of the most highly expressed DUBs in cells is OTUB1 [20, 72]. Remarkably, OTUB1 possesses both catalytic and non-catalytic activities. Through its catalytic activity, OTUB1 cleaves Lys48-linked polyubiquitin chains [22, 129]. Non-catalytically, OTUB1 inhibits the formation of Lys48- and Lys63-linked polyubiquitin chains by the inhibition of E2 ubiquitin-conjugating enzymes [19, 24, 25, 130]. OTUB1 participates in diverse cellular processes including fibrosis [19], inflammation [77-79], DNA repair [24], apoptosis [77] and proliferation [80]. We previously showed that OTUB1 is also the substrate of the oxygen-sensing factor FIH, which hydroxylates OTUB1 Asn 22, regulating cellular energy metabolism [85].

We provided detailed insights into the molecular interplay between FIH and OTUB1. We showed that FIH and OTUB1 likely interact through a covalent bond catalyzed by FIH, forming a heterodimer. Following the heterodimer formation, the catalytic cleavage of Lys48-linked ubiquitin chains by OTUB1 was maintained and regulated by the E2 enzyme UBCH5B [83]. Additionally, we showed a metabolic phenotype in mice with *Otub1* deletion, which was comparable to the published phenotype of *Hif1an* KO mice [9, 114]. To know if the downstream mTOR/AKT activation under OTUB1 deletion in mice is also observed under deletion of FIH, the mTOR/AKT pathway could be studied under FIH deletion in mice. Currently, it is known that overexpressed FIH in cells decreases the levels of AKT and GSK phosphorylation [131, 132] with silencing of FIH having the opposite effect [131]. Furthermore, it would be interesting to study if the FIH-dependent hydroxylation of OTUB1 and/or the FIH-OTUB1 heterodimer occur *in vivo* and if the FIH-dependent regulation of OTUB1 is linked to the observed metabolic phenotype in both mouse models. Distinct mouse organs could be tested for the presence of the heterodimer via co-IP against FIH and OTUB1. The likelihood to detect the heterodimer is the bigger in tissues with the highest FIH and OTUB1 expression levels, which are the brain, skeletal muscle and kidney [114, 133]. Under a double inducible knock-out for OTUB1 and FIH in mice, the presence of the heterodimer could also be studied in distinct organs. Unfortunately, an antibody detecting asparagine hydroxylated proteins is not available. If such an antibody could be developed, the inter- and intra-organ localization of OTUB1 Asn22 hydroxylation could be detected in mice to give insights into the most important organs for FIH-dependent

OTUB1 regulation. To clearly determine the physiological relevance of the FIH-dependent regulation of OTUB1 *in vivo*, a transgenic mouse strain carrying OTUB1 with a mutated Asn22 to Ala would be needed. We showed that OTUB1 Asn22 is necessary for both OTUB1 hydroxylation by FIH as well as the FIH-OTUB1 heterodimer formation *in vitro* and that Asn22Ala mutation abrogates both. Hence, if FIH solely regulates energy metabolism through OTUB1 Asn22, mice with OTUB1 Asn22Ala mutation should display the same phenotype as *Hif1an* KO mice (Figure 1).

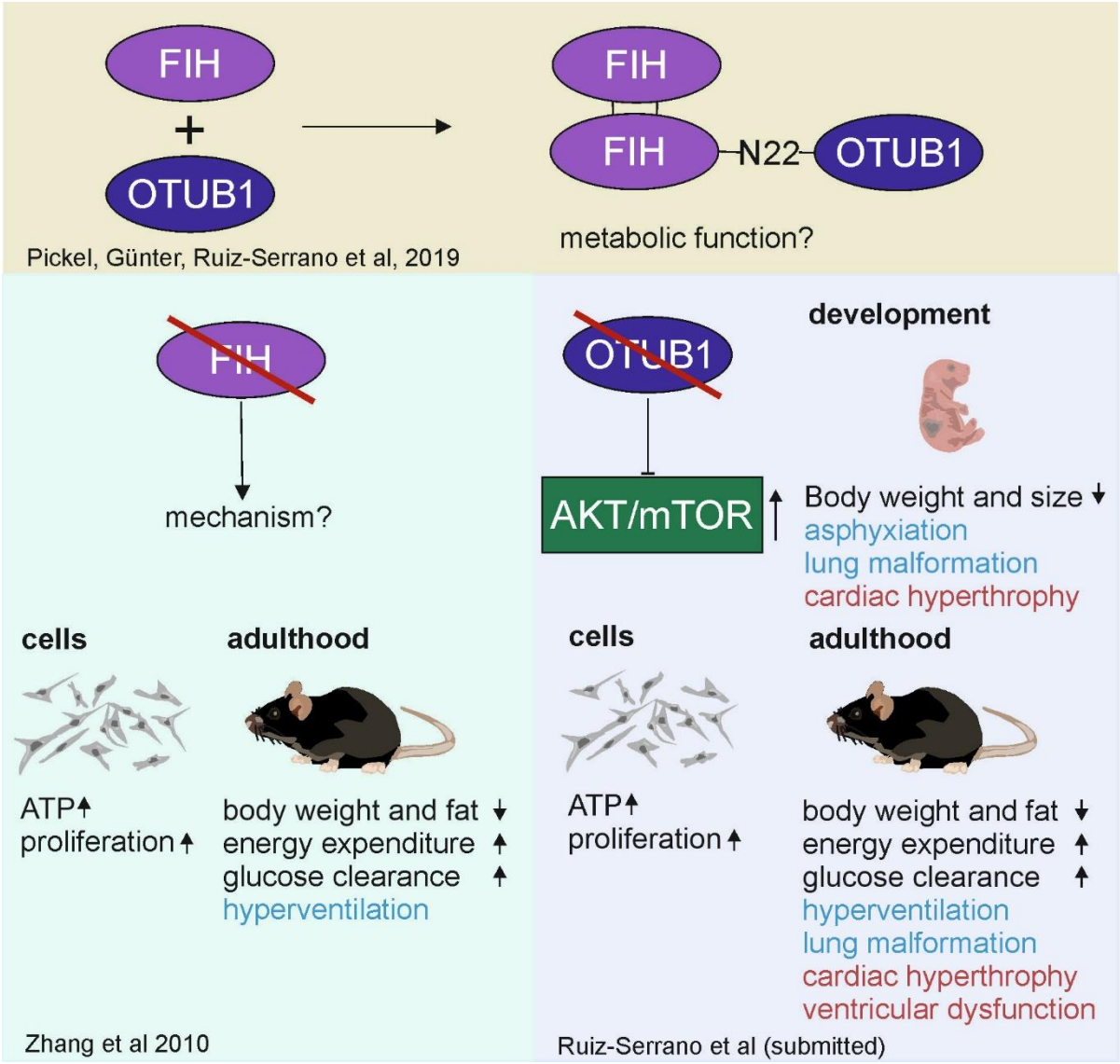

Figure 1: Summary of OTUB1 and FIH-dependent physiological functions. FIH and OTUB form a heterodimer with two FIH proteins likely covalently bound to one OTUB1 protein (top). FIH deletion leads to increased ATP levels in cells. In mice, deletion of FIH led to decreased body weight and fat mass, increased energy expenditure and increased glucose clearance (bottom left). Our results from mice with *Otub1* deletion suggest that OTUB1 is an inhibitor of the AKT/mTOR pathway. Following the deletion of OTUB1, we observed an increased proliferation and ATP production in cells. OTUB1 deletions also led to a perinatal lethality due to asphyxiation and lung malformation, to cardiac hypertrophy and to a decreased body weight

and size. Following induction of OTUB1 knock-out, adult mice show a decreased body weight and fat as well as an increased energy expenditure and glucose clearance, hyperventilation, lung malformation, cardiac hypertrophy, and ventricular dysfunction (bottom right).

In vivo, we found that perinatal lethality observed in homozygous *Otub1* KO mice was due to asphyxiation with a decreased airway space and increased cell proliferation. Furthermore, the animals showed a cardiac hypertrophy and a decreased body weight and length. The analyses of the embryonic lungs were performed at E18.5, just before the mice are born. Homozygous *Otub1* KO mice at E18.5 showed an increased cell proliferation; however, the type of cell(s) was not identified. Hence, to analyze which type(s) of cells were proliferating in *Otub1* KO mice, co-staining analysis of the proliferation marker with different cell type markers could be performed. These results could help to understand the effect of OTUB1 in the lung in more detail. Surfactant protein C levels and lamellar body morphology were similar in homozygous *Otub1* KO mice compared with *Wt* mice at E18.5. Nonetheless, an embryonic time point study could be used to understand OTUB1 levels, pulmonary histopathology, developmental gene expression and early lethality throughout the different embryonic stages. This development studies could determine the specific time during which OTUB1 is most relevant for lung development.

A cardiac phenotype was also observed in induced adult *Otub1* KO mice with cardiac hypertrophy, decreased heart rate, impaired systolic and diastolic function. To analyze the cause of the observed decrease in heart rate, electrocardiography (ECG) could be performed. ECG will further help to understand the transmission of the electric signal in the heart of induced adult *Otub1* KO mice and will identify whether the cells transmitting the electric impulse along the heart were damaged or not and a potential different input from the central nervous system. The increased left ventricular mass and impaired systolic function of the heart could be explained by an impaired mTOR pathway signaling. At a protein level in the heart, phosphorylated S6K was increased and in MEFs phosphorylated AMPK was decreased. Phosphorylated AMPK has been shown to inhibit the activity of mTORC1. Additionally, mTORC1 inhibits autophagy avoiding the development of cardiac hypertrophy [134]. Therefore, decreased phosphorylated AMPK could increase mTORC1 activity inhibiting autophagy and as a result leading to the observed cardiac hypertrophy. At an experimental level, this could be analyzed by deletion and overexpression of OTUB1 in cardiomyocytes and in *Otub1* KO mouse hearts. In the cardiomyocytes and hearts, pAMPK/AMPK levels could be studied since we previously observed the decrease in pAMPK in MEFs but did not investigate the heart. Furthermore, autophagy could be measured by investigating the autophagosome markers LC3B-II/LC3B-I ratio, Atg4 protease and beclin-1 protein levels [135]. To further

characterize the cardiac hypertrophy, the expression of different pro-hypertrophic genes may be analyzed, such as Hey2 and TGF-β [136, 137]. Furthermore, the investigation of lung and heart specific *Otub1* KO mice would determine whether the lung malformation alone is responsible for the embryonic death and/or the organ malformations in the embryos and adults are completely independent.

Regarding the metabolic phenotype, induced adult *Otub1* KO mice displayed decreased insulin levels but similar glucose basal levels as well an enhanced glucose clearance under glucose challenge. These glucose/insulin signaling differences might be due to an increased number or activity of the insulin receptors that activates downstream IRS proteins and the Akt signaling pathway. To study the insulin receptor signaling, total amount of insulin receptors and IRS activation could be assessed. To further understand the reason of the reduced insulin plasma amount under deletion of OTUB1 in mice, the direct study of insulin production via b-cells from the pancreas could be analyzed. The mTOR pathway participates in fatty acid oxidation and glycolysis pathways. We observed a decreased body weight with an increased food intake under deletion of OTUB1 as well as increased liver weight. Further analysis of the glycolytic enzymes might give insights into whether glycolysis is altered or regulated by OTUB1/mTOR signaling.

Additionally, the study of specific KO mice could provide insight in the specific relevance of OTUB1 at an organ level as well as understand the molecular mechanism behind. For example, heart inducible KO mice could be studied by cardiomyocyte-specific OTUB1 deletion could use by alpha-myosin heavy chain promoter directing the expression of a tamoxifen inducible Cre recombinase to cardiac myocytes (αMHC-MerCreMer) [138]. Also, liver-specific KO mice could be studied by Cre recombinase under the control of albumin promoter (Alb-Cre) [139]. Furthermore, overexpression of OTUB1 levels *in vivo* would be interesting to assess whether the observed phenotype will be reversed, compensated, or maintained, information that could also determine the most relevant function of OTUB1 *in vivo*. To optimize time and costs, a previous study on overexpression of OTUB1 in organ specific cell lines could provide information that could be further analyzed *in vivo.*

Furthermore, OTUB1 is highly expressed in the brain and in our studies, *Otub1* KO mice showed increased brain weight normalized to total body weight. Because of an impaired neural regulation, the metabolic and cardiac phenotype may also be explained. Also, brain FIH KO mice phenocopies partly whole-body FIH KO mice, showing decreased body weight, increased oxygen consumption and increased insulin sensitivity [114]. Therefore, the study of OTUB1 function in the brain could provide information whether OTUB1 is the substrate of FIH leading

to the metabolic phenotype. For example, food intake and body weight are regulated by the hypothalamus via insulin, leptin and ghrelin [140, 141]. We found that insulin levels in *Otub1* KO are decreased with similar TSH hormone levels, which does not support a direct effect of the hypothalamus. However, alterations in ghrelin level by an impaired hypothalamic regulation can produce differences in insulin levels [142]. Hence, the assessment of ghrelin and leptin levels could help to determine if the brain function leads to metabolic changes in *Otub1* KO mice.

To understand the molecular mechanism behind the observed differences, the overall cellular ubiquitin chain levels were studied in the presence and absence of OTUB1. MEFs and organs from adult knock-out mice showed no differences in the total ubiquitin levels, Lys48- and Lys63-linked ubiquitin chains. In the future, it would be interesting to analyze if following proteasomal inhibition with MG-132 ubiquitin chain levels change in the absence of OTUB1.

OTUB1 is raising interest in cancer and immune research, due to its major role in cancer development and progression as well as in the regulation of immune cells. In our research, we not only identify and analyze the interaction among OTUB1 and FIH at a cellular level, but we also characterized the phenotype of OTUB1 deletion *in vivo*. The functional consequence of the stable FIH-OTUB1 complex has not yet been studied, but a potential field of study would be the regulation of energy metabolism *in vitro* and *in vivo.* Besides the metabolic phenotype, OTUB1 has a pleiotropic role *in vivo*, including the regulation of embryonic development, cardiac and pulmonary functions. The phenotypes observed under the deletion of OTUB1 could be explained by OTUB1 regulation of the AKT/mTOR pathway. OTUB1 is a potential pharmacologic target where the side effects should be carefully considered. Our analyses indicate that non-targeted inhibition of OTUB1 may lead to severe side effects. Overall, our results show that further understanding in the molecular and physiological interplay of FIH and OTUB1 may help targeting novel therapeutic treatments.

References

1. Semenza, G.L., *Regulation of oxygen homeostasis by hypoxia-inducible factor 1.* Physiology, 2009. **24**: p. 97-106.
2. Kaelin, W.G., Jr. and P.J. Ratcliffe, *Oxygen sensing by metazoans: the central role of the HIF hydroxylase pathway.* Mol Cell, 2008. **30**(4): p. 393-402.
3. Schofield, C.J. and P.J. Ratcliffe, *Oxygen sensing by HIF hydroxylases.* Nat Rev Mol Cell Biol, 2004. **5**(5): p. 343-54.
4. Scholz, C.C. and C.T. Taylor, *Hydroxylase-dependent regulation of the NF-κB pathway.* Biol. Chem., 2013. **394**(4): p. 479-93.
5. Ploumakis, A. and M.L. Coleman, *OH, the Places You'll Go! Hydroxylation, Gene Expression, and Cancer.* Mol Cell, 2015. **58**(5): p. 729-41.
6. Islam, M.S., et al., *2-Oxoglutarate-Dependent Oxygenases.* Annu Rev Biochem, 2018. **87**: p. 585-620.
7. Masson, N., et al., *The FIH hydroxylase is a cellular peroxide sensor that modulates HIF transcriptional activity.* EMBO reports, 2012. **13**(3): p. 251-7.
8. Zhang, N., et al., *The asparaginyl hydroxylase factor inhibiting HIF-1alpha is an essential regulator of metabolism.* Cell metabolism, 2010. **11**(5): p. 364-78.
9. Sim, J., et al., *The Factor Inhibiting HIF Asparaginyl Hydroxylase Regulates Oxidative Metabolism and Accelerates Metabolic Adaptation to Hypoxia.* Cell Metab, 2018. **27**(4): p. 898-913.e7.
10. Cockman, M.E., et al., *Posttranslational hydroxylation of ankyrin repeats in IkappaB proteins by the hypoxia-inducible factor (HIF) asparaginyl hydroxylase, factor inhibiting HIF (FIH).* PNAS, 2006. **103**(40): p. 14767-72.
11. Cockman, M.E., J.D. Webb, and P.J. Ratcliffe, *FIH-dependent asparaginyl hydroxylation of ankyrin repeat domain-containing proteins.* Ann N Y Acad Sci., 2009. **1177**: p. 9-18.
12. Karttunen, S., et al., *Oxygen-dependent hydroxylation by FIH regulates the TRPV3 ion channel.* J. Cell Sci., 2015. **128**(2): p. 225-31.
13. Rodriguez, J., et al., *Substrate-Trapped Interactors of PHD3 and FIH Cluster in Distinct Signaling Pathways.* Cell Rep., 2016. **14**(11): p. 2745-60.
14. Nagarajan, Y., G.Y. Rychkov, and D.J. Peet, *Modulation of TRP Channel Activity by Hydroxylation and Its Therapeutic Potential.* Pharmaceuticals (Basel), 2017. **10**(2).
15. Janke, K., et al., *Factor inhibiting HIF-1 (FIH-1) modulates protein interactions of apoptosis-stimulating p53 binding protein 2 (ASPP2).* J Cell Sci, 2013. **126**(Pt 12): p. 2629-40.
16. Devries, I.L., et al., *Consequences of IkappaB alpha hydroxylation by the factor inhibiting HIF (FIH).* FEBS letters, 2010. **584**(23): p. 4725-30.
17. Scholz, C.C., et al., *Regulation of IL-1β-induced NF-κB by hydroxylases links key hypoxic and inflammatory signaling pathways.* PNAS, 2013. **110**(46): p. 18490-5.
18. Scholz, C.C., et al., *FIH regulates cellular metabolism through hydroxylation of the deubiquitinase OTUB1.* PLoS Biol., 2016. **14**(1): p. e1002347.
19. Herhaus, L., et al., *OTUB1 enhances TGFbeta signalling by inhibiting the ubiquitylation and degradation of active SMAD2/3.* Nat Commun, 2013. **4**: p. 2519.
20. Clague, M.J., C. Heride, and S. Urbe, *The demographics of the ubiquitin system.* Trends Cell Biol, 2015. **25**(7): p. 417-26.
21. Edelmann, M.J., et al., *Structural basis and specificity of human otubain 1-mediated deubiquitination.* Biochem. J., 2009. **418**(2): p. 379-90.
22. Wang, T., et al., *Evidence for bidentate substrate binding as the basis for the K48 linkage specificity of otubain 1.* J Mol Biol, 2009. **386**(4): p. 1011-23.
23. Wiener, R., et al., *The mechanism of OTUB1-mediated inhibition of ubiquitination.* Nature, 2012. **483**(7391): p. 618-22.
24. Nakada, S., et al., *Non-canonical inhibition of DNA damage-dependent ubiquitination by OTUB1.* Nature, 2010. **466**(7309): p. 941-6.

25. Juang, Y.C., et al., *OTUB1 co-opts Lys48-linked ubiquitin recognition to suppress E2 enzyme function.* Mol Cell, 2012. **45**(3): p. 384-97.
26. Wiener, R., et al., *E2 ubiquitin-conjugating enzymes regulate the deubiquitinating activity of OTUB1.* Nat. Struct. Mol. Biol., 2013. **20**(9): p. 1033-9.
27. Wolberger, C., *Mechanisms for regulating deubiquitinating enzymes.* Protein Sci., 2014. **23**(4): p. 344-53.
28. Mevissen, T.E.T. and D. Komander, *Mechanisms of Deubiquitinase Specificity and Regulation.* Annu Rev Biochem, 2017. **86**: p. 159-192.
29. Stiehl, D.P., et al., *Increased prolyl 4-hydroxylase domain proteins compensate for decreased oxygen levels. Evidence for an autoregulatory oxygen-sensing system.* J. Biol. Chem., 2006. **281**(33): p. 23482-91.
30. Wenger, R.H., et al., *Frequently asked questions in hypoxia research.* Hypoxia, 2015. **3**: p. 35-43.
31. Lando, D., et al., *FIH-1 is an asparaginyl hydroxylase enzyme that regulates the transcriptional activity of hypoxia-inducible factor.* Genes Dev., 2002. **16**(12): p. 1466-71.
32. Sun, X.X., K.B. Challagundla, and M.S. Dai, *Positive regulation of p53 stability and activity by the deubiquitinating enzyme Otubain 1.* EMBO J., 2012. **31**(3): p. 576-92.
33. Tan, S., *A modular polycistronic expression system for overexpressing protein complexes in Escherichia coli.* Protein Expr. Purif., 2001. **21**(1): p. 224-34.
34. Pickel, C., C.T. Taylor, and C.C. Scholz, *Genetic Knockdown and Pharmacologic Inhibition of Hypoxia-Inducible Factor (HIF) Hydroxylases.* Methods Mol Biol, 2018. **1742**: p. 1-14.
35. Gutsche, K., et al., *Intermittent hypoxia confers pro-metastatic gene expression selectively through NF-kappaB in inflammatory breast cancer cells.* Free Radic. Biol. Med., 2016. **101**: p. 129-142.
36. Peach, M., N. Marsh, and D.J. Macphee, *Protein solubilization: attend to the choice of lysis buffer.* Methods Mol. Biol., 2012. **869**: p. 37-47.
37. Anderson, B.L., R.W. Berry, and A. Telser, *A sodium dodecyl sulfate--polyacrylamide gel electrophoresis system that separates peptides and proteins in the molecular weight range of 2500 to 90,000.* Anal Biochem, 1983. **132**(2): p. 365-75.
38. Bradford, M.M., *A rapid and sensitive method for the quantitation of microgram quantities of protein utilizing the principle of protein-dye binding.* Anal. Biochem., 1976. **72**: p. 248-54.
39. Swamy, M., et al., *Blue native polyacrylamide gel electrophoresis (BN-PAGE) for the identification and analysis of multiprotein complexes.* Sci STKE, 2006. **2006**(345): p. pl4.
40. Camacho-Carvajal, M.M., et al., *Two-dimensional Blue native/SDS gel electrophoresis of multi-protein complexes from whole cellular lysates: a proteomics approach.* Mol. Cell Proteomics, 2004. **3**(2): p. 176-82.
41. Neuhoff, V., et al., *Improved staining of proteins in polyacrylamide gels including isoelectric focusing gels with clear background at nanogram sensitivity using Coomassie Brilliant Blue G-250 and R-250.* Electrophoresis, 1988. **9**(6): p. 255-62.
42. Cox, J. and M. Mann, *MaxQuant enables high peptide identification rates, individualized p.p.b.-range mass accuracies and proteome-wide protein quantification.* Nat. Biotechnol., 2008. **26**(12): p. 1367-72.
43. Cox, J., et al., *Andromeda: a peptide search engine integrated into the MaxQuant environment.* J. Proteome Res., 2011. **10**(4): p. 1794-805.
44. Wolski, W., J. Grossmann, and C. Panse. *SRMService - R-Package to Report Quantitative Mass Spectrometry Data.* 2018; Available from: http://github.com/protViz/SRMService.
45. Turker, C., et al. *B-Fabric: The Swiss Army Knife for Life Sciences.* in *EDBT 2010*. 2010. Lausanne, Switzerland.
46. Vizcaino, J.A., et al., *2016 update of the PRIDE database and its related tools.* Nucleic Acids Res, 2016. **44**(D1): p. D447-56.

47. Ciechanover, A., et al., *ATP-dependent conjugation of reticulocyte proteins with the polypeptide required for protein degradation.* PNAS, 1980. **77**(3): p. 1365-8.
48. Hershko, A., et al., *Proposed role of ATP in protein breakdown: conjugation of protein with multiple chains of the polypeptide of ATP-dependent proteolysis.* PNAS, 1980. **77**(4): p. 1783-6.
49. Kostiuk, M.A., B.O. Keller, and L.G. Berthiaume, *Non-radioactive detection of palmitoylated mitochondrial proteins using an azido-palmitate analogue.* Methods Enzymol., 2009. **457**: p. 149-65.
50. Yeh, T.L., et al., *Molecular and cellular mechanisms of HIF prolyl hydroxylase inhibitors in clinical trials.* Chem. Sci., 2017. **8**(11): p. 7651-7668.
51. Singleton, R.S., et al., *Quantitative mass spectrometry reveals dynamics of factor-inhibiting hypoxia-inducible factor-catalyzed hydroxylation.* J. Biol. Chem., 2011. **286**(39): p. 33784-94.
52. Tian, Y.M., et al., *Differential sensitivity of hypoxia inducible factor hydroxylation sites to hypoxia and hydroxylase inhibitors.* J. Biol. Chem., 2011. **286**(15): p. 13041-51.
53. Lancaster, D.E., et al., *Disruption of dimerization and substrate phosphorylation inhibit factor inhibiting hypoxia-inducible factor (FIH) activity.* Biochem J, 2004. **383**(Pt. 3): p. 429-37.
54. Emmerich, C.H. and P. Cohen, *Optimising methods for the preservation, capture and identification of ubiquitin chains and ubiquitylated proteins by immunoblotting.* Biochem. Biophys. Res. Commun., 2015. **466**(1): p. 1-14.
55. Wells, J.N., L.T. Bergendahl, and J.A. Marsh, *Co-translational assembly of protein complexes.* Biochem Soc Trans, 2015. **43**(6): p. 1221-6.
56. Pao, K.C., et al., *Activity-based E3 ligase profiling uncovers an E3 ligase with esterification activity.* Nature, 2018. **556**(7701): p. 381-385.
57. Termathe, M. and S.A. Leidel, *The Uba4 domain interplay is mediated via a thioester that is critical for tRNA thiolation through Urm1 thiocarboxylation.* Nucleic Acids Res, 2018. **46**(10): p. 5171-5181.
58. Yang, M., et al., *Substrate selectivity analyses of factor inhibiting hypoxia-inducible factor.* Angew Chem Int Ed Engl, 2013. **52**(6): p. 1700-4.
59. Yang, M., et al., *Asparagine and aspartate hydroxylation of the cytoskeletal ankyrin family is catalyzed by factor-inhibiting hypoxia-inducible factor.* J. Biol. Chem., 2011. **286**(9): p. 7648-60.
60. Yang, M., et al., *Factor-inhibiting hypoxia-inducible factor (FIH) catalyses the post-translational hydroxylation of histidinyl residues within ankyrin repeat domains.* The FEBS journal, 2011. **278**(7): p. 1086-97.
61. Friedrich, M.G., et al., *Spontaneous cross-linking of proteins at aspartate and asparagine residues is mediated via a succinimide intermediate.* Biochem. J., 2018. **475**(20): p. 3189-3200.
62. Sridharan, U. and K. Ponnuraj, *Isopeptide bond in collagen- and fibrinogen-binding MSCRAMMs.* Biophys. Rev., 2016. **8**(1): p. 75-83.
63. Dann, C.E., 3rd, R.K. Bruick, and J. Deisenhofer, *Structure of factor-inhibiting hypoxia-inducible factor 1: An asparaginyl hydroxylase involved in the hypoxic response pathway.* PNAS, 2002. **99**(24): p. 15351-6.
64. Elkins, J.M., et al., *Structure of factor-inhibiting hypoxia-inducible factor (HIF) reveals mechanism of oxidative modification of HIF-1 alpha.* J. Biol. Chem., 2003. **278**(3): p. 1802-6.
65. Stolze, I.P., et al., *Genetic analysis of the role of the asparaginyl hydroxylase factor inhibiting hypoxia-inducible factor (FIH) in regulating hypoxia-inducible factor (HIF) transcriptional target genes [corrected].* J. Biol. Chem., 2004. **279**(41): p. 42719-25.
66. Wilkins, S.E., et al., *Differences in hydroxylation and binding of Notch and HIF-1alpha demonstrate substrate selectivity for factor inhibiting HIF-1 (FIH-1).* Int J Biochem Cell Biol, 2009. **41**(7): p. 1563-71.

67. Ehrismann, D., et al., *Studies on the activity of the hypoxia-inducible-factor hydroxylases using an oxygen consumption assay.* Biochem. J., 2007. **401**(1): p. 227-34.
68. Jewell, U.R., et al., *Induction of HIF-1alpha in response to hypoxia is instantaneous.* Faseb J., 2001. **15**(7): p. 1312-4.
69. Singleton, R.S., et al., *OGFOD1 catalyzes prolyl hydroxylation of RPS23 and is involved in translation control and stress granule formation.* PNAS, 2014. **111**(11): p. 4031-6.
70. Horita, S., et al., *Structure of the ribosomal oxygenase OGFOD1 provides insights into the regio- and stereoselectivity of prolyl hydroxylases.* Structure, 2015. **23**(4): p. 639-52.
71. Paolini, N.A., et al., *A Ribosomopathy Reveals Decoding Defective Ribosomes Driving Human Dysmorphism.* Am. J. Hum. Genet., 2017. **100**(3): p. 506-522.
72. Clague, M.J., S. Urbe, and D. Komander, *Breaking the chains: deubiquitylating enzyme specificity begets function.* Nat Rev Mol Cell Biol, 2019. **20**(6): p. 338-352.
73. Günter, J., et al., *The functional interplay between the HIF pathway and the ubiquitin system - more than a one-way road.* Exp Cell Res, 2017. **356**(2): p. 152-159.
74. Vandenabeele, P. and M.J. Bertrand, *The role of the IAP E3 ubiquitin ligases in regulating pattern-recognition receptor signalling.* Nat Rev Immunol, 2012. **12**(12): p. 833-44.
75. Edelmann, M.J., et al., *Structural basis and specificity of human otubain 1-mediated deubiquitination.* Biochem J, 2009. **418**(2): p. 379-90.
76. Wolberger, C., *Mechanisms for regulating deubiquitinating enzymes.* Protein Sci, 2014. **23**(4): p. 344-53.
77. Goncharov, T., et al., *OTUB1 modulates c-IAP1 stability to regulate signalling pathways.* Embo j, 2013. **32**(8): p. 1103-14.
78. Li, S., et al., *Regulation of virus-triggered signaling by OTUB1- and OTUB2-mediated deubiquitination of TRAF3 and TRAF6.* J Biol Chem, 2010. **285**(7): p. 4291-7.
79. Peng, Y., R. Xu, and X. Zheng, *HSCARG negatively regulates the cellular antiviral RIG-I like receptor signaling pathway by inhibiting TRAF3 ubiquitination via recruiting OTUB1.* PLoS Pathog, 2014. **10**(4): p. e1004041.
80. Lin, J.T., et al., *Naive CD4 t cell proliferation is controlled by mammalian target of rapamycin regulation of GRAIL expression.* J Immunol, 2009. **182**(10): p. 5919-28.
81. Zhou, K., et al., *OTUB1-mediated deubiquitination of FOXM1 up-regulates ECT-2 to promote tumor progression in renal cell carcinoma.* Cell Biosci, 2020. **10**: p. 50.
82. Sulser, P., et al., *HIF hydroxylase inhibitors decrease cellular oxygen consumption depending on their selectivity.* FASEB J., 2020. **34**(2): p. 2344-2358.
83. Pickel, C., et al., *Oxygen-dependent bond formation with FIH regulates the activity of the client protein OTUB1.* Redox Biol, 2019. **26**: p. 101265.
84. Scholz, C.C., et al., *Regulation of IL-1beta-induced NF-kappaB by hydroxylases links key hypoxic and inflammatory signaling pathways.* PNAS, 2013. **110**(46): p. 18490-5.
85. Scholz, C.C., et al., *FIH Regulates Cellular Metabolism through Hydroxylation of the Deubiquitinase OTUB1.* PLoS Biol, 2016. **14**(1): p. e1002347.
86. Pasupala, N., et al., *OTUB1 non-catalytically stabilizes the E2 ubiquitin-conjugating enzyme UBE2E1 by preventing its autoubiquitination.* J Biol Chem, 2018. **293**(47): p. 18285-18295.
87. Wang, X., et al., *OTUB1 inhibits CNS autoimmunity by preventing IFN-gamma-induced hyperactivation of astrocytes.* EMBO J, 2019. **38**(10).
88. Mulas, F., et al., *The deubiquitinase OTUB1 augments NF-kappaB-dependent immune responses in dendritic cells in infection and inflammation by stabilizing UBC13.* Cell Mol Immunol, 2020.
89. Li, Y., et al., *Preventing abnormal NF-kappaB activation and autoimmunity by Otub1-mediated p100 stabilization.* Cell Res, 2019. **29**(6): p. 474-485.
90. Zhou, X., et al., *The deubiquitinase Otub1 controls the activation of CD8(+) T cells and NK cells by regulating IL-15-mediated priming.* Nat Immunol, 2019. **20**(7): p. 879-889.

91. Saldana, M., et al., *Otubain 1: a non-canonical deubiquitinase with an emerging role in cancer.* Endocr Relat Cancer, 2019. **26**(1): p. R1-R14.
92. Ikeda, H., et al., *Increased Akt-mTOR signaling in lung epithelium is associated with respiratory distress syndrome in mice.* Mol Cell Biol, 2011. **31**(5): p. 1054-65.
93. Lertkiatmongkol, P., et al., *Endothelial functions of platelet/endothelial cell adhesion molecule-1 (CD31).* Curr Opin Hematol, 2016. **23**(3): p. 253-9.
94. Costantino, S., et al., *Obesity-induced activation of JunD promotes myocardial lipid accumulation and metabolic cardiomyopathy.* Eur Heart J, 2019. **40**(12): p. 997-1008.
95. Riehle, C. and J. Bauersachs, *Small animal models of heart failure.* Cardiovasc Res, 2019. **115**(13): p. 1838-1849.
96. Zhao, L., et al., *OTUB1 protein suppresses mTOR complex 1 (mTORC1) activity by deubiquitinating the mTORC1 inhibitor DEPTOR.* J Biol Chem, 2018. **293**(13): p. 4883-4892.
97. Land, S.C., C.L. Scott, and D. Walker, *mTOR signalling, embryogenesis and the control of lung development.* Semin Cell Dev Biol, 2014. **36**: p. 68-78.
98. Wang, J., et al., *PI3K-AKT pathway mediates growth and survival signals during development of fetal mouse lung.* Tissue Cell, 2005. **37**(1): p. 25-35.
99. Iturri, P., et al., *Inhibition of Protein Kinases AKT and ERK1/2 Reduce the Carotid Body Chemoreceptor Response to Hypoxia in Adult Rats.* Adv Exp Med Biol, 2015. **860**: p. 269-77.
100. Xu, L. and M. Brink, *mTOR, cardiomyocytes and inflammation in cardiac hypertrophy.* Biochim Biophys Acta, 2016. **1863**(7 Pt B): p. 1894-903.
101. Dummler, B. and B.A. Hemmings, *Physiological roles of PKB/Akt isoforms in development and disease.* Biochem Soc Trans, 2007. **35**(Pt 2): p. 231-5.
102. Saxton, R.A. and D.M. Sabatini, *mTOR Signaling in Growth, Metabolism, and Disease.* Cell, 2017. **168**(6): p. 960-976.
103. Caron, A., et al., *DEPTOR at the Nexus of Cancer, Metabolism, and Immunity.* Physiol Rev, 2018. **98**(3): p. 1765-1803.
104. Manning, B.D. and A. Toker, *AKT/PKB Signaling: Navigating the Network.* Cell, 2017. **169**(3): p. 381-405.
105. Hahn-Windgassen, A., et al., *Akt activates the mammalian target of rapamycin by regulating cellular ATP level and AMPK activity.* J Biol Chem, 2005. **280**(37): p. 32081-9.
106. De Leo, S., S.Y. Lee, and L.E. Braverman, *Hyperthyroidism.* Lancet, 2016. **388**(10047): p. 906-918.
107. Haeusler, R.A., T.E. McGraw, and D. Accili, *Biochemical and cellular properties of insulin receptor signalling.* Nat Rev Mol Cell Biol, 2018. **19**(1): p. 31-44.
108. Taniguchi, C.M., B. Emanuelli, and C.R. Kahn, *Critical nodes in signalling pathways: insights into insulin action.* Nat Rev Mol Cell Biol, 2006. **7**(2): p. 85-96.
109. Lopez-Barneo, J., et al., *Carotid body oxygen sensing and adaptation to hypoxia.* Pflugers Arch, 2016. **468**(1): p. 59-70.
110. Akasaki, Y., et al., *Glycolytic fast-twitch muscle fiber restoration counters adverse age-related changes in body composition and metabolism.* Aging Cell, 2014. **13**(1): p. 80-91.
111. Chakraborty, A., et al., *Inositol pyrophosphates inhibit Akt signaling, thereby regulating insulin sensitivity and weight gain.* Cell, 2010. **143**(6): p. 897-910.
112. Carracedo, A., A. Alimonti, and P.P. Pandolfi, *PTEN level in tumor suppression: how much is too little?* Cancer Res, 2011. **71**(3): p. 629-33.
113. Osman, M.A., F.H. Sarkar, and E. Rodriguez-Boulan, *A molecular rheostat at the interface of cancer and diabetes.* Biochim Biophys Acta, 2013. **1836**(1): p. 166-76.
114. Zhang, N., et al., *The asparaginyl hydroxylase factor inhibiting HIF-1alpha is an essential regulator of metabolism.* Cell Metab, 2010. **11**(5): p. 364-78.
115. Dickinson, M.E., et al., *High-throughput discovery of novel developmental phenotypes.* Nature, 2016. **537**(7621): p. 508-514.

116. Gutsche, K., et al., *Intermittent hypoxia confers pro-metastatic gene expression selectively through NF-kappaB in inflammatory breast cancer cells.* Free Radic Biol Med, 2016. **101**: p. 129-142.
117. Emmerich, C.H. and P. Cohen, *Optimising methods for the preservation, capture and identification of ubiquitin chains and ubiquitylated proteins by immunoblotting.* Biochem Biophys Res Commun, 2015. **466**(1): p. 1-14.
118. Imeri, F., et al., *Generation of renal Epo-producing cell lines by conditional gene tagging reveals rapid HIF-2 driven Epo kinetics, cell autonomous feedback regulation, and a telocyte phenotype.* Kidney Int, 2019. **95**(2): p. 375-387.
119. Uhlen, M., et al., *Proteomics. Tissue-based map of the human proteome.* Science, 2015. **347**(6220): p. 1260419.
120. Bradford, M.M., *A rapid and sensitive method for the quantitation of microgram quantities of protein utilizing the principle of protein-dye binding.* Anal Biochem, 1976. **72**: p. 248-54.
121. Sun, X.X., K.B. Challagundla, and M.S. Dai, *Positive regulation of p53 stability and activity by the deubiquitinating enzyme Otubain 1.* EMBO J, 2012. **31**(3): p. 576-92.
122. Schindelin, J., et al., *Fiji: an open-source platform for biological-image analysis.* Nat Methods, 2012. **9**(7): p. 676-82.
123. Schneider, C.A., W.S. Rasband, and K.W. Eliceiri, *NIH Image to ImageJ: 25 years of image analysis.* Nat Methods, 2012. **9**(7): p. 671-5.
124. Weir, J.B., *New methods for calculating metabolic rate with special reference to protein metabolism.* J Physiol, 1949. **109**(1-2): p. 1-9.
125. Wielinga, P.Y., B. Alder, and T.A. Lutz, *The acute effect of amylin and salmon calcitonin on energy expenditure.* Physiol Behav, 2007. **91**(2-3): p. 212-7.
126. Clapcote, S.J. and J.C. Roder, *Simplex PCR assay for sex determination in mice.* Biotechniques, 2005. **38**(5): p. 702, 704, 706.
127. Meyer-Schwesinger, C., *The ubiquitin–proteasome system in kidney physiology and disease.* Nature Reviews Nephrology, 2019. **15**(7): p. 393-411.
128. Harrigan, J.A., et al., *Deubiquitylating enzymes and drug discovery: emerging opportunities.* Nature Reviews Drug Discovery, 2018. **17**(1): p. 57-78.
129. Edelmann, M.J., et al., *Structural basis and specificity of human otubain 1-mediated deubiquitination.* Biochem J, 2009. **418**(2): p. 379-90.
130. Wolberger, C., *Mechanisms for regulating deubiquitinating enzymes.* Protein science : a publication of the Protein Society, 2014. **23**(4): p. 344-353.
131. Peng, H., et al., *MicroRNA-31 targets FIH-1 to positively regulate corneal epithelial glycogen metabolism.* FASEB journal : official publication of the Federation of American Societies for Experimental Biology, 2012. **26**(8): p. 3140-3147.
132. Mahon, P.C., K. Hirota, and G.L. Semenza, *FIH-1: a novel protein that interacts with HIF-1alpha and VHL to mediate repression of HIF-1 transcriptional activity.* Genes Dev, 2001. **15**(20): p. 2675-86.
133. Fagerberg, L., et al., *Analysis of the human tissue-specific expression by genome-wide integration of transcriptomics and antibody-based proteomics.* Molecular & cellular proteomics : MCP, 2014. **13**(2): p. 397-406.
134. Li, Y., et al., *AMPK inhibits cardiac hypertrophy by promoting autophagy via mTORC1.* Archives of Biochemistry and Biophysics, 2014. **558**: p. 79-86.
135. Barth, S., D. Glick, and K.F. Macleod, *Autophagy: assays and artifacts.* The Journal of pathology, 2010. **221**(2): p. 117-124.
136. Dong, W., et al., *Activated Protein C Ameliorates Renal Ischemia-Reperfusion Injury by Restricting Y-Box Binding Protein-1 Ubiquitination.* J Am Soc Nephrol, 2015. **26**(11): p. 2789-99.
137. Liu, G., et al., *Transforming growth factor β and its role in heart disease.* Experimental and therapeutic medicine, 2017. **13**(5): p. 2123-2128.

138. Sohal, D.S., et al., *Temporally regulated and tissue-specific gene manipulations in the adult and embryonic heart using a tamoxifen-inducible Cre protein.* Circ Res, 2001. **89**(1): p. 20-5.
139. Yakar, S., et al., *Normal growth and development in the absence of hepatic insulin-like growth factor I.* Proc Natl Acad Sci U S A, 1999. **96**(13): p. 7324-9.
140. Vercruysse, P., et al., *Hypothalamic Alterations in Neurodegenerative Diseases and Their Relation to Abnormal Energy Metabolism.* Frontiers in Molecular Neuroscience, 2018. **11**(2).
141. Levin, B.E. and T.A. Lutz, *Amylin and Leptin: Co-Regulators of Energy Homeostasis and Neuronal Development.* Trends Endocrinol Metab, 2017. **28**(2): p. 153-164.
142. Yada, T., et al., *Ghrelin regulates insulin release and glycemia: physiological role and therapeutic potential.* Curr Diabetes Rev, 2008. **4**(1): p. 18-23.

6. Contributions to publications

Original research publications mentioned in this thesis

Ruiz-Serrano A, Monné Rodríguez J, Boyle CN, Günter J, Constantino S, Flüchter P, Pfundstein S, Bapst A, Pellegrini G, Wagner CA, Lutz TA, Paneni F, Wenger RH, Scholz CC. The deubiquitinase OTUB1 is essential for development, energy metabolism respiration and cardiac function. (Submitted)

All figures

Pickel C, Günter J, **Ruiz-Serrano A**, Spielmann P, Fabrizio J-A, Wolski W, Peet DJ, Wenger RH, Scholz CC. Oxygen-dependent bond formation with FIH regulates the activity of the client protein OTUB1. Redox Biol. 2019 Sep;26:101265.

To supplementary figure 1

Reviews

Günter J*, **Ruiz-Serrano A***, Pickel C*, Wenger RH, Scholz CC The functional interplay between the HIF pathway and the ubiquitin system - more than a one-way road. Exp Cell Res. 2017 Jul 15;356(2):152-159.

* These authors contributed equally to this manuscript.

Wrote part of the review article and contributed figures

7. Curriculum Vitae

Personal details

Name: **Amalia Ruiz Serrano**
Nationality: Spanish

Education

10.2015-present **PhD student** in the Cellular Oxygen Physiology research group
Institute of Physiology, University of Zurich, Switzerland
Supervision by Dr Carsten Scholz

09.2014-09.2015 **MSc** in Cell and Tissue Engineering
Institute of Science & Technology in Medicine, Keele University, UK
Thesis: Effect of micropatterned and collagen coated surfaces in tenocytes and TSCPs
Supervision by Prof Nicholas R Forsyth and Dr Paul Roach

09.2010-07.2014 **BSc** in Biotechnology
Experimental Sciences Faculty, Pablo de Olavide University, Spain
Thesis: Effect of *Arx* mutation in the olfactory bulb
Cell therapy for neuropathology group, CABIMER-CSIC
Supervision by Prof Manuel Álvarez Dolado

Grants & Awards

10.2019 **Hartmann Mueller travel grant**
98th meeting of the German Physiological Society, Ulm, Germany

05.2019 **Life Sciences Switzerland travel grant**
Knowledge transfer in Mouse Embryology practical course, PHENOMIN-ICS, France

04.2018 **Scholarship for the Keystone Symposia**
Therapeutic Targeting of Hypoxia-Sensitive Pathways, Oxford, UK

Scientific communication and meetings

2019 Oral presentation - 98th meeting of the German Physiological Society (Ulm, DE)

2018 Oral presentation - Keystone Symposia, (Oxford, UK)

2016-2018 1 oral and 3 Poster presentations Swiss Physiology Meeting (CH)

2016-2017 2 Poster presentations - ZIHP Symposium (Zurich, CH)

Publications

Original research publications

Ruiz-Serrano A, Monné Rodríguez J, Boyle CN, Günter J, Constantino S, Flüchter P, Pfundstein S, Bapst A, Pellegrini G, Wagner CA, Lutz TA, Paneni F, Wenger RH, Scholz CC. The deubiquitinase OTUB1 is essential for development, energy metabolism respiration and cardiac function. (Submitted)

Hopp A-K, Schlicker L, **Ruiz-Serrano A**, Hetzel U, Kipar A, Scholz CC, Hiller K, Verdeguer F, Pedrioli DML, Hottiger MO. Loss of MacroD1 rewires mitochondrial oxidative metabolism towards glycolysis *in vivo* and *in vitro*. (Submitted)

Pickel C, Günter J, **Ruiz-Serrano A**, Spielmann P, Fabrizio J-A, Wolski W, Peet DJ, Wenger RH, Scholz CC. Oxygen-dependent bond formation with FIH regulates the activity of the client protein OTUB1. Redox Biol. 2019 Sep;26:101265.

Reviews

Günter J*, **Ruiz-Serrano A***, Pickel C*, Wenger RH, Scholz CC The functional interplay between the HIF pathway and the ubiquitin system - more than a one-way road. Exp Cell Res. 2017 Jul 15;356(2):152-159.
* These authors contributed equally to this manuscript.

8. Acknowledgements

Foremost, I would like to thank my supervisor Dr. Carsten Scholz for giving me the opportunity to work on this exciting project. I appreciate his patience and time investment during my PhD. Thanks, Carsten for your continuous advice, understanding, time for meetings and scientific feedback. Thanks to his support in all the research time and writing of this thesis. Not every supervisor gives a lift to Schlieren to help with an experiment! Danke.

Special thanks go to Prof. Roland H. Wenger for suggestions, critical discussion and always challenging questions that have help me to grow as a scientist. Also, thanks to transmit your passion for hiking and Fondue to us, I have learned a lot about science and Switzerland thanks to you. Merci.

The completion of this project could not have been accomplished without the valuable feedback of my other thesis committee members Prof. Dr. Thomas A. Lutz and Prof. Dr. Hugo H. Marti. Thank you for their insightful comments and to find time to be present during my four committee meetings.

I would like to thank current and former members of the group of Roli, Carsten, Tanja and Stellor. I had the best welcoming ever possible in the group and found together with colleagues, friends with whom the lab has been even nicer. Also, I thank you my friends in the institute of physiology which makes the PhD experience more enjoyable. Thanks also to Brigitte for helping whenever possible with the bureaucracy and Patrick to be always available for any question!

Most importantly, thanks to my family, boyfriend, and friends whose support and encouragement has always been present.